博士論文

Response Based Track Profile Estimation Using Observable Train Models with Numerical and Experimental Validations

可観測な車両モデルを利用した応答計測型軌道変位推定とその検証

シヤガラジャン ジョシ サラバナン

Thiyagarajan Jothi Saravanan

Department of Civil Engineering
Graduate School of Engineering
The University of Tokyo, Japan

A dissertation submitted in partial fulfillment for the degree of

Doctor of Philosophy

March, 2018

This page is intentionally left blank

Dedicated to my mother

ACKNOWLEDGEMENTS

<div align="right">

シヤガラジャン ジョシ サラバナン
Thiyagarajan Jothi Saravanan,
March, 2018.

</div>

ABSTRACT

Railway technology has developed in line with Japanese social and economic changes and has seen rising speeds, cost saving and safety, as well as falling environmental impact. However, local railway networks suffer from age-related deterioration and poor maintenance and also it might be unable to perform adequate monitoring. It is essential to improve the comfort level and service life of local railway lines. Track profile which directly influences the ride quality and safety of rail tracks need to be estimated for the maintenance purpose. Currently, Track Recording Vehicle (TRV) like Doctor Yellow, one high speed test train in Japan is utilized for the track condition monitoring. But the demerits of TRV are, that it is expensive and cannot be frequently used for local railway lines. It is used only once in a year for most of lines. So, track profile estimation through vehicle response measurements potentially provides efficient and frequent measurement. However, the current onboard measurement system still stays on the qualitative inspection by repetitive tests. The main challenge to detect the vertical and lateral track profile and the other rail track irregularities is the unstable solution for the inverse analysis. A simpler, more robust and cost effective system for in-service train vehicle is desirable. Thus, data assimilation method is necessary for estimating the unknown inputs. For inverse analysis technique generally augmented Kalman Filter is being utilized. However, issue of un-observability need to be solved.

From the above background study, the research objectives of this dissertation are as follows,

• To propose extended Augmented State Kalman Filter (ASKF) technique to solve the Observability Rank Condition (ORC) for the state space model.

• To estimate both vertical and lateral railway track profile using extension of ASKF data assimilation technique for a rigid body motion train model.

• To perform Multi-Body Simulations (MBS) using SIMPACK to investigate the influence from different factors under various scenarios and to validate the proposed estimation algorithm.

• To validate the proposed inverse analysis on experimental measurements obtained from in-service local railway line.

Firstly, while the measurement of track profile or vehicle's absolute displacement on board is not practical, but the acceleration and angular velocity measurements are feasible. Prevalent

sensing devices such as smartphones have been potentially being utilized in vehicle body motion measurement. However, the applicability of inverse analysis for track profile estimation from such measurement is not clarified yet. Hence, from the perspective of observability, sensor installation location's effect needs to be investigated. Observability is the method or a concept to explain whether the particular state of the dynamic system can be identified under a given subset of limited measurements. In this study, ORC analysis of various time invariant linear vehicle dynamic models with different measurement layout are carried out to obtain the appropriate sensor placement strategy. The analysis shows that the profile becomes unobservable under acceleration and angular velocity measurements. To overcome this issue, in this dissertation the second derivative of the profile is proposed to be augmented in the state vector as one of the additional state variable, and thus the track profile component can be obtained through double integration of it. The proposed approaches theoretically solved the issue of un-observability and also revealed a sensor type and placement strategy, which can be used as the guideline in the track profile estimation through train vehicle response measurement.

Secondly, for numerical analysis purpose, vehicle body acceleration (vertical and lateral) and angular velocity measurements (pitching and yawing) are considered. In this dissertation, Kalman filter technique is employed for state space models termed as conventional ASKF and two extended approaches for the track profile estimation by augmenting the second derivative of profile directly or adopting the first derivative of the original state vector. The recommended estimation algorithm ASKF is robust and fast, which competently process the data collected from sensors through a simple linear rigid body train vehicle model. The verification study for simplified train models (4 DOF) and 6 DOF train models, accounting for both vertical and lateral track profile estimation are carried out and results are found to be in good agreement. In order to obtain the quantitative comparison of two waveforms, phase-shift correction is carried out using the misfit criteria through Hilbert transform. The statistical metrics are utilized for obtaining the single-valued misfit between two waveforms. Therefore, depending upon the sensors availability and feasible sensor placement locations, track profile can be reconstructed using extended ASKF algorithm with proposed method.

Thirdly, to perform MBS using SIMPACK: Rail, to generate more realistic responses by considering the influence from different factors under various scenarios, namely straight track and splined track sections. The sensors are placed just above the rail tracks on both the sides and used to measure the acceleration and angular velocity responses from the car body and both bogie masses of running train model on simulated track sections with vertical and lateral excitations. These vehicle measurement responses are utilized to estimate the vertical and lateral track profile using the 6 DOF train model and it is validated using the proposed estimation algorithm. The suggested sensor placement strategy is compared with maximum sensor location case and found to perform well.

For straight track section (ideal case), it shows a good agreement for vertical track profile while it can estimate only above 8 m wavelength irregularity for lateral track profile. The statistical metrics are utilized for comparison between various cases and the proposed approach is verified. Also, MBS are carried out for understanding the influence of rolling motion of train vehicle. For curved track section, the results show good agreement for vertical track profile estimation, while it shows large variation for lateral profile estimation. This is due to hunting oscillation phenomenon. Exactly the splined section of the track cannot be evaluated, because of wheel-rail interaction problem.

Lastly, to perform the rail track profile estimation from the in-service vehicle response measurement proposed extended ASKF method is employed. The smartphones (low cost sensors) are mounted on the train car body floor to collect the train vehicle dynamic responses. Inverse analysis is carried out to estimate both the vertical and lateral track irregularity by reconstructing the track profile waveform as well as converted 10 m chord versine waveform. The results are found with slight deviations due to simplified 4 DOF model and other phenomenon like hunting oscillation motion. This is due to practical limitations of sensor placement only on the car body. In future experimental measurements, the optimal sensor placement is recommended to mount sensors on car body and bogie masses. Thus, by utilizing 6 DOF train model accounting for bogie pitching/yawing motion, rail track profile can be estimated more precisely.

In summary, this dissertation proposes and realizes an inverse analysis scheme for the railway track profile estimation from in-service vehicle response measurements. The results obtained from this research exposed that the recommended, data assimilation ASKF method is efficient for condition assessment of local railway track lines with satisfactory correctness.

LIST OF CONTENTS

LIST OF FIGURES

LIST OF TABLES

Chapter 1 INTRODUCTION

1.1 Importance of Railway Infrastructure

Japan is an extended and elongated archipelago on the Pacific Ocean at the edge of Asian continent. Around 73% of the total land area is hilly region, henceforth almost 127 million people population are living on the coastline or nearby rivers. So, the cities alongside the shoreline have dense population and are interconnected by railways. Railroad vehicles are among the most widely used transportation methods for moving passengers and goods. Trains have been used in commerce for more than a century since its commencement at England in 1825 and have been used for services in Japan for 143 years since 1872. Over the last 40 years or so, railways have seen some significant progress in rail transportation technology. To minimize costs and transportation time railway operational speeds have been increased substantially however safety and comfort remain to be of paramount importance. Track irregularities have been a problem troubling railway scientists and engineers ever since the initiation of railway networks. Nowadays, the prominence of infrastructure maintenance is highlighted, as Japan has constructed a lot of infrastructure facilities since 1960s which is considered as the '*era of high economic growth*'. They are deteriorating badly which should be preserved appropriately in order to provide good service and prevent dangerous accidents [1]. As a result of absolute length of the railway system, the assessment of infrastructure is challenging and costly process. Furthermore, the issue of identification and probable restoration of damaged segments are difficult due to extreme usage of these infrastructures by frequent and heavy traffic. Timely cautioning systems that diminish the interruption of the railway networks are required and beneficial.

Many factors influence the cause of irregularities of a railway tracks. Features that influence irregularities can be grouped as railway vehicle and track engineering factors. The safe operation of a railway vehicle is dependent on the delicate interaction of dynamics of the railway vehicle and track infrastructures. Some significant vehicle engineering factors include but are not limited to the axle load, imbalance between the right and left static wheel load, spring stiffness of the suspension system, height of the vehicle, the location of the vehicles' center-of gravity etc. The condition of the track (maintenance grading), minimum curve radius,

super-elevation, track twists, cross overs, switches, rail profile, type of sleepers, ballast, etc. are some of the factors which falls under track engineering. The term '*real-world train dynamics*' refers to the dynamic behavior of rolling stock and in-service trains that can be found in local railway lines under operation. The vehicle dynamics of a train vehicle while in operation is a highly complex system. Furthermore, in real conditions various features of tracks are experienced such as straight tracks, tangent tracks, turnouts and curved tracks. It would be a difficult assignment to bring a concept of single mathematical model that might be comprehensively addressing all features of train-track interactions.

According to [2], the study of the dynamic behavior of the rolling stock and train can be divided into two basic groups. Figure 1.1 illustrates the schematic diagram of rolling stock [2]. The dynamic response refers to the behavior of the system owing to dynamic inputs and the stability study aims at investigating the system under various functioning circumstances. The rail vehicle components consist of,

(a) Wheel set bearing (axle box);
(b) A bogie (wheeled wagon or trolley), framework carrying wheels, a subassembly of wheels and axles (Figure 1.2) [2];
(c) Vehicle body, over the center of the bogie frame.
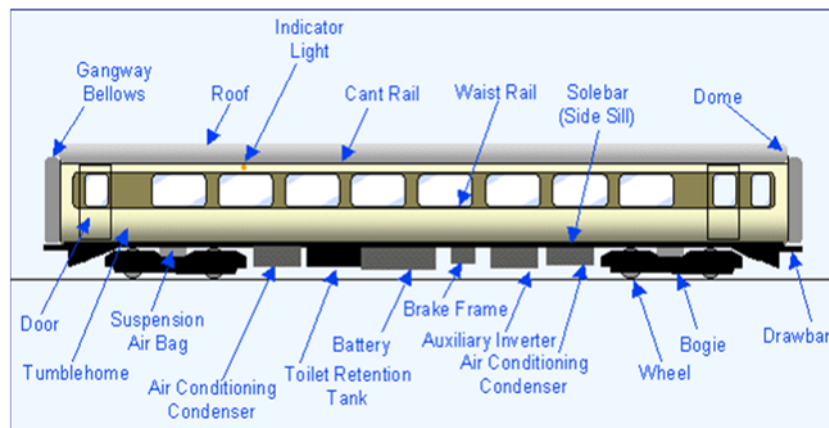
Figure 1.1 Schematic diagram of rolling stock [2]

The paper [4] explains about the overview of rail irregularities and its effect on the dynamic characteristics of the train vehicle. The vehicle responses directly effect in the ride comfort and safety of the passengers. Normally, track geometry (design shape or layout) and defects are classified under the category of long wavelength and short wavelength respectively. A wheel-

rail contact surface relationship is a significant issue for a running train, which may cause instability and contact stress amongst wheel and rail, which correspondingly result in wear, fatigue cracks and higher noise. Figures 1.3 – 1.4 represent the types of rail degradation and classification of track irregularities respectively [2]. The types of track irregularity considered for local railway tracks are classified as short and long track irregularities in Figures 1.5 and 1.6 respectively [4]. The schematic diagram for types of track geometry, namely vertical profile (elevation), lateral profile (alignment), gauge deformation, cant and twist are shown in Figure 1.7 [4].
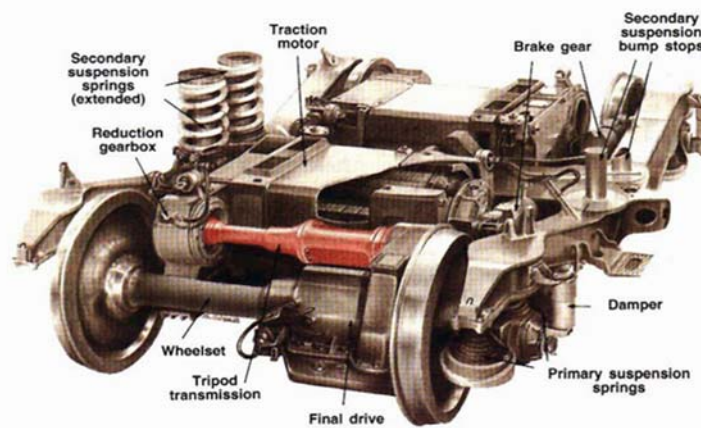
Figure 1.2 Bogie and its spare parts [2]
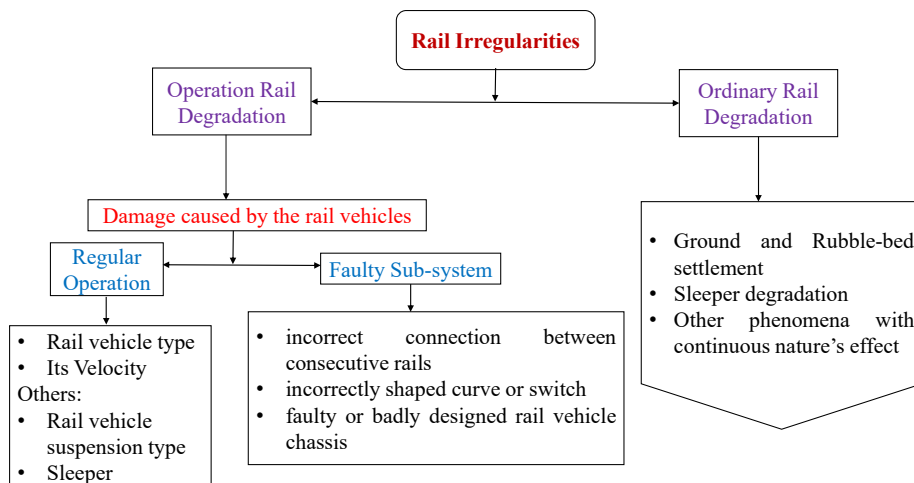
Figure 1.3 Types of rail degradation [2]

3

Type	Long Track Irregularities	Short Track Irregularities
Phenomenon	poor track alignments, switches, level crossings and bridges	squats, corrugation, thermite welds with poor finishing quality, insulated joints, blades and frogs of switches and crossings
Wavelength	length > 3 meters	length < 3 meters
Frequency Range	low frequency vibrations	mid (40-400 Hz) and high (400-2000 Hz or even more) frequency vibrations
Demerits	discomfort to passengers and damages to cargo	large dynamic contact forces and wheel-rail vibrations

Figure 1.4 Classification of track irregularities [2]

(a) Corrugation

(b) Squat

(c) Insulated joints

(d) Thermite welding

Figure 1.5 Short track irregularities [4]

(a) Poor track alignments

(b) Switches

(c) Level crossing

Figure 1.6 Long track irregularities [4]

To prevent a condition that would result in a derailment, the existing rails need to inspected and replaced if necessary. For track condition inspection, there are three main approaches available as shown in the Figure 1.8 [3], namely:

(a) Portable driven device manually - which can be used to gain information of a comparatively low length of track
(b) Movable device - which can be used for longer distances and is completely mechanically driven. These inspection vehicles which gives track status can be used during night time (i.e. when traffic is halted)
(c) Axle-box acceleration method (ABA) - which is used to detect track irregularity conditions. It is fixed on an axle-box supporting the axle of at least one bogie of an ordinary functioning train vehicle.
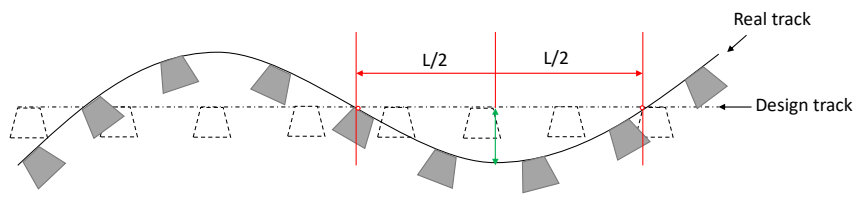
(a) vertical irregularity
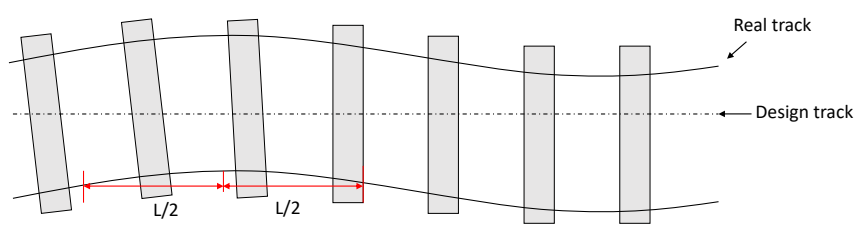
(b) alignment irregularity
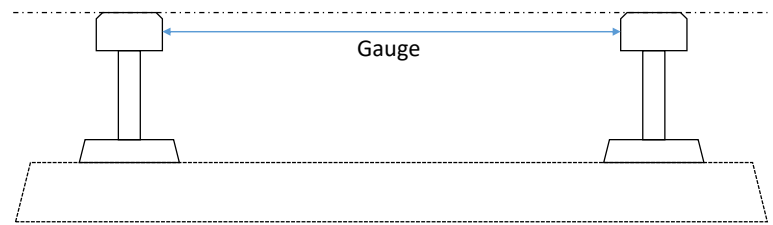
(c) gauge deformation
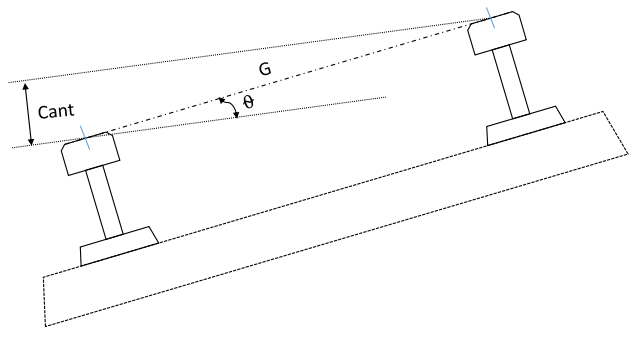
(d) Cant
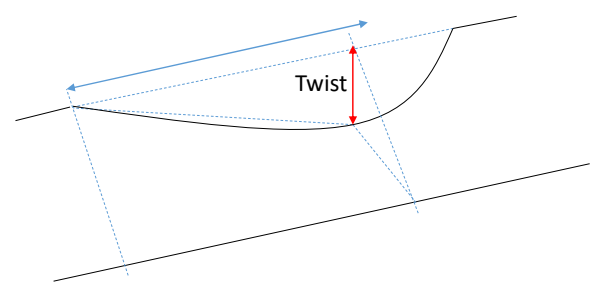
(e) twist

Figure 1.7 Types of track geometry [4]
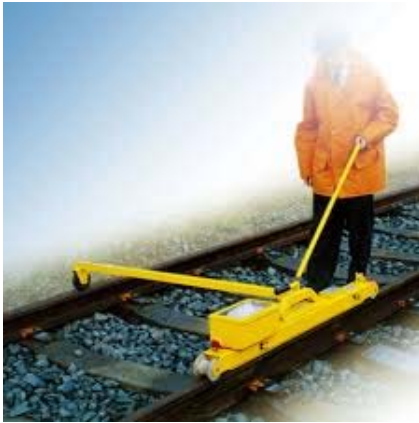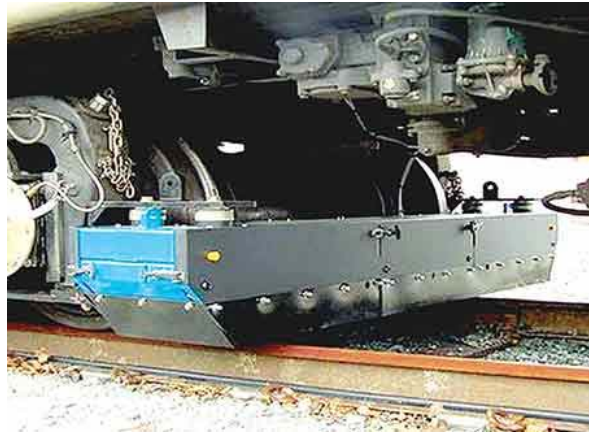
(a) Portable device   (b) Movable device
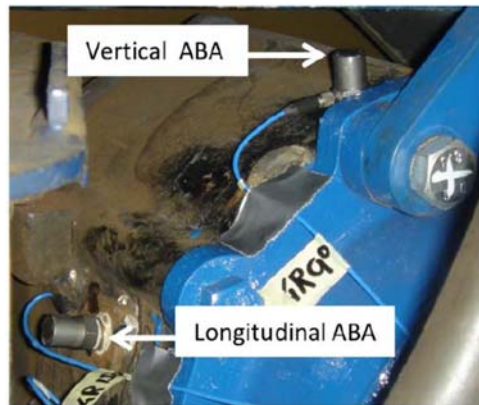
(c) ABA method

Figure 1.8 Existing railway track condition estimation method [3]

1.2   Literature Review: Track Profile Estimation

A railway vehicle running on tracks is one of the most complex dynamical systems in engineering due to many nonlinear components in the system. To minimize costs and transportation time railway operational speed has increased however safety and comfort remain to be of paramount importance. The necessary inspections need to be performed for determining the track condition due to bigger demand on railway networks. Sensors are mounted on in-service vehicles for collecting the acceleration and other dynamic parameters which are suitable more for condition monitoring of railway tracks. Track irregularities have been a problem troubling railway scientists and engineers since railways initiation. The exhaustive list of researchers has worked in perspective of track profile estimation from

measurements obtained from in-service train vehicle. The following state-of-the-art literature review presents a view on the existing condition monitoring technology; some data processing techniques and how research has been evolving over the decade of time.

1.2.1 Existing track condition monitoring methods

Several efforts are carried out to improve systems for the assessment of track environment. The objective is to attain a measureable or qualitative evaluation of serviceability of track and comfort to passengers which plays a significant role for rail management [5-7]. According to [8], rail track inspection emphases on fault identification, finding the reasons for defects and predicting for major damages to occur. Safety of the track is conventionally guaranteed by towed track recording coach (TRC) or track recording vehicle (TRV). Conventionally, track geometry estimation is done using TRC/TRV which is used to traverse over rail tracks. Development of electronic robust sensor technology made conceivable track profile assessment systems that can be mounted on in-service railway vehicles. More innovative tools are established to comprehend the exhaustive track-train interaction and also to forecast the possible problems confronted. Maintenance of in-service system is further difficult as the measurements are expected to come to halt more often when comparing to TRV/TRC. Thus the loss of accuracy in the measured data is the drawback of the in-service system.

Firstly, Federal Railroad Administration (FRA) – US, introduced condition monitoring system mounted on car-body and bogie of high-speed trains to measure vertical and lateral accelerations. It also used Global Positioning System (GPS) for locating the train within 60-90 m of precise location. The results are reported using mobile technology and are found triggered by excess acceleration. This error is substantial and might be due to GPS position which seems to be on the side of bogie [9]. In [10], track monitoring of in-service London Underground vehicles using vertical and lateral accelerometers are discussed in a detailed manner. Drawback appears that the vehicle speed is not considered in the processing, thus the acceleration will upsurge with speed. In [11]，it discussed about online monitoring of Chinese railway vehicle distortion from accelerometers placed on bogie and car body of train. The paper [12] explained about measurement system employed on an Italian metro vehicle to identify corrugation problems using axle-box mounted accelerometers as well as track conditions using sensor mounted on car body and bogie. In order to attain location, few sensors are used in addition to detect curving as Global Navigation Satellite System is not possible to use for underground purpose.

In [13], it described about the on-board measurement system of high-speed train in Italy with acceleration sensors placed on car body, bogie and axle-boxes to assess irregularities with wavelengths greater than 20 m on rail track. The data processing in frequency domain is

utilized with an effort to invert the train suspension dynamics considering the ambiguity in the suspension system parameters and also comprises problems associated to senor noise from accelerometers. The research in [14] illustrated the improvement of an unattended track geometry measurement system (UGMS) to monitor the frequently used lines devoid of disturbing the normal traffic. Apart from UGMS many track monitoring devices were developed and few were commercialized. Even though UGMS provide decent idea of what and how much data will be collected, it fails in providing filtering process required. Subsequently, due to in-service robustness issue, [15] explained about the accelerometers usage alone, on ICE 2 trains (second series of German high-speed trains) for improved track maintenance scheme on regularly scheduled high-speed trains. The results are found favorable to provide efficient information on track geometry maintenance.

The interesting work in [16, 17] presented the monitoring system used on in-service vehicles to detect vertical and lateral track irregularity respectively. Sensors placed on an in-service train vehicle collects enormous amount of data since the vehicle covers the same track several times every day compared to TRVs which pass through only once every few weeks. Hence, these collected data need to be handled carefully such that there is no loss of data and at the same time proper data reduction should be adopted in order to handle appropriately by the server.

The paper [18] investigated the condition monitoring prospects using vehicle mounted sensors. During inspection track geometry parameters like right and left vertical rail profile, lateral alignment, gauge, cross-level, dipped joints, corrugation is being collected. Specific track geometry requirements i.e., threshold defined for individual faults, are derived from the reports which were historically assured for safe running of vehicles on the track. Currently advanced tools are utilized in order to predict issues like wheel climb to understand train-track interaction well. A bogie-mounted sensors system based on an inertial measurement unit (IMU) alone is used on the Southern network in UK to understand the dynamics of a third rail condition monitoring system [19]. Comparison of track condition monitoring results obtained from axle-box and bogie mounted accelerometers on in-service Korean high-speed vehicle is discussed in [20]. Also the same team used a simplified sensor set with mixed filtering approach and compared the results with UGMS attached to the same vehicle. The system can practically detect the irregularities but the difficulties exist in replicating the UGMS track geometry [21]. Many track features can be identified with an IMU in the car body of German in-service regional railway vehicle. The IMU detects train vibrations and other undesirable signals and the system is at its early stage development [22]. It has been found that at times a clarification to a specific problem is defined in the literature.

In [23] it explained to detect corrugation and to monitor joints with the use of axle-box vertically sensing accelerometers. This describes that the sensors can be preferred for a specific application to focus on one characteristic of track geometry but mostly cannot be utilized for supplementary functions. Notable technical information on handling of the accelerometer data

to obtain versine (chord) type data has been reported in [24]. The in-service measurement system consists of bogie-mounted vertical accelerometer with additional vertical displacement sensor to measure vertical track geometry. In [25] developed low-cost TIMS (Train Intelligent Monitoring System) for monitoring railway track irregularities in local railways and also train position identification method using GPS sensor and train velocity where there is no connection with tachometer signal. The field measurements have been carried out using tri-axial accelerometers on the train car body floor. The root mean square values for vertical and lateral accelerations are being considered as threshold for estimating vertical and lateral track geometry respectively. These values increase with increasing vehicle speed. In [26, 27], illustrated the notable research on Japanese in-service track geometry monitoring system. In order to detect the track geometry faults and vehicle faults, vertically and laterally sensing accelerometers are attached on car body and axle-boxes in addition with microphone and particularly no sensors on bogie frame.

Mostly, a dynamic system model and its inverse can be represented either in non-parametric or parametric representation in frequency/time domain. Based on direct vehicle vibration measurements, possibility of reconstruction of track geometry is an example for inverse analysis problem. In the research carried out by [28], a parametric system identification and model inversion approach is suggested for real time application. The limitation of the proposed approach is that the model estimated for system identification is effective only about the velocity value as a result of which it was achieved. Later, the main objective is to use sensors only on the car body and also developed multi-resolution analysis of data processing using wavelet.

In [29] it described about the Japanese in-service rail-vehicle system measuring vertical and lateral track geometry irregularities using accelerometers mounted on the car body floor. Dynamic modelling of primary and secondary suspension systems are the requirements for that approach. Also a microphone (an acoustic sensor) is utilized for detecting corrugation faults. Although the proposed system is found to be employed on high-speed lines, the newly developed *N700 Shinkansen trains* (network of high-speed railway lines in Japan) which have good suspension system, made no longer suitable to apply. A new system was made in response to this, '*RAIDARSS-3*' with axle box-mounted, vertically sensing accelerometers, which employ doubly integrated and processed with a 10 m chord versine measurement procedure to obtain track geometry. Procedures are well-defined such as accelerations surpassing a threshold value or track irregularities exceeding assumed threshold levels. This distinctive system is exclusively for sensing trains passing, apparently as this causes substantial body accelerations that could else be detected as track irregularities. Nevertheless, the authors summarize that axle box-mounted accelerometers are challenging to maintain, so there is presently an improved work for reconstructing track geometry from car–body accelerations, using a Kalman filter and inverse modelling [30]. This system is still in a

developing stage The research carried out in [31], examined the connection between train dynamic characteristics, rail track irregularities, vehicle speed and irregularity wavelength.

Axle-box mounted accelerometers are frequently believed as a promising method to detect the vertical track geometry. Nevertheless, the prerequisite double integration results rise to certain complications, and upholding the sensors on axle-boxes has shown challenging in practice. Hence, a precise method is to mount the sensors on the bogie, comprising the full UGMS with an IMU on the bogie and optical sensors observing the rails.

The better robust solution is to utilize body-mounted sensors, however there are few difficulties triggered by the separation of the primary and secondary suspension systems. Also, there are certain common problems faced with track geometry monitoring systems namely, sensor inaccuracies and location problems. The faults in turnouts can be determined in terms of wavelength and Power Spectral Density functions. It can be utilized in more precise manner for locating geometric degradation and it is less time consuming which in turn helps in cutting down the maintenance cost [32]. This method is explicitly more attractive, because different maintenance approach can be utilized to maintain the different wavelength faults. In [33], the new parametric stochastic model is utilized to estimate the track geometry from the dynamics response of the in-service vehicle namely, vertical acceleration and the wheel load.

In later years, [101] introduced the probe vehicle which vividly alter the concept of railway track monitoring and therefore contributes to the safety of railways system. Also introduced wavelet based multi-resolution analysis method for detecting rail defects by disintegrating the obtained data into a detailed component of high frequency and an approximation component of low frequency. In [102] used frequency domain technique through inertial methods to estimate vertical rail track profile. An overview on the modern intelligent systems available for the maintenance of train infrastructure is well presented in [103], by examining the benefits and limitations of the monitoring system.

In [104], it proposed a different approach for estimating more realistic rail track geometry based on stochastic modelling and statistical properties of measured response. The interesting research on damage detection in railway infrastructure using wavelet transform on acceleration response obtained from the train vehicle is carried out by [105]. For Italian railway network, novel measurement methods for detecting rail corrugation and other track irregularities are discussed in detail by [106]. It also proposed a method for calculating the acoustic roughness spectrum for track maintenance. In [107], a method was proposed for determination of the vertical track profile through dynamic response obtained from bogie using accelerometer and gyroscope. In order to determine the track profile, the cross-entropy optimization technique was applied to match the data with the measured dynamic response of a train bogie. [108, 109] explain about the development of a compact size onboard sensor system for monitoring tracks. The measured responses from developed onboard system

showed promising and effective results for evaluating the quality of existing railway tracks in robust manner.

1.2.2 Literature Survey on Observability Theory

Constructing mathematical model for dynamic system from observed input/output data and which also comprises the ideal design of experiments for competently creating instructive data suitable for such models is termed as system identification [34-36]. In recent years, much attention for optimal sensor placement strategies has been received because of the development of system identification and health monitoring methodologies. Henceforth, the assortment of optimal sensor arrangement for parameter approximation in structural dynamics is important [37]. The aim in an experimental design is to create actual choice of the optimum number and placement of sensors such that the subsequent measured data are helpful in revealing the condition of the structure [38]. In many structural dynamics problems, understanding the output unknown force acting on a dynamic system is the most important step. Nevertheless, measuring the external force directly with sensors is a tough job, whereas appropriately obtaining the vibration responses are reasonable. Thus, the importance of external force identification through inverse analysis from measured responses are frequently preferred comparing to direct measurement. Numerous force reconstruction approaches have been recommended through inverse analysis in recent years [39-41].

With this background, once mathematical model is determined, it can be utilized to simulate the performance of the system influenced by numerous external forcing conditions. Thus, observability is the method or a concept to explain whether the particular state of the dynamic system can be identified under a given subset of limited measurements [42]. The observability of linear systems are vital structural properties which have close relationship with the state observers. In control system it is well-defined as the probability to infer the state of the system from observing its input-output behavior [43]. Particularly, observability can govern the stability of the Kalman filter [44]. Based on Lie algebra, Observability Rank Condition (ORC) method is developed for handling nonlinear systems which is an extension of concept of observability for linear system [45]. On the other hand, rank test can be utilized to obtain parameter identifiability which is a distinct case of the observability problem [46]. A detailed study on robust implementation of Observability Test by algebraic and geometric observability methods are presented in the work of [47, 48]. For a sensor setup to be effective, the important prerequisite is that interested states and parameters of the system should be observable. If the system is observable, the capability to exactly evaluate the state vector variables of an observable system is influenced by system noise [49]. Still, when the system is unobservable, an exact evaluation of the variable in state vector is not possible although the

noise level is insignificant [50]. This is agreed by many researchers who developed response-based road and rail profile estimation methods [30, 51-54]. However, the prerequisite on the types and locations of sensors are not theoretically explained for various type of vehicle model.

1.2.3 Literature Survey on Kalman Filtering Technique

In structural dynamics, certain classic examples of stochasticity loading comprise spatial variability of road roughness and track geometry irregularities, which affect the dynamics of vehicles. Profile estimation is considered to be an essential input which affect vehicle dynamics and control systems design. Henceforth, widespread research is in progress to improve techniques and methods that are efficient for obtaining unknown dynamic input forces. The aim of this research is to establish a method to estimate profile by using state-space representation with observing acceleration and angular velocity measurements, whose accuracy is dependent on the sensor location and vehicle type. A number of research works have been carried out using vibration response of ordinary vehicles [57-62]. When only dynamic acceleration response is observed, the location of an accelerometer in the vehicle is critical. Similarly, when only angular velocity is measured, there are certain undetectable frequency ranges which exist due to the difference in vehicle wheel base length. Therefore, observing either acceleration or angular velocity is not enough to capture the exact dynamic response. Also in order to process acceleration and angular velocity measurements, transfer function method is not sufficient to describe the model since it is designed for single-input and single-output model. Instead, the state-space representation is essential to achieve multi-input model. The following paragraphs discuss about a detailed background study on existing Kalman filtering approach [63, 64], which supports recursive techniques that are well known in system identification theory.

When the direct measurements of unknown forces on the structural dynamic systems are not feasible, it is essential to determine the excitation sources through inverse analysis. Thus, force identification method was utilized to obtain unknown input forces from the responses collected on the structure through system identification technique [65]. For the past three decades, input dynamic force reconstruction techniques were established using transfer function in frequency domain. Subsequently several other time domain methods were also established, which predominantly ensuing a deterministic approach [66, 67]. Instead, an approach based on sensitivity of system's output is illustrated for identifying both the input excitation force and the physical parameters of a structure [68]. In early stages, [69], presented a notable work on force estimation from the response measured on the structural system by a data assimilation inverse algorithm through the application of Kalman filtering techniques. Later, improvement on combined deterministic-stochastic methods which is derived from

13

control engineering where the noise is modelled as stochastic processes and considered to be exist in both state variable and measurements [70, 71].

In civil and mechanical engineering, structural modeling particularly considered in system identification approach, benefits both from displacement and acceleration responses. It is obtained through non-contact techniques/GPS based measurements and accelerometer sensors respectively. Hence it is recommended to study on the measured sensors information and fusion of collocated displacement and acceleration data such that, it result in precise motion data. However, the low-frequency noise amplification occurs during the integration of acceleration response and the high-frequency noise amplification take place during the differentiation of displacement response. Likewise, in contrast to displacement sensors which are inaccurate for higher frequencies and utilize low sampling rates, accelerometer sensors are further precise for higher sampling rates and higher frequencies. Thus the issue related to data sampled at dissimilar rates, can be dealt using multi-rate Kalman filtering technique along with new smoothing technique [72]. In this regard, further research was carried out for data fusion of acceleration and intermittent displacement response measurements in dynamic system for estimating autonomous dynamic displacement measurement [73]. In recent times, Kalman filter was utilized to obtain a precise estimate of the external dynamic loads from unmeasured responses of the structural system, using the state-space configuration where the state vector is derived by pseudo-inverse method [74]. On the other hand, the fusion of heterogeneous non-collocated data of measured acceleration and displacement responses using Kalman filtering data assimilation inverse analysis technique is being widely studied for linear and non-linear structural system identification problem predominantly with joint state-parameter estimation procedures [75, 76].Herein, an Augmented State Kalman filter (ASKF) estimation method is recommended for dynamic force reconstruction, where joint input-state estimation can be attained by adding the unknown external dynamic forces variables in the state-vector and it can be determined using a standard Kalman filter [77].

Following this research, a numerical study was presented for understanding the stability of ASKF when utilized for estimating joint input-state parameters and concluded that using acceleration measurement only can result in unpredictable outcomes. In an attempt to solve this difficulty, dummy displacement measurements are augmented to the observation state vector [78]. Later a notable research has recommended solving the problems associated with displacement estimates affected due to spurious low frequency components, by augmenting artificial white noise displacement measurements into the state vector for solving joint state-parameter estimation problems [79]. It is worth to mention that a dual execution of the Kalman filtering technique was implemented for obtaining the unknown dynamic inputs and other states of a linear state-space configuration model by means of sparse noisy acceleration data measured on the dynamic structural system [80]. Also the same researchers discussed about the experimental justification of the dual Kalman filters for real-time state input estimation of

14

systems through sparse acceleration measurements [81]. In more recent years, research on a two-stage Kalman filter technique, which estimates dynamic displacement with high accuracy by augmenting high-sampling rate acceleration measurements with low-sampling rate displacement data was presented [82]. Also some researchers proposed method for an improved Kalman filter-unknown input estimation algorithm using data fusion of partial acceleration and displacement measurements [69, 83].

With this comprehensive background research, this chapter discusses the problem of reconstructing the dynamic states of a vibrating system, using limited output-only (response) vibration measurements. According to the research carried out by [52], linear ASKF technique has been used for effective road profile estimation purpose using quarter car (2-DOF) state-space configuration model and also compared with experimental results gathered from laboratory test vehicle. Also in [84], road profile estimation was carried out using Kalman filtering theory for responses obtained from vehicles and confirmed using true profile data got from profiler. Later by following the previous work, [51] concentrated on profile estimation of off-road terrain which is noticeably uneven than usual surfaced road. It discusses about estimating the off-road terrain profile using a full car model (7-DOF) by ASKF approach and was also compared with experimental study using all-terrain Prowler ATV vehicle.

In railway infrastructure maintenance, track irregularity measurements are necessary to check for safe and comfortable transportation. Following this, ASKF technique for inverse analysis, has been utilized for estimating track geometry irregularities (input signal) from car-body acceleration measurements (output signal) through reduced model of 4-DOF train model (simplified vehicle model) [30] (Figures 1.9 and 1.10). This technique is normally employed for the force reconstruction of unknown input (track profile geometry) from a known output of measurement data (car-body responses). It is found that the estimated outcomes are in decent agreement with the track irregularity in vertical direction. But the drawback of this proposed method is that, the state space model considered in this research is a simplified train model (4 DOF), which do not consider the bogie pitching motion. Also the measurement vector considered for inverse analysis consist of only car body acceleration and body pitch rate response data, which incidentally makes the system unobservable. Henceforth, the unknown input (track profile) reconstructed using cannot be considered for the further evaluation. In future, there is a scope for improving the present technique to make the system considered in the state-space representation to be observable and also utilize the correct vehicle model which included bogie pitching motion to replicate the real train vehicle. This system is still in a developing stage. The research carried out by [110, 111] also explained about the estimation of track profile from car-body responses only and the results are compared using statistical metrics.
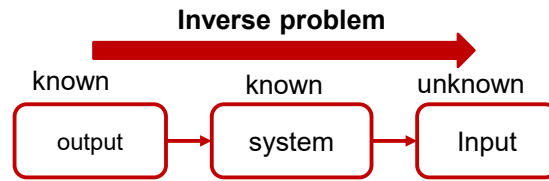
Figure 1.9 Inverse analysis for input identification
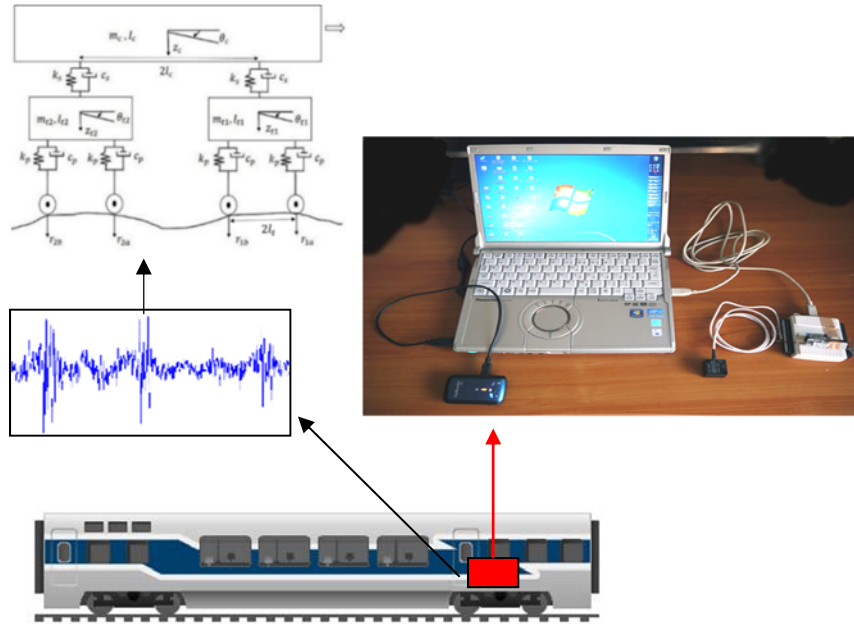
Figure 1.10 Online Monitoring Sensor System for detecting local railway-track profile

1.2.4 Literature Survey on Multi-Body Simulation

The Multi-Body Simulation (MBS) of train vehicles models is carried out to most likely to obtain the real time replica of the in-service train vehicle measurements. Since the field experiments generally involve lot of unpredicted incidences, it is advisable to carry out multi-body system dynamics [132, 133]. Many research on dynamic response analyses of train – track interaction using simulation for local as well as high speed railway networks are studied [91] [134-138]. Commonly, finite element analysis (FEA) models are not well suitable for dealing with complex dynamic systems like coupled train-track interaction. FEA involves more number of degrees-of freedom (DOFs) and hence the simulation becomes computationally expensive and time consuming. In order to overcome this drawback, the MBS method can be utilized [129].

MBS are utilized as a vital tool for the new vehicle design and also for examining service complications with prevailing train vehicles [139-141]. The significant aim of this MBS is to construct all train vehicle parts and assemble along with track as rigid bodies and with the help of force and kinematic constraint elements to link each other together. The MBS tool utilized in this research study is SIMPACK: Rail, which aids in carrying out the simulation at short duration with high accuracy results for vehicle systems and dynamics [142, 143]. In recent research work carried by [144], illustrated the differences between simple and complex models in the MBS of long train dynamics. Thus, MBS has been proved to be an effective way to model and analyze rail dynamic tests. In [145], the estimation of vertical and lateral track irregularities based on the displacement signals obtained through double integration of acceleration measurements obtained from the car body and bogie mass using the MBS – SIMPACK software are discussed and results are analyzed in time-frequency domain. This system is still in a developing stage.

1.3 Motivation for Research

The Japanese railways have increased several trains for the service purpose in recent decades and the number is still accumulating. Such a trend of increase in service frequency continues to spread in the near future. Since much high speed railway systems are being currently in service, the commercial railway infrastructures are not maintained properly. Currently, Track Recording Vehicle (TRV) like Doctor Yellow – high speed test train is utilized for the track condition monitoring. But the demerits of TRV are, it is expensive and cannot be frequently used for local railway lines. It is used only once in a year. Henceforth it is clear that the necessity for condition assessment and maintenance for the local railway network is of primary importance. So, track profile evaluation through vehicle response measurements potentially provides efficient solutions. It has been done by many researchers in past decades. However, there are still many problems which require further studies. A brief review of previous researchers on the track geometry estimation have been presented in this chapter. Apart from this method, recently few researchers work on obtaining the track geometry profile by placing the senor on the wheel-axle box. This approach is commonly used in high speed railway network around the world for the daily maintenance purpose. But this method of mounting sensor on the axle box is difficult in the local railway infrastructure. Thus, there is a need to solve this sensor placement so as to obtain the track profile.

A simpler, more robust and cost effective system for in-service train vehicle is desirable. Thus, data assimilation method is necessary for estimating the unknown inputs. For inverse analysis technique generally augmented Kalman filter is being utilized. However, issue of un-observability need to be solved. Only few researchers have implemented inverse analysis

technique and succeeded in track profile estimation. In [30] it utilized Kalman filter inverse analysis technique for reconstructing input force (track profile) from the car body measurements for the Japanese Shinkansen railway system. The numerical study suggested averaged simplified train model for carrying out inverse analysis while the issue of un-observability is not solved yet. The experimental study does not clearly illustrate the sensor placement strategy and also reconstructed track profile is not clear for the track maintenance community. There are many drawbacks mentioned in that research and hence it need to be solved. The main challenge is to detect the vertical and lateral track profile and the existing rail track irregularities. Hence proper inverse analysis algorithm and sensor placement strategy need to be recommended for the precise track profile estimation for the commercial railway networks. The proposed estimation algorithm need to be validated for many cases using multi-body dynamics train simulation.

1.4   Research Objective

The objective of this present research work is to propose a precise and efficient response based track profile estimation methods by measuring multiple responses from sensors mounted on in-service train vehicles which are simulated by rigid body motion linear vehicle models. The objective of the research is in four-folds:

1. To propose extended Augmented State Kalman Filter (ASKF) technique to solve the Observability Rank Condition (ORC) analysis for the state space model. It is conducted for determining the optimal observations.
2. To estimate both vertical and lateral railway-track profile using extension of ASKF data assimilation technique for a rigid body motion train model.
3. To gain an in-depth understanding, multi-body simulations are performed to replicate the true system with various conditions and track irregularities and validate the proposed estimation algorithm and optimal sensor placement.
4. To validate proposed inverse analysis on experimental field measurements obtained from in-service local railway lines.

The proposed methodology is tabulated in Table 1.1 which explains clearly that the low cost prevalent sensors like smartphones or any wireless sensors network can be mounted just above the front wheelset of the front bogie on the train car body floor and the bogie mass for obtaining the dynamic response from the in-service commercial train railway vehicle. Later, the proposed extended ASKF technique is used for estimating the railway track profile. Therefore, this study recommends a track condition monitoring practice by an in-service train vehicle for safety of railway infrastructure.

Table 1.1 Proposed Methodology

Mechanism	Method	Sensor type	Inverse Analysis	Sensor Location	Target
Indirect (Response based)	Sensors on in-service vehicle	Low cost Accelerometers Gyroscopes	Extension on ASKF Technique	Car body and Bogie mass	Vertical and Lateral Track Profile

1.5 Dissertation outline

The following is the outline of the chapters and a short description of each,

Chapter 1 - Introduction: A state-of-the-art-review of the research work on the track geometry estimation especially on the indirect mechanism- response based, including numerical analysis and measurement investigation, have been given in this chapter. The different types of track irregularities and rail degradations are explained. Thus the importance of the railway infrastructure is mentioned clearly by evaluating the existing track condition monitoring techniques. This chapter ends with the research motivation, objective and organization of this thesis.

Chapter 2 – Observability theory and proposed approaches: The observability rank condition (ORC) analysis to theoretically obtain the appropriate sensor types and their placements for estimating vertical and lateral rail track profile is presented in this chapter. The measurement matrix consists of only acceleration and angular velocity responses collected from the dynamic characteristics of vehicle body. In order to estimate the profile through inverse analysis, the second derivative of the profile is included in the state vector as one of the additional state variable, and thus the non-static component can be obtained through double integration of it. Different types of vehicle models are considered with appropriate sensor types and their locations, for the numerical analyses and the results are presented. The two approaches to obtain the second derivative of profile as an observable state variable are examined. Approach (a) includes the second derivative of the profile in the state vector. Although the system is unobservable the augmented state variable is observable. Approach (b) alters state space model by taking the first derivative of the system equation. The second derivative component is observable. These analyses indicate that the profile can be estimated by an accelerometer and a gyro mounted on car body and bogie. At last some discussions about the sensor placement strategy and track profile estimation are presented in this chapter.

Chapter 3 - Numerical study on extension of Augmented State Kalman Filter: The vertical and lateral track profile estimation from the in-service vehicle response measurement by

employing inverse analysis based on extended ASKF method is being studied in this chapter. Acceleration and angular velocities are assumed to be observed variables. The two approaches to obtain the second derivative of profile as an observable state variable are examined as explained in the previous chapter. The performances are compared numerically using linear half car train vehicle models namely simplified model (4 DOF) and 6 DOF model, accounting for both vertical and lateral track profile estimation and results are found to be in good agreement. In order to obtain the quantitative comparison of two waveforms, phase-shift correction is carried out using the misfit criteria through Hilbert transform. The statistical metrics are utilized for obtaining the single-valued misfit between two waveforms.

Chapter 4 – Multi-Body Simulation for Track Profile Estimation from Vehicle Responses: The multi-body dynamics modeling of train vehicle is presented to replicate the real field test. The multi-body simulation is carried out both on straight track and splined track sections and results are verified. The sensors are placed just above the rail tracks on both the sides and used to measure the acceleration and angular velocity responses from the car body and both bogie masses of running train model on simulated track excitations. These vehicle measurement responses are utilized to estimate the vertical and lateral track profile using 6 DOF train models and it is validated for the proposed estimation algorithm. The suggested sensor placement strategy is verified with all possible sensor location results. For straight track section (ideal case), it shows a good agreement for vertical track profile while it can estimate only above 8 m wavelength irregularity for lateral track profile. Also, MBS are carried out for understanding the influence of rolling motion of train vehicle. For curved track section, the results show good agreement for vertical track profile estimation, while it shows large variation for lateral profile estimation. Exactly the splined section of the track cannot be evaluated, because of wheel-rail interaction problem.

Chapter 5 - Railway Track Monitoring using In-Service Vehicle Responses: The rail track profile estimation from the in-service vehicle response measurement by employing inverse analysis based on extended augmented state Kalman filtering analyses is being studied in this chapter. Inverse analysis is carried out to estimate both the vertical and lateral track irregularity by reconstructing the track profile geometry for 10 m chord versine waveform. Thus, depending upon the sensors availability and feasible sensor placement locations in the real field measurement, rail track profile can be evaluated using proposed extended ASKF algorithm. The results are found with slight deviations due to simplified 4 DOF model and other phenomenon like hunting oscillation motion. This is due to practical limitations of sensor placement only on the car body. The optimal sensor placement is recommended to mount sensors on car body and bogie masses. Thus, by utilizing 6 DOF train model accounting for bogie pitching/yawing motion, rail track profile can be estimated more precisely.

Chapter 6 – Conclusions and future research scope are presented.

Chapter 2 OBSERVABILITY THEORY AND PROPOSED APPROACHES

2.1 Introduction

Towards maintaining the railway infrastructure effectively, the rail track geometry need to be examined regularly. Estimating profile geometry from the in-service vehicle response measurements possibly offers effective results. Still, the appropriate profile estimation for different vehicle dynamic models with efficient sensor placement strategy is not clarified. Therefore, from the perspective of observability concept, effective sensor installation locations need to be investigated. Observability is the method or a concept to explain whether the particular state of the dynamic system can be identified under a given subset of limited measurements. In order to estimate the profile, the Observability Rank Condition (ORC) analysis of various time invariant linear vehicle dynamic models are carried out to obtain the appropriate sensor placement strategy. Since the practice of displacement sensors are costly and also obtaining the absolute displacement is impractical, accelerometers and gyros are utilized for the measurements. Hence, the profile becomes unobservable under this measurement matrix. Consequently, to estimate the profile through inverse analysis, the second derivative of the profile is included in the state vector as one of the additional state variable, and thus the non-static component can be obtained through double integration of it. The ORC analysis is carried out based on two proposed approaches in order to study whether the second derivative of profile is observable. Henceforth, ORC analysis theoretically exposed a sensor placement strategy and its type, which can be utilized as the recommendation for effective profile estimation through in-service vehicle response measurements. In this chapter, 6 DOF vehicle model (train) and 7 DOF full car model are considered with appropriate effective sensor types, namely acceleration and gyro and their locations for profile estimation. Hence, its requirements are studied through the ORC analysis.

2.2 Observability

2.2.1 Observability Rank Condition of Linear System

For the continuous time-invariant system, the state space model is represented as,

$$\dot{x}(t) = Ax(t) + Bu(t) \qquad\qquad (2.1)$$

$$y(t) = Cx(t) + Du(t) \qquad\qquad (2.2)$$

where x is the state vector, y is the output vector, u is the input vector, A is the transition/state matrix, B is the input matrix, C is the output/measurement matrix, and D is the feedback matrix. A system is observable if, for any probable arrangement of state vectors, the present state can be obtained in finite time using only the outputs [45]. If a system is unobservable, some of its state variables cannot be estimated through output measurements. A continuous time-invariant linear state-space model with N states is observable if and only if, the rank of the observability matrix (O) is equal to N, where,

$$O = \begin{bmatrix} C \\ CA \\ CA^2 \\ \vdots \\ CA^{N-1} \end{bmatrix} \qquad\qquad (2.3)$$

2.2.2 Observability Rank Condition of Nonlinear System

Generally, the analytic system can cover vast range of systems demonstrating nonlinearities that are encountered in structural engineering field. An analytic system is considered that of affine-input nonlinear system, which is represented as [45, 55]:

$$\dot{x} = f(x) + \sum_{j=1}^{l} g_j(x)U_j \qquad\qquad (2.4)$$

$$y_i = h_i(x), i = 1, \ldots\ldots, n \qquad\qquad (2.5)$$

where x is the state vector of size m, U_j, $j=1,\ldots,l$ are inputs which are locally constant and also independent, h is the measurement matrix expressing a measured value of 'n' observation equations.

A basic tool used in this algorithm is the Lie derivative which evaluates the change of a tensor field, $L_v\big(s(x)\big)$ of scalar function $s(x)$ along the flow of a function of a space whose value at

each point is a vector quantity, $v(x) = [v_1 \ldots \ldots v_v]^T$ and Lie derivative of a vector, $\Omega = [s_1(x), \ldots, s_k(x)]$ beside the vector field $v\ (x)$ is given in equation (2.6) and (2.7) respectively.

$$L_v\big(s(x)\big) = \nabla s . v \qquad\qquad (2.6)$$

$$L_v(\Omega) = d\Omega . v \qquad\qquad (2.7)$$

The method can be explained in following steps:

1. Initial, $k=0$; $\Omega_0 = [h_1, h_2, \ldots, h_n]$, $\Delta\Omega_0 = \Omega_0$
2. $\Delta\Omega_{k+1} = [(L_f(\Delta\Omega_k))^T, \quad (L_{g1}(\Delta\Omega_k))^T \ldots, \quad (L_{gl}(\Delta\Omega_k))^T]^T$
3. $\Omega_{k+1} = \Omega_k \cup \Delta\Omega_{k+1}$
4. Compute $d\Omega_{k+1}$ then $d\Omega_{k+1} = d\Omega_k \cup d\Omega_{k+1}$
5. If rank $(d\Omega_{k+1})$ = rank $(d\Omega_k)$ or rank $(d\Omega_{k+1})$ = m or $k=m-2$ end; then $k=k+1$ and go to step 2.

Hence, the rank condition is contended only if the final rank of $d\Omega_{k+1}$ is equal to dimension of x (i.e. m) at the final stage of the analysis. For any classic structural engineering problem, the displacement measurements make the system observable rather than the acceleration or velocity measurements at the similar point. The inference through these mathematical expressions is that observability theory results do not get affected by the influence of noise either in the measurements or in the process equations.

2.2.3 Separating Observable Variables from an Unobservable System

When the system is unobservable, the measurement vector variables do not allow identifying all the states in the state vector. Hence it is necessary from the observability perspective to search for at least the smaller subset of the state vector which is being considered as observable state variable [55]. It is feasible to differentiate observable and unobservable state variable only by considering a system with equations as rational, which in turn can be defined by the rational fraction. The observability algorithm for nonlinear system can directly separate the states into these classifications by excluding the ith column of the final matrix $d\Omega_k$, and the occurring matrix's $d\Omega_k^i$ rank is calculated. If the rank of $d\Omega_k^i$ is reduced value than the rank of $d\Omega_k$, then the ith state is observable; otherwise it is not. Subsequently, it is viable to differentiate the states. Likewise, it can be adopted for linear system as well. Hence, the observable state variables alone can be separated from the unobservable system. It is desirable for the purpose of system identification to consider parameter θ as known candidates, which result in observable for reduced system.

For example, consider any parameter θ_i is known, and after ORC analysis is carried out for the reduced new system, Σ'_{θ_i}, then if the rank for Σ'_{θ_i} is equal to the original system rank, Σ then the considered known parameter is a good candidate. But the process includes iteration of whole ORC algorithm many times and therefore it is time consuming process. Hence, assumed parameter θ_i is the jth state of x, the jth column of the final matrix $d\Omega_\lambda$ of Σ can be excluded and the matrix $d\Omega_\lambda^j$ rank calculation can be done for the reduced system. Thus it can be explained in the following lines:

(a) The new reduced system have state x_r separated from state x, likewise, the vectors f and g_i can be separated as $f = [f_r^T, 0]$ and $g = [g_{i_r}^T, 0]$. Then, the ORC analysis is applied to estimate the rank of the reduced system.

(b) After applying step 2 and 3,

$\Omega_{k+1} = \Omega_k \cup [(L_{f_r}(\Delta\Omega_k))^T, \quad (L_{g1_r}(\Delta\Omega_k))^T \, \dots, \quad (L_{gl_r}(\Delta\Omega_k))^T]^T$ and hence step 4 would lead to $d\Omega_{k+1} = [\nabla_{x_r}\Omega_{(k+1)_1} \dots\dots \nabla_{x_r}\Omega_{(k+1)_l}]'$, where Ω_{k+1} has a size l.

(c) ORC is applied for obtaining the rank of the original system Σ and application of step 2 and 3 would lead to:

$$\Omega_{k+1} = \Omega_k \cup [(L_f(\Delta\Omega_k))^T, \quad (L_{g_1}(\Delta\Omega_k))^T \, \dots, \quad (L_{g_l}(\Delta\Omega_k))^T]^T$$

$$= \Omega_k \cup [(d_{x_r}(\Delta\Omega_k).f_r, \quad d_{x_r}(\Delta\Omega_k).g_{1_r})^T \, \dots, \quad (d_{x_r}(\Delta\Omega_k).g_{l_r})^T]^T + \{0\}$$
$$= \Omega_k \cup [(L_{f_r}(\Delta\Omega_k))^T, \quad (L_{g_{1_r}}(\Delta\Omega_k))^T \, \dots, \quad (L_{g_{l_r}}(\Delta\Omega_k))^T]^T$$

(d) Ω_{k+1} is denoted same for both Σ and Σ'_{θ_i}. Consequently, following step 4:

$$d\Omega_{k+1} = \begin{bmatrix} \nabla_{x_r}\Omega_{(k+1)_1} & \frac{\partial\Omega_{(k+1)_1}}{\partial\theta_i} \\ \vdots & \vdots \\ \nabla_{x_r}\Omega_{(k+1)_l} & \frac{\partial\Omega_{(k+1)_l}}{\partial\theta_i} \end{bmatrix}$$

(e) Hence, if the column corresponding to the partial derivatives with respect to θ_i is cut off from this matrix, the remaining part $d\Omega_{k+1}^j$ has the same structure as $d\Omega_{k+1}$ for Σ'_{θ_i}, including for the final matrix where $k + 1 = \lambda$.

2.3 Proposed Approaches for Profile Estimation

For estimating the rail track profile using train vehicle, the location of sensors and their types are important. Although sensors to obtain displacement and rotational angle are expected to

provide the profile component, they are not practical to use in the measurement field. Only acceleration and angular velocity are easily measurable in the field. Installation locations also have practical limitations. For high speed trains, axle-box accelerometers are used to obtain the profile directly [56]. However, for the normal commercial trains, axle-box accelerometers are not feasible to install. Because mounting sensor externally at bogie masses is practical difficulty and risk as well. Car body and bogies are preferred as sensor installation locations. Under these limitations, profile estimation is normally difficult as explained in this chapter. The second derivative of profile is first estimated through acceleration and angular velocity measurement and integrated twice with high pass filter to evaluate profile. Observability of the second derivative of the profile is studied herein.

For the continuous time-invariant system, the state space model is denoted as,

$$\dot{x}(t) = Ax(t) + Bu(t); y(t) = Hx(t) \qquad (2.8)$$

where x is the system state vector, u is the input vector, y is the measurement vector, A is the state matrix, B is the input matrix and H is the measurement matrix. In this study the state vector is augmented with the input vector. Hence, the state matrix is given by including the input matrix to the original state matrix and thus the state matrix size increases.

$$\tilde{x} = \begin{bmatrix} x \\ u \end{bmatrix} \qquad (2.9)$$

The measurement matrix is appended by a null matrix because inputs are assumed unmeasured.

$$\tilde{H} = [H \quad 0] \qquad (2.10)$$

The two approaches for the estimation of profile as a part of the state vector are considered.

2.3.1 Approach (a)

It is to augment the state variables with the second derivative of the profile and estimate the second derivative. The motivation for proposing this approach is from the practical sensor types. Since, acceleration measurements are carried out, it is being expected that second derivative state variable component can be observable. The profile is estimated directly from the state vector as its double integration; however, it has a large low frequency estimation error. A high-pass filter is needed to be applied for accurate results.

2.3.2 Approach (b)

The other is to alter state space model by adopting the first derivative of the state vector as new state vector. Thus, only the dynamic components are considered while the static components (i.e., displacement) are excluded from the state vector. The profile is estimated as the double integration of a state vector component. This process makes the second derivative of profile as an observable state even though the profile is not observable. The altered state space model is,

$$\ddot{\tilde{x}}(t) = A\dot{\tilde{x}}(t) ; \quad \dot{y}(t) = \widetilde{H}\dot{\tilde{x}}(t) \tag{2.11}$$

where $\tilde{x}$ is augmented state vector and only the measurement matrix H, is modified while the transition matrix A, is unaltered.

2.4 Analysis of Vehicle Models

In order to obtain theoretically the appropriate locations and types of sensors to estimate the profile as the 'observable state', the different linear rigid body vehicle models with varying degree-of-freedom (DOF) are considered for the analysis, namely:

- 6 DOF model: vertical and lateral track profile estimation

- Simplified 4 DOF averaged geometry vehicle model

- 7 DOF full car model: for vertical profile (real car)

Practical sensor types are accelerometers and gyros and their installation locations are car body and bogies. In these analyses the parameters of the vehicle models are considered known. The analyses are carried out using both the linear and non-linear observability check methods and are found to be consistent. The proposed approaches are investigated for all vehicle models. All possible combination of measurements at car body and bogies with accelerometers and gyros are analyzed in terms of ORC and all cases where the profile or its derivatives are observable are extracted for each vehicle model. Note that only minimum combination of measurements is listed in the following sections.

2.4.1 6 DOF train vehicle model considering vertical displacement

The 6 DOF vehicle model depicts the linear train vehicle model with car body and two bogies in vertical direction as shown in Figure 2.1. In this model, z_c and θ_c are the car body displacement and pitch angle, z_{t1} and z_{t2} are front and rear bogie displacement, θ_{t1} and θ_{t2} are front and rear bogie pitch angle. The inputs r_{1a}, r_{1b}, r_{2a}, r_{2b} denote the track displacement.
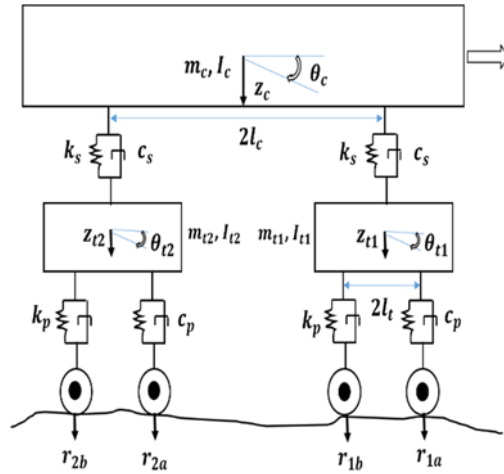
Figure 2.1 A free-body diagram of 6 DOF train vehicle model: vertical displacement

For deriving the dynamic equation of motion for 6 DOF model Lagrange function is utilized,

$$M\ddot{z} + C\dot{z} + Kz = Dr + E\dot{r} \qquad (2.12)$$

$$M = \begin{bmatrix} m_c & 0 & 0 & 0 & 0 & 0 \\ 0 & I_c & 0 & 0 & 0 & 0 \\ 0 & 0 & m_{t1} & 0 & 0 & 0 \\ 0 & 0 & 0 & I_{t1} & 0 & 0 \\ 0 & 0 & 0 & 0 & m_{t2} & 0 \\ 0 & 0 & 0 & 0 & 0 & I_{t2} \end{bmatrix} \qquad (2.13)$$

$$C = \begin{bmatrix} 2c_s & 0 & -c_s & 0 & -c_s & 0 \\ 0 & 2c_s l_c^2 & -c_s l_c & 0 & c_s l_c & 0 \\ -c_s & -c_s l_c & 2c_p + c_s & 0 & 0 & 0 \\ 0 & 0 & 0 & 2c_p l_t^2 & 0 & 0 \\ -c_s & c_s l_c & 0 & 0 & 2c_p + c_s & 0 \\ 0 & 0 & 0 & 0 & 0 & 2c_p l_t^2 \end{bmatrix} \quad (2.14)$$

$$K = \begin{bmatrix} 2k_s & 0 & -k_s & 0 & -k_s & 0 \\ 0 & 2k_s l_c^2 & -k_s l_c & 0 & k_s l_c & 0 \\ -k_s & -k_s l_c & 2k_p + k_s & 0 & 0 & 0 \\ 0 & 0 & 0 & 2k_p l_t^2 & 0 & 0 \\ -k_s & k_s l_c & 0 & 0 & 2k_p + k_s & 0 \\ 0 & 0 & 0 & 0 & 0 & 2k_p l_t^2 \end{bmatrix} \quad (2.15)$$

$$D = \begin{bmatrix} 0 & 0 & 0 & 0 \\ 0 & 0 & 0 & 0 \\ c_p & c_p & 0 & 0 \\ l_t c_p & -l_t c_p & 0 & 0 \\ 0 & 0 & c_p & c_p \\ 0 & 0 & l_t c_p & -l_t c_p \end{bmatrix} \quad E = \begin{bmatrix} 0 & 0 & 0 & 0 \\ 0 & 0 & 0 & 0 \\ k_p & k_p & 0 & 0 \\ l_t k_p & -l_t k_p & 0 & 0 \\ 0 & 0 & k_p & k_p \\ 0 & 0 & l_t k_p & -l_t k_p \end{bmatrix} \quad (2.16)$$

where m_c is the mass for the vehicle car body; I_c is the mass moment of inertia for the vehicle car body; m_{t1} and m_{t2} are the masses of the front/rear bogies respectively; I_{t1} and I_{t2} are the mass moment of inertia for the front/rear bogies respectively; c_p and c_s are the vertical damping coefficients of primary and secondary suspensions respectively; k_p and k_s are the vertical spring stiffness of primary and secondary suspensions respectively; $2l_c$ and $2l_t$ are car-body base and bogie-wheel base respectively (Figure 2.1).

Consider x (t) be a vector containing state variables and r (t) be a profile vector containing inputs from four wheels. Sensors are presumed to be placed at the center of car body and bogies respectively. The state vector is as follows,

$$x^a = [z_c \; \theta_c \; z_{t1} \; \theta_{t1} \; z_{t2} \; \theta_{t2} \; \dot{z}_c \; \dot{\theta}_c \; \dot{z}_{t1} \; \dot{\theta}_{t1} \; \dot{z}_{t2} \; \dot{\theta}_{t2} \; r_{1a} \; r_{1b} \; r_{2a} \; r_{2b} \; \dot{r}_{1a} \; \dot{r}_{1b} \; \dot{r}_{2a} \; \dot{r}_{2b}]^T \quad (2.17)$$

Then, the transition/state matrix of the system in the state-space representation takes the form:

$$A = \begin{bmatrix} 0_{6 \times 6} & I_{6 \times 6} & 0_{8 \times 8} \\ -M^{-1}K_{6 \times 6} & -M^{-1}C_{6 \times 6} & a^* \\ 0_{8 \times 8} & 0_{8 \times 8} & \begin{matrix} I_{4 \times 4} \\ 0_{4 \times 4} \end{matrix} \end{bmatrix} \quad (2.18)$$

$$
\text{where,} \quad a^* = \begin{bmatrix} \dfrac{k_p}{m_{t1}} & \dfrac{k_p}{m_{t1}} & 0 & 0 & \dfrac{c_p}{m_{t1}} & \dfrac{c_p}{m_{t1}} & 0 & 0 \\[2.5ex] \dfrac{l_t k_p}{I_{t1}} & \dfrac{-l_t k_p}{I_{t1}} & 0 & 0 & \dfrac{l_t c_p}{I_{t1}} & \dfrac{-l_t c_p}{I_{t1}} & 0 & 0 \\[2.5ex] 0 & 0 & \dfrac{k_p}{m_{t2}} & \dfrac{k_p}{m_{t2}} & 0 & 0 & \dfrac{c_p}{m_{t2}} & \dfrac{c_p}{m_{t2}} \\[2.5ex] 0 & 0 & \dfrac{l_t k_p}{I_{t2}} & \dfrac{-l_t k_p}{I_{t2}} & 0 & 0 & \dfrac{l_t c_p}{I_{t2}} & \dfrac{-l_t c_p}{I_{t2}} \end{bmatrix}.
$$

The results of ORC analysis of 6 DOF vehicle model is shown in Table 2.1. The proposed two approaches are executed with the following state vectors. In approach (a), the new state vector is,

$$\widetilde{x^a} = [z_c\ \theta_c\ z_{t1}\ \theta_{t1}\ z_{t2}\ \theta_{t2}\ \dot{z}_c\ \dot{\theta}_c\ \dot{z}_{t1}\ \dot{\theta}_{t1}\ \dot{z}_{t2}\ \dot{\theta}_{t2}\ r_{1a}\ r_{1b}\ r_{2a}\ r_{2b}\ \dot{r}_{1a}\ \dot{r}_{1b}\ \dot{r}_{2a}\dot{r}_{2b}\ \ddot{r}_{1a}\ \ddot{r}_{1b}\ \ddot{r}_{2a}\ \ddot{r}_{2b}]^T$$

$$(2.19)$$

In approach (b), the new state vector is,

$$\dot{x}^a = [\dot{z}_c\ \dot{\theta}_c\ \dot{z}_{t1}\ \dot{\theta}_{t1}\ \dot{z}_{t2}\ \dot{\theta}_{t2}\ \ddot{z}_c\ \ddot{\theta}_c\ \ddot{z}_{t1}\ \ddot{\theta}_{t1}\ \ddot{z}_{t2}\ \ddot{\theta}_{t2}\ \dot{r}_{1a}\ \dot{r}_{1b}\ \dot{r}_{2a}\ \dot{r}_{2b}\ \ddot{r}_{1a}\ \ddot{r}_{1b}\ \ddot{r}_{2a}\ \ddot{r}_{2b}]^T$$

$$(2.20)$$

Table 2.2 shows the observable states for the two approaches. The acceleration and angular velocity of car body and bogie mass are the minimum combination of measurements, which results in observable profile derivatives. By implementing both the approaches, the second derivative component of the profile is observable.

Table 2.1 ORC analysis results for 6 DOF train model (for vertical displacement)

Measurements	Observable states
$\ddot{z}_c\ \dot{\theta}_c\ \dot{\theta}_{t1}\ \dot{\theta}_{t2}$	$\dot{\theta}_c\ \dot{\theta}_{t1}\ \dot{\theta}_{t2}$
$\ddot{z}_{t1}\ \ddot{z}_{t2}\ \dot{\theta}_{t1}\ \dot{\theta}_{t2}$	$\dot{\theta}_{t1}\ \dot{\theta}_{t2}$
$\ddot{z}_c\ \dot{\theta}_c\ \ddot{z}_{t1}\ \ddot{z}_{t2}\ \dot{\theta}_{t1}\ \dot{\theta}_{t2}$	$\dot{\theta}_c\ \dot{\theta}_{t1}\ \dot{\theta}_{t2}$

Table 2.2 ORC analysis for 6 DOF model (for vertical displacement) using proposed approaches

Measurements	Observable states

	Approach (a)	Approach (b)
$\ddot{z}_c\ \dot{\theta}_c\ \dot{\theta}_{t1}\ \dot{\theta}_{t2}$	$\dot{\theta}_c\ \dot{\theta}_{t1}\ \dot{\theta}_{t2}\ \ddot{r}_{1a}\ \ddot{r}_{1b}\ \ddot{r}_{2a}\ \ddot{r}_{2b}$	$\dot{\theta}_c\ \dot{\theta}_{t1}\ \dot{\theta}_{t2}\ \ddot{z}_{t1}\ \ddot{\theta}_{t1}\ \ddot{z}_{t2}\ \ddot{\theta}_{t2}\ \ddot{r}_{1a}\ \ddot{r}_{1b}\ \ddot{r}_{2a}\ \ddot{r}_{2b}$
$\ddot{z}_{t1}\ \ddot{z}_{t2}\ \dot{\theta}_{t1}\ \dot{\theta}_{t2}$	$\dot{\theta}_{t1}\ \dot{\theta}_{t2}\ \ddot{r}_{1a}\ \ddot{r}_{1b}\ \ddot{r}_{2a}\ \ddot{r}_{2b}$	$\dot{\theta}_{t1}\ \dot{\theta}_{t2}\ \ddot{z}_{t1}\ \ddot{\theta}_{t1}\ \ddot{z}_{t2}\ \ddot{\theta}_{t2}\ \ddot{r}_{1a}\ \ddot{r}_{1b}\ \ddot{r}_{2a}\ \ddot{r}_{2b}$
$\ddot{z}_c\ \dot{\theta}_c\ \ddot{z}_{t1}\ \ddot{z}_{t2}\ \dot{\theta}_{t1}\ \dot{\theta}_{t2}$	$\dot{\theta}_c\ \dot{\theta}_{t1}\ \dot{\theta}_{t2}\ \ddot{r}_{1a}\ \ddot{r}_{1b}\ \ddot{r}_{2a}\ \ddot{r}_{2b}$	$\dot{\theta}_c\ \dot{\theta}_{t1}\ \dot{\theta}_{t2}\ \ddot{z}_{t1}\ \ddot{\theta}_{t1}\ \ddot{z}_{t2}\ \ddot{\theta}_{t2}\ \ddot{r}_{1a}\ \ddot{r}_{1b}\ \ddot{r}_{2a}\ \ddot{r}_{2b}$

2.4.2 4 DOF train vehicle model with averaged track geometry considering vertical displacement

The equation of motion for a 6 DOF vehicle model with averaged track geometry is derived as described in the previous section. As given in Equation 2.12, for a numerical model, an input vector contains track profile at four axles and their first derivatives (eight elements). Only D and E matrix gets modified while other matrices remain the same.
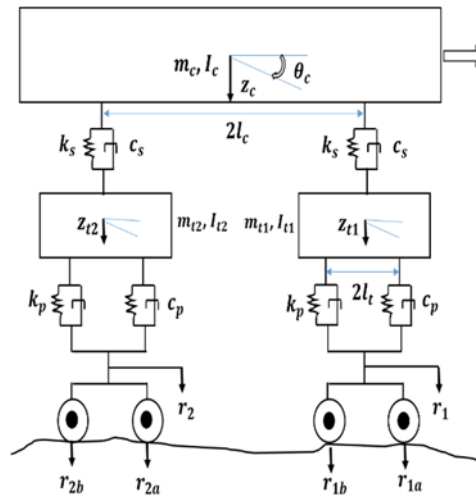
Figure 2.2 Simplified train model with averaged geometry: vertical displacement

For inverse analysis, a reduced vehicle model is presented in Figure 2.2. The equation of motion,

$$M\ddot{z} + C\dot{z} + Kz = Dr + E\dot{r} \qquad (2.21)$$

$$D = \begin{bmatrix} 0 & 0 \\ 0 & 0 \\ 2c_p & 0 \\ 0 & 0 \\ 0 & 2c_p \\ 0 & 0 \end{bmatrix} \qquad E = \begin{bmatrix} 0 & 0 \\ 0 & 0 \\ 2k_p & 0 \\ 0 & 0 \\ 0 & 2k_p \\ 0 & 0 \end{bmatrix} \qquad (2.22)$$

In order to improve the results, state vector need to be reduced. Thus an averaged geometry is obtained at vehicle body by transferring the averaged track profile input measured at front and rear axle, which is given as, $r_1 = \frac{r_{1a}+r_{1b}}{2}$; $r_2 = \frac{r_{2a}+r_{2b}}{2}$ do not comprise frequency components corresponding to the wavelength of bogie wheel base.

Thus, input vector, $$r^T(t) = [r_1, r_2] \qquad (2.23)$$

The state vector is as follows,

$$x^a = [z_c \ \theta_c \ z_{t1} \ \theta_{t1} \ z_{t2} \ \theta_{t2} \ \dot{z}_c \ \dot{\theta}_c \ \dot{z}_{t1} \ \dot{\theta}_{t1} \ \dot{z}_{t2} \ \dot{\theta}_{t2} \ r_1 \ r_2 \ \dot{r}_1 \ \dot{r}_2]^T \qquad (2.24)$$

However, the pitching motion of the bogie is not considered in this averaged 6 DOF model, thus it is a simplified model same as the half car model.

Hence the state vector reduces to,

$$x^a = [z_c \ \theta_c \ z_{t1} \ z_{t2} \ \dot{z}_c \ \dot{\theta}_c \ \dot{z}_{t1} \ \dot{z}_{t2} \ r_1 \ r_2 \ \dot{r}_1 \ \dot{r}_2]^T \qquad (2.25)$$

Then, the transition/state matrix of the system in the state-space representation takes the form:

$$A_a = \begin{bmatrix} 0_{4x4} & I_{4x4} & 0_{6x6} \\ -M^{-1}K_{4x4} & -M^{-1}C_{4x4} & a^* \\ 0_{4x4} & 0_{4x6} & \begin{matrix} I_{2x2} \\ 0_{2x2} \end{matrix} \end{bmatrix} \qquad (2.26)$$

where, $a^* = \begin{bmatrix} \frac{k_p}{m_{t1}} & 0 & 0 & 0 \\ 0 & 0 & \frac{k_p}{m_{t2}} & 0 \end{bmatrix}$.

The results of ORC analysis of Simplified 4 DOF train vehicle model is shown in Table 2.3. The proposed two approaches are executed with the following state vectors.

Table 2.3 ORC analysis results for 4 DOF train model (for vertical displacement)

Measurements	Observable states
$\ddot{z}_c\ \dot{\theta}_c$	$\dot{\theta}_c$
$\ddot{z}_{t1}\ \ddot{z}_{t2}$	Nil
$\ddot{z}_c\ \dot{\theta}_c\ \ddot{z}_{t1}\ \ddot{z}_{t2}$	$\dot{\theta}_c$

In approach (a), the new state vector is,

$$\widetilde{x^a} = [z_c\ \theta_c\ z_{t1}\ z_{t2}\ \dot{z}_c\ \dot{\theta}_c\ \dot{z}_{t1}\ \dot{z}_{t2}\ r_1\ r_2\ \dot{r}_1\ \dot{r}_2\ \ddot{r}_1\ \ddot{r}_2]^T \qquad (2.27)$$

In approach (b), the new state vector is,

$$\dot{x}^a = [\dot{z}_c\ \dot{\theta}_c\ \dot{z}_{t1}\ \dot{z}_{t2}\ \ddot{z}_c\ \ddot{\theta}_c\ \ddot{z}_{t1}\ \ddot{z}_{t2}\ \dot{r}_1\ \dot{r}_2\ \ddot{r}_1\ \ddot{r}_2]^T \qquad (2.28)$$

Table 2.4 shows the observable states for the two approaches. The acceleration and angular velocity of car body and un-sprung mass are the minimum combination of measurements, which results in observable profile derivatives. By implementing both the approaches, the second derivative component of the profile is observable.

Table 2.4 ORC analysis for 4 DOF train model (for vertical displacement) using proposed approaches

Measurements	Observable states	
	Approach (a)	**Approach (b)**
$\ddot{z}_c\ \dot{\theta}_c$	$\dot{\theta}_c\ \ddot{r}_1\ \ddot{r}_2$	$\dot{\theta}_c\ \ddot{z}_c\ \ddot{\theta}_c\ \ddot{z}_{t1}\ \ddot{z}_{t2}\ \ddot{r}_1\ \ddot{r}_2$
$\ddot{z}_{t1}\ \ddot{z}_{t2}$	$\ddot{r}_1\ \ddot{r}_2$	$\ddot{z}_c\ \ddot{\theta}_c\ \ddot{z}_{t1}\ \ddot{z}_{t2}\ \ddot{r}_1\ \ddot{r}_2$
$\ddot{z}_c\ \dot{\theta}_c\ \ddot{z}_{t1}\ \ddot{z}_{t2}$	$\dot{\theta}_c\ \ddot{r}_1\ \ddot{r}_2$	$\dot{\theta}_c\ \ddot{z}_c\ \ddot{\theta}_c\ \ddot{z}_{t1}\ \ddot{z}_{t2}\ \ddot{r}_1\ \ddot{r}_2$

2.4.3 6 DOF train vehicle model considering lateral displacement

The 6 DOF vehicle model depicts the linear train vehicle model with car body and two bogies in lateral direction as shown in Figure 2.3. In this model, y_c and φ_c are the car body lateral displacement and yaw angle, y_{b1} and y_{b2} are front and rear bogie lateral displacement, φ_{b1}

and φ_{b2} are front and rear bogie yaw angle. The inputs s_{1a}, s_{1b}, s_{2a}, s_{2b} denote the lateral track displacement.
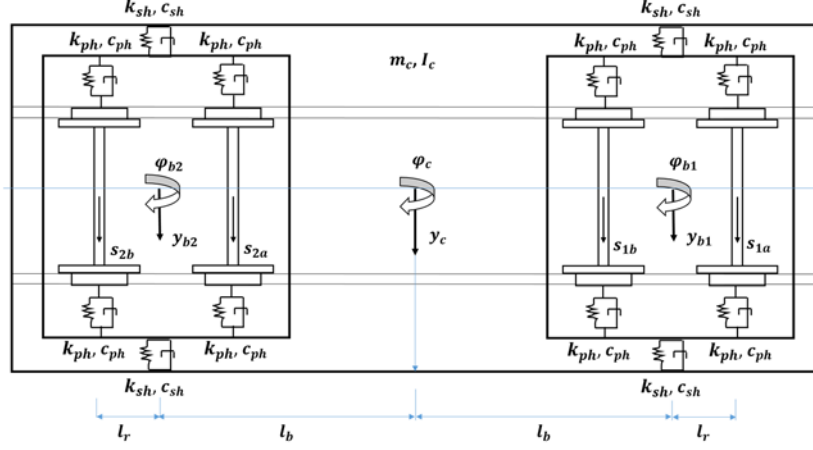
Figure 2.3 A free-body diagram of 6 DOF train vehicle model: lateral displacement

For deriving the dynamic equation of motion for 6 DOF model Lagrange function is utilized,

$$M\ddot{y} + C\dot{y} + Ky = Ds + E\dot{s} \tag{2.29}$$

$$
M = \begin{bmatrix}
m_c & 0 & 0 & 0 & 0 & 0 \\
0 & I_c & 0 & 0 & 0 & 0 \\
0 & 0 & m_{b1} & 0 & 0 & 0 \\
0 & 0 & 0 & I_{b1} & 0 & 0 \\
0 & 0 & 0 & 0 & m_{b2} & 0 \\
0 & 0 & 0 & 0 & 0 & I_{b2}
\end{bmatrix} \tag{2.30}
$$

$$
C = \begin{bmatrix}
2c_{sh} & 0 & -c_{sh} & 0 & -c_{sh} & 0 \\
0 & 2c_{sh}l_b^2 & -c_s l_b & 0 & c_{sh}l_b & 0 \\
-c_{sh} & -c_{sh}l_b & 2c_{ph}+c_{sh} & 0 & 0 & 0 \\
0 & 0 & 0 & 2c_{ph}l_r^2 & 0 & 0 \\
-c_{sh} & c_{sh}l_b & 0 & 0 & 2c_{ph}+c_{sh} & 0 \\
0 & 0 & 0 & 0 & 0 & 2c_{ph}l_r^2
\end{bmatrix} \tag{2.31}
$$

$$K = \begin{bmatrix} 2k_{sh} & 0 & -k_{sh} & 0 & -k_{sh} & 0 \\ 0 & 2k_{sh}l_b^2 & -k_{sh}l_b & 0 & k_{sh}l_b & 0 \\ -k_{sh} & -k_{sh}l_b & 2k_{ph}+k_{sh} & 0 & 0 & 0 \\ 0 & 0 & 0 & 2k_{ph}l_r^2 & 0 & 0 \\ -k_{sh} & k_{sh}l_b & 0 & 0 & 2k_{ph}+k_{sh} & 0 \\ 0 & 0 & 0 & 0 & 0 & 2k_{ph}l_r^2 \end{bmatrix} \quad (2.32)$$

$$D = \begin{bmatrix} 0 & 0 & 0 & 0 \\ 0 & 0 & 0 & 0 \\ c_{ph} & c_{ph} & 0 & 0 \\ l_r c_{ph} & -l_r c_{ph} & 0 & 0 \\ 0 & 0 & c_{ph} & c_{ph} \\ 0 & 0 & l_r c_{ph} & -l_r c_{ph} \end{bmatrix} \quad E = \begin{bmatrix} 0 & 0 & 0 & 0 \\ 0 & 0 & 0 & 0 \\ k_{ph} & k_{ph} & 0 & 0 \\ l_r k_{ph} & -l_r k_{ph} & 0 & 0 \\ 0 & 0 & k_{ph} & k_{ph} \\ 0 & 0 & l_r k_{ph} & -l_r k_{ph} \end{bmatrix} \quad (2.33)$$

where m_c is the mass for the vehicle car body; I_c is the mass moment of inertia for the vehicle car body; m_{b1} and m_{b2} are the masses of the front/rear bogies respectively; I_{b1} and I_{b2} are the mass moment of inertia for the front/rear bogies respectively; c_{ph} and c_{sh} are the horizontal damping coefficients of primary and secondary suspensions respectively; k_{ph} and k_{sh} are the horizontal spring stiffness of primary and secondary suspensions respectively; $2l_b$ and $2l_r$ are car-body base and bogie-wheel base respectively (Figure 2.5). Consider $x(t)$ be a vector containing state variables and $s(t)$ be a profile vector containing inputs from four wheels. Sensors are presumed to be placed at the center of car body and bogies respectively. The state vector is as follows,

$$x^a = [y_c\ \varphi_c\ y_{b1}\ \varphi_{b1}\ y_{b2}\ \varphi_{b2}\ \dot{y}_c\ \dot{\varphi}_c\ \dot{y}_{b1}\ \dot{\varphi}_{b1}\ \dot{y}_{b2}\ \dot{\varphi}_{b2}\ s_{1a}\ s_{1b}\ s_{2a}\ s_{2b}\ \dot{s}_{1a}\ \dot{s}_{1b}\dot{s}_{2a}\dot{s}_{2b}]^T$$

$$(2.34)$$

Then, the transition/state matrix of the system in the state-space representation takes the form:

$$A = \begin{bmatrix} 0_{6x6} & I_{6x6} & 0_{8x8} \\ -M^{-1}K_{6x6} & -M^{-1}C_{6x6} & a^* \\ 0_{8x8} & 0_{8x8} & \begin{matrix} I_{4x4} \\ 0_{4x4} \end{matrix} \end{bmatrix} \quad (2.35)$$

34

where,

$$a^* = \begin{bmatrix} \dfrac{k_{ph}}{m_{b1}} & \dfrac{k_{ph}}{m_{b1}} & 0 & 0 & \dfrac{c_{ph}}{m_{b1}} & \dfrac{c_{ph}}{m_{b1}} & 0 & 0 \\[3mm] \dfrac{l_r k_{ph}}{I_{b1}} & \dfrac{-l_r k_{ph}}{I_{b1}} & 0 & 0 & \dfrac{l_r c_{ph}}{I_{b1}} & \dfrac{-l_r c_{ph}}{I_{b1}} & 0 & 0 \\[3mm] 0 & 0 & \dfrac{k_{ph}}{m_{b2}} & \dfrac{k_{ph}}{m_{b2}} & 0 & 0 & \dfrac{c_{ph}}{m_{b2}} & \dfrac{c_{ph}}{m_{b2}} \\[3mm] 0 & 0 & \dfrac{l_r k_{ph}}{I_{b2}} & \dfrac{-l_r k_{ph}}{I_{b2}} & 0 & 0 & \dfrac{l_r c_{ph}}{I_{b2}} & \dfrac{-l_r c_{ph}}{I_{b2}} \end{bmatrix}.$$

The results of ORC analysis of 6 DOF vehicle model is shown in Table 2.5.

Table 2.5 ORC analysis results for 6 DOF train model (for lateral displacement)

Measurements	Observable states
$\ddot{y}_c \ \dot{\varphi}_c \ \dot{\varphi}_{b1} \ \dot{\varphi}_{b2}$	$\dot{\varphi}_c \ \dot{\varphi}_{b1} \ \dot{\varphi}_{b2}$
$\ddot{y}_{b1} \ \ddot{y}_{b2} \ \dot{\varphi}_{b1} \ \dot{\varphi}_{b2}$	$\dot{\varphi}_{b1} \ \dot{\varphi}_{b2}$
$\ddot{y}_c \ \dot{\varphi}_c \ \ddot{y}_{b1} \ \ddot{y}_{b2} \ \dot{\varphi}_{b1} \ \dot{\varphi}_{b2}$	$\dot{\varphi}_c \ \dot{\varphi}_{b1} \ \dot{\varphi}_{b2}$

The proposed two approaches are executed with the following state vectors. In approach (a), the new state vector is,

$$\widetilde{x^a} = [y_c \ \varphi_c \ y_{b1} \ \varphi_{b1} \ y_{b2} \ \varphi_{b2} \ \dot{y}_c \ \dot{\varphi}_c \ \dot{y}_{b1} \ \dot{\varphi}_{b1} \ \dot{y}_{b2} \ \dot{\varphi}_{b2} \ s_{1a} \ s_{1b} \ s_{2a} \ s_{2b} \dots..$$

$$\dots \dot{s}_{1a} \ \dot{s}_{1b} \ \dot{s}_{2a} \ \dot{s}_{2b} \ \ddot{s}_{1a} \ \ddot{s}_{1b} \ \ddot{s}_{2a} \ \ddot{s}_{2b}]^T \tag{2.36}$$

In approach (b), the new state vector is,

$$\dot{x}^a = [\dot{y}_c \ \dot{\varphi}_c \ \dot{y}_{b1} \ \dot{\varphi}_{b1} \ \dot{y}_{b2} \ \dot{\varphi}_{b2} \ \ddot{y}_c \ \ddot{\varphi}_c \ \ddot{y}_{b1} \ \ddot{\varphi}_{b1} \ \ddot{y}_{b2} \ \ddot{\varphi}_{b2} \ \dot{s}_{1a} \ \dot{s}_{1b} \ \dot{s}_{2a} \ \dot{s}_{2b} \ \ddot{s}_{1a} \ \ddot{s}_{1b} \ \ddot{s}_{2a} \ \ddot{s}_{2b}]^T$$

$$\tag{2.37}$$

Table 2.6 shows the observable states for the two approaches. The acceleration and angular velocity of car body and bogie mass are the minimum combination of measurements, which results in observable profile derivatives. By implementing both the approaches, the second derivative component of the profile is observable.

Table 2.6 ORC analysis for 6 DOF model (for lateral displacement) using proposed approaches

Measurements	Observable states

	Approach (a)	**Approach (b)**
$\ddot{y}_c\ \dot{\varphi}_c\ \dot{\varphi}_{b1}\ \dot{\varphi}_{b2}$	$\dot{\varphi}_c\ \dot{\varphi}_{b1}\ \dot{\varphi}_{b2}\ \ddot{s}_{1a}\ \ddot{s}_{1b}\ \ddot{s}_{2a}\ \ddot{s}_{2b}$	$\dot{\varphi}_c\ \dot{\varphi}_{b1}\ \dot{\varphi}_{b2}\ \ddot{y}_c\ \ddot{\varphi}_c\ \ddot{y}_{b1}\ \ddot{\varphi}_{b1}\ \ddot{y}_{b2}\ \ddot{\varphi}_{b2}$ $\ddot{s}_{1a}\ \ddot{s}_{1b}\ \ddot{s}_{2a}\ \ddot{s}_{2b}$
$\ddot{y}_{b1}\ \ddot{y}_{b2}\ \dot{\varphi}_{b1}\ \dot{\varphi}_{b2}$	$\dot{\varphi}_{b1}\ \dot{\varphi}_{b2}\ \ddot{s}_{1a}\ \ddot{s}_{1b}\ \ddot{s}_{2a}\ \ddot{s}_{2b}$	$\dot{\varphi}_{b1}\ \dot{\varphi}_{b2}\ \ddot{y}_c\ \ddot{\varphi}_c\ \ddot{y}_{b1}\ \ddot{\varphi}_{b1}\ \ddot{y}_{b2}\ \ddot{\varphi}_{b2}$ $\ddot{s}_{1a}\ \ddot{s}_{1b}\ \ddot{s}_{2a}\ \ddot{s}_{2b}$
$\ddot{y}_c\ \dot{\varphi}_c\ \ddot{y}_{b1}\ \ddot{y}_{b2}\ \dot{\varphi}_{b1}\ \dot{\varphi}_{b2}$	$\dot{\varphi}_c\ \dot{\varphi}_{b1}\ \dot{\varphi}_{b2}\ \ddot{s}_{1a}\ \ddot{s}_{1b}\ \ddot{s}_{2a}\ \ddot{s}_{2b}$	$\dot{\varphi}_c\ \dot{\varphi}_{b1}\ \dot{\varphi}_{b2}\ \ddot{y}_c\ \ddot{\varphi}_c\ \ddot{y}_{b1}\ \ddot{\varphi}_{b1}\ \ddot{y}_{b2}\ \ddot{\varphi}_{b2}$ $\ddot{s}_{1a}\ \ddot{s}_{1b}\ \ddot{s}_{2a}\ \ddot{s}_{2b}$

2.4.4 4 DOF train vehicle model with averaged track geometry considering lateral displacement

The equation of motion for a 6 DOF vehicle model with averaged track geometry is derived as described in the previous section. As given in Equation 2.29, for a numerical model, an input vector contains track profile at four axles and their first derivatives (eight elements). Only D and E matrix gets modified while other matrices remain the same. For inverse analysis, a reduced vehicle model is presented in Figure 2.4. The equation of motion,

$$M\ddot{y} + C\dot{y} + Ky = Ds + E\dot{s} \tag{2.38}$$

$$D = \begin{bmatrix} 0 & 0 \\ 0 & 0 \\ 2c_{ph} & 0 \\ 0 & 0 \\ 0 & 2c_{ph} \\ 0 & 0 \end{bmatrix} \qquad E = \begin{bmatrix} 0 & 0 \\ 0 & 0 \\ 2k_{ph} & 0 \\ 0 & 0 \\ 0 & 2k_{ph} \\ 0 & 0 \end{bmatrix} \tag{2.39}$$
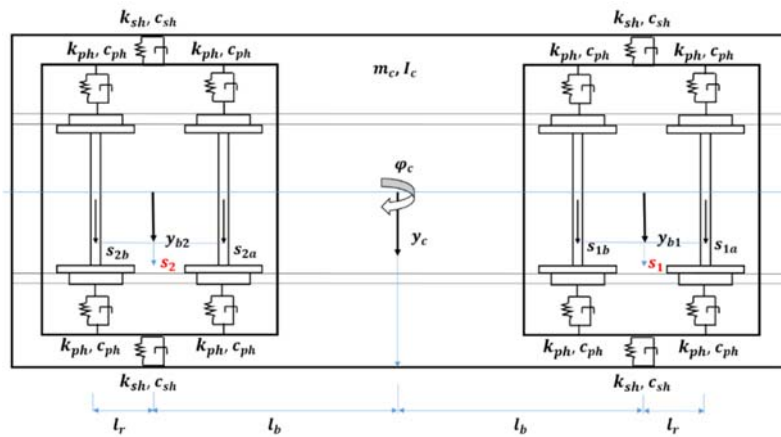
Figure 2.4 Simplified train model with averaged geometry: lateral displacement

In order to improve the results, state vector need to be reduced. Thus an averaged geometry is obtained at vehicle body by transferring the averaged track profile input measured at front and rear axle, which is given as, $s_1 = \frac{s_{1a}+s_{1b}}{2}$; $s_2 = \frac{s_{2a}+s_{2b}}{2}$ do not comprise frequency components corresponding to the wavelength of bogie wheel base.

Thus, input vector, $$s^T(t) = [s_1, s_2] \tag{2.40}$$

The state vector is as follows,

$$x^a = [y_c \; \varphi_c \; y_{b1} \; \varphi_{b1} \; y_{b2} \; \varphi_{b2} \; \dot{y}_c \; \dot{\varphi}_c \; \dot{y}_{b1} \; \dot{\varphi}_{b1} \; \dot{y}_{b2} \; \dot{\varphi}_{b2} \; s_1 \; s_2 \; \dot{s}_1 \; \dot{s}_2]^T \tag{2.41}$$

However, the yawing motion of the bogie is not considered in this averaged 6 DOF model, thus it is a simplified model same as the half car model with 4 DOF. Hence the state vector reduces to,

$$x^a = [y_c \; \varphi_c \; y_{b1} \; y_{b2} \; \dot{y}_c \; \dot{\varphi}_c \; \dot{y}_{b1} \; \dot{y}_{b2} \; s_1 \; s_2 \; \dot{s}_1 \; \dot{s}_2]^T \tag{2.42}$$

The results and inferences are same as explained for 4 DOF simplified train car model for vertical displacement (2.4.3).

2.4.5 7 DOF - full car model

A 7-DOF full car model, as presented in Figure 2.5, comprises heave (z), roll (φ_r) and pitch (θ_p) of the sprung mass in addition to four un-sprung masses which demonstrate translation at respective corner of the vehicle (w_{ij}), where the subscripts i and j correspond to the side of the vehicle and axle respectively. The stiffness of spring, stiffness of tire and coefficient of damping are considered to be linear and in addition it is also presumed that the pitch and roll angles remain small. The four inputs (u_{ij}) to the system are the profile obtained from displacement at all vehicle corners. Even though model dynamics is free from derivatives of input, they are augmented in the input vector to support in the input estimation.
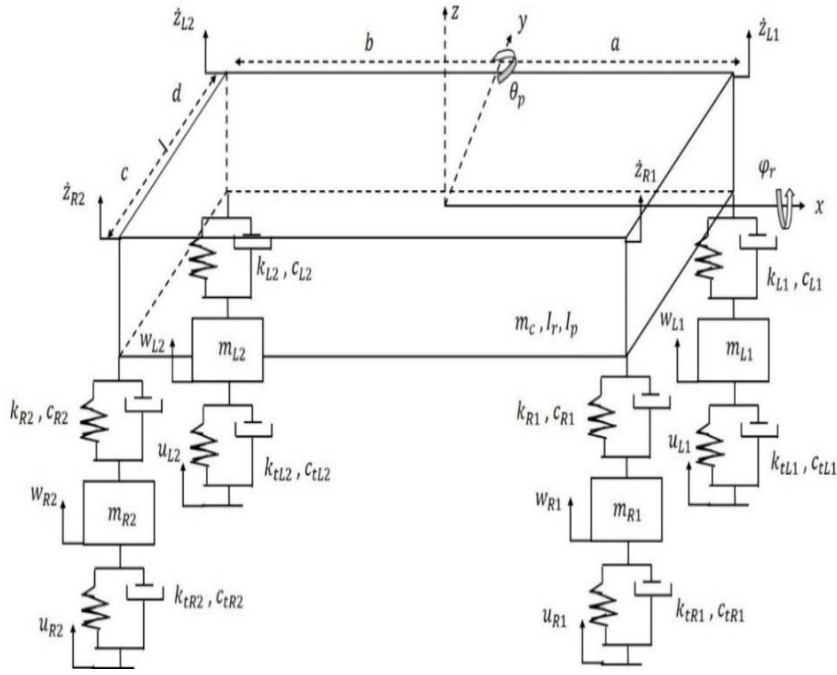
Figure 2.5 The free body diagram of 7-DOF full car model

The dynamic equation of motion for 7-DOF full car model is derived using Lagrange function.

$$M\ddot{x} + C\dot{x} + Kx = Du + E\dot{u} \tag{2.43}$$

$$
M = \begin{bmatrix}
m_{L1} & 0 & 0 & 0 & 0 & 0 & 0 \\
0 & m_{R1} & 0 & 0 & 0 & 0 & 0 \\
0 & 0 & m_{L2} & 0 & 0 & 0 & 0 \\
0 & 0 & 0 & m_{R2} & 0 & 0 & 0 \\
0 & 0 & 0 & 0 & m_c & 0 & 0 \\
0 & 0 & 0 & 0 & 0 & I_r & 0 \\
0 & 0 & 0 & 0 & 0 & 0 & I_p
\end{bmatrix}
\tag{2.44}
$$

$$
K = \begin{bmatrix}
k_{tL1}+k_{L1} & 0 & 0 & 0 & -k_{L1} & k_{L1}(d) & -k_{L1}(a) \\
0 & k_{tR1}+k_{R1} & 0 & 0 & -k_{R1} & -k_{R1}(d) & -k_{R1}(b) \\
0 & 0 & k_{tL2}+k_{L2} & 0 & -k_{L2} & k_{L2}(c) & k_{L2}(a) \\
0 & 0 & 0 & k_{tR2}+k_{R2} & -k_{R2} & -k_{R2}(c) & k_{R2}(b) \\
-k_{L1} & -k_{R1} & -k_{L2} & -k_{R2} & a^* & b^* & c_1^* \\
k_{L1}(d) & -k_{R1}(d) & k_{L2}(c) & -k_{R2}(c) & b^* & d^* & e_1^* \\
-k_{L1}(a) & -k_{R1}(a) & k_{L2}(b) & k_{R2}(b) & c_2^* & e_2^* & f^*
\end{bmatrix}
\tag{2.45}
$$

38

$$a^* = k_{L1} + k_{R1} + k_{L2} + k_{R2}$$

$$b^* = -k_{L1}(d) + k_{R1}(d) - k_{L2}(c) + k_{R2}(c)$$

$$c_1^* = k_{L1}(a) + k_{R1}(b) - k_{L2}(a) - k_{R2}(b)$$

$$c_2^* = k_{L1}(a) + k_{R1}(a) - k_{L2}(a) - k_{R2}(b)$$

$$d^* = k_{L1}(d^2) + k_{R1}(d^2) + k_{L2}(c^2) + k_{R2}(c^2)$$

$$e_1^* = -k_{L1}(ad) + k_{R1}(bd) + k_{L2}(ac) - k_{R2}(bc)$$

$$e_2^* = -k_{L1}(ad) + k_{R1}(ad) + k_{L2}(bc) - k_{R2}(bc)$$

$$f^* = k_{L1}(a^2) + k_{R1}(ab) + k_{L2}(ab) + k_{R2}(b^2)$$

where m_c is the mass for the vehicle car body; I_r and I_p is the mass moment of inertia for the vehicle car body for rolling and pitching respectively; m_{L1}, m_{R1} and m_{L2}, m_{R2} are the masses of the left-right front and rear bogies respectively; k_{L1}, k_{R1} and k_{L2}, k_{R2} are the vertical spring stiffness of left-right front and rear suspensions respectively; k_{tL1}, k_{tR1} and k_{tL2}, k_{tR2} are the stiffness of left-right front and rear tires respectively; a, b, c, d represents the distance from the center of gravity of the car body to front/rear suspension locations respectively as shown in Figure 2.5.

The damping matrix [C] is identical in form to [K] given in equation (2.46) except that the corresponding term 'k' should be replaced by 'c'.

$$D = \begin{bmatrix} k_{tL1} & 0 & 0 & 0 \\ 0 & k_{tR1} & 0 & 0 \\ 0 & 0 & k_{tL2} & 0 \\ 0 & 0 & 0 & k_{tR2} \\ 0 & 0 & 0 & 0 \\ 0 & 0 & 0 & 0 \\ 0 & 0 & 0 & 0 \end{bmatrix} \quad E = \begin{bmatrix} c_{tL1} & 0 & 0 & 0 \\ 0 & c_{tR1} & 0 & 0 \\ 0 & 0 & c_{tL2} & 0 \\ 0 & 0 & 0 & c_{tR2} \\ 0 & 0 & 0 & 0 \\ 0 & 0 & 0 & 0 \\ 0 & 0 & 0 & 0 \end{bmatrix} \tag{2.46}$$

The system state vector is given as,

$$x^a = [w_{L1} \ w_{R1} \ w_{L2} \ w_{R2} \ z \ \varphi_r \ \theta_p \ \dot{w}_{L1} \ \dot{w}_{R1} \ \dot{w}_{L2} \ \dot{w}_{R2} \ \dot{z} \ \dot{\varphi}_r \ \dot{\theta}_p \ u_{L1} \ u_{R1} \ u_{L2} \ u_{R2} \ldots$$
$$\ldots \dot{u}_{L1} \ \dot{u}_{R1} \ \dot{u}_{L2} \ \dot{u}_{R2}]^T \tag{2.47}$$

The results of ORC analysis of 7-DOF full suspension model is shown in Table 2.7. Because observation matrix depends on sensor location, the sensors are presumed to be placed at the center of car body and bogies respectively.

Table 2.7 ORC analysis results for 7-DOF full suspension model

Measurements	Observable states
$\ddot{z}\ \dot{\varphi}_r\ \dot{\theta}_p\ \ddot{w}_{L1}\ \ddot{w}_{R1}\ \ddot{w}_{L2}\ \ddot{w}_{R2}$	$\dot{\varphi}_r\ \dot{\theta}_p$
$\dot{\varphi}_r\ \dot{\theta}_p\ \ddot{w}_{L1}\ \ddot{w}_{R1}\ \ddot{w}_{L2}\ \ddot{w}_{R2}$	$\dot{\varphi}_r\ \dot{\theta}_p$
$\ddot{z}\ \ \dot{\varphi}_r\ \dot{\theta}_p$	$\dot{\varphi}_r\ \dot{\theta}_p$
$\dot{\varphi}_r\ \dot{\theta}_p$	$\dot{\varphi}_r\ \dot{\theta}_p$
$\ddot{z}\ \ \ddot{w}_{L1}\ \ddot{w}_{R1}\ \ddot{w}_{L2}\ \ddot{w}_{R2}$	Nil
$\ddot{w}_{L1}\ \ddot{w}_{R1}\ \ddot{w}_{L2}\ \ddot{w}_{R2}$	Nil

The proposed two approaches are executed with the following state vectors.

In approach (a), the new state vector is,

$$\widetilde{x^a} = [w_{L1}\ w_{R1}\ w_{L2}\ w_{R2}\ z\ \varphi_r\ \theta_p\ \dot{w}_{L1}\ \dot{w}_{R1}\ \dot{w}_{L2}\ \dot{w}_{R2}\ \dot{z}\ \dot{\varphi}_r\ \dot{\theta}_p\ u_{L1}\ u_{R1}\ u_{L2}\ u_{R2} ...$$
$$..\dot{u}_{L1}\ \dot{u}_{R1}\ \dot{u}_{L2}\ \dot{u}_{R2}\ \ddot{u}_{L1}\ \ddot{u}_{R1}\ \ddot{u}_{L2}\ \ddot{u}_{R2}]^T \qquad (2.48)$$

In approach (b), the new state vector is,

$$\dot{x}^a = [\dot{w}_{L1}\ \dot{w}_{R1}\ \dot{w}_{L2}\ \dot{w}_{R2}\ \dot{z}\ \dot{\varphi}_r\ \dot{\theta}_p\ \ddot{w}_{L1}\ \ddot{w}_{R1}\ \ddot{w}_{L2}\ \ddot{w}_{R2}\ \ddot{z}\ \ddot{\varphi}_r\ \ddot{\theta}_p\ \dot{u}_{L1}\ \dot{u}_{R1}\ \dot{u}_{L2}\ \dot{u}_{R2} ...$$
$$... \ddot{u}_{L1}\ \ddot{u}_{R1}\ \ddot{u}_{L2}\ \ddot{u}_{R2}]^T \qquad (2.49)$$

Table 2.8 shows the observable states for the two approaches. The acceleration and angular velocity of car body and bogie masses are the minimum combination of measurements, which results in observable profile derivatives. By implementing both the approaches, the second derivative component of the profile is observable.

Table 2.8 ORC results for 7-DOF full suspension model using proposed approach

Measurements	Observable states	
	Approach (a)	**Approach (b)**
$\ddot{z}\ \ \dot{\varphi}_r\ \dot{\theta}_p\ \ddot{w}_{L1}\ \ddot{w}_{R1}\ \ddot{w}_{L2}\ \ddot{w}_{R2}$	$\dot{\varphi}_r\ \dot{\theta}_p$ $\ddot{u}_{L1}\ \ddot{u}_{R1}\ \ddot{u}_{L2}\ \ddot{u}_{R2}$	$\dot{\varphi}_r\ \dot{\theta}_p\ \ddot{w}_{L1}\ \ddot{w}_{R1}\ \ddot{w}_{L2}\ \ddot{w}_{R2}\ \ddot{z}\ \ddot{\varphi}_r\ \ddot{\theta}_p$ $\ddot{u}_{L1}\ \ddot{u}_{R1}\ \ddot{u}_{L2}\ \ddot{u}_{R2}$
$\dot{\varphi}_r\ \dot{\theta}_p\ \ddot{w}_{L1}\ \ddot{w}_{R1}\ \ddot{w}_{L2}\ \ddot{w}_{R2}$	$\dot{\varphi}_r\ \dot{\theta}_p$ $\ddot{u}_{L1}\ \ddot{u}_{R1}\ \ddot{u}_{L2}\ \ddot{u}_{R2}$	$\dot{\varphi}_r\ \dot{\theta}_p\ \ddot{w}_{L1}\ \ddot{w}_{R1}\ \ddot{w}_{L2}\ \ddot{w}_{R2}\ \ddot{z}\ \ddot{\varphi}_r\ \ddot{\theta}_p$ $\ddot{u}_{L1}\ \ddot{u}_{R1}\ \ddot{u}_{L2}\ \ddot{u}_{R2}$
$\ddot{z}\ \ \dot{\varphi}_r\ \dot{\theta}_p$	$\dot{\varphi}_r\ \dot{\theta}_p$	$\dot{\varphi}_r\ \dot{\theta}_p\ \ddot{w}_{L1}\ \ddot{w}_{R1}\ \ddot{w}_{L2}\ \ddot{w}_{R2}\ \ddot{z}\ \ddot{\varphi}_r\ \ddot{\theta}_p$

$\dot{\varphi}_r \ \dot{\theta}_p$	$\dot{\varphi}_r \ \dot{\theta}_p$	$\dot{\varphi}_r \ \dot{\theta}_p \ \ddot{w}_{L1} \ \ddot{w}_{R1} \ \ddot{w}_{L2} \ \ddot{w}_{R2} \ \ddot{z} \ \ddot{\varphi}_r \ \ddot{\theta}_p$
$\ddot{z} \ \ \ddot{w}_{L1} \ \ \ddot{w}_{R1} \ \ \ddot{w}_{L2} \ \ \ddot{w}_{R2}$	$\ddot{u}_{L1} \ \ddot{u}_{R1} \ \ddot{u}_{L2} \ \ddot{u}_{R2}$	$\ddot{w}_{L1} \ \ddot{w}_{R1} \ \ddot{w}_{L2} \ \ddot{w}_{R2} \ \ddot{z} \ \ddot{\varphi}_r \ \ddot{\theta}_p$ $\ddot{u}_{L1} \ \ddot{u}_{R1} \ \ddot{u}_{L2} \ \ddot{u}_{R2}$
$\ddot{w}_{L1} \ \ddot{w}_{R1} \ \ddot{w}_{L2} \ \ddot{w}_{R2}$	$\ddot{u}_{L1} \ \ddot{u}_{R1} \ \ddot{u}_{L2} \ \ddot{u}_{R2}$	$\ddot{w}_{L1} \ \ddot{w}_{R1} \ \ddot{w}_{L2} \ \ddot{w}_{R2} \ \ddot{z} \ \ddot{\varphi}_r \ \ddot{\theta}_p$ $\ddot{u}_{L1} \ \ddot{u}_{R1} \ \ddot{u}_{L2} \ \ddot{u}_{R2}$

2.5 Discussions and Summary

The observability analysis to theoretically obtain the appropriate sensor types and their placements for estimating rail track profile are illustrated in this chapter. The measurement matrix consists of only acceleration and angular velocity responses collected from the dynamic characteristics of vehicle body. In order to estimate the profile through inverse analysis, the second derivative of the profile is included in the state vector as one of the additional state variable, and thus the non-static component can be obtained through double integration of it. Different types of vehicle models are considered with appropriate sensor types and their locations, for the numerical analyses and the results are presented. The two approaches to obtain the second derivative of profile as an observable state variable are examined. Approach (a) includes the second derivative of the profile in the state vector. Although the system is unobservable the augmented state variable is observable. Approach (b) alters state space model by taking the first derivative of the system equation. The second derivative component is observable. These analyses indicate that the profile can be estimated by an accelerometer and a gyro on car body or bogie. The profile is expected to be obtained by the double integration of the high pass-filtered second derivative.

Chapter 3 NUMERICAL STUDY ON EXTENSION OF AUGMENTED STATE KALMAN FILTER

3.1 Introduction

In order to maintain the railway infrastructure competently, the prerequisite is to monitor the vertical and lateral direction of profile regularly. While the measurement of profile or vehicle's absolute displacement is not practical, but the acceleration and angular velocity measurements are feasible. Prevalent sensing devices such as smartphones have been potentially being utilized in vehicle body motion measurement. However, the applicability of such measurement for profile estimation is not clarified yet. In this chapter a numerical analysis for track profile estimation by various vehicle dynamics models are presented. In previous chapter, an observability analysis on the profile estimation through augmented state space model as well as two other extended formulations has been performed. For inverse analysis purpose, vehicle body acceleration and angular velocity measurements are considered in measurement matrix. In the two approaches, the second derivative of the profile is included in the state vector along with other state variables. While the profile itself is not observable in any formulation, the second derivative of profile was shown to be observable. In this chapter, Kalman filter technique (data assimilation for inverse problem) is employed for three state space models mentioned above, termed as conventional Augmented State Kalman Filter (ASKF) and two extended approaches (a) and (b) for the profile estimation. Thus, a numerical study on extension of ASKF for input dynamic force reconstruction is presented. The performances are compared numerically using linear vehicle models, namely, simplified train model (4 DOF) and 6 DOF vehicle model (train).

3.2 Mathematical Formulation

The recommended method basically comprises of a standard linear Kalman filter data assimilation inverse analysis technique performed on an augmented state-space representation wherein the dynamic input forces are augmented to the unknown state vector [63, 64]. The augmented state-space model has been derived using the filter equations as presented below [77] [84].

3.2.1 Augmented State-Space Model

Consider a linear, classical discrete-time dynamical system represented in state-space configuration model with a state vector, x_k. It consists of least amount of data that is adequate to exclusively define the unforced dynamical performance of the system which is required to forecast its upcoming performance; the subscript k represents discrete time.

$$x_{k+1} = Ax_k + Bu_k + w_k \tag{3.1}$$

$$y_k = Hx_k + Du_k + v_k \tag{3.2}$$

where A and B represent transition matrix and input matrix respectively; w_k denotes stochastic process noise vector, $\{w_k \in R^{n_s}\}_{k=0}^{\infty}$, where n_s mentions number of states, assumed to be additive, white, and Gaussian with zero mean; u_k denotes the dynamic input excitation vector with η_k a component of the stochastic process $\{\eta_k \in R^{n_u}\}_{k=0}^{\infty}$ can be shown as, $u_{k+1} = u_k + \eta_k$; y_k is the measured data vector at time k; H is the measurement matrix; D is direct transmission matrix; v_k is the measurement noise, $\{v_k \in R^{n_d}\}_{k=0}^{\infty}$, assumed to be additive, white, and Gaussian with zero mean and it is uncorrelated with the process noise. By redefining the state vector by adding the unknown input vector, an augmented state equation is achieved with noise vector, $\varepsilon_k \in R^{n_s+n_u}$.

$$x_k^a = \begin{bmatrix} x_k \\ u_k \end{bmatrix} \tag{3.3}$$

$$x_{k+1}^a = \begin{bmatrix} A & B \\ 0 & I \end{bmatrix} x_k^a + \begin{Bmatrix} w_k \\ \eta_k \end{Bmatrix} \tag{3.4}$$

$$x_{k+1}^a = A_a x_k^a + \varepsilon_k \tag{3.5}$$

where, $A_a \in R^{(n_s+n_u)x(n_s+n_u)}$, is the system matrix.

The measurement equation in augmented state-space model will have the following form:

$$y_k = H_a x_k^a + v_k \tag{3.6}$$

where, H_a is the new measurement matrix constructed from original output matrix and direct transmission matrix, represented as $H_a = [H \ \ D]$. Hence, the formulation for augmented state-space model defining state and observation equations are given in Equations (3.5) and (3.6) respectively.

3.2.2 Augmented State Kalman Filter for Input-state Estimation

An alternative prevailing method for recursive joint state-input estimation is the Augmented State Kalman Filter (ASKF) data assimilation inverse analysis technique, which is considered to be optimal estimator in a minimum-variance unbiased sense, i.e. to ultimately infer parameters from indirect and uncertain measurements. Thus, the best estimate is obtained from noisy data by filtering out noise and by predicting those observations against the state estimate. The application of augmented state-space configuration is extensively utilized in automatic control field with the purpose of concurrently estimating the states and parameters of the dynamic system. In this background, the aforementioned objective to extract excitation data from measurement can be achieved by implementing Kalman filtering technique which conventionally follows recursive prediction-correction pattern.

Let $\hat{x}_{k|l}^a$ be the estimate of x_k^a given, $\{y_n\}_{n=0}^l$. Without observed data at time $k = 0$, the initial state estimate is given as, $\hat{x}_{0|-1}^a$ and it is assumed to be random variable. A posterior state estimate is derived by combining the prior estimate $\hat{x}_k^{a^-}$ (Prediction step) and the weighted difference between an actual measurement and a measurement prediction $H_a \hat{x}_k^{a^-}$ (Update step) as illustrated below.

$$\hat{x}_k^a = \hat{x}_k^{a^-} + L(y_k - H_a \hat{x}_k^{a^-}) \tag{3.7}$$

The difference $(y_k - H_a \hat{x}_k^{a^-})$ is known as measurement residual which reveals the inconsistency between the predicted and the actual measurement. The matrix L is called the Kalman gain, an essential factor which minimizes the posterior error covariance. Henceforth, the error covariance matrix $P_{k|l} \in R^{(n_s+n_u)x(n_s+n_u)}$ will have the following form with assumption that $P_{0|-1}$ and $\hat{x}_{0|-1}^a$ are known.

$$P_{k|l} = E\left[(x_k^a - \hat{x}_{k|l}^a)(x_k^a - \hat{x}_{k|l}^a)^T\right] \tag{3.8}$$

The noise processes for state, excitation and measurement $\{w_k\}, \{\eta_k\}$ and $\{v_k\}$ are assumed to be known discrete vectors, which are mutually uncorrelated stochastic processes with zero mean and Gaussian white processes of covariance matrices Q, S and R represented by,

$$E[w_k w_l^T] = Q\delta_{k-l} \qquad E[\eta_k \eta_l^T] = S\delta_{k-l} \, E[v_k v_l^T] = R\delta_{k-l} \tag{3.9}$$

where δ_{k-l} is the Kronecker delta. The influence of process covariance matrix Q is based on the model of the system used and the observation noise covariance matrix R depends on the accuracy of sensors used for the measurements and however the obtained solution is less sensitive to these matrices when compared with the covariance matrix S which is considered as regularization matrix. The ASKF formulation for the discrete-time state-space model of a

physical system as mentioned in Equations (3.5) and (3.6) are presented in terms of time update and measurement update.

Time update:

$$\hat{x}^a_{k+1|k} = A_a \hat{x}^a_{k|k} \tag{3.10}$$

$$P_{k+1|k} = A_a P_{k|k} A_a{}^T + Q_a \tag{3.11}$$

Measurement update:

$$L_{k+1} = P_{k+1|k} H_a^T (H_a P_{k+1|k} H_a^T + R)^{-1} \tag{3.12}$$

$$\hat{x}^a_{k+1|k+1} = \hat{x}^a_{k+1|k} + L_{k+1}(y_{k+1} - H_a \hat{x}^a_{k+1|k}) \tag{3.13}$$

$$P_{k+1|k+1} = P_{k+1|k} - L_{k+1} H_a P_{k+1|k} \tag{3.14}$$

Considering the aforementioned expressions, if the observation noise covariance matrix R approaches zero, the Kalman gain L affects the residual severely, i.e. actual measurement is trusted more. Instead, if prior estimate error covariance matrix approaches zero, then the influence of gain matrix on residual is less, else the predicted measurement is trusted. In combination with the augmented noise vector ε_k of Equation (3.5), the augmented covariance matrix $Q_a \in R^{(n_s+n_u)x(n_s+n_u)}$ is given as, $Q_a = \begin{bmatrix} Q & 0 \\ 0 & S \end{bmatrix}$.

The augmented state-space model and its utilization in Kalman filtering techniques are developed and formulated in detailed manner by using the filter equations and it is briefly illustrated in Table 3.1. The proposed ASKF method by [77], for unknown input force reconstruction in structural dynamic system have determined that the ASKF is likely to have numerical instabilities owing to problems of the augmented state-space model. In order to overcome this issue of un-observability, two approaches are proposed as an extension of augmented state-space model. The two approaches for the estimation of profile as a part of the state vector are considered. One is to augment the state variables with the second derivative of the profile and estimate the second derivative. The profile is estimated directly from the state vector as its double integration; however, it has a large low frequency estimation error. A high-pass filter is needed to be applied for accurate results.

Table 3.1 A general scheme of augmented state Kalman filter-based joint input-state estimation algorithm [63, 64] [77]

Augmented state-space model

$$x_{k+1}^a = A_a x_k^a + \varepsilon_k$$

$$y_k = H_a x_k^a + v_k$$

where ε_k and v_k are independent, zero-mean, Gaussian noise processes of covariance matrices Q_a and R, respectively.

Initialization:

    For $k = 0$, set $\qquad \hat{x}_0^a = E[x_0^a]$

$$P_0 = E[(x_0^a - E[x_0^a])(x_0^a - E[x_0^a])^T]$$

Computation:

    For $k = 1, 2, \ldots\ldots,$ compute

State estimate propagation

$$\hat{x}_{k+1|k}^a = A_a \hat{x}_{k|k}^a$$

Error covariance propagation

$$P_{k+1|k} = A_a P_{k|k} A_a^T + Q_a$$

Kalman gain matrix

$$L_{k+1} = P_{k+1|k} H_a^T (H_a P_{k+1|k} H_a^T + R)^{-1}$$

State estimate update

$$\hat{x}_{k+1|k+1}^a = \hat{x}_{k+1|k}^a + L_{k+1}(y_{k+1} - H_a \hat{x}_{k+1|k}^a)$$

Error covariance update

$$P_{k+1|k+1} = P_{k+1|k} - L_{k+1} H_a P_{k+1|k}$$

The other is to alter state space model by adopting the first derivative of the state vector as new state vector. Thus, only the dynamic components are considered while the static components (i.e., displacement) are excluded from the state vector. The profile is estimated as the double integration of a state vector component. This process makes the second derivative of profile as an observable state even though the profile is not observable. The altered state space model is,

$$\ddot{x}_k^a = A_a \dot{x}_k^a; \qquad \dot{y}_k = \widetilde{H_a} \dot{x}_k^a \qquad\qquad (3.15)$$

where x_k^a is augmented state vector and only the measurement matrix H_a, is modified while the transition matrix A_a, is unaltered.

3.3   Proposed Implementation of Estimation Algorithm

In this chapter, an inverse analysis algorithm is utilized to reconstruct the dynamic input force excitation (profile information) from the multiple observables on a vehicle model. This specific problem of force extraction from the response collected on a multi-body dynamic system through the Kalman filtering technique is a data assimilation inverse problem categorized in a stochastic basis. In order to obtain theoretically the appropriate locations and types of sensors to estimate the profile as the 'observable state', the different vehicle models are considered for the observability analysis as explained in the previous chapter. Practical sensor types are accelerometers and gyros and their installation locations are car body and bogies. In these analyses the parameters of the vehicle models are considered known. The analyses are carried out using both the linear and non-linear observability check methods and are found to be consistent. The proposed approaches are investigated for all vehicle models. All possible combination of measurements at car body and bogies with accelerometers and gyros are analyzed in terms of ORC and all cases where the profile or its derivatives are observable are extracted for each vehicle model. The subsequent sections give a brief overview of generating profiles according to available standards and utilizing it for the inverse problem by implementing on various vehicle models which includes simplified 4 DOF model and 6 DOF vehicle model respectively. The simulation results from proposed approach of extension on ASKF method is compared with the results obtained from conventional ASKF and it is found to perform well. The application of the ASKF profile estimation algorithm explicitly recommended in this chapter is explained in Figure 3.1.
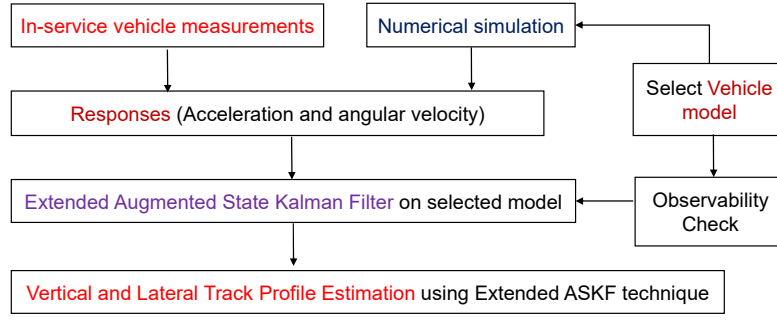
Figure 3.1 Profile estimation algorithms to reconstruct from measurement responses

3.3.1 Quantification through various Statistical Metrics

To validate the estimation algorithm, the following metrics have been used to quantify the signature variations. In this framework, estimated profile and true profile are utilized in simulating the responses from the same dynamic vehicle model and consequently, an indirect criterion is evaluated, based on a damage estimation value obtained from the vehicle measurement to the true profile. The assessment of these criteria help in understanding the consequence of potential errors have on the estimated profile from responses collected from vehicle.

3.3.1.1 Root Mean Square Error

The Root-Mean-Square Error (RMSE) is a commonly used statistical metrics to measure the residuals (prediction errors), which serves to aggregate error into a single measure of predictive power [85]. The RMSE expressed below is a dimensional error estimation value,

$$RMSE(mm) = \sqrt{\frac{\Sigma(x_i^0 - x_i^1)^2}{N}} \qquad (3.16)$$

where x_i^0, x_i^1 are the ith value of reference series and compared series respectively and N is the number of data samples.

3.3.1.2 Root Mean Square Deviation

The Root-Mean-Square Deviation (RMSD) is a commonly used statistical metrics to measure the residuals (prediction errors), which signifies the sample standard deviation of the differences between estimated values and true values [85]. The RMSD expressed below is a normalized value which is a non-dimensional metrics.

$$RMSD(\%) = \sqrt{\frac{\Sigma(x_i^0 - x_i^1)^2}{\Sigma(x_i^0)^2}} \times 100 \qquad (3.17)$$

where x_i^0, x_i^1 are the ith value of reference series and compared series respectively.

3.3.1.3 Correlation Coefficient

Correlation identifies similarity and dependency amongst two waveforms. An exact resemblance indicates that the Correlation Coefficient (CC) is unity (or -1). Two randomly generated time series will be hardly correlated amid each other, to the extent that the sum of the factored pairs will tend towards zero. CC is calculated for a subset of the total block of data with overlapped pairs [86]. Therefore, CC is obtained by the computational implementation as the mean of the products of the standard scores and it is beneficial in predictive damage assessment.

$$CC = \frac{1}{n-1}\Sigma_{i=1}^n \left(\frac{X_i - \bar{X}}{s_X}\right)\left(\frac{Y_i - \bar{Y}}{s_Y}\right) \qquad (3.18)$$

$$\bar{X} = \frac{1}{n}\Sigma_{i=1}^n X_i \quad ; \qquad s_X = \sqrt{\frac{1}{n-1}\Sigma_{i=1}^n (X_i - \bar{X})^2} \qquad (3.19)$$

Based on the sample of the paired data (X_i, Y_i), the CC is derived by the Equation (3.18), where sample mean and sample standard deviation are specified in Equations (3.19) respectively.

3.3.2 Estimation of Track Profile from Vehicle Responses

In the current research work, the estimation algorithm employed is based on an augmented Kalman filtering theory, which is capable of solving the inverse analysis in a stochastic context. Track profile estimation from vehicle measurement responses is feasible with the usage of a priori information on possible modelling deficits and dynamic input excitation. The aim of the mathematical simulations is to understand the vibration generated by vehicles due to the dynamic interaction amongst train vehicle and track profile surface. For practical application of the approach, two things must be completely defined for the execution of estimation algorithm, namely vehicle model and the analogous measurement system, i.e. matrices *A, B, C, D* along with covariance matrices *Q, S* and *R*, which are found to be tuning parameters. Perhaps, it is not an optimum solution but it is very pragmatic. However, this issue is rarely discussed in literature and no solution can be derived from severe mathematical reflection. Certainly, tuning parameters utilized in this estimation algorithm should consider the actuality of the measurement arrangement with all feasible errors and model restrictions, and thus it marks the usage of empirical parameter inevitable. Generally, the results obtained in

the subsequent sections prove that the recommended data assimilation inverse analysis algorithm is an appreciable method for the vertical and lateral track profile estimation. Accordingly, these results approve the rationality of carefully chosen tuning parameter.

With the background of an inverse analysis, the quality of evaluation of measured responses through direct problem, influence extremely the reliability of the estimated excitation. Henceforth, Kalman filter technique is employed for three state space models mentioned above, termed as conventional ASKF and two extended approaches (a) and (b) for the track profile estimation. The further studies on different vehicle models are being conducted for the effective track profile estimation using practical sensors and its installation locations. Thus, robustness and competence of the proposed approaches will be broadly assessed by conducting numerical analyses of train vehicle models.

3.4   Simulated Railway Track Profile

Track irregularity record obtained from real field measurement is essential to detect the influence of irregularities, however attaining such record is inappropriate. Alternative solution is to use simulation result of the track geometry [4]. Thus, track irregularities can be given as random functions with reference to the longitudinal coordinate axis '*x*'. Numerous measurements have shown that the track irregularities may be frequently described by a one-sided PSD function of the track geometry [87]. PSD functions utilized in this study are expressed in Equations (3.20) and (3.21) for elevation, alignment and cross irregularities respectively.

$$S_{v,a}\left(\Omega\right)=\frac{A_v\Omega_c^2}{(\Omega^2+\Omega_r^2)(\Omega^2+\Omega_c^2)} \tag{3.20}$$

$$S_c\left(\Omega\right)=\frac{A_v\Omega_c^2\Omega^2/l_a^2}{(\Omega^2+\Omega_r^2)(\Omega^2+\Omega_c^2)(\Omega^2+\Omega_s^2)} \tag{3.21}$$

where $S_{v,a}$ is PSD function for the elevation and alignment irregularity; S_c is PSD function for the cross level irregularity; $\Omega = 1/L_r$ represents the spatial frequency (Hz) and L_r is the length of the irregularity (m). Table 3.2 illustrates the coefficients value representing the above equations given by the Federal Railroad Administration (FRA) for Classes 4, 5 and 6 of tracks, with Class 6 representing the best and Class 4 the worst [87-90]. However, the track irregularity represented by PSD method cannot be applied in the simulation directly, since the record in time domain is needed in the analysis. The sample of rail irregularities can be produced by inverse Fourier transform method and so on.

Table 3.2 Track PSD model parameter [92]

Quality (FRA)	Very poor (4)	Poor (5)	Moderate (6)
A_v (m)	2.39×10^{-5}	9.35×10^{-6}	1.50×10^{-6}
Ω_s (rad/m)	1.130	0.821	0.438
Ω_r (rad/m)	2.06×10^{-2}	2.06×10^{-2}	2.06×10^{-2}
Ω_c (rad/m)	0.825	0.825	0.825

In this study the spectral representation method [93] is applied to obtain the profiles for the deviation in the elevation, alignment and cross level, i.e., $r_v(x)$, $r_h(x)$ and $r_c(x)$, of the twin rail system can be established.

$$r_v(x) = \sqrt{2}\sum_{n=0}^{N-1}A_n\cos(\Omega_n x + \alpha_n) \tag{3.22}$$

$$r_h(x) = \sqrt{2}\sum_{n=0}^{N-1}B_n\cos(\Omega_n x + \beta_n) \tag{3.23}$$

$$r_c(x) = \sqrt{2}\sum_{n=0}^{N-1}C_n\cos(\Omega_n x + \gamma_n) \tag{3.24}$$

where N represents the total number of discrete spatial frequencies considered, and the independent random phase angles α_n, β_n, γ_n ($n = 1, 2, \ldots, N-1$) are random phase angle uniformly distributed from 0 to 2π.

Ω_n is the nth discrete frequency, which is computed as Equation (3.25),

$$\Omega_n = n\Delta\Omega = \frac{n(\Omega_u - \Omega_l)}{N} \tag{3.25}$$

where $n = 1, 2, \ldots, N-1$; Ω_u and Ω_l denote the upper bound and lower bound of the circle frequencies considered respectively. Coefficients, A_n, B_n and C_n in Equations (3.22 – 3.24) can be defined as in Equations (3.26 - 3.29).

$$A_0 = B_0 = C_0 = 0 \tag{3.26}$$

$$A_1 = B_1 = \sqrt{\left(\frac{1}{2\pi}S_{v,a}(\Delta\Omega) + \frac{1}{3\pi}S_{v,a}(0)\right)\Delta\Omega}\ ; \quad C_1 = \sqrt{\left(\frac{1}{2\pi}S_c(\Delta\Omega) + \frac{1}{3\pi}S_c(0)\right)\Delta\Omega}$$

$$\tag{3.27}$$

$$A_2 = B_2 = \sqrt{\left(\frac{1}{2\pi}S_{v,a}\left(2\Delta\Omega\right)+\frac{1}{12\pi}S_{v,a}\left(0\right)\right)\Delta\Omega} \; ; C_2 = \sqrt{\left(\frac{1}{2\pi}S_c\left(2\Delta\Omega\right)+\frac{1}{12\pi}S_c\left(0\right)\right)\Delta\Omega}$$

(3.28)

$$A_n = B_n = \sqrt{\left(\frac{1}{2\pi}S_{v,a}\left(n\Delta\Omega\right)\right)\Delta\Omega} \; ; \qquad C_n = \sqrt{\left(\frac{1}{2\pi}S_c\left(n\Delta\Omega\right)\right)\Delta\Omega}$$

(3.29)

Note that the results of $r_v(x)$, $r_h(x)$ and $r_c(x)$ generated by above method may not satisfy the control standard of the track. The normalization process to the maximum tolerable deviations of the track is necessary according to the different track quality. From Equations (3.33 – 3.35), the vertical and alignment profile irregularities for the right and left rails can be calculated respectively.

$$r_{vr}\left(x\right) = r_v\left(x\right) - \frac{1}{2}r_c(x)$$

(3.30)

$$r_{vl}\left(x\right) = r_v\left(x\right) + \frac{1}{2}r_c(x)$$

(3.31)

$$r_{hr}\left(x\right) = r_{hl}\left(x\right) = r_h\left(x\right)$$

(3.32)

For numerical simulation, the subsequent parameters are considered as, $\Omega_l = 0.0209 \; rad/m$, $\Omega_u = 12.566 \; rad/m$, $N = 4000$ and length of the track profile is 1000 m. The profiles of the two rails used for rail track in the simulation are plotted in Figure 3.2. The corresponding wavelength is 0.5 m to 300 m, which covers whole length of track irregularities (both short and long wavelength).

(a)
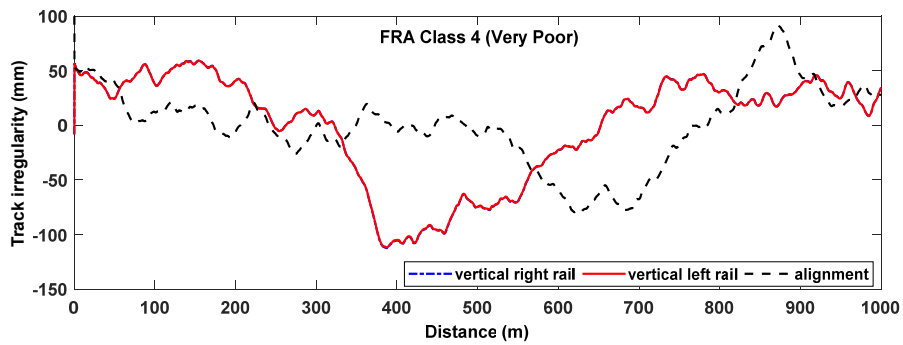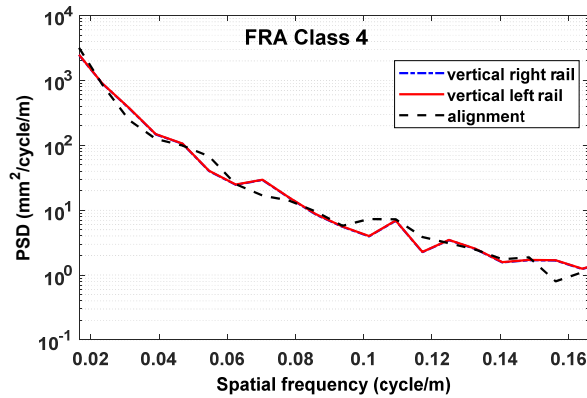
FRA Class 4

(b)

Figure 3.2 Rail Track profile: (a) generated from FRA Class 4; (b) PSD plot

3.4.1 4 DOF train vehicle model with averaged track geometry

3.4.1.1 A Simplified train vehicle model for estimating vertical track geometry

Local railways suffer from age-related deterioration and poor maintenance, which is unable to perform adequate monitoring. It is necessary to enhance the comfort level and service life of railway transportation. Track profile estimation from response measurements possibly offers effective results. A simpler, more robust and cost effective system for use on in-service vehicle is desirable. For railway track vertical profile estimation, numerical simulation using ASKF method for 4 DOF vehicle model with averaged track geometry (Figure 2.4) (a simplified vehicle model as explained in the previous chapter) is carried out in detailed manner. The accelerometer and rate gyro sensors are considered to be mounted on the car body floor just above the front bogie mass of the 6 DOF train model for the data assimilation inverse analyses. The car body vertical acceleration and pitch rate measurement responses are collected from 6 DOF train model (Figure 2.3) and utilized as the input response for simplified train model with 4 DOF where ASKF technique in implemented as inverse analysis. Based on three formulations, railway track profile estimation is numerically studied employing ASKF data assimilation inverse analysis technique on the artificial profile generated using FRA standards. The reference vehicle parameters for train vehicle model are obtained from [94, 95] representing local railway network parameters as shown in Table 3.3. Furthermore, the vehicle is supposed to retain a constant velocity of 90 km/h with simulated distance of 1000 m and sampling frequency of 100 Hz.

53

Table 3.3 Train vehicle model parameters

Parameter	Value
Car body mass (m_c)	11571.5 kg
Front bogie mass (m_{t1})	2042.5 kg
Rear bogie mass (m_{t2})	2042.5 kg
Car body mass moment of inertia (I_c)	416574 kgm^2
Front bogie mass moment of inertia (I_{t1})	1211 kgm^2
Rear bogie mass moment of inertia (I_{t2})	1211 kgm^2
Primary vertical suspension stiffness (k_p)	1150 kN/m
Secondary vertical suspension stiffness (k_s)	290 kN/m
Primary vertical suspension damping (c_p)	115 kN.s/m
Secondary vertical suspension damping (c_s)	29 kN.s/m
Primary horizontal suspension stiffness (k_{ph})	3840 kN/m
Secondary horizontal suspension stiffness (k_{sh})	176 kN/m
Primary horizontal suspension damping (c_{ph})	384 kN.s/m
Secondary horizontal suspension damping (c_{sh})	17.6 kN.s/m
Half of car-body base (l_c)	7.2 m
Half of bogie-wheel base (l_t)	1.125 m

Numerical simulation is incorporated with vehicle model errors and various measurement noise levels determined by Gaussian white noise which is produced as a random walk model and also initial condition error in the stochastic framework iteration so as to approximately estimate the exact profile. The noisy response is simulated by adding noise components to the unpolluted vehicle responses as,

$$x_{noise} = x + \in_{\%} \gamma_{noise} \sigma(x) \qquad (3.33)$$

where $\in_{\%}$ is the percentage noise level, γ_{noise} is a noise with a standard normal distribution, $\sigma(x)$ is the standard deviation of the "measured" response.

A typical case of simulated profile after using band pass filter with cut off frequency of 0.0166 – 0.166 cycle/m, by incorporating noise level of 5% (standard deviation of measured response and random error). Noise is augmented to estimated data based on the features of practical sensors used to obtain the measurement response signals. To remove the integration error, a 0.15 Hz high-pass filter is employed. The vehicle model parameters are estimated based on the real vehicle. The filter considered in this simulation helps to evaluate wavelengths ranging

between 6 m – 60 m, which covers ranges comprising from short to long wavelength irregularities as mentioned in [96]. Table 3.4 gives the natural frequency estimation of simplified train model (4 DOF) accounting for vertical displacement.

Table 3.4 Natural frequency estimation of 4 DOF train model: for vertical displacement

Natural frequency	1st (car body vertical translation)	2nd (car body pitching)	3rd (front bogie vertical translation)	4th (rear bogie vertical translation)
Value (Hz)	1.0594	1.2699	5.6804	5.6804

For the simulation purpose, the estimation algorithm makes use of the available practical sensors and its installation locations. Henceforth, acceleration and angular velocity measurements at train car body are considered. The conventional Kalman filtering technique causes numerical instabilities in augmented state-space model as the system itself is unobservable. In order to solve observability issue, two proposed approaches are utilized and results are presented. Figure 3.3 represents the numerical study results on reconstructing vertical track irregularity, using a Kalman filter and inverse modelling. Exactly assessing the track profile in the spatial domain is not as significant as precisely evaluating it in the spatial frequency domain. In order to relate the estimated and simulated true profile, PSD plots in frequency domain, considered by means of Welch's method need to be utilized. The statistical metrics of RMSD, RMSE and CC are calculated and illustrated in Table 3.5 which indicates that the performance of the proposed Approach (a) is better than the conventional ASKF and Approach (b). Since estimated track profile differs with the simulated FRA Class 4 profile, it must be illustrious that certain error is being occurred due to the simplified model. If pitching motion at bogie is considered, this issue can be rectified. Thus, 6 DOF train model need to be incorporated which includes bogie pitching motion.
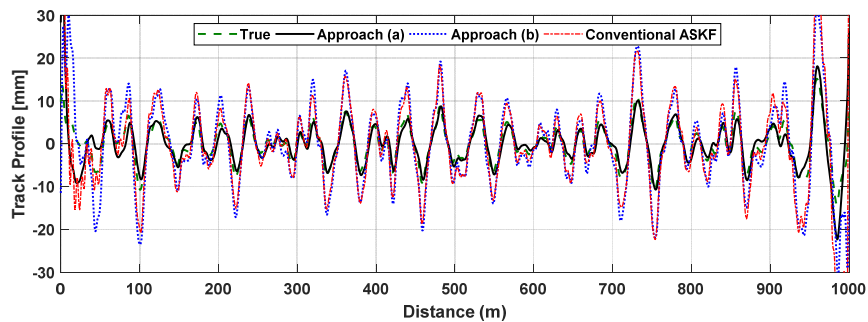
(a) Vertical track irregularity from from simplified 4DOF train vehicle model

55
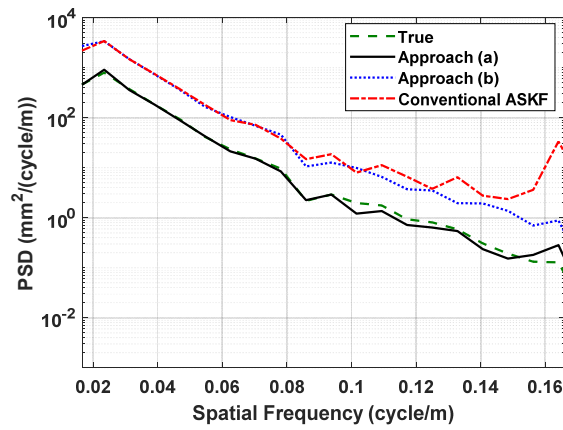
(b) PSD plot
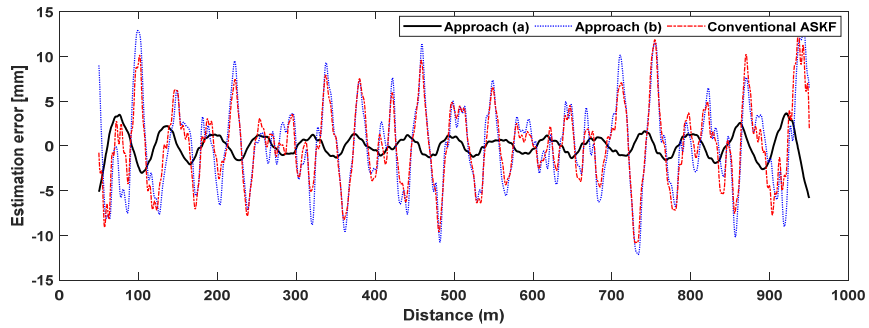
(c) Comparison of estimation error (for track length, 50 – 950 m)

Figure 3.3 Estimation results for vertical track irregularity

Table 3.5 Comparison of statistical metrics for estimation algorithms on 4 DOF train vehicle model for vertical track irregularity (for track length, 50 – 950 m)

Description	Statistical Metrics	Conventional ASKF	Approach (a)	Approach (b)
Vertical acceleration and pitch rate measurements at train car body	RMSD (%)	109.5	33.38	121.1
	CC	0.88	0.94	0.86
Comparison of estimation error	RMSE (mm)	4.34	1.32	4.74

3.4.1.2 A Simplified train vehicle model for estimating lateral track geometry

The condition monitoring of the lateral track alignment irregularity is extremely significant for the safe passage of railway vehicle. The lateral track profile can be estimated using the accelerometer and yaw rate gyro sensors mounted on to the in-service train vehicle. The lateral acceleration measurement and yaw angular velocity provides consistent estimate of the lateral track irregularity. For railway track profile estimation, numerical simulation using ASKF method for 4 DOF vehicle model with averaged track geometry (Figure 2.6) (a simplified vehicle model as explained in the previous chapter) is carried out in detailed manner. The accelerometer and rate gyro sensors are considered to be mounted on the car body floor just above the front bogie mass of the 6 DOF train model for the data assimilation inverse analyses. The car body lateral acceleration and yaw rate measurement responses are collected from 6 DOF train model (Figure 2.3) and utilized as the input response for simplified train model with 4 DOF where augmented Kalman filtering technique in implemented as inverse analysis.

Based on three formulations, railway track alignment profile estimation is numerically studied employing augmented Kalman filtering technique on the artificial profile generated using FRA standards. The reference vehicle parameters for train vehicle model are obtained from [94, 95] representing local railway network parameters as shown in Table 3.3. Furthermore, the vehicle is assumed to maintain a constant velocity of 90 km/h with simulated distance of 1000 m and sampling frequency of 100 Hz. Numerical simulation is incorporated with measurement noise levels generated as a random walk driven by Gaussian white noise and also initial condition error in the Kalman filter iteration in order to approximately obtain the exact profile. A typical case of simulated profile after using band pass filter with cut off spatial frequency of 0.0166 – 0.166 cycle/m, by incorporating noise level of 5 % (standard deviation of measured response and random error). Noise is added to simulated data based on the characteristics of practical sensors used to measure the respective signals. The parameters of the model are approximated based on the real vehicle. The filter considered in this simulation helps to evaluate wavelengths ranging between 6 m – 60 m, which covers ranges comprising from short to long wavelength irregularities as mentioned in [96]. Table 3.6 gives the natural frequency estimation of simplified train model (4 DOF) (for accounting lateral displacement). By using conventional Kalman filtering technique, the system becomes unobservable for the acceleration and angular velocity measurements at train car body. This causes numerical instabilities in augmented state-space model. In order to solve observability, issue two proposed approaches are utilized and results are presented.

Table 3.6 Natural frequency estimation of 4 DOF train model: for lateral displacement

Natural frequency	1st (car body lateral translation)	2nd (car body yawing)	3rd (front bogie lateral translation)	4th (rear bogie lateral translation)
Value (Hz)	0.8678	1.0414	9.8714	9.8718

Figure 3.4 represents the numerical study results on lateral track irregularity by reconstructing track geometry, using a Kalman filter and inverse modelling. Exactly assessing the track profile in the spatial domain is not as significant as precisely evaluating it in the spatial frequency domain. In order to relate the estimated and simulated true profile, PSD plots in frequency domain, considered by means of Welch's method need to be utilized. The statistical metrics of RMSD, RMSE and CC are calculated and illustrated in Table 3.7 which indicates that the performance of the proposed approach (a) and (b) are better than the conventional ASKF. This is due to the un-observability system in conventional ASKF method.
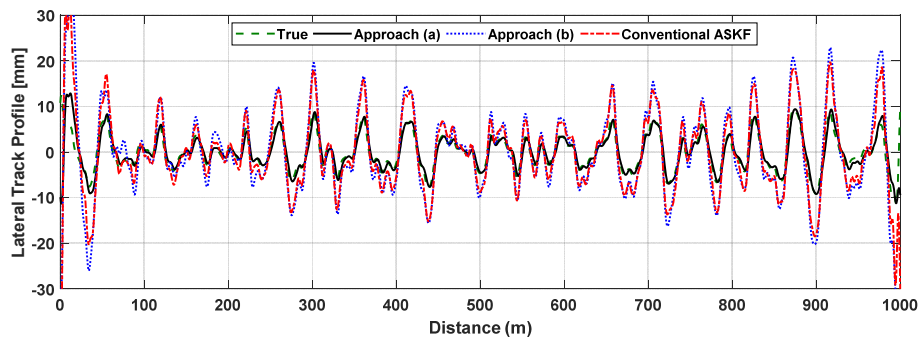
(a) Lateral track irregularity from simplified 4DOF train vehicle model
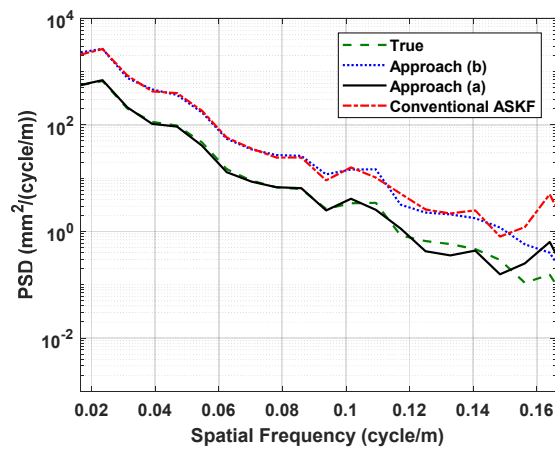
(b) PSD plot
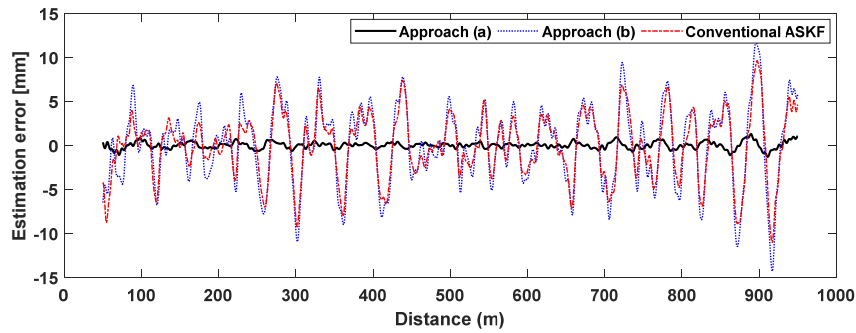
(c) Comparison of estimation error (for track length, 50 – 950 m)

Figure 3.4 Estimation results for lateral track irregularity

Since estimated track profile differs with the simulated FRA Class 4 vertical profile, it must be illustrious that certain error is being occurred due to the simplified model. If yawing motion at bogie is considered, this issue can be rectified. Thus, 6 DOF train model need to be incorporated which includes bogie yawing motion.

Table 3.7 Comparison of statistical metrics for estimation algorithms on 4 DOF train vehicle model for lateral track irregularity (for track length, 50 – 950 m)

Description	Statistical Metrics	Conventional ASKF	Approach (a)	Approach (b)
Lateral acceleration and yaw rate measurements at train car body	RMSD (%)	99.37	11.1	109.0
	CC	0.93	0.99	0.84
Comparison of estimation error	RMSE (mm)	3.65	0.41	4.37

3.4.2 Misfits Criteria for the Phase-Shift-Modified Signals

Quantitative assessment of time signals is frequently essential in many problems. There are many time-frequency misfit and goodness-of-fit criteria in the past [91-92]. Comparison of two measured signals considerably benefits in the analysis and interpretation of the process under investigation. A single-valued integral quantity is more is more appropriate if a set of signals is to be compared with the another set of signals. Finally, it is not clear whether they are able to accurately measure the difference. Therefore, there is necessity to use time-frequency envelope and phase misfit criteria to properly quantify and characterize a difference between two signals.

In this research, the profile obtained from Approach (a) using ASKF technique is performing better than the conventional method. But it is clear that some phase modification of the signal can be more understandable in the distance domain. This modification is carried out using the time-frequency misfit criteria using Hilbert transform technique. It returns a complex helical sequence, sometimes called the analytic signal, from a real data sequence. The discrete-time analytic signal comprises of real part, which is the original data, and an imaginary part, which contains the Hilbert transform. The imaginary part is a version of the original real sequence with a 90° phase shift. Sines are therefore transformed to cosines and conversely. The Hilbert transformed series has the same amplitude and frequency content as the original sequence and includes phase information that depends on the phase of the original. The Hilbert transform is useful in calculating instantaneous attributes of a time series, especially the amplitude and frequency. The instantaneous amplitude is the amplitude of the complex Hilbert transform; the instantaneous frequency is the time rate of change of the instantaneous phase angle. For a pure sinusoid, the instantaneous amplitude and frequency are constant. The instantaneous phase, however, is a saw-tooth, reflecting how the local phase angle varies linearly over a single cycle. For mixtures of sinusoids, the attributes are short term, or local, averages spanning no more than two or three points.

The Hilbert transform is applied to true signal and analytic signal is obtained is as shown below,

$$x_{true} = Hilbert\ Transform\ (x_{true\_real}) \qquad (3.34)$$

Discrete-time analytic signal, $\quad x_{true} = x_{real} + i * x_{img} \qquad (3.35)$

The phase of the true signal is obtained using the four-quadrant inverse tangent, which must be real,

$$\theta_{true} = tan^{-1}\left(\frac{x_{img}}{x_{real}}\right) \qquad (3.36)$$

Similarly, HT is applied to the estimated signal and the phase of the estimated signal is modified with the phase of the true signal obtained in Eq. (3.36),

$$x_{estimated} = Hilbert\ Transform\ (x_{est\_real}) \qquad (3.37)$$

$$x_{estimated} = x_{e\_real} + i * x_{e\_img} \qquad (3.38)$$

$$x_{updated} = absolute\ (x_{estimated}) * e^{i\theta_{true}} \qquad (3.39)$$

$$x_{updated\_real} = real\ (x_{updated}) \qquad (3.40)$$

Phase Correction, $\quad x_{est\_real} \rightarrow x_{updated\_real} \qquad (3.41)$

Estimated signal is updated with the phase angle of the true signal, thus, x_{true_real} and $x_{updated\_real}$ can be compared.

The profile obtained from Approach (a) method in both vertical and lateral track irregularity (as shown in Figures 3.3 and 3.4), need to be modified for phase shift error. By applying the proposed misfit criteria, the phase shift correction is carried out as shown in the Figure 3.5. Now the statistical metrics is evaluated for both old and updated waveform obtained from Approach (a) method and it is tabulated in the Table 3.8. After misfit criteria, the single-valued metrics show good improvement comparing to the old values. This phase modification criterion is utilized throughout the thesis to improve the profile obtained from Approach (a) method for both vertical and lateral profiles estimation.
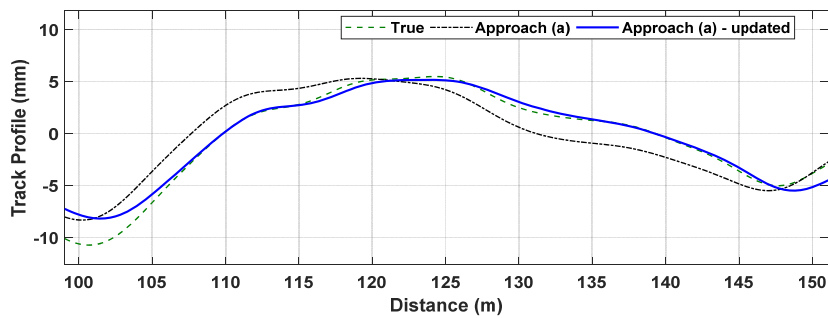
(a) Vertical profile
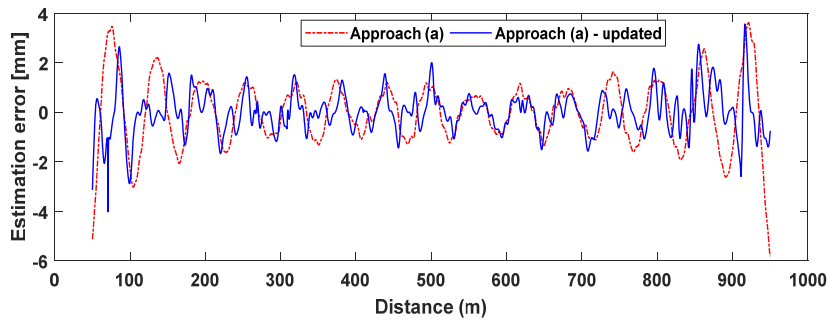
(b) Estimation error for vertical profile

(c) Lateral profile

61
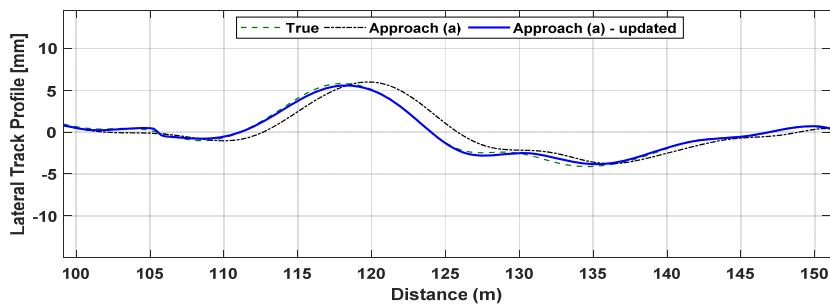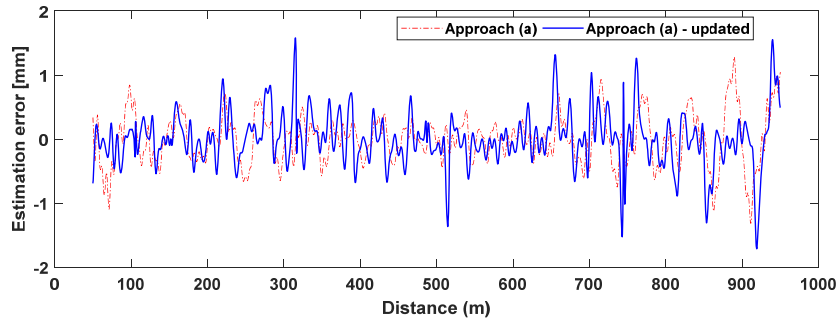
(d) Estimation error for lateral profile

Figure 3.5 Phase Correction for quantitative comparison of two waveforms

Table 3.8 Comparison of statistical metrics for misfit criteria (for track length, 50 – 950 m)

Description	Statistical Metrics	Vertical track profile		Lateral track profile	
		App (a)	App (a)-updated	App (a)	App (a)-updated
Phase correction for quantitative comparison of two waveforms	RMSD (%)	33.38	21.1	11.1	10.4
	CC	0.94	0.99	0.99	0.99
	RMSE (mm)	1.32	0.83	0.41	0.38

3.4.3 Train vehicle: 6 DOF model for vertical displacement

In order to assess the behavior of proposed ASKF estimation algorithm for railway track profile estimation, 6 DOF train vehicle model for vertical displacement with senor placement (Figure 3.6) is considered for numerical simulation which represents the real train where pitching motion in bogie mass is included. The estimated profile is the front wheel of the front bogie mass as shown in the Figure 3.6. Based on three formulations, railway track profile estimation is numerically studied employing ASKF technique on the artificial profile generated using FRA standards: Class 4 (very poor). The reference vehicle parameters for 6 DOF train model are shown in Table 3.3. Furthermore, numerical simulation is incorporated with the same assumptions as mentioned in the previous section (3.4.1.1). Table 3.9 gives the natural frequency estimation of 6 DOF train vehicle model accounting for vertical displacement.
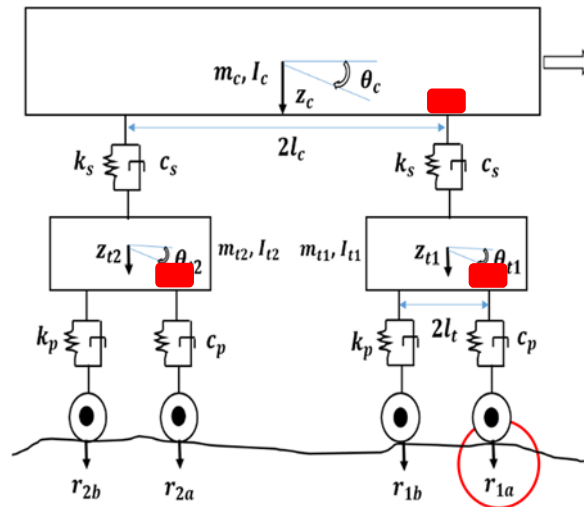
Figure 3.6 6 DOF train vehicle model (for vertical displacement) with sensor placement

Table 3.9 Natural frequency of 6 DOF train model: for vertical displacement

Natural frequency of Vehicle	Value (Hz)
1st (car body vertical translation)	1.0666
2nd (car body pitching)	1.2788
3rd (front bogie vertical translation)	5.9874
4th (front bogie pitching)	5.9925
5th (rear bogie vertical translation)	7.8031
6th (rear bogie pitching)	7.8031

Before carrying out the inverse analysis for vertical track profile estimation using 6 DOF, the vehicle model verification is done by implementing Kalman filtering technique with zero model error and zero noise. The measurement vector consists of six variables namely, displacements and thetas measured at train car body, front and rear bogies. From Figure 3.7, it can have observed that the estimated vertical and lateral track profile are in good agreement with the simulated rail track profile (FRA Class 4: very poor). The statistical metrics value for RMSD error are 3 % and 4 % for vertical and lateral profile respectively, which is negligible. For CC, it is 0.999 and 0.989 for vertical and lateral profile respectively, which shows it is well correlated.
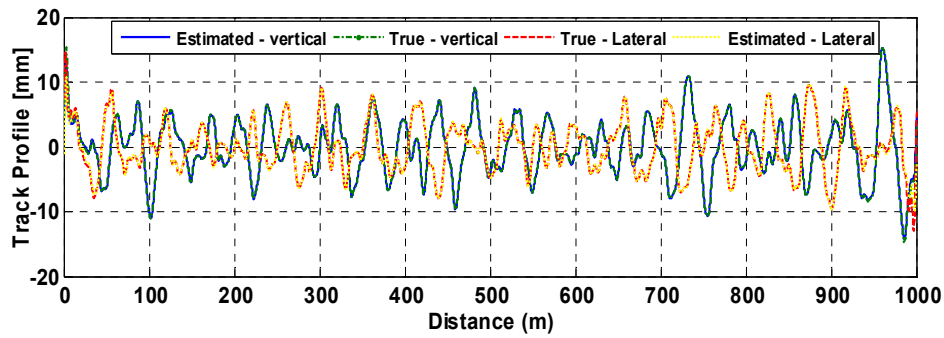
(a)
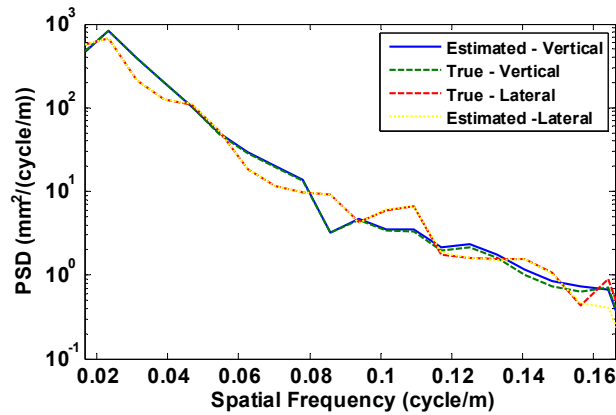
(b)

Figure 3.7 6 DOF train vehicle model for vertical and lateral displacement: (a) Comparison of estimated track profile with simulated FRA profile; (b) PSD plot

3.4.3.1 Measurement set up

For the simulation purpose, the following types of measurements are considered for the 6 DOF train vehicle model as per the ORC analysis results as discussed in the previous Chapter 2.

- M1: Vertical acceleration and pitching angular velocity measurements at car body only.
- M2: Vertical acceleration and pitching angular velocity measurements at car body, front and rear bogie masses.
- M3: Vertical acceleration and pitching angular velocity measurements at car body and front bogie masses.
- M4: Vertical acceleration measurement at car body and pitching angular velocity measurement at car body, front and rear bogie masses.
- M5: Vertical acceleration measurement at car body and pitching angular velocity measurement at car body and front bogie masses.

- M6: Vertical acceleration and pitching angular velocity measurements at front and rear bogie masses.
- T: Vertical acceleration and pitching angular velocity measurements at car body only in simplified 4 DOF train model for vertical displacement.

The measurement set: M1 do not satisfy observability condition. Even the second derivative of the profile remains unobservable. Still, it is considered in the numerical simulation for comparing with measurement set: T. Figures 3.8 - 3.13 are the rail track profile estimation results obtained from ASKF estimation algorithm for the simulated FRA Class - 4 vertical track profile, from the vehicle response measurement set-up as mentioned above (M1 – M6) and also measurement set: T. From the Figures 3.8 - 3.13, Approach (a) is performing better when comparing to conventional ASKF and Approach (b). Also measurement: M6 is performing poor when comparing to other measurement sets. The statistical metrics of RMSD and CC are calculated as per Equations (3.16) and (3.17) are tabulated in Table 3.10, which also indicate that the performance of the proposed Approach (a) is better than the conventional ASKF and Approach (b).
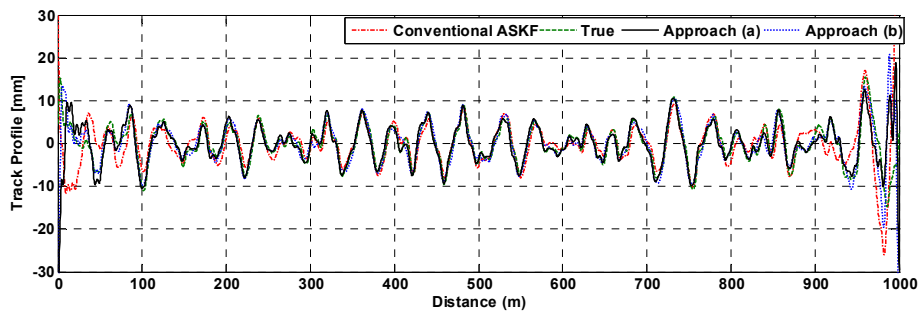
(a)
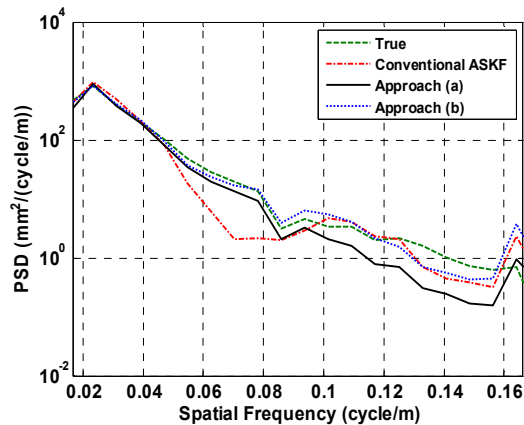
(b)

Figure 3.8 Comparison of estimated and simulated FRA - Class 4 track profile: (a) From measurement-M1 ($\ddot{z}_c$ $\dot{\theta}_c$); (b) PSD plot
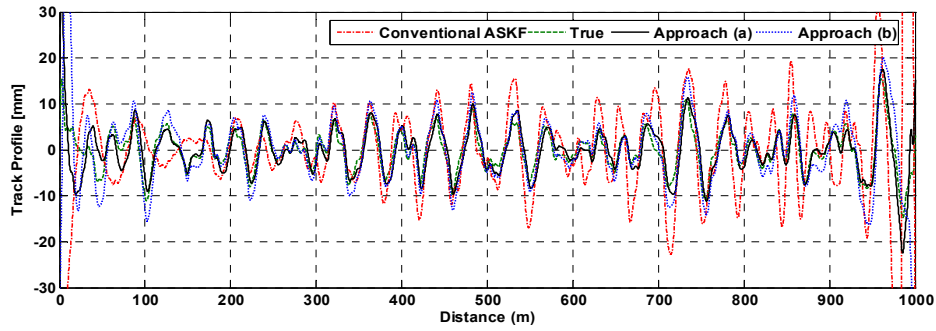
(a)
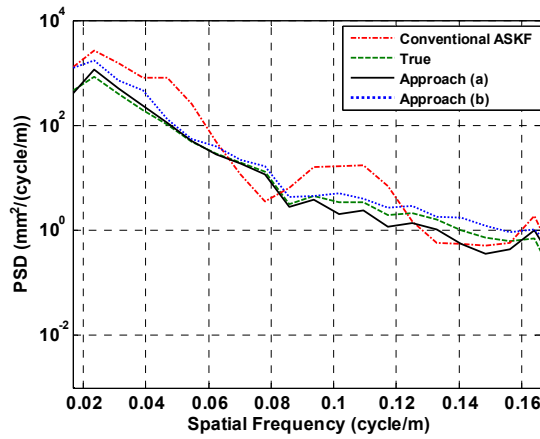
(b)

Figure 3.9 Comparison of estimated and simulated FRA - Class 4 vertical track profile: (a) From measurement-M2 ($\ddot{z}_c$ $\dot{\theta}_c$ $\ddot{z}_{t1}$ $\ddot{z}_{t2}$ $\dot{\theta}_{t1}$ $\dot{\theta}_{t2}$); (b) PSD plot

Exactly assessing the track profile in the spatial domain is not as significant as precisely evaluating it in the spatial frequency domain. In order to relate the estimated and simulated true profile, PSD plots in frequency domain, considered by means of Welch's method need to be utilized. Henceforth, the rail track profile estimated using proposed algorithm Approach (a), is considered for all measurement sets and a comparison PSD plot is shown in Figure 3.14. The inference obtained from Figure 3.14 (b) confirms that the measurement: M1 is performing poor when comparing to all other measurement sets, which resulted in second derivative of profile unobservable. It explains that even though M2 to M6 is performing relatively in similar manner, PSD plot clearly illustrates the difference among them. The measurement- M2 ($\ddot{z}_c$ $\dot{\theta}_c$ $\ddot{z}_{t1}$ $\ddot{z}_{t2}$ $\dot{\theta}_{t1}$ $\dot{\theta}_{t2}$) is the maximum possibility for the sensor placement which in turn must produce the good results in ASKF inverse analysis technique. On the other hand, since the front wheel profile of front bogie mass is utilized for estimation, the measurement-M3 ($\ddot{z}_c$ $\dot{\theta}_c$ $\ddot{z}_{t1}$ $\dot{\theta}_{t1}$) is sufficient for estimating the vertical track profile geometry. It is evident from the comparison of statistical metrics (Table 3.10) and PSD plot (Figure 3.14 (b)).

66
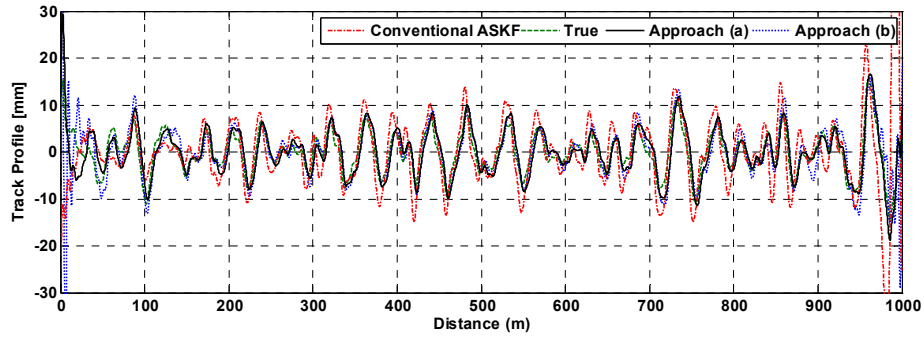
(a)
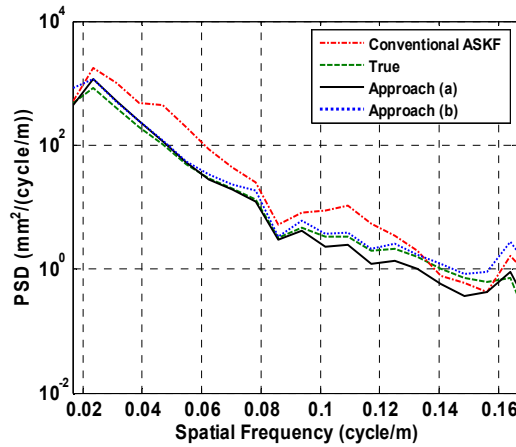
(b)

Figure 3.10 Comparison of estimated and simulated FRA - Class 4 track vertical profile: (a) From measurement-M3 ($\ddot{z}_c$ $\dot{\theta}_c$ $\ddot{z}_{t1}$ $\dot{\theta}_{t1}$); (b) PSD plot

Also, the estimated track profile using conventional method (T) considered in [30] is performing poor and hence it is comparatively improved by the proposed ASKF method: Approach (a). Thus, by utilizing 6 DOF train model which considers bogie pitching motion, vertical rail track profile can be estimated accurately using proposed ASKF method.

(a)

67
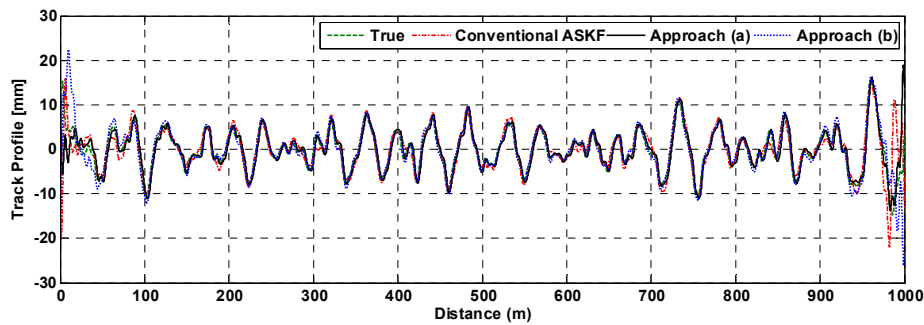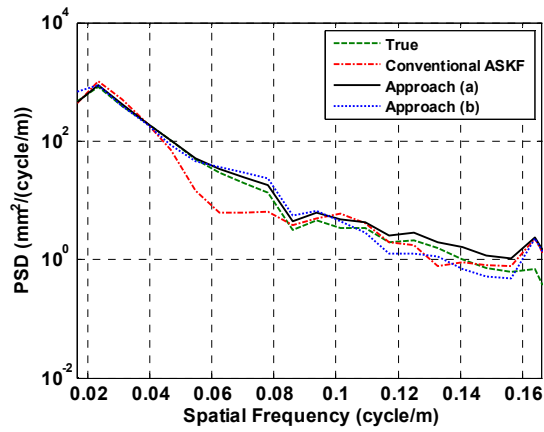
(b)

Figure 3.11 Comparison of estimated and simulated FRA - Class 4 track vertical profile: (a) From measurement-M4 ($\ddot{z}_c\ \dot{\theta}_c\ \dot{\theta}_{t1}\ \dot{\theta}_{t2}$); (b) PSD plot
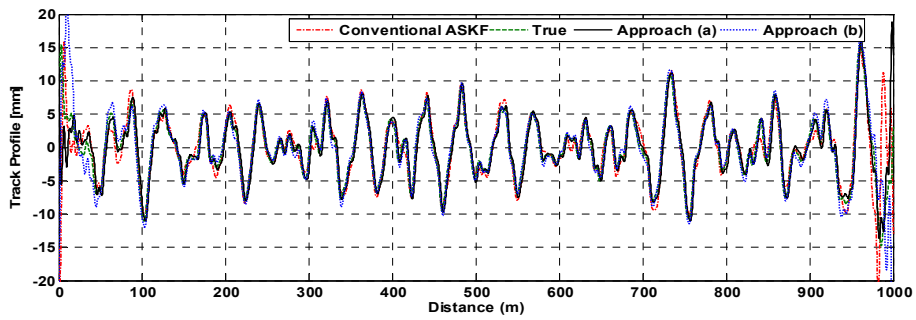
(a)
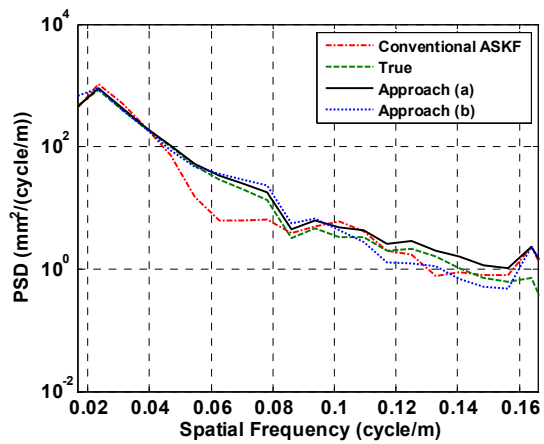
(b)
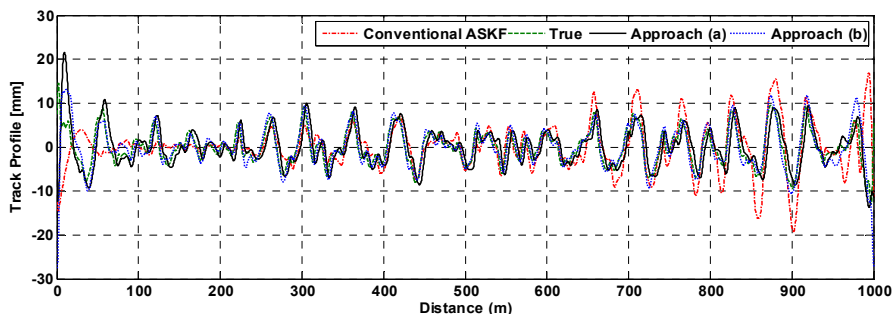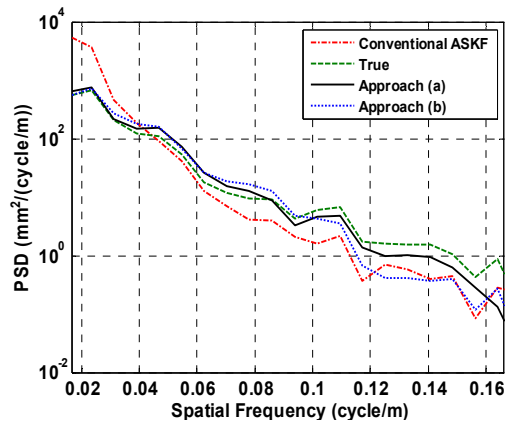
Figure 3.12 Comparison of estimated and simulated FRA - Class 4 track vertical profile: (a) From measurement-M5 ($\ddot{z}_c\ \dot{\theta}_c\ \dot{\theta}_{t1}$); (b) PSD plot
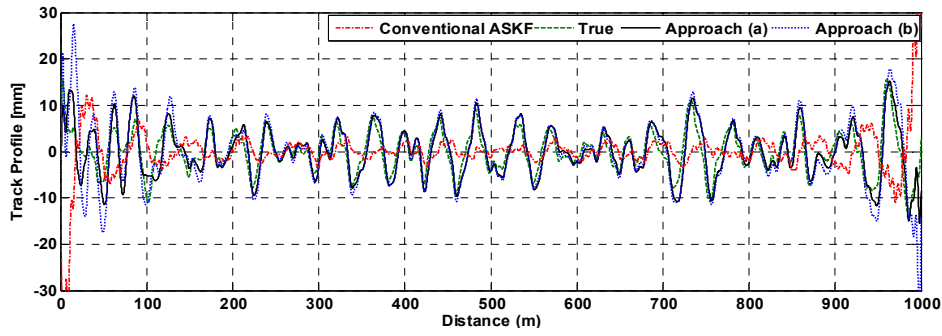
(a)
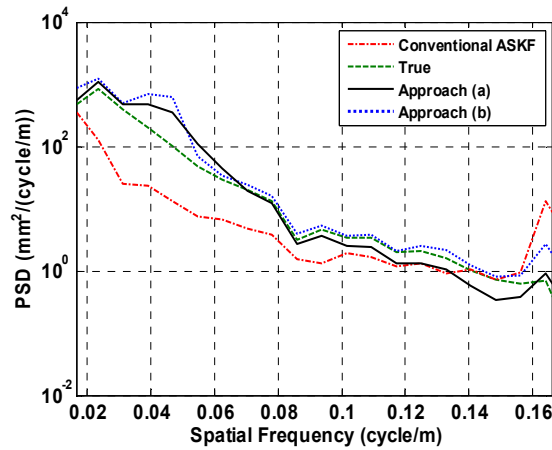
(b)

Figure 3.13 Comparison of estimated and simulated FRA - Class 4 track vertical profile: (a) From measurement-M6 ($\ddot{z}_{t1}$ $\ddot{z}_{t2}$ $\dot{\theta}_{t1}$ $\dot{\theta}_{t2}$); (b) PSD plot

Figure 3.14 (c) gives the comparison of estimation error for M2 and M3 which has value less than ± 1.5 mm. Also second part of the Table 3.10 shows that the comparison of statistical metrics after applying misfit criteria and it can be concluded that the measurement set M3 is performing close to M2. Therefore, depending upon the sensors availability and feasible sensor placement locations in the real field measurement, vertical rail track geometry can be reconstructed using inverse modelling and extended ASKF algorithm with proposed Approach (a) method. For the optimal sensor placement, the measurement set M3 ($\ddot{z}_c$ $\dot{\theta}_c$ $\ddot{z}_{t1}$ $\dot{\theta}_{t1}$) can be utilized for mounting on in-service railway vehicle for robust track condition monitoring using proposed data assimilation inverse analysis ASKF technique.
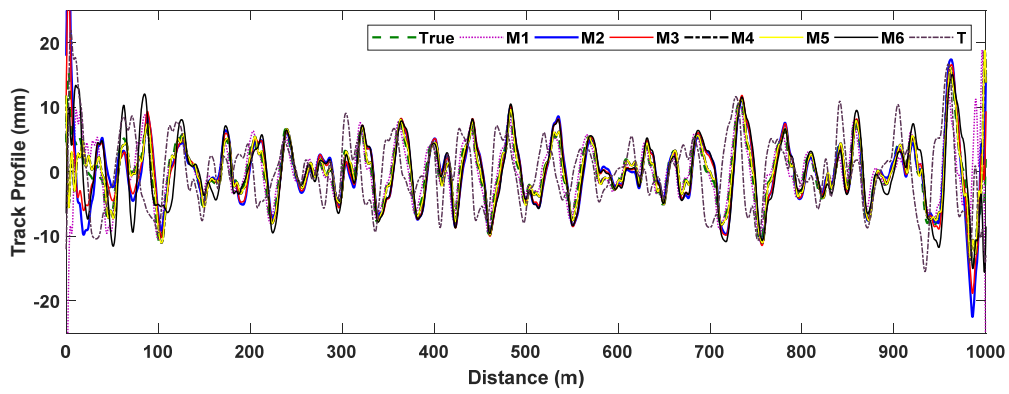
(a)
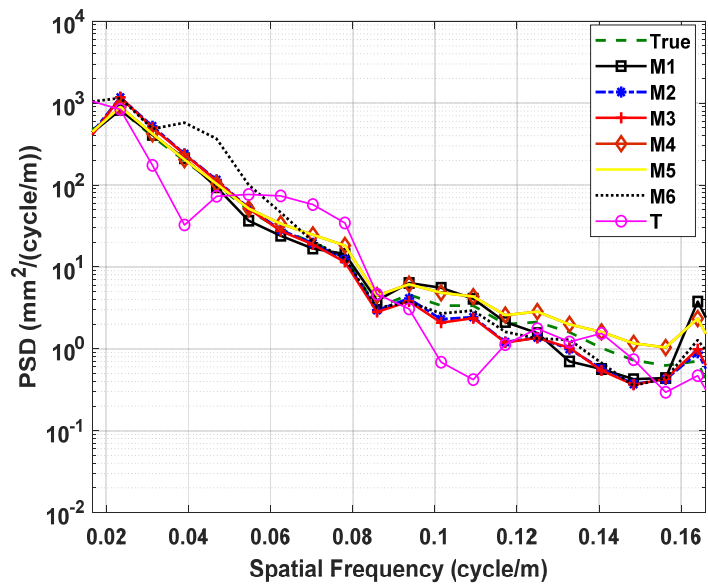
(b)
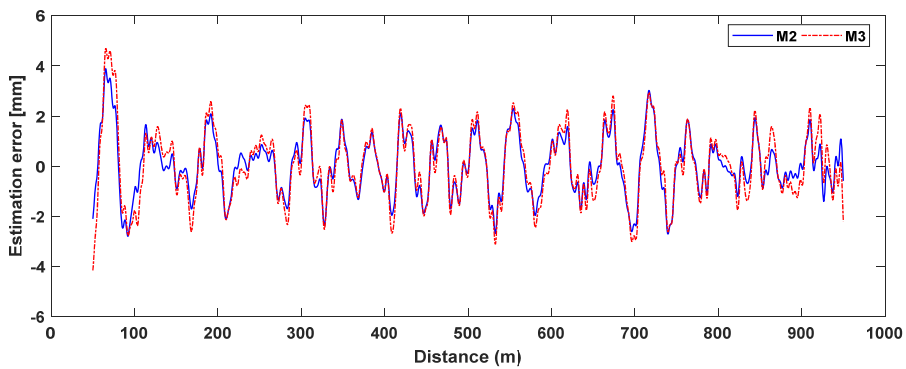
(c)

Figure 3.14 Profile obtained from Approach (a): (a) Comparison of estimated profile with simulated FRA - Class 4 vertical track profile; (b) PSD plot; (c) Estimation error after misfit criteria (for track length of 50-950 m)

70

Table 3.10 Comparison of estimation algorithms on 6 DOF train vehicle model using statistical metrics for FRA - Class: 4 vertical track profile

Measurements	Statistical Metrics	Conventional ASKF	Approach (a)	Approach (b)
M1	RMSD (%)	146.9	133.9	192.7
	CC	0.43	0.53	0.48
M2	RMSD (%)	135.9	50.1	118.2
	CC	0.26	0.89	0.78
M3	RMSD (%)	157.6	53.2	68.1
	CC	0.28	0.89	0.87
M4	RMSD (%)	154.9	45.8	52.3
	CC	0.30	0.89	0.89
M5	RMSD (%)	162.8	45.9	52.1
	CC	0.32	0.89	0.89
M6	RMSD (%)	203.1	61.8	90.7
	CC	0.30	0.85	0.82
Comparison of Estimation error after misfit criteria (length of 50-950 m):				
M2	RMSD (%)	105.5	28.9	87.4
	CC	0.68	0.97	0.84
	RMSE (mm)	4.27	1.17	3.87
M3	RMSD (%)	154.1	34.2	58.7
	CC	0.55	0.94	0.89
	RMSE (mm)	6.23	1.38	4.22

3.4.4 Train vehicle: 6 DOF model for lateral displacement

In order to assess the behavior of proposed ASKF estimation algorithm for lateral track profile estimation, 6 DOF train vehicle model for lateral displacement (Figure 3.15) is considered for numerical simulation which represents the real train where yawing in bogie is included. The estimated profile is the front wheel of the front bogie mass (s_{1a}). Based on three formulations, lateral track profile estimation is numerically studied employing ASKF technique on the simulated profile generated using FRA standards. The reference vehicle parameters for 6 DOF train model are shown in Table 3.3. Furthermore, numerical simulation is incorporated with the same assumptions as mentioned in the previous section (3.4.1.2). Table 3.11 gives the natural frequency estimation of 6 DOF train vehicle model accounting for lateral displacement.
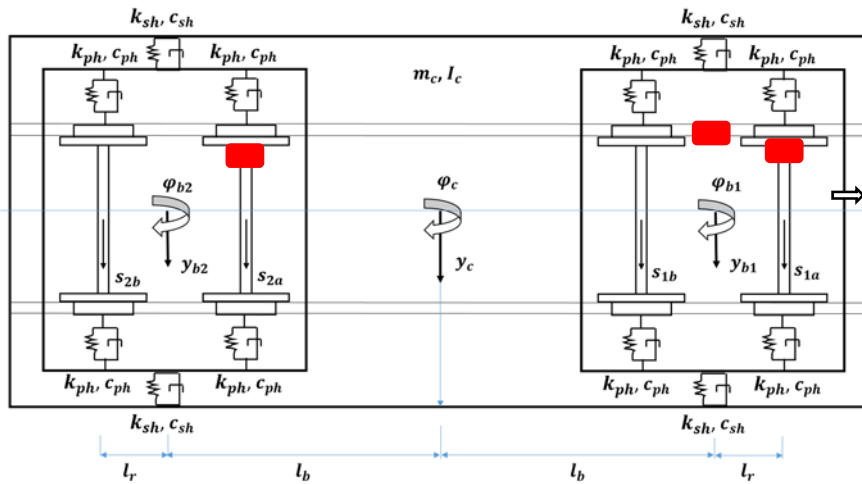
Figure 3.15 6 DOF train vehicle model (for lateral displacement) with sensor placement

Table 3.11 Natural frequency estimation of 6 DOF train model: for lateral displacement

Natural frequency of Vehicle	Value (Hz)
1st (car body lateral translation)	0.8681
2nd (car body yawing)	1.0416
3rd (front bogie lateral translation)	9.9813
4th (front bogie yawing)	9.9817
5th (rear bogie lateral translation)	14.2587
6th (rear bogie yawing)	14.2587

3.4.4.1 Measurement set up

- A1: Lateral acceleration and yawing angular velocity measurements at car body only.
- A2: Lateral acceleration and yawing angular velocity measurements at car body, front and rear bogie masses.
- A3: Lateral acceleration and yawing angular velocity measurements at car body and front bogie masses.
- A4: Lateral acceleration measurement at car body and yawing angular velocity measurement at car body, front and rear bogie masses.
- A5: Lateral acceleration measurement at car body and yawing angular velocity measurements at car body and front bogie masses.
- A6: Lateral acceleration and yawing angular velocity measurements at front and rear bogie masses.

- S: Lateral acceleration and yawing angular velocity measured at car body in simplified 4 DOF train model with averaged track geometry (Figure 2.6)

Figures 3.16 - 3.21 are the rail track profile estimation results obtained from ASKF estimation algorithm for the simulated FRA Class - 4 vertical track profile, from the vehicle response measurement set-up as mentioned above (A1 – A6) and also measurement set (S). From the Figures 3.16 - 3.21, Approach (a) is performing better when comparing to conventional ASKF and Approach (b). The statistical metrics of RMSD and CC are tabulated in Table 3.12, which also indicate that the performance of the proposed Approach (a) is better than the conventional ASKF and Approach (b). In order to relate the estimated and simulated true profile, PSD plots in frequency domain, considered by means of Welch's method need to be utilized. Henceforth, the rail track alignment profile estimated using proposed algorithm Approach (a), is considered for all measurement sets and a comparison PSD plot is shown in Figure 3.22 (b). It explains that even though A2 to A5 is performing relatively in similar manner, PSD plot clearly illustrates the difference among them.

(a)

(b)
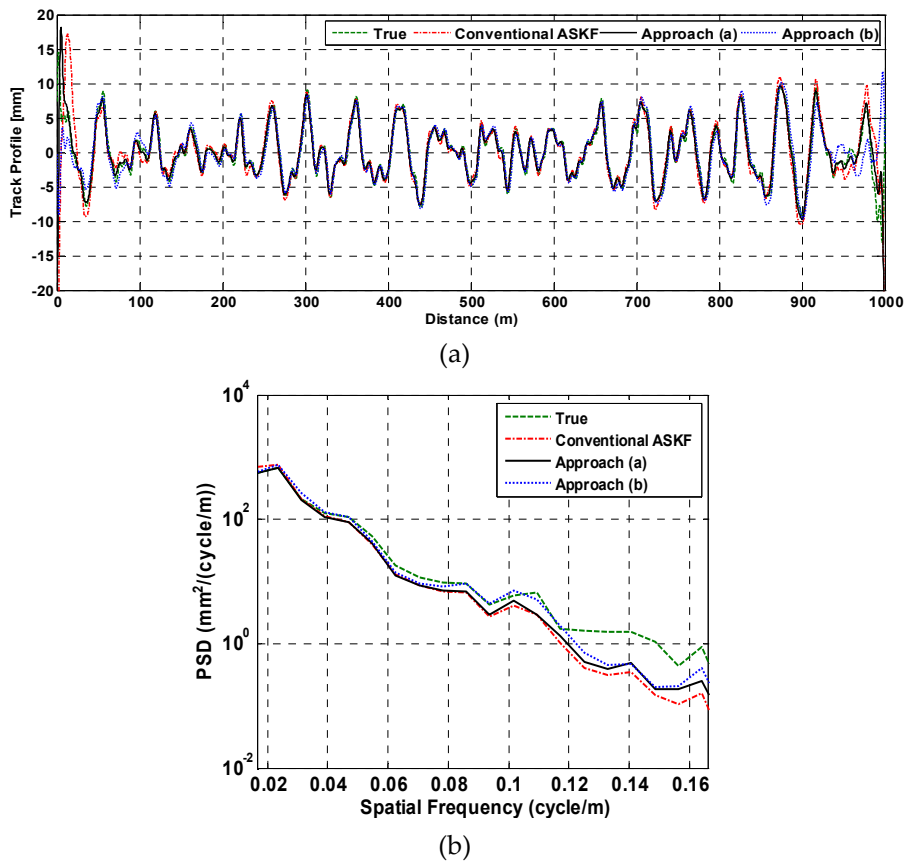
Figure 3.16 Comparison of estimated and simulated FRA - Class 4 alignment track profile: (a) From measurement-A1 ($\ddot{y}_c$ $\dot{\varphi}_c$); (b) PSD plot
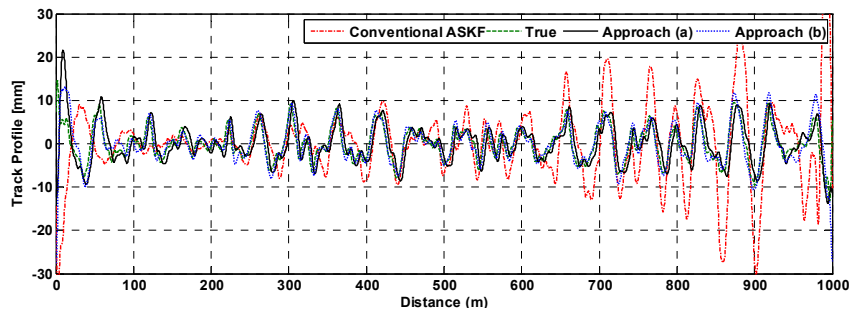
(a)
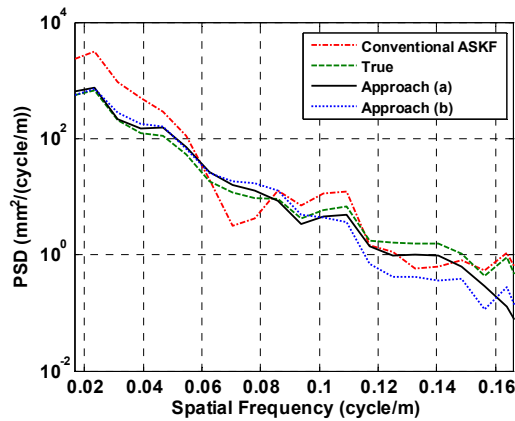
(b)

Figure 3.17 Comparison of estimated and simulated FRA - Class 4 alignment track profile: (a) From measurement-A2 ($\ddot{y}_c\ \dot{\varphi}_c\ \ddot{y}_{b1}\ \ddot{y}_{b2}\ \dot{\varphi}_{b1}\ \dot{\varphi}_{b2}$); (b) PSD plot

The inference obtained from Figure 3.22 confirms that the measurement: A1 is performing slightly poor when comparing to other measurement sets, which is in turn the unobservable system. The measurement A2 ($\ddot{y}_c\ \dot{\varphi}_c\ \ddot{y}_{b1}\ \ddot{y}_{b2}\ \dot{\varphi}_{b1}\ \dot{\varphi}_{b2}$) with the maximum number of sensor placement should produce good results in ASKF inverse analysis technique as mentioned in the Table 3.11. Also, the estimated profile using simplified 4 DOF model (S) is poor when comparing with A2 and A3 cases.

(a)

(b)

Figure 3.18 Comparison of estimated and simulated FRA - Class 4 alignment track profile: (a) From measurement-A3 ($\ddot{y}_c$ $\dot{\varphi}_c$ $\ddot{y}_{b1}$ $\dot{\varphi}_{b1}$); (b) PSD plot
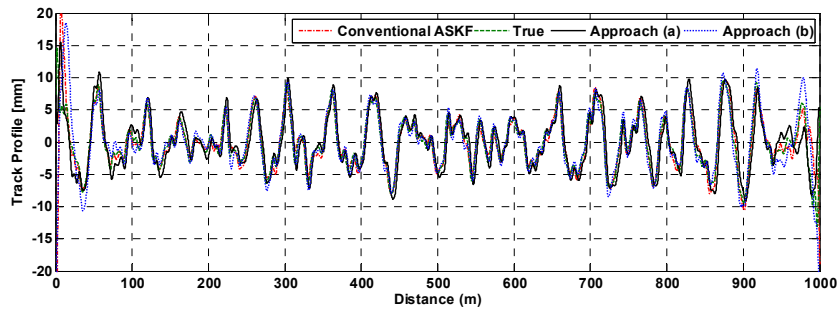
(a)
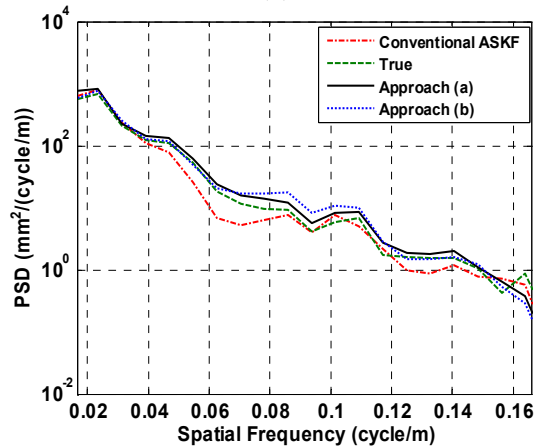
(b)

Figure 3.19 Comparison of estimated and simulated FRA - Class 4 alignment track profile: (a) From measurement-A4 ($\ddot{y}_c$ $\dot{\varphi}_c$ $\dot{\varphi}_{b1}$ $\dot{\varphi}_{b2}$); (b) PSD plot

On the other hand, since the front wheel profile of front bogie mass is utilized for estimation in the numerical simulation using ASKF techniques, the measurement-A3 ($\ddot{y}_c$ $\dot{\varphi}_c$ $\ddot{y}_{b1}$ $\dot{\varphi}_{b1}$) is sufficient for estimating the lateral track profile geometry. It is evident from the comparison of statistical metrics (Table 3.12) and PSD plot (Figure 3.22 (b)). From Figure 3.22 (c), the

comparison of estimation error for A2 and A3 is less than ± 2 mm. Also second part of the Table 3.12 shows that the comparison of statistical metrics after applying misfit criteria and it can be concluded that the measurement set A3 is performing close to A2.
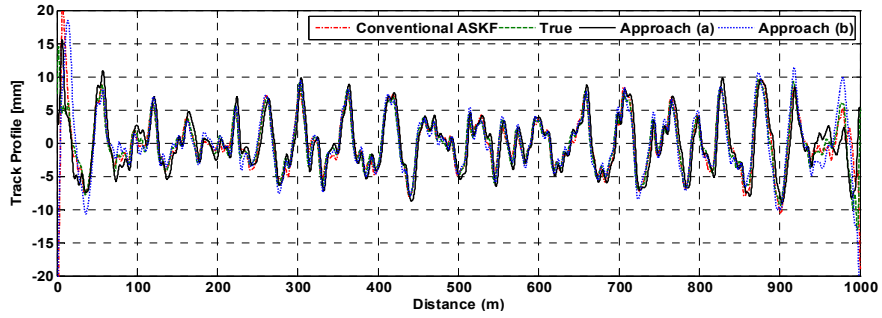
(a)
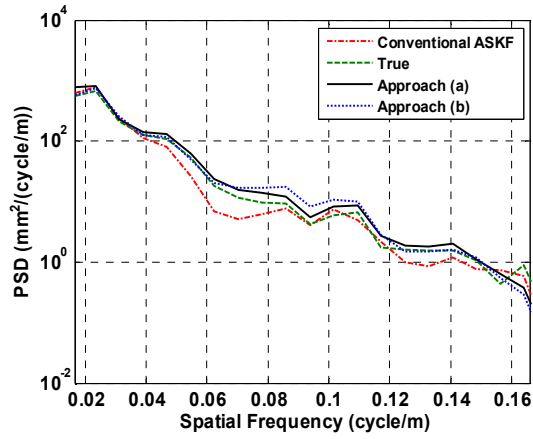
(b)

Figure 3.20 Comparison of estimated and simulated FRA - Class 4 alignment track profile: (a) From measurement-A5 ($\ddot{y}_c$ $\dot{\varphi}_c$ $\dot{\varphi}_{b1}$); (b) PSD plot
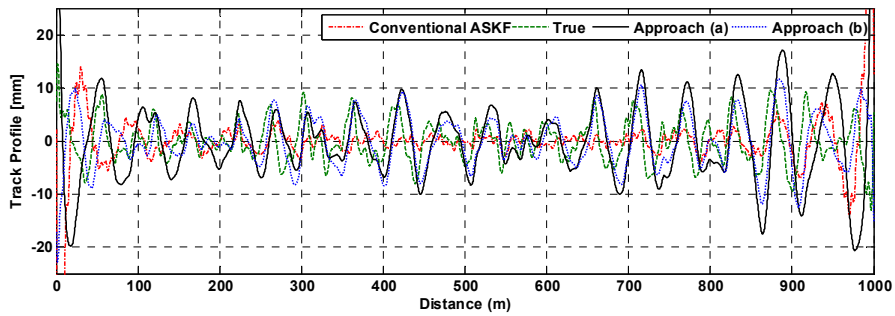
(a)
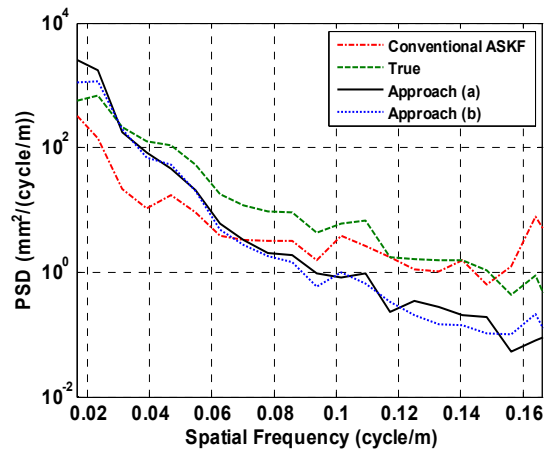
(b)

Figure 3.21 Comparison of estimated and simulated FRA - Class 4 alignment track profile: (a) From measurement-A6 ($\ddot{y}_{b1}$ $\ddot{y}_{b2}$ $\dot{\varphi}_{b1}$ $\dot{\varphi}_{b2}$); (b) PSD plot
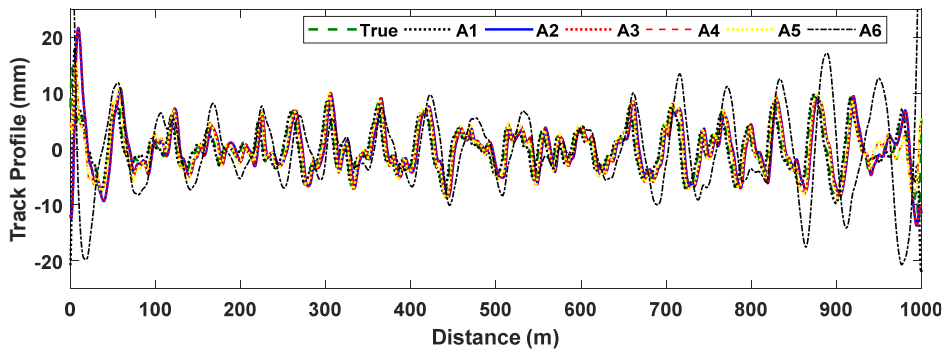
(a)
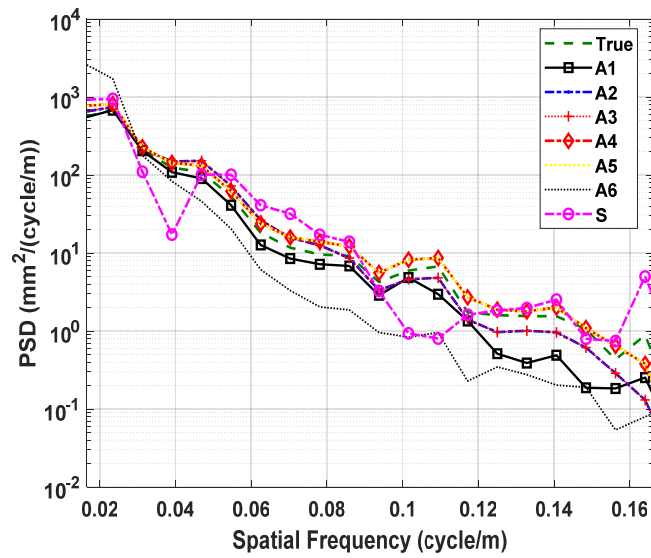
(b)
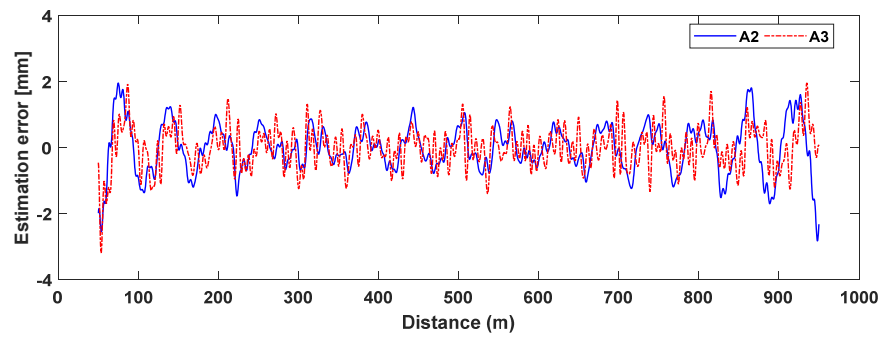
(c)

Figure 3.22 Profile obtained from Approach (a): (a) Comparison of estimated profile with simulated FRA - Class 4 alignment profile; (b) PSD plot; (c) Estimation error after misfit criteria (for track length of 50-950 m)

Table 3.12 Comparison of estimation algorithms on 6 DOF train vehicle model

Measurements	Statistical Metrics	Conventional ASKF	Approach (a)	Approach (b)
A1	RMSD (%)	98.1	56.7	75.1
	CC	0.69	0.84	0.76
A2	RMSD (%)	219.1	56.1	97.3
	CC	0.19	0.88	0.73
A3	RMSD (%)	278.8	52.6	92.3
	CC	0.29	0.88	0.76
A4	RMSD (%)	268.4	52.3	65.7
	CC	0.29	0.88	0.83
A5	RMSD (%)	263.1	52.2	65.6
	CC	0.32	0.88	0.83
A6	RMSD (%)	225.4	176.7	156.4
	CC	0.11	0.26	0.27
Comparison of Estimation error after misfit criteria (length of 50-950 m):				
A2	RMSD (%)	155.5	16.3	72.1
	CC	0.67	0.99	0.76
	RMSE (mm)	5.87	0.61	2.72
A3	RMSD (%)	142.2	18.1	39.8
	CC	0.79	0.99	0.91
	RMSE (mm)	2.39	0.68	1.88

Therefore, depending upon the sensors availability and feasible sensor placement locations in the real field measurement, alignment track geometry can be reconstructed using inverse modelling and extended ASKF algorithm with proposed Approach (a) method.

3.5 Discussions and Summary

The track profile estimation from the in-service vehicle response measurement by employing inverse analysis based on extended augmented state Kalman filtering analyses is being studied in this chapter. The measurement matrix consists of only acceleration and angular velocity responses. In inverse analysis, the second derivative of the profile is included in the state vector as one of the additional state variable, and thus the profile can be obtained through double integration of it. Different types of vehicle models are considered with appropriate sensor types and their locations, for the numerical analyses and the results are presented. The two approaches to obtain the second derivative of profile as an observable state variable are examined. These analyses indicate that the profile can be estimated by an accelerometer and a gyro on car body and bogie. The profile is expected to be obtained by the double integration of the high pass-filtered second derivative. Thus, a numerical study on extension of ASKF for input dynamic force reconstruction is presented. The performances are compared numerically using linear vehicle models, namely, simplified train model (4 DOF) and 6 DOF vehicle model (train). The further studies are being conducted for the effective track profile estimation using practical sensors and its installation locations on in-service train vehicle.

Chapter 4   MULTI-BODY SIMULATION FOR TRACK PROFILE ESTIMATION FROM VEHICLE RESPONSES

4.1   Introduction

The multibody system approach, with the development of computer technology, is clearly an added value in the analysis and design of mechanical and mechatronic systems. In vehicle system dynamics, the Multi-Body Simulation (MBS) software tool helps to integrate the simulation, analysis and optimization of the non-linear dynamic performance of the vehicle and it components [2, 128-131]. In this chapter, multi-body dynamics modelling of train vehicle is presented and the measurement responses from the car body and bogie mass are obtained while running on the track from MBS – SIMPACK: Rail software. The measured responses are utilized in the data assimilation inverse analysis problem to estimate the vertical and lateral track geometry profile. The proposed estimation algorithm based on extension of Augmented State Kalman Filter (ASKF) technique is being validated using the simulation results. All the obtained simulation results are reported in the following sections of this chapter.

4.2   Workflow for modelling MBS train vehicle

The following paragraphs describes about the significance of the modelling elements that need to be utilized for multi-body dynamics modelling of train vehicle using SIMPACK: Rail [128-131].

The SIMPACK: *Pre View Set* is the main pre-processor used for creating and editing models and starting online or offline *Solvers*. *Bodies* are the basic modelling elements and introduce mass and inertia properties. Rigid Bodies, which do not change their geometry or mass

properties during the simulation. They may be rigid or flexible. All components of the train - vehicle dynamics model are considered as rigid. *Bodies* are connected to other *Bodies* or *Reference Systems* by means of *Joints*, forming a kinematic tree.

Each *Body* has a *Body Reference Frame* (BRF) that represents the main coordinate system and follows its movement during the simulation. Most parts of a rail vehicle model in SIMPACK are made of standard Modelling Elements. Only the contact between the rails and wheels and the track require specialized Modelling Elements. *Wheelsets* relate one left-hand and one right-hand *Rail-Wheel Pair* to each other. They additionally contain the necessary information for the contact quasilinearization. *Rails* are passive modelling elements that hold all information about the rail profile and the built-in geometry.

In rail vehicle models, Rails are mandatory because they are referenced by *Rail-Wheel Pairs*. It contains all settings needed to bring one rail and one wheel into contact. They control the associated *Force Element*, *Markers* and *Primitives*. The modelling element *Rail-Wheel Contacts* define how the tangential forces and the tangential torque for the rail-wheel contact patches are calculated. It is referenced by a *Rail-Wheel Pair*. It provides the functionality for the tangential forces and torque in contact patches when the equivalent elastic rail-wheel contact is used.

The discrete elastic contact always uses a method that is derived from *Rail-Wheel Contact FASTSIM* (A Fast Algorithm for the Simplified Non-Linear Theory of Contact) according to [147]. It is well-accepted and the most common method in multibody simulation for determining the tangential rail-to-wheel contact forces in vehicle dynamics calculations. The method assumes that the contact patch is elliptical and provides rail-to-wheel tangential forces. The method is quasi static its validity is generally accepted for excitation frequencies up to about 20 Hz (i.e. excitations from track irregularities). *Excitation* for creating Track irregularity signals in distance domain is from *Input Functions*. It also ensures a reasonable spline interpolation and derivative handling. Track or rail related irregularities (*Track Excitation*) to be used in time domain simulations are defined in the *Track* element. They apply to the rail profile reference *Markers* of all *Rail-Wheel Pairs* automatically, including the appropriate time delay according to the position of the respective wheel along the track.

The modelling element '*Sensors*' provide an easy way to measure distances and angles including the related velocities and accelerations. *Sensors* do not influence the model topology, states or behaviour. As a consequence, only the *Measurements solver* needs to be re-run when *Sensors* are added, modified or removed and the solver splits its calculation in the actual solution run and an additional *Measurements* run, e.g. Time Integration, Kinematics or Equilibrium. Sensors are mounted between two *Markers*, namely the *From Marker* and the *To Marker*, and perform their measurements between these Markers. For absolute measurements, use the *Isys Marker* as *From Marker*.

The *Equilibrium solvers* try to bring a model into a static (or quasi-static) equilibrium. They do this by modifying the *Joint* and *Body* position and/or velocity states, which define the kinematic state of the model, and the dynamic states of *Force* or *Control Elements*. The *Static Equilibrium solvers* fully consider all non-linearities in the model. Non-linear models may have more than one equilibrium state. In these cases, it strongly depends on the initial model state and their parameters which equilibrium state will actually be found. The *Preload solver* tries to bring the model into an equilibrium by calculating the necessary preloads (nominal forces) in *Force Elements* and some *Control Elements*. These elements provide the possibility to define a constant nominal or preload force or torque, which is added to the force or torque from the actual characteristics.

The simplest case is a pre-loaded linear spring where, $F = c \cdot x + F_{preload}$. *Preloads* are most often used to resemble a pre-stressing of a spring due to the gravity. It calculates the preloads automatically so that the model is in an equilibrium, i.e. the residual accelerations become zero or at least very small. The automatic solution is helpful or even indispensable for complex models with many preloads in different directions where a manual calculation is difficult or impossible.

The *Time Integration solver* calculates the complete behaviour of the multibody model in time domain. There is both an online and an offline *Time Integration solver*. The online solver animates the motion in the 3D Page as the solver runs, the offline solver outputs the results to file. It determines the complete behaviour of the fully non-linear model in time, by solving the full set of non-linear equations of motion over the time. The *Measurements solver* must be used to generate the full set of results. *SODASRT* 2 is SIMPACK's default integrator. This integrator is accurate, very fast and very robust, i.e. it can start from extreme non-equilibrium situations. It is a BDF integrator (backward differentiation formula, an implicit multistep integration scheme), that make highly efficient multibody simulation possible. *SIMPACK Post* is required for visualizing results generated by the other SIMPACK modules.

4.3   Multi-body Dynamics Modelling of Train

As the literature review in Chapter 1, there were various models of train vehicle systems in the previous research. The model used in this research study is introduced in this section. Multi-body system simulation or multi-body dynamics is used to predict and optimize the behaviour of any type of multibody system by solving the equations of motion. The bodies of a multibody system are linked by means of joints and kinematic constraints, which allow certain relative motions and restrict others. The bodies themselves can be rigid or flexible. The DOFs are represented by a number of independent state variables that define the motion of the body

(displacement, deformation). The movements within these DOFs are influenced by arbitrary forces and torques provided by according elements. The system is finished by input excitation and sensors for measuring the preferred outputs. In describing the kinematic behaviour, the motion or the position of the multi- body system is studied with respect to the kinematic joints [146]. The SIMPACK solvers convert the Modelling Elements and model structure into a set of non-linear ordinary differential equations. The complete set of equations is then called differential-algebraic equations. SIMPACK models can built up from multiple so-called *sub-models*. Different components of the complete model can be defined in separate SIMPACK models. These individual sub-models can then be loaded into parent models to provide a modular construction of the entire system. The sub-modelling approach, via the Modelling Element Substructures, allows varying complexity for different analyses; the respective sub-models need only to be switched in the Substructure. Substructures themselves can also contain Substructures; these Substructures are called nested Substructures. There is no limit to the number of nesting levels. In this present research, for MBS train vehicle is modeled as a 42 DOFs multi-body system, which considers the dynamic features of the suspension systems and the longitudinal motion of the vehicle components. It includes seven rigid components namely, a car body, two bogie masses and four wheelsets. Individually all module of the train car has six DOFs: X (longitudinal displacement), Y (lateral displacement), Z (vertical displacement), θ (pitch angle), ψ (roll angle) and φ (yaw angle). The complete train vehicle model is built as the prototype of the commercial train, which contains all seven components along with the defined track. The multi-body model of train is constructed as shown in the topology diagram in Figure 4.1.
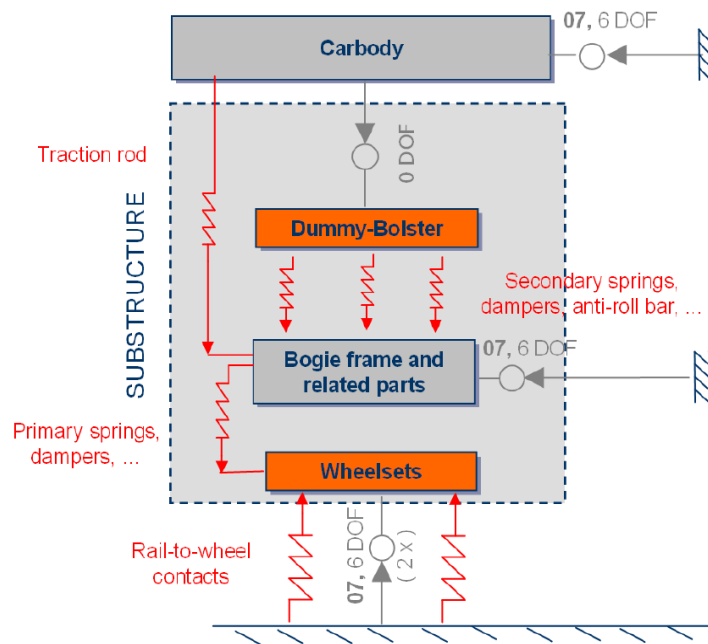
Figure 4.1 Schematic model topology of a train vehicle (2D block diagram) [128]

After assembling various components of vehicle along with primary and secondary suspension system, the complete 3D train model can be obtained as shown in Figure 4.2.
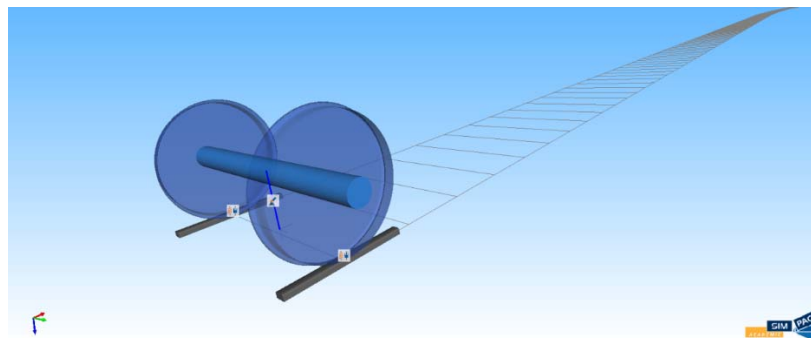
(a) Wheel set
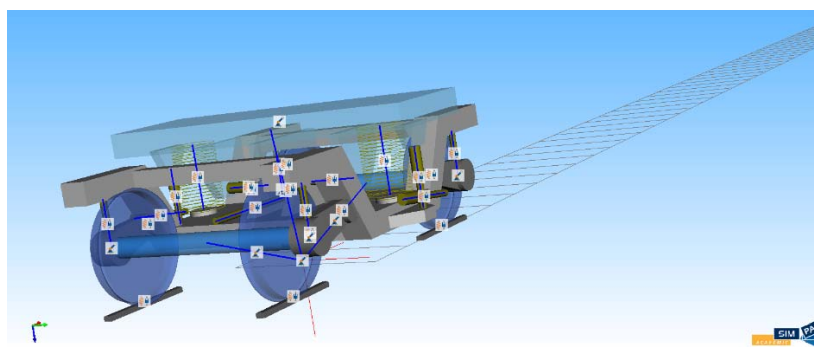
(b) Bogie mass
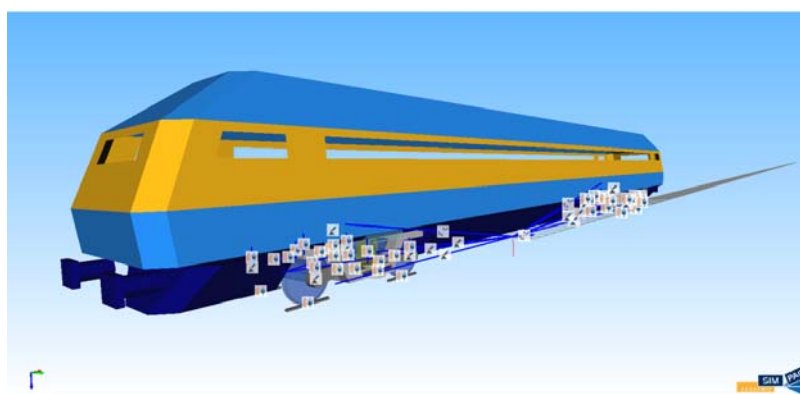
(c) Train car

Figure 4.2 Multi-body model of a train vehicle with track (3D model)

4.4   Modelling assumptions and implementation

For MBS: train vehicle model, the assemblage of various rigid components like wheelsets, bogie mass and car body are considered. A *Track* element defines the three-dimensional run of a route, the track line, in space. Tracks are usually intended for providing a virtual guideway for train vehicles with wheelsets remain in contact with the track and never derail. Here, straight track is considered for the simulation. A standard ERRI *S1002 Wheel Profile* and *UIC 60 Rail Profile* are used along with rail inclination of 1:40 (cant) in the MBS according to [148]. There was no kind of untrueness considered in wheel. Also rails are mounted on *Inertia-Fixed* track. The method for locating the contact patches between rail and wheel is *Equivalent elastic method* which converts the actual contact patch shape into an equivalent ellipse. The normal force method recommended is *Hertzian*. The combined Young's modulus of the rail and wheel material, $E = 2.1 \times 10^{11}$ N/m^2 used for the Hertzian normal force and the tangential forces. The common Poisson number, ν of the rail and wheel material is 0.28. The physical parameters of the MBS train vehicle model considered for present study are two sets as illustrated in the Table 4.1 [94, 95, 143]. The vertical and lateral track profile excitation for left and right rail are shown in the Figure 4.3. The accelerometers and gyros are placed on car body and two bogie mass above the rail on both sides for estimating the left and right rail track profile.
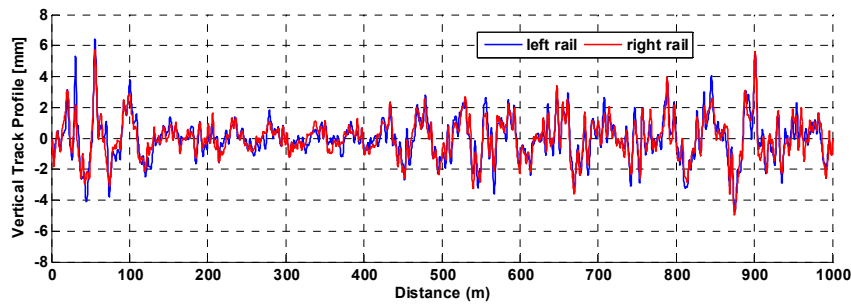
(a) Vertical True track profile
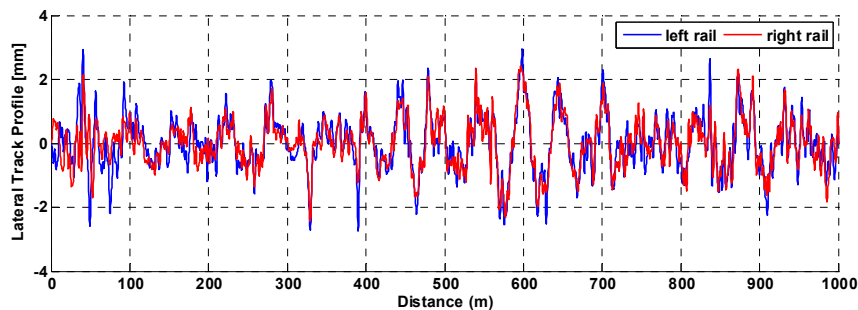
(b) Lateral True track profile

Figure 4.3 Rail track profile irregularities

Table 4.1 Properties of train vehicle model system [94, 95, 143]

Parameter	SET I	SET II
Car body mass (m_c)	23143 kg	20000 kg
Car body mass moment of inertia about x axis (I_{cx})	33326 kgm²	29998 kgm²
Car body mass moment of inertia about y axis (I_{cy})	833148 kgm²	1229932 kgm²
Car body mass moment of inertia about z axis (I_{cz})	833148 kgm²	1229932 kgm²
Bogie mass (m_b)	3925 kg	2615 kg
Bogie mass moment of inertia about x axis (I_{bx})	1105 kgm²	1722 kgm²
Bogie mass moment of inertia about y axis (I_{by})	2177 kgm²	1476 kgm²
Bogie mass moment of inertia about z axis (I_{bz})	2422 kgm²	3076 kgm²
Wheelset mass (m_w)	1645 kg	1200 kg
Wheelset mass moment of inertia about x axis (I_{wx})	633 kgm²	740 kgm²
Wheelset mass moment of inertia about y axis (I_{wy})	103 kgm²	74 kgm²
Wheelset mass moment of inertia about z axis (I_{wz})	633 kgm²	740 kgm²
Primary vertical suspension stiffness (k_p)	1150 kN/m	1220 kN/m
Secondary vertical suspension stiffness (k_s)	290 kN/m	430 kN/m
Primary vertical suspension damping (c_p)	115 kN.s/m	122 kN.s/m
Secondary vertical suspension damping (c_s)	29 kN.s/m	25 kN.s/m
Primary horizontal suspension stiffness (k_{ph})	3840 kN/m	3884 kN/m
Secondary horizontal suspension stiffness (k_{sh})	176 kN/m	160 kN/m
Primary horizontal suspension damping (c_{ph})	384 kN.s/m	388.4 kN.s/m
Secondary horizontal suspension damping (c_{sh})	17.6 kN.s/m	16 kN.s/m
Half of car-body base (l_c)	7.2 m	9.5 m
Half of bogie-wheel base (l_t)	1.125 m	1.28 m
Track gauge	1.067 m	1.435 m
Nominal wheel radius	0.405 m	0.46 m
Lateral Wheel distance	0.55 m	0.75 m
Friction coefficient (μ)	0.4	0.4

4.5 Track geometry estimation from measurement responses obtained from MBS

In order to assess the behavior of proposed extended Augmented State Kalman filter (ASKF): Approach (a) estimation algorithm for railway track profile estimation, 6 DOF train vehicle model for vertical and lateral displacement with senor placements (Figures 3.6 and 3.15) are considered for inverse analysis which represents the real train where pitching and yawing motion in bogie mass included. The estimated profile is the front wheel of the front bogie mass as shown in the Figures 3.6 and 3.15. The reference vehicle parameters for 6 DOF train model are considered from the Table 4.1 accordingly. Inverse analysis is incorporated with various measurement noise levels generated as a random walk driven by Gaussian white noise and also initial condition error in the Kalman filter iteration in order to approximately obtain the exact profile. For true track profile, left rail - vertical track irregularity, is considered for comparison with the estimated track profile (Figure 4.3). Furthermore, for MBS the vehicle is supposed to retain a constant velocity of 90 km/h with simulated distance of 1000 m and sampling frequency of 100 Hz. A typical case of track profile after using band pass filter with cut off spatial frequency of 0.0166 – 0.166 cycle/m, by incorporating noise level of 10 % (standard deviation of measured response and random error). The filter considered in this simulation helps to evaluate wavelengths ranging between 6 m – 60 m, which covers ranges comprising from short to long wavelength irregularities as mentioned in [96].

4.5.1 Measurement set up

In this section implementation details of numerical simulation are introduced. The vehicle parameters Set- I is considered for MBS (Table 4.1).

The measurement set up for estimating vertical track profile,

- M1: Vertical acceleration and pitching angular velocity measurements at car body only.
- M2: Vertical acceleration and pitching angular velocity measurements at car body, front and rear bogie masses.
- M3: Vertical acceleration and pitching angular velocity measurements at car body and front bogie mass.
- M4: Vertical acceleration measurement at car body and pitching angular velocity measurement at car body and front bogie masses.

The measurement set up for estimating lateral track profile,

- A1: Lateral acceleration and yawing angular velocity measurements at car body only.
- A2: Lateral acceleration and yawing angular velocity measurements at car body, front and rear bogie masses.
- A3: Lateral acceleration and yawing angular velocity measurements at car body and front bogie mass.
- A4: Lateral acceleration measurement at car body and yawing angular velocity measurements at car body and front bogie masses.

4.5.1.1 Different Track Excitation

This section explains the estimation of both vertical and lateral track profile when different track excitations are given for left and right track respectively. And also reveals how varying train speed affect during the inverse analysis using 6 DOF. The results are shown below and inferences are provided. The train speed considered in this MBS study corresponds to low speed (30 km/h), average speed (90 km/h) and high speed (160 km/h).

For all train speed cases, the set M1 ($\ddot{z}_c\ \dot{\theta}_c$) has an issue of un-observability. Also, M4 ($\ddot{z}_c\ \dot{\theta}_c\ \dot{\theta}_{t1}$) is performing poor comparing with M2 ($\ddot{z}_c\ \dot{\theta}_c\ \ddot{z}_{t1}\ \dot{\theta}_{t1}\ \ddot{z}_{t2}\ \dot{\theta}_{t2}$) and M3 ($\ddot{z}_c\ \dot{\theta}_c\ \ddot{z}_{t1}\ \dot{\theta}_{t1}$). Similar conclusion is arrived for the lateral measurement set up. The estimation results for vertical and lateral left track profile under different excitations for low, average and high train speeds are shown in the Figures 4.4 to 4.9 respectively. The statistical metrics results are given in Table 4.2. Since the front wheel profile of front bogie mass is utilized for estimation, the measurement-M3 ($\ddot{z}_c\ \dot{\theta}_c\ \ddot{z}_{t1}\ \dot{\theta}_{t1}$) is sufficient for estimating the vertical track profile geometry. The measurement set M3 ($\ddot{z}_c\ \dot{\theta}_c\ \ddot{z}_{t1}\ \dot{\theta}_{t1}$) is performing close to M2 ($\ddot{z}_c\ \dot{\theta}_c\ \ddot{z}_{t1}\ \dot{\theta}_{t1}\ \ddot{z}_{t2}\ \dot{\theta}_{t2}$). Similar conclusion is arrived for estimating lateral track profile. The measurement set A3 ($\ddot{y}_c\ \dot{\varphi}_c\ \ddot{y}_{b1}\ \dot{\varphi}_{b1}$) is performing close to A2 ($\ddot{y}_c\ \dot{\varphi}_c\ \ddot{y}_{b1}\ \ddot{y}_{b2}\ \dot{\varphi}_{b1}\ \dot{\varphi}_{b2}$).

Figures 4.4 (c) to 4.9 (c) give the comparison of estimation error among measurement set for both vertical and lateral profile respectively. It has error value less than ± 1 mm for vertical and lateral track profile geometry. Hence, the optimal sensor placement can be at car body and front bogie mass (measurement set: M3 and A3). The illustrated PSD plot for lateral profile estimation has certain variation in spatial frequency above 0.12 cycle/m. Hence it could not detect track irregularity wavelength below 8 m for lateral profile. This phenomenon may occur due to the simplified model used for inverse analysis. Also considered rigid body model do not account for rolling motion of train vehicle. It could not replicate the vehicle dynamic characteristics exactly, similar to hunting oscillation phenomenon.
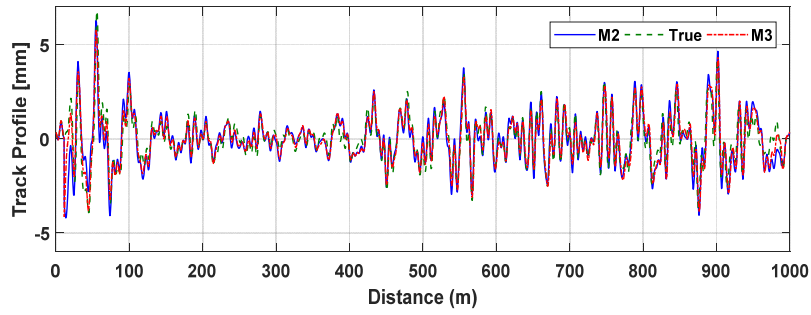
(a) Comparison plot
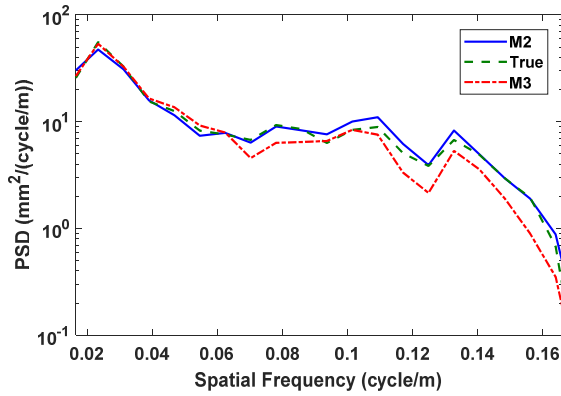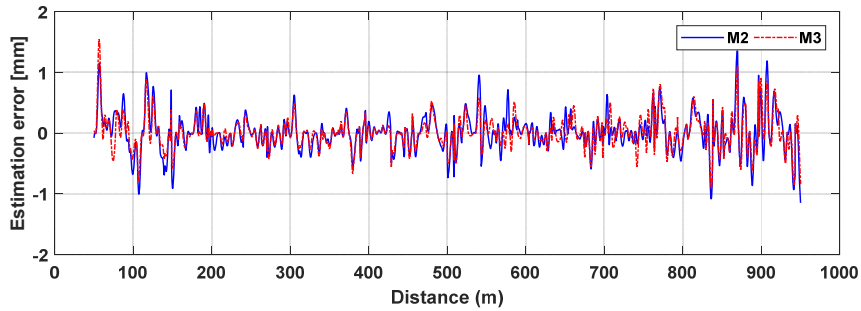
(b) PSD plot

(c) Estimation error after misfit criteria (for track length 50m to 950m)

Figure 4.4 Estimation of vertical track irregularity for low train speed (30 km/h)
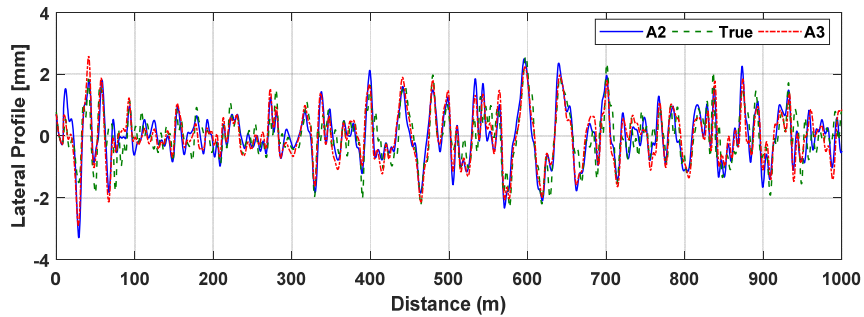
(a) Comparison plot
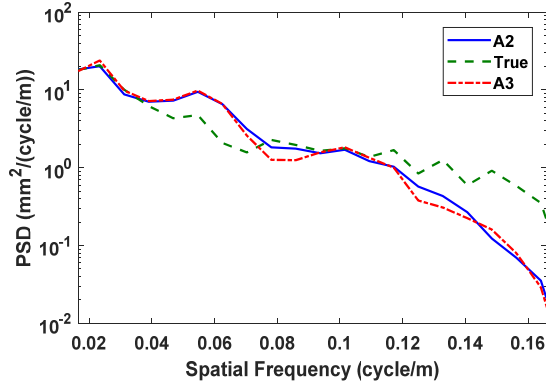
(b) PSD plot
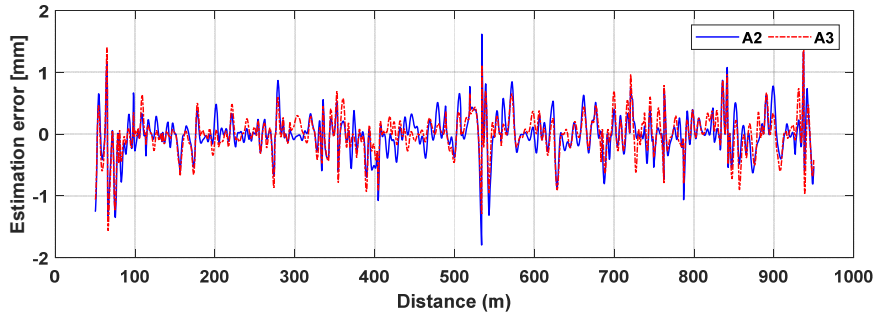
(c) Estimation error after misfit criteria (for track length 50m to 950m)

Figure 4.5 Estimation of lateral track irregularity for low train speed (30 km/h)

From the Table 4.3, the metrics are calculated after applying misfit criteria and it shows that the vertical and lateral track profile estimated for low train speed (30 km/h as shown in Figures 4.6 and 4.7) is performing slightly poor comparing to other verified train speed. This is due to the high pass filter utilized. In the inverse analysis, after force reconstruction in Kalman filtering, the high pass filter of 0.15 Hz is introduced to avoid offset drifts during double integration. The relationship between the wavelength (λ), velocity (v) and frequency (f) is, $\lambda = v/f$. Hence, for v = 30 km/h, and f = 0.15 Hz, the calculated spatial frequency ($1/\lambda$), is 0.018 cycle/m. But the band pass filter used is 0.0166 -0.16 cycle/m (for wavelength 6 m to 60 m). Since the value is greater than the band pass filter (0.018 cycle/m > 0.0166 cycle/m), it is performing slightly poor comparing to higher train speed. Hence for high pass filter of 0.15 Hz, if train speed is above 35 km/h, the performance will be good (i.e., $1/\lambda$ will be < 0.0166 cycle/m). Thus, by utilizing 6 DOF train model which considers bogie pitching/yawing motion, rail track profile can be estimated accurately using proposed ASKF method: Approach (a). Therefore, depending upon the sensors availability and feasible sensor placement locations in the real field measurement, track geometry can be reconstructed. For the optimal sensor placement, the measurement set M3 ($\ddot{z}_c$ $\dot{\theta}_c$ $\ddot{z}_{t1}$ $\dot{\theta}_{t1}$) and A3 ($\ddot{y}_c$ $\dot{\varphi}_c$ $\ddot{y}_{b1}$ $\dot{\varphi}_{b1}$) can be utilized for mounting on in-service railway vehicle for robust vertical and lateral track profile estimation respectively.
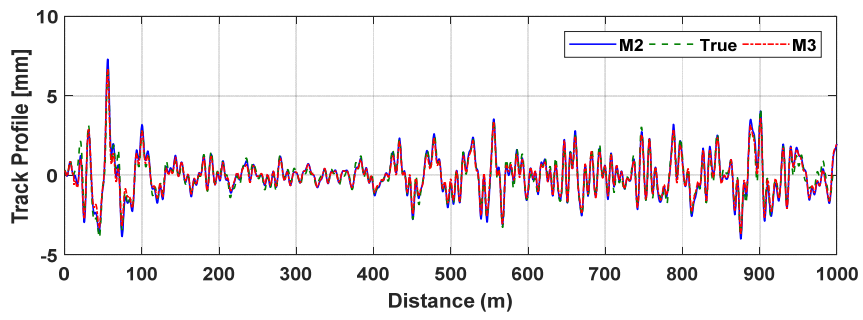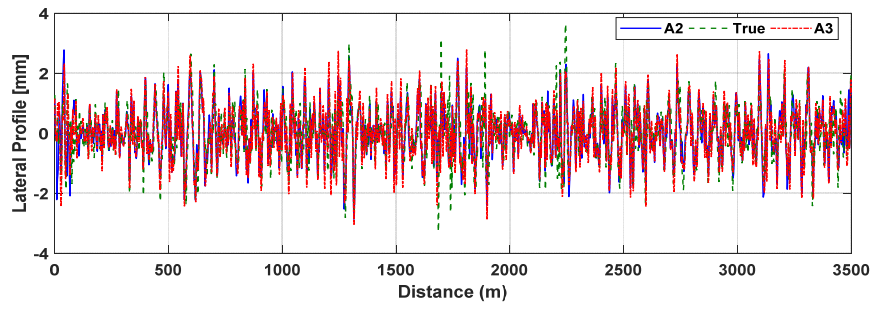
(a) Comparison plot
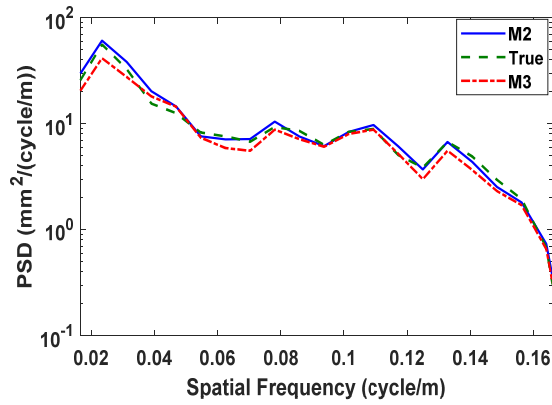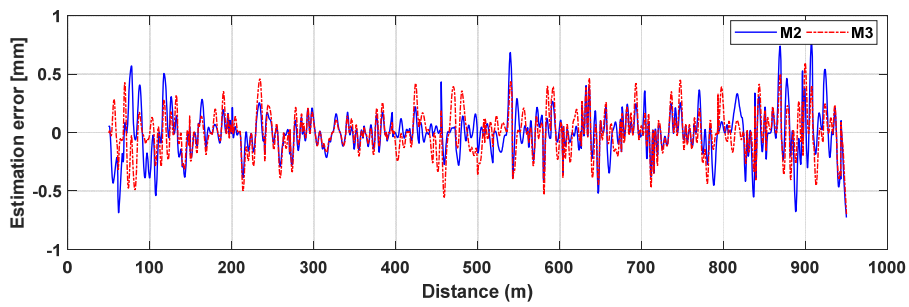
(b) PSD plot

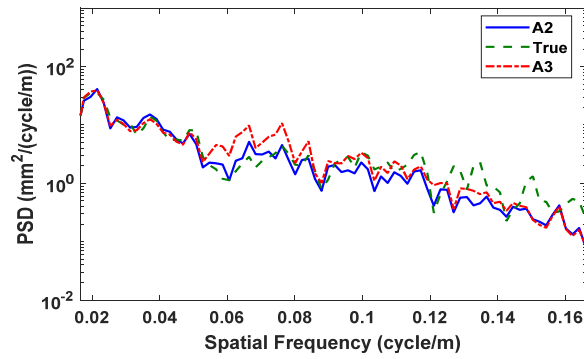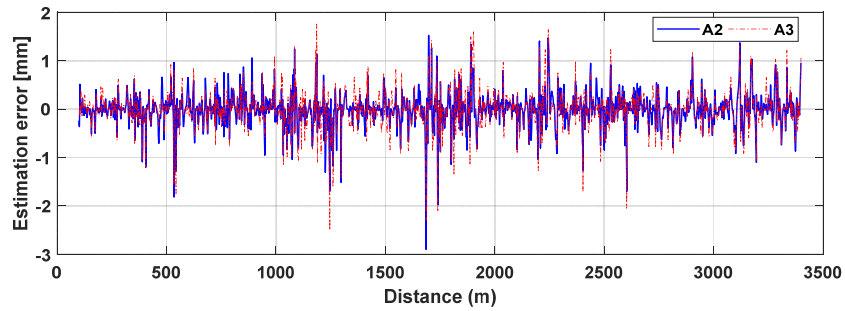(c) Estimation error after misfit criteria (for track length 50m to 950m)

Figure 4.6 Estimation of vertical track irregularity for average train speed (90 km/h)
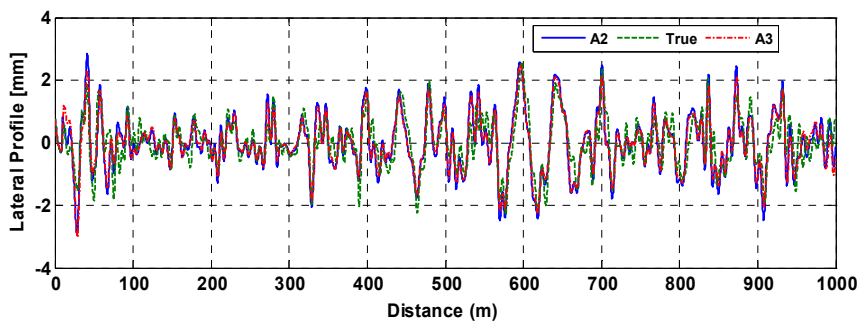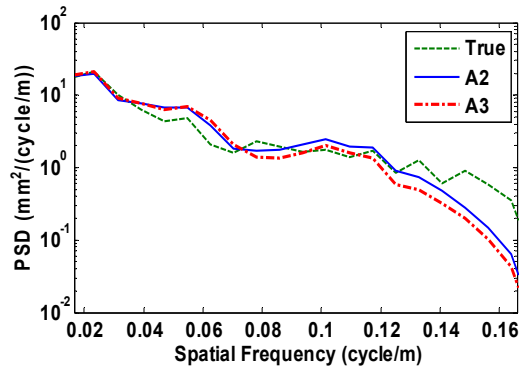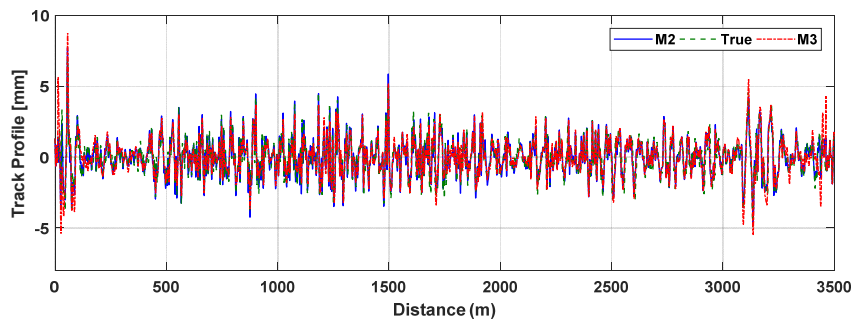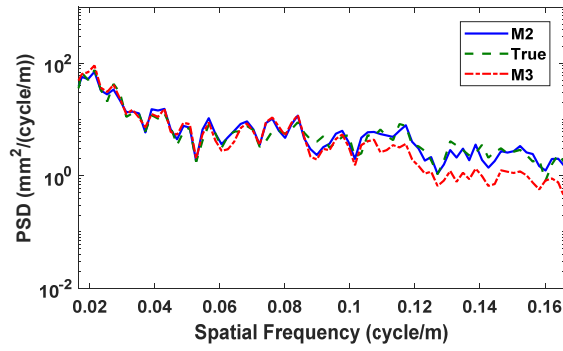

(a) Comparison plot
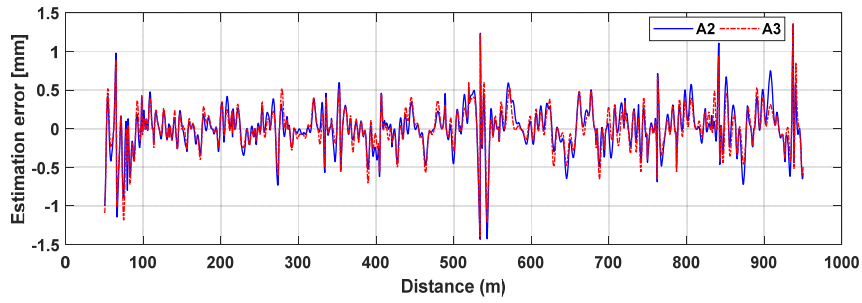
(b) PSD plot

(c) Estimation error after misfit criteria (for track length 50m to 950m)

Figure 4.7 Estimation of lateral track irregularity for average train speed (90 km/h)
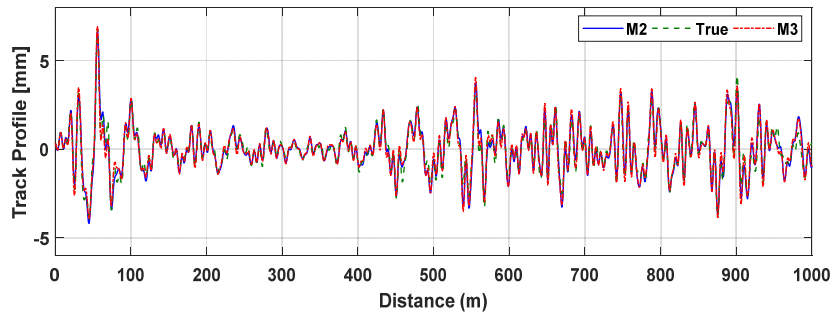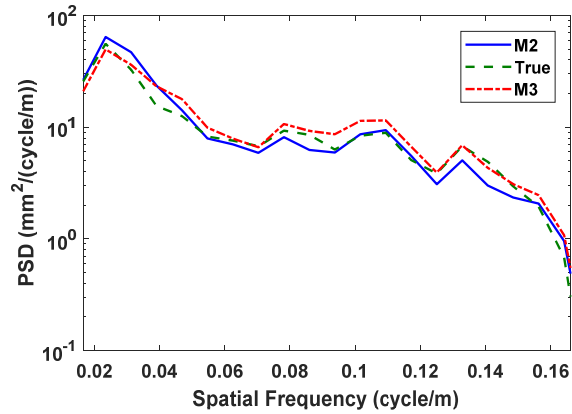
(a) Comparison plot
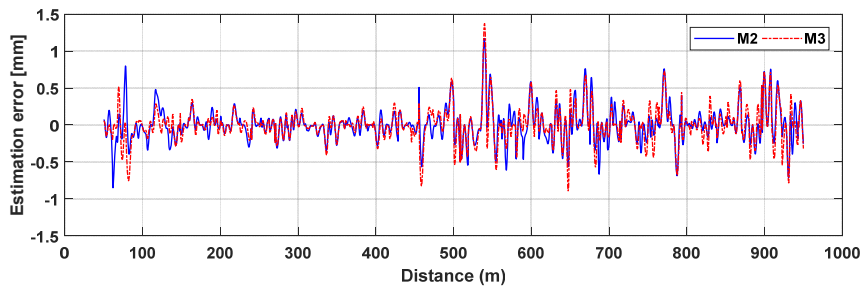
(b) PSD plot

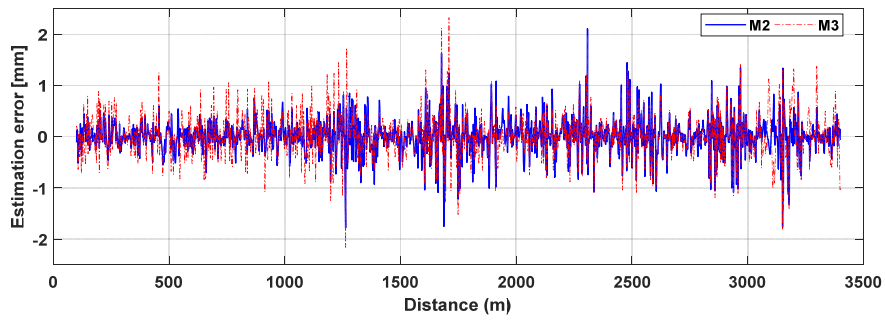(c) Estimation error after misfit criteria (for track length 50m to 950m)

Figure 4.8 Estimation of lateral track irregularity for high train speed (160 km/h)
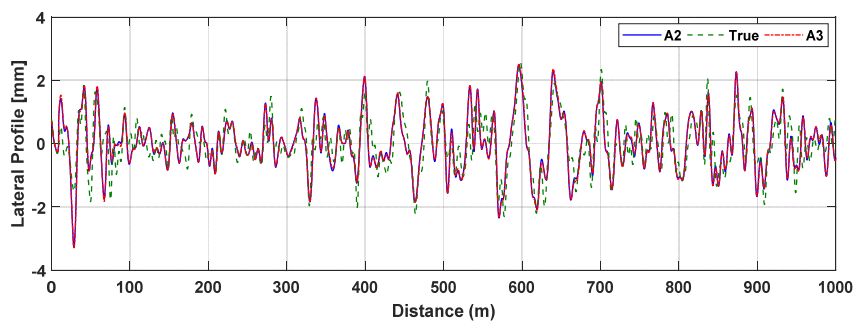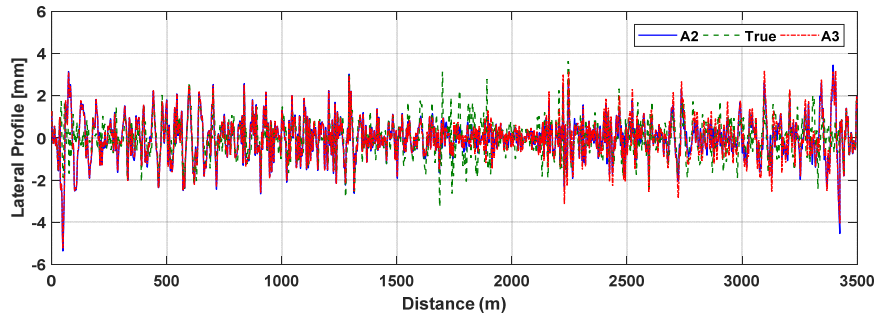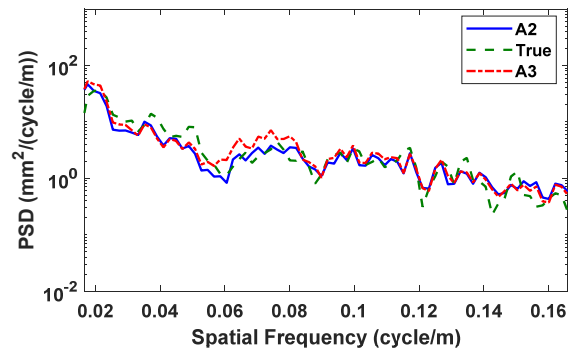

(a) Comparison plot
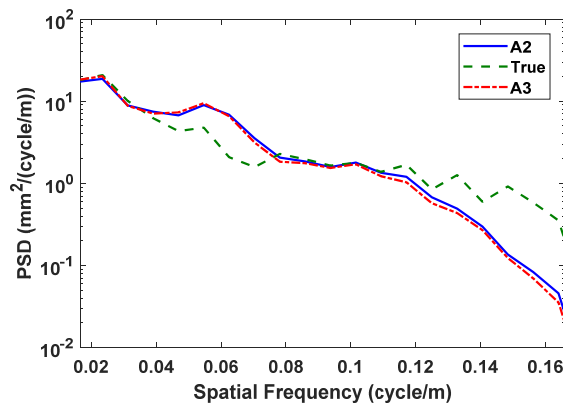
(b) PSD plot
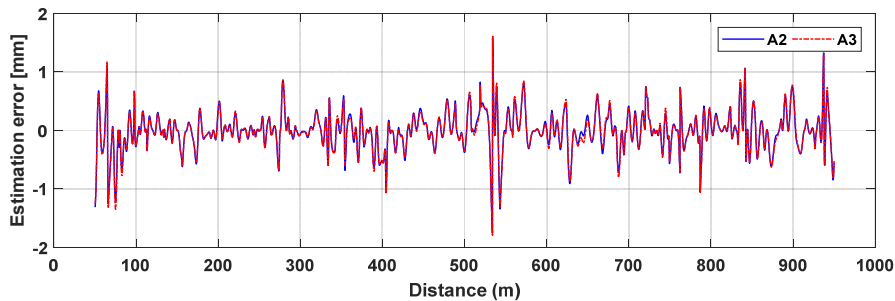
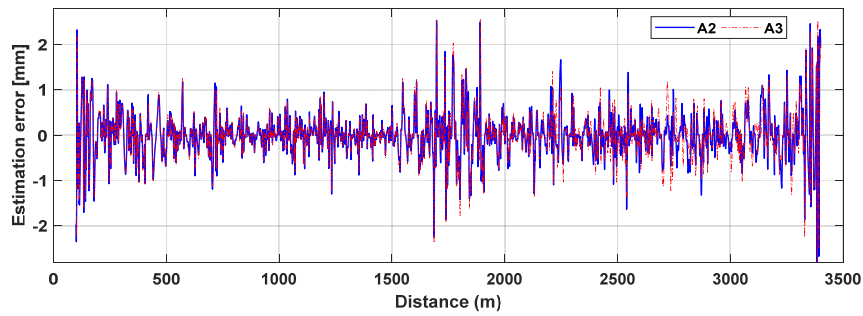(c) Estimation error after misfit criteria (for track length 50m to 950m)

Figure 4.9 Estimation of lateral track irregularity for high train speed (160 km/h)

93

Table 4.2 Comparison of left track profile under different excitation using statistical metrics for varying train speed

Train speed	Track profile	Approach (a)	Statistical Metrics		
			RMSD (%)	CC	RMSE (mm)
Low (30 km/h)	Vertical	M2	25.3	0.97	0.30
		M3	22.3	0.98	0.27
	Lateral	A2	39.2	0.93	0.32
		A3	37.8	0.93	0.31
Average (90 km/h)	Vertical	M2	15.8	0.99	0.19
		M3	15.1	0.99	0.18
	Lateral	A2	33.9	0.95	0.28
		A3	31.7	0.95	0.26
High (160 km/h)	Vertical	M2	18.9	0.98	0.23
		M3	19.4	0.98	0.23
	Lateral	A2	38.7	0.93	0.31
		A3	39.2	0.93	0.32

In Appendix: A, the estimation results for vehicle parameter SET-I (Table 4.1) are shown in the Figure A.1 and A.2 for vertical and lateral right track profile under different excitations (Figure 5.3) for the average train speed (90 km/h) respectively. The statistical metrics are evaluated after applying misfit criteria and results are given in Table A.1.

4.5.2 Curved track section

Rail vehicles are steered by their rails, that follow the *Track*. Cartographic Track is considered as the *Track* kind. The *Track Line* is assembled from various segments in the three directions horizontal, superelevation and vertical that are stringed together (Figure 4.10). Horizontal Cartographic Track segment types consist of Straight track (STR), Circular arc (CIR), Clothoid transition (CLO) - the curvature increases or decreases linearly from 1/R1 to 1/R2. The splined discretization for the curved track length of 3500 m can be defined as, 700 m STR $\rightarrow$ 500 m (R2) CLO $\rightarrow$ 1000 m CIR $\rightarrow$ 500 m (R1) CLO $\rightarrow$ 800 m STR. It is illustrated in the Figure 4.12 (a) and the curvature of the splined track is shown in Figure 4.10 (b). For MBS under curved track section is carried out in this section at the average train speed of 90 km/h. The vertical and lateral excitations of the track section are shown in the Figure 4.11. By utilizing 6 DOF train model which considers bogie pitching/yawing motion, rail track profile can be estimated using proposed ASKF method: Approach (a).
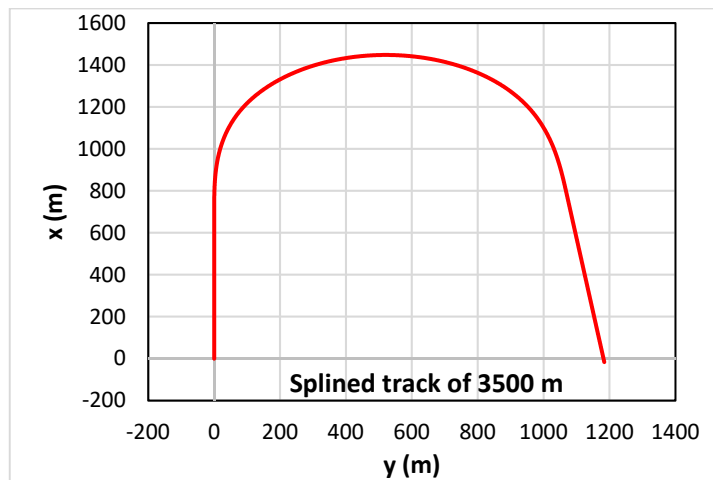
(a) Curved track section

(b) Curvature of splined track

Figure 4.10 Rail track profile irregularities for curved section

The estimation results for straight track section (3.5 km) for vehicle parameter SET-I (Table 4.1) are shown in the Figures 4.12 and 4.13 for vertical and lateral left track profile respectively. These results are illustrated for comparing with the results obtained from the splined track section. The estimation results for curved track section are shown in the Figures 4.14 and 4.15 for vertical and lateral left track profile respectively. The statistical metrics results are given in Table 4.4. Comparing the statistical metrics RMSD and CC, with the estimated results obtained for straight track, it is clear that influence of splined section has affected the track profile estimation. Figures 4.12 (c) - 4.15 (c) give the comparison of estimation error among measurement set after applying misfit criteria for both vertical and lateral profile respectively.

The statistical metrics are evaluated after applying the misfit criteria and results are given in Table 4.3. Comparing the statistical metrics RMSD and CC, with the estimated results obtained for straight track, it is clear that influence of splined section has affected the track profile estimation. The RMSE value shows that splined track section has high error comparing to the straight track. Still, the illustrated PSD plots (Figures 4.14 (b) and 4.15 (b)) have certain variation for wavelength less than 7 m. This phenomenon may occur due to the simplified model used for inverse analysis. It could not replicate the vehicle dynamic characteristics exactly. Also, the estimation results of curved track section, performs slightly poor comparing to straight track section., which can be clearly illustrated from Table 4.3.
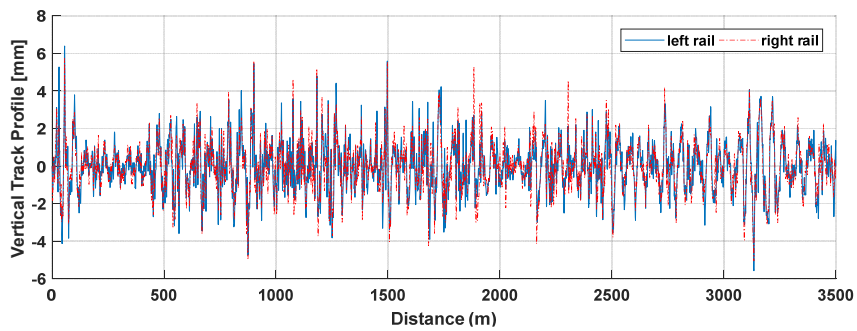
(A) Vertical profile
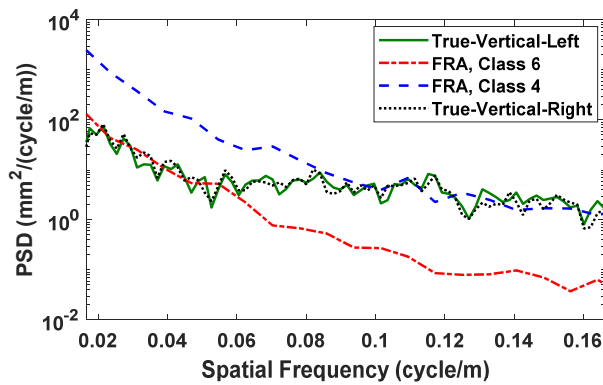
(B) PSD plot

(a) Vertical true track profile
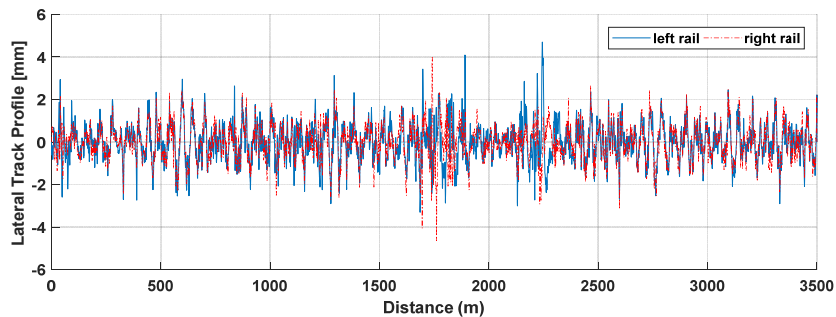
(A) Alignment profile

96
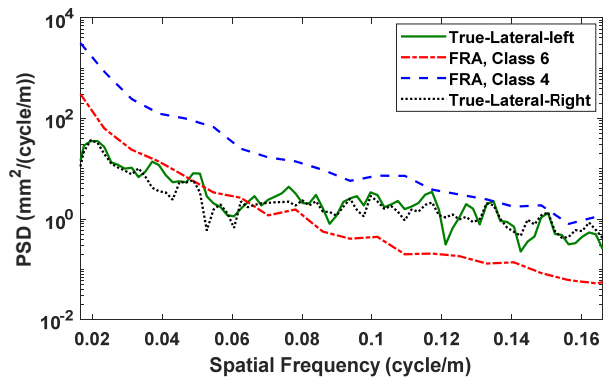
(B) PSD plot

(b) Lateral true track profile

Figure 4.11 Rail track profile (True) irregularities for 3.5 km
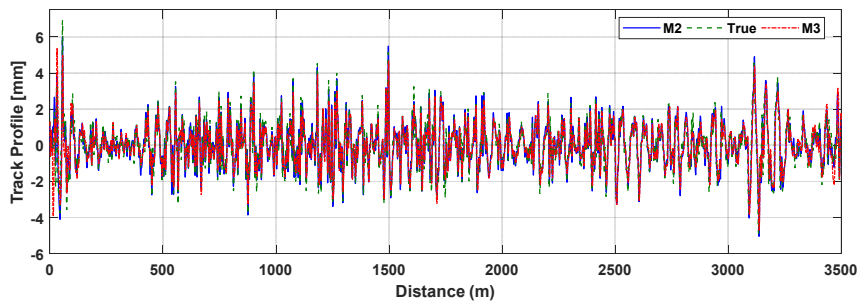
(a) Comparison plot
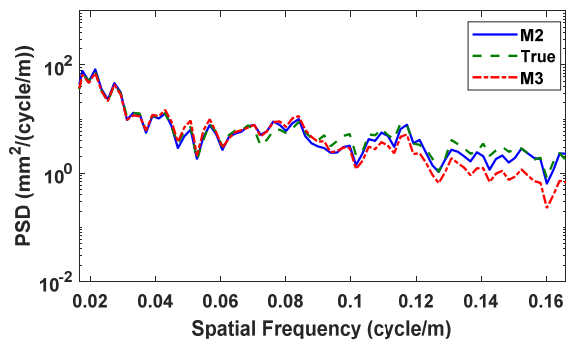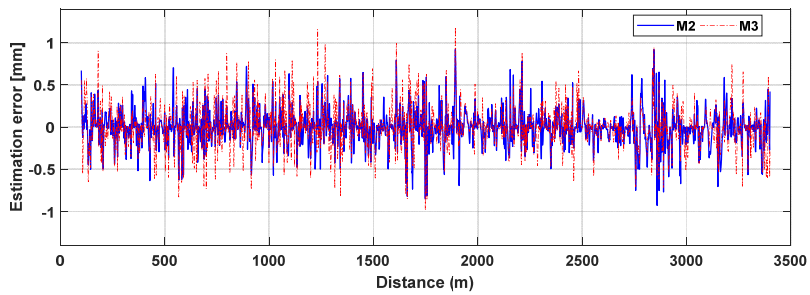
(b) PSD plot

(c) Estimation error after misfit criteria (for track length, 100-3400 m)

Figure 4.12 Estimation of vertical track irregularity for straight track section (90 km/h)

(a) Comparison plot

(b) PSD plot

(c) Estimation error after misfit criteria (for track length, 100-3400 m)

Figure 4.13 Estimation of lateral track irregularity for straight track section (90 km/h)

(a) Comparison plot

98

(b) PSD plot

(c) Estimation error after misfit criteria (for track length, 100-3400 m)

Figure 4.14 Estimation of vertical track irregularity for splined track section (90 km/h)

(a) Comparison plot

(b) PSD plot

(c) Estimation error after misfit criteria (for track length, 100-3400 m)

Figure 4.15 Estimation of vertical track irregularity for splined track section (90 km/h)

Table 4.3 Comparison of straight vs splined track profile (left) under different excitation (for 90 km/h) using statistical metrics (for track length, 100-3400 m)

Track profile	Measurement: Approach (a)	Statistical Metrics		
		RMSD (%)	CC	RMSE (mm)
Straight track section (3.5 km)				
Vertical	M2	16.5	0.99	0.20
	M3	19.4	0.98	0.23
Lateral	A2	39.3	0.93	0.22
	A3	43.9	0.92	0.27
Splined track section (3.5 km)				
Vertical	M2	25.3	0.97	0.31
	M3	30.9	0.95	0.37
Lateral	A2	59.6	0.83	0.49
	A3	60.7	0.82	0.50

4.5.2.1 Same Track Excitation for Splined section

This study reveals whether the rolling motion is affected much during the inverse analysis using 6 DOF. The results are shown below and inferences are provided.

In order to study the influence of rolling motion of train vehicle, same track excitation is applied for left and right rail. Hence the MBS results are influenced much by pitching and yawing motion rather than rolling motion. For similar track excitation with train traversing at average speed of 90 km/h, the results are given in Figure 4.16 and 4.17 for vertical and lateral track profile respectively. The statistical metrics results are given in Table 4.4. Figures 4.16 (c) and 4.17 (c) give the comparison of estimation error among measurement set after applying misfit criteria, for both vertical and lateral profile respectively. Comparing the statistical

metrics RMSD and CC, with the estimated results obtained for different excitations, it is clear that influence of rolling motion is avoided. Still, the illustrated PSD plots (Figures 4.18 (b) and 4.19 (b)) have certain variation as seen for the different excitation case. This phenomenon may occur due to the simplified model used for inverse analysis. It could not replicate the vehicle dynamic characteristics exactly.
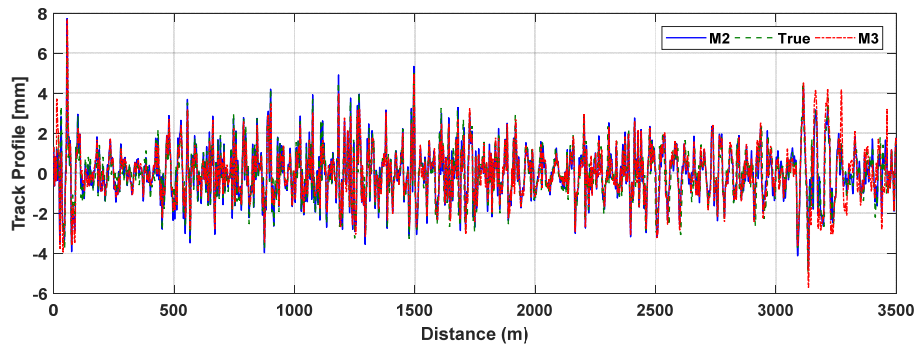
(a) Comparison plot
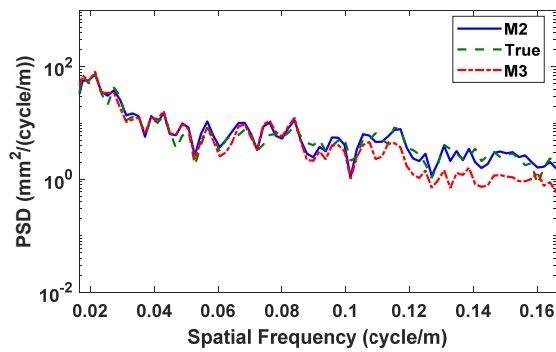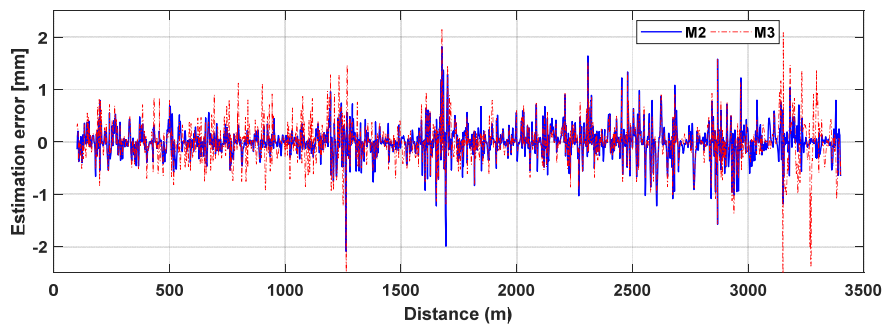
(b) PSD plot

(c) Estimation error after misfit criteria (for track length, 100-3400 m)

Figure 4.16 Estimation of vertical track irregularity for splined section with same track excitation (90 km/h)
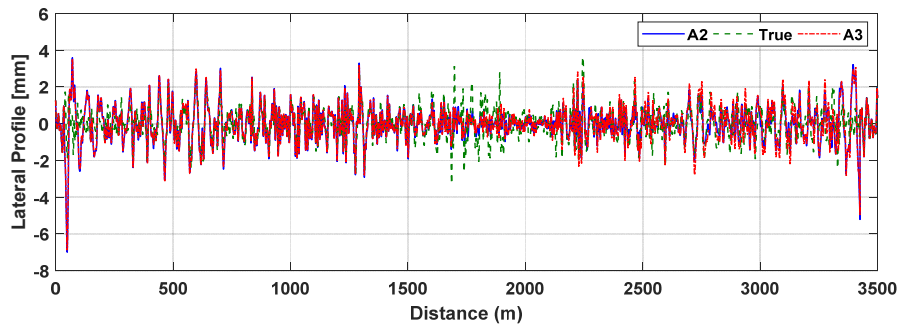
(a) Comparison plot
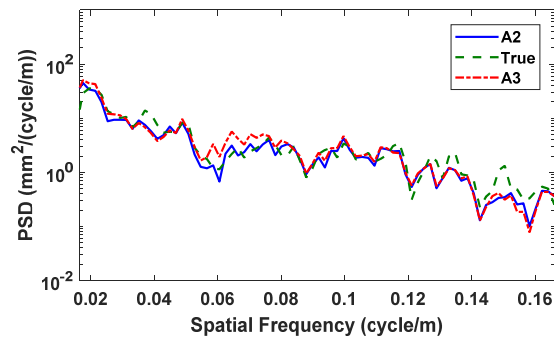
(b) PSD plot
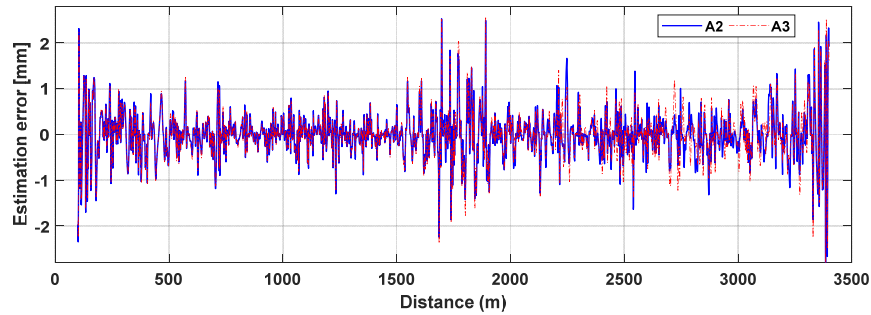
(c) Estimation error after misfit criteria (for track length, 100-3400 m)

Figure 4.17 Estimation of lateral track irregularity for splined section with same track excitation (90 km/h)

Table 4.4 Comparison of left track profile under same excitation for splined track section using statistical metrics (for track length, 100-3400 m)

Track profile	Measurement: Approach (a)	Statistical Metrics		
		RMSD (%)	CC	RMSE (mm)
Vertical	M2	22.6	0.98	0.27
	M3	28.9	0.96	0.35
Lateral	A2	57.6	0.85	0.47
	A3	57.9	0.84	0.48

4.6   Discussion and Summary

Currently, the significance of the MBS for solving the train vehicle dynamics is frequently utilized. The MBS software is progressively accepted for obtaining the rail dynamics solutions and it has been established as a conceivable means to decrease the number of on-track investigations and amount of costs. The simulations are carried out for varying train speed: low (30 km/h), average (90 km/h) and high (160 km/h). The sensors are placed just above the rail tracks on both the sides and used to measure the acceleration and angular velocity responses from the car body and both bogie masses of running train model on simulated track excitations. These vehicle measurement responses are utilized to estimate the vertical and lateral track profile using the 6 DOF train model and it is validated for the proposed estimation algorithm. The suggested sensor placement strategy is verified with all possible sensor location results. For straight track section (ideal case), it shows a good agreement for vertical track profile while it can estimate only above 8 m wavelength irregularity for lateral track profile. The statistical metrics are utilized for comparison between various cases and the proposed approach is verified. Also, MBS are carried out for understanding the influence of rolling motion of train vehicle. So, similar track excitations are given for both left and right rail and MBS is carried out. For curved track section, the results show good agreement for vertical track profile estimation, while it shows large variation for lateral profile estimation. This is due to hunting oscillation phenomenon. Exactly the splined section of the track cannot be evaluated, because of wheel-rail interaction problem. Henceforth it can be summarized that MBS – SIMPACK: Rail can be significantly utilized for the usage of track maintenance as one of its several practices.

Chapter 5 RAILWAY TRACK MONITORING USING IN-SERVICE VEHICLE RESPONSES

5.1 Introduction

For confirming the safety of railway infrastructure, monitoring of rail track is necessary [26, 97, 98]. Equipping sensitive sensors like optical displacement transducers are difficult in operating railway system. Collecting measurement data from in-service train has become common practice for track condition assessment [10]. In last decade, mounting miniaturized track recording vehicle equipment on traversing train vehicle for track geometry estimation has been utilized. Another possibility is to attach practical sensors namely accelerometers and rate gyroscopes on bogie mass and axle-boxes of an in-service train vehicle for monitoring ride quality. The drawback of this method is that, the track data obtained is inadequate. In pioneering work carried out by Japanese railway researchers, vertically sensing axle-box accelerometers to observe rail track corrugation, from in-service vehicles have been investigated [99]. Later, [100] introduced an economical way for track maintenance planning which utilized online digital data processing, viz. inertia method and inverse filtering method. Thus by taking into account both vehicle dynamics and human sensitivity; control over track can be achieved.

In the field of railways, obtaining real time vehicle vibration from simple sensors system equipped on in-service train vehicle is the promising future research for maintenance purpose. Hence it is aiming towards the development of conventional railways by monitoring effectively. Eccentricities from the real case can effect in poor ride quality caused due to undesirable characteristics of vehicle dynamics. The objective of this chapter is to carry out the rail track monitoring concept using in-service vehicle responses for local railway system using prevalent sensing device like smartphone and other low cost sensors. Also implementing the proposed data assimilation inverse analysis approach on the measurement response collected from the in-service vehicle. Correspondingly, track recording vehicle (TRV) is utilized to obtain the existing condition of the conventional railway line considered for the research study. All the obtained results are reported in the following sections of this chapter.

5.2 Conventional Railway Track Condition Monitoring

5.2.1 Detection of railway track conditions from TRV

A TRV is utilized to obtain the existing track condition and its irregularities by measuring the linear and gradient curves of each rail using an optical displacement sensor system. Conversely, TRV's are very costly and displacement transducers are very sensitive to dirt found in the rail tracks. Therefore, repetitive upkeep of the railway track is not feasible and also the track recording car may cause hindrance to the regular traffic flow of train vehicle. In order to overcome this issue, there is a necessity to record the rail track profile using the equipment attached to the in-service vehicle. The following content explains about the various parameters measured using the TRV for the inspection purpose. The railways track chosen for the inspection was under one railway operator, which is about 80 km in distance. Table 5.1 illustrates the distance chart between each station (S) for the traversing train vehicle.

Table 5.1 Distance chart between stations

Station 1 to 2	3.53 km
Station 2 to 3	9 km
Station 3 to 4	18.1 km
Station 4 to 5	31.97 km
Station 5 to 6	17.4 km

Some of the geometric parameters of the rail track generally measured using TRV inspection car to test the rail condition are position, gauge, curvature and alignment of the track, twist, unevenness and the cross-level of the two rails. Track geometry includes the track layouts with related measurements used in design, construction and maintenance of rail tracks. The TRV cars use a variety of optical and inertial sensors, other measuring systems, and data management systems to reproduce the rail track profile being inspected. The velocity profile of the TRV car run over the selected rail track is shown in the Figure 5.1. The station numbers are illustrated in the following figures respectively.
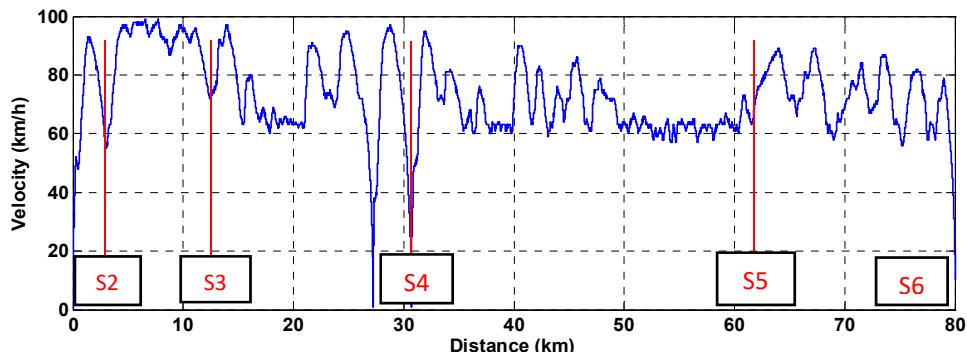
Figure 5.1 Velocity profile of the TRV inspection car

5.2.1.1 Gauge

It is the distance between the interior of left and right load bearing rails that makes up the single railway track line as presented in the Figure 5.2. In this railway operator, the track gauge is maintained at 1067 mm (narrow gauge). In the curved part, gauge distance is represented with "plus" for enlargement and with "minus" for the shrinkage.
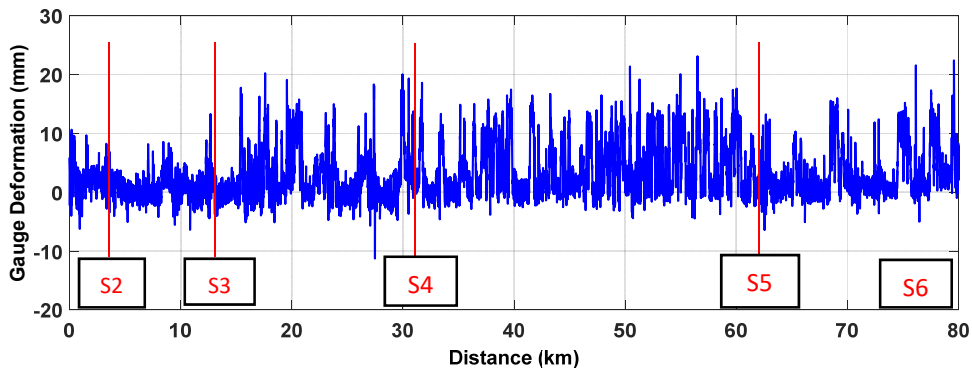
Figure 5.2 Track gauge distance

5.2.1.2 Cross-level

It refers to the difference in height amongst top surface of the left and right rails at any point of the rail track as shown in the Figure 5.3. Meanwhile the rail can marginally move up and down and henceforth the measurement should be done under loaded condition. On the curved tracks, the rate of change of elevation is measured in terms of 'cant' or 'super elevation',

which is maintained such that it assists traversing vehicle to direct round the curve such that the wheel flanges are intact with the rails by reducing the wear and friction.
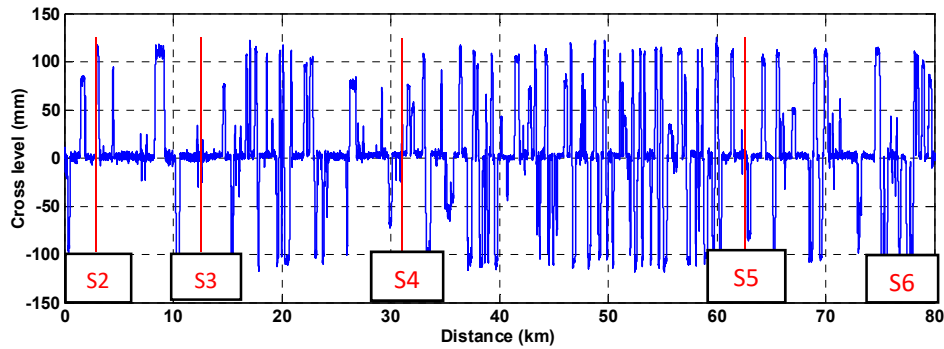
Figure 5.3 Rail Cross-level

5.2.1.3 Twist

Conversely, rolling stock can engage wide variation of the cross-levels as they are very sensitive to it. Track twist can be well-defined as the change in cross-levels over a certain length of rail track, which is shown in the Figure 5.4. In Japan, the track twist is measured on the loaded track, by obtaining the variation of cross-level over an interval of 5 m since the maximum axis distance of the conventional railway vehicle is 4.6 m. Generally, twist measured on the right side is represented as 'plus' and the case measured on left side is represented as 'minus'.
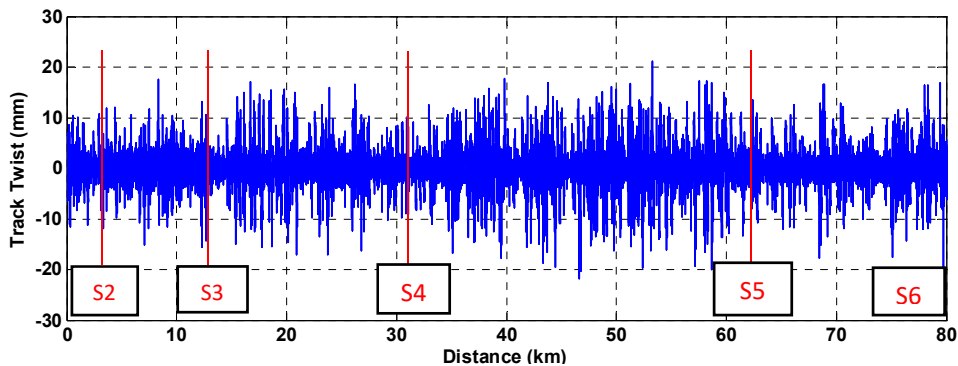
Figure 5.4 5 m - Twist of track

107

5.2.1.4 Unevenness

In order to measure the unevenness of the rail joint for the loaded track, the relative vertical depression value with respect to line joining two points at a distance of 5 m is to be estimated on either side of the rail joint. Track irregularities occur in rails due to the effect caused by the deterioration of rail track as a result of repeated traffic. The track irregularity measurement is based on 10 m chord versine method which comes under the category of mid chord based measuring system [24, 112-114]. But the measured waveform through this method is different from its original profile corresponding to the true track irregularity on real condition. Normally, 10 m chord versine method shows the precise frequency characteristic with magnitude and phase. Hence its transfer function has different magnitude gains for each wavelength component of a track irregularity, which in turn affect the characteristics of running vehicle. From Figure 5.5 (a), the gain in wavelength (λ) of 5 m is zero, which is inappropriate for the assessment of the track irregularity. Also gain is two for the wavelength of 10 m, which has a good correlation with the running safety of the train vehicle. Hence the desired wavelength band for the 10 m chord versine is, $6 \leq \lambda$ (m) ≤ 60 (which covers ranges comprising from short to long wavelength irregularities), where the gain exceeds 0.2. For a given base length of a rail, unevenness is defined as the vertical depression at the center, which is obtained for each loaded rail track separately for a base length of 10 m as shown in Figure 5.5 (b - c) for left and right rail respectively. This measurement is spontaneously obtained from TRV and also from flexi-meters. The left track irregularity is utilized in inverse analysis as shown in Figure 5.5 (d).
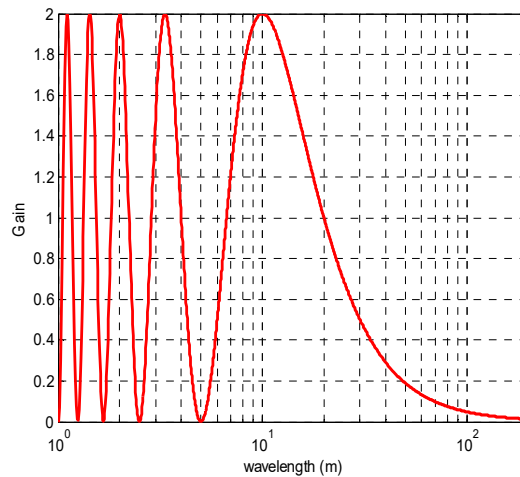
(a) Transfer function of 10 m chord method
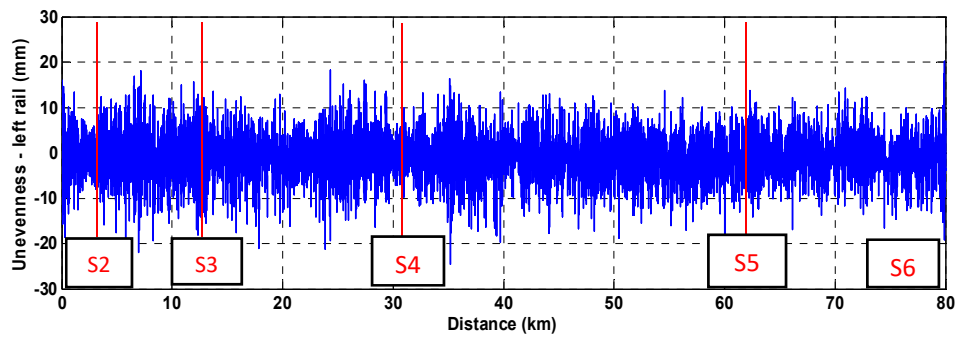
(b) For left rail
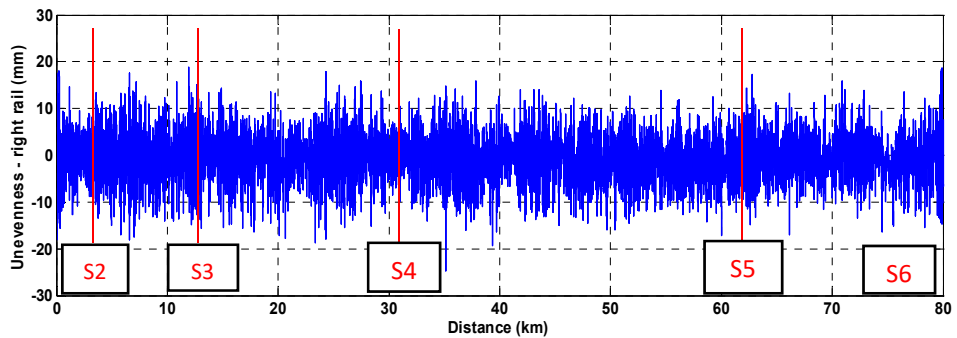
(c) For right rail
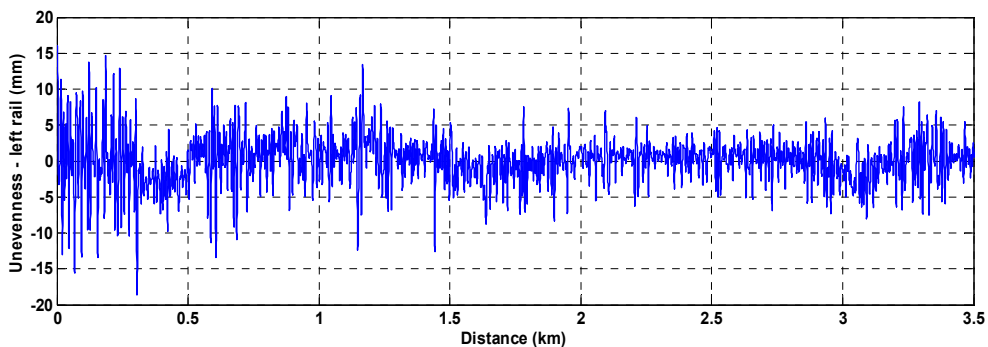
(d) 10 m chord versine: Left track irregularity (zoomed response: Station 1-2)

Figure 5.5 10 m - Unevenness of track

5.2.1.5 Alignment of track

For measuring the horizontal alignment (lateral) of the track, a chord of 10 m length is selected along each rail track and versine is measured at the center of the stretched chord. In Figure 5.6 (a-b), illustrates the alignment of the left and right rail respectively. Both the linear and gradient tracks have their separate tolerance value and it can be measured either in unloaded or loaded tracks. Thus, alignment is utilized to define the straightness of the track.

109
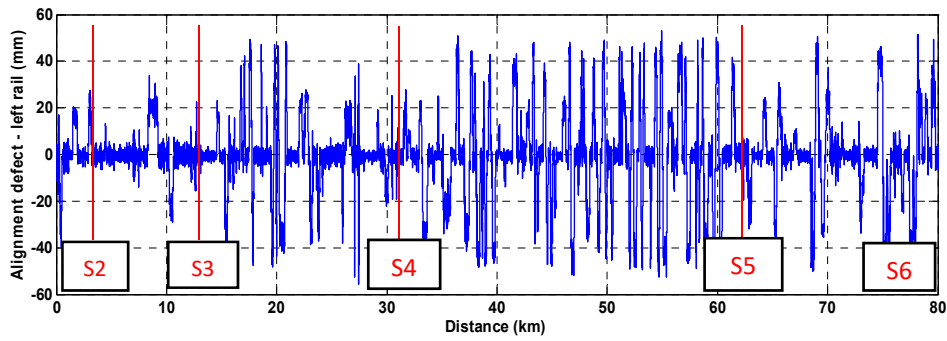
(a) For left rail
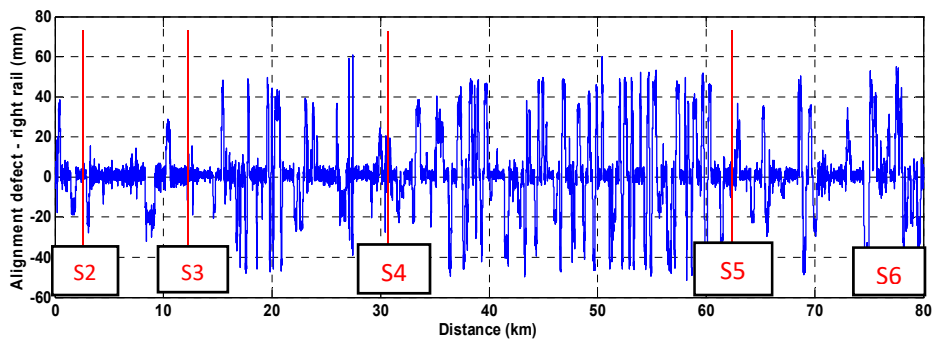
(b) For right rail
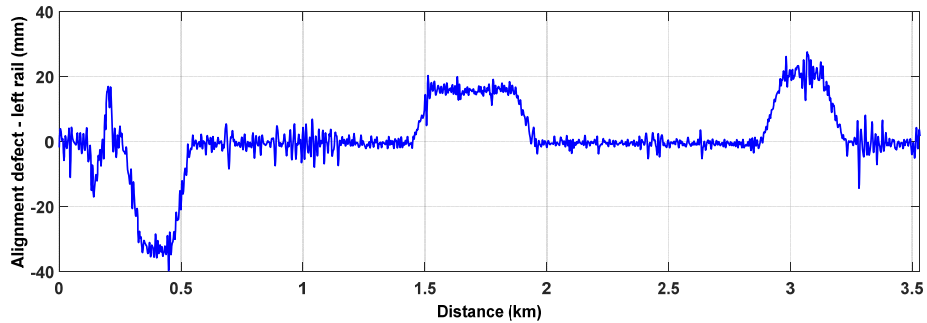
(c) 10 m chord versine: Left track irregularity (zoomed response: Station 1-2)

Figure 5.6 10 m - Alignment of track

5.2.1.6 Restoration of true track irregularity

In the 10 m chord versine measured data, an extra component due to curvature of the true track geometry (horizontal or vertical curves) is included which is not a track irregularity. Hence this component needs to be removed. Thus, restoration is an estimate of a true track irregularity waveform from the measured 10 m chord versine data. This is carried out using the digital inverse filter as explained by [115]. In the inverse filtering method, a complete restoration is not feasible in theory and hence only a partial filtering is done with limited

frequency band. Thus, even if the restored waveform is band limited, it is significant and valuable in practice when vehicle vibrations are taken into consideration. In this particular case, a restoration wavelength band is considered between $6 \leq \lambda$ (m) ≤ 60. The restored waveform for both vertical and lateral track profile (left and right rails) are provided in Figures 5.7 (A) and 5.7 (B) respectively.
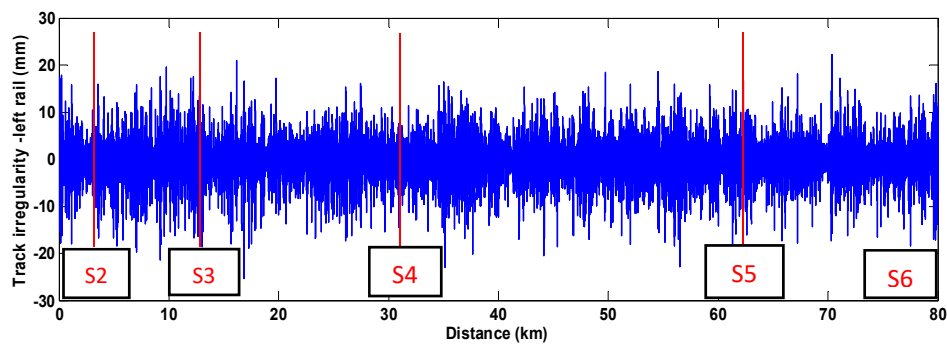
(a) Restored waveform- for left rail
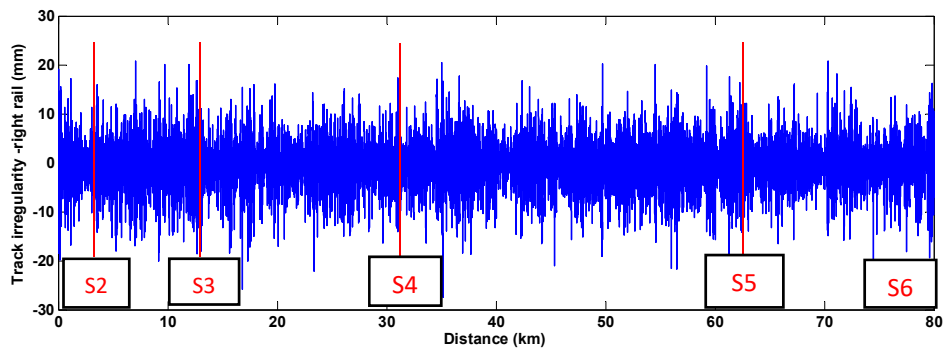
(b) Restored waveform- for right rail
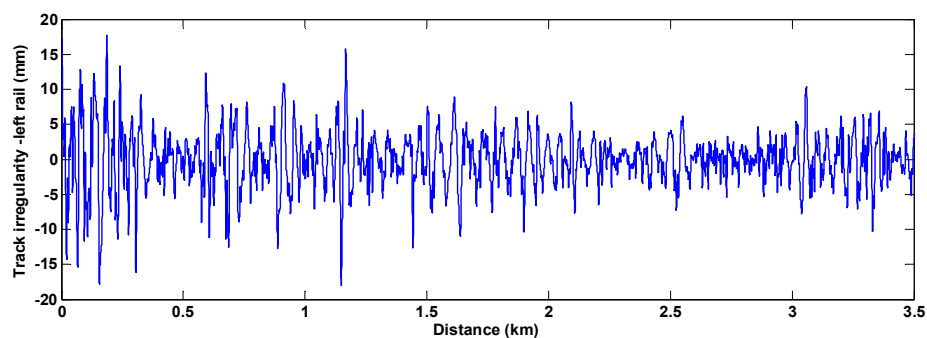
(c) Restored left rail waveform: vertical track (Station 1-2)

(A) Restored True Vertical Track irregularity
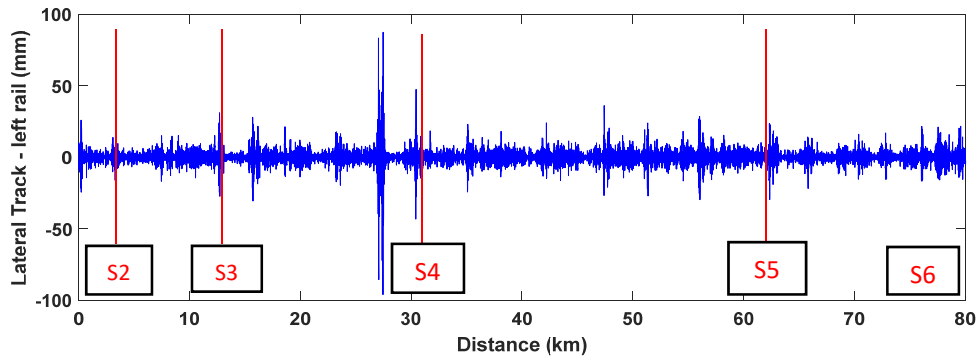
111

(a) Restored waveform- for left rail
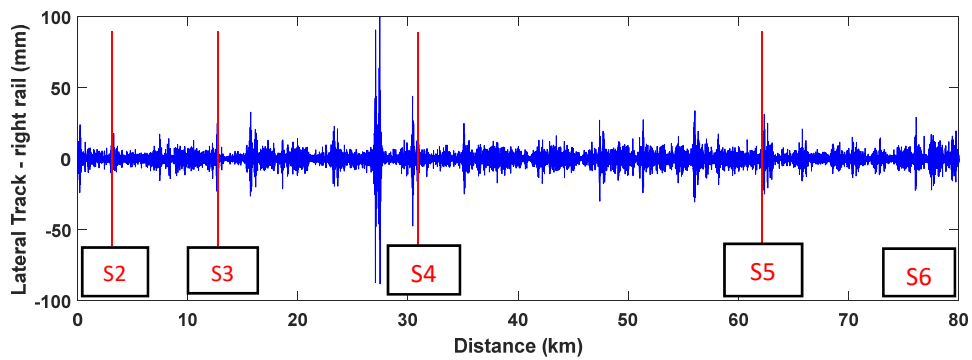
(b) Restored waveform- for right rail
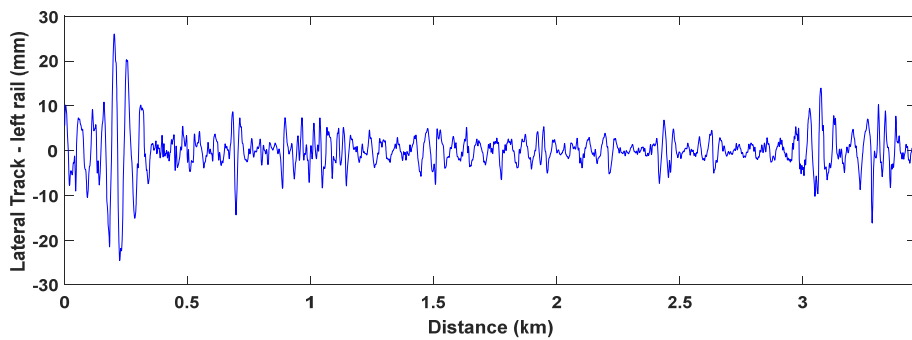
(c) Restored left rail waveform: lateral track (Station 1-2)

(B) Restored True Lateral Track irregularity

Figure 5.7 Restoration of True Track irregularity

5.2.1.7 Spiral easement

A rail track curve should have progressive increase in radius over time instead of becoming straight all together. An easement curve, also known as a transition curve, a spiral easement, is

a gradual curve starting from infinite radius (straight) where it meets the adjacent straight ('tangent') track and decreasing in radius until it matches the desired curve radius (as shown in Figure 5.8 (a)). This reduces the sideways force applied to a train entering or leaving a curve, which in turn reduces wear on prototype wheels and track and for both prototype and model, reduces the potential for derailments. If such easement is not provided, then the lateral acceleration of the train will change abruptly at the tangent point where the straight section meets the curved track. The minimum curve radius must be provided in order to satisfy the allowable design radius and also maintain the operation cost. Cant is defined as the difference in elevation of two rails, which is also known as super elevation, as shown in Figure 5.8 (b). It helps train to traverse on a curved section with wheel flanges in contact with the rails, with less wear and friction. Taking into account, the easement curve and super elevation, the maximum safe speed of a curve can be determined. The maximum cant value provided for the standard gauge railway track under measurement is about 105 mm (from Figure 5.8 (b)). A vertical easement, also known as a grade transition, and it takes a longer linear distance to climb a hill of a given height using a maximum grade.
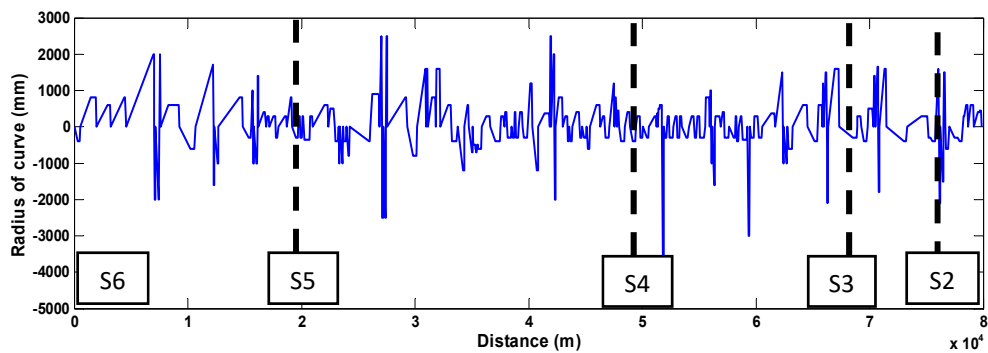
(a)
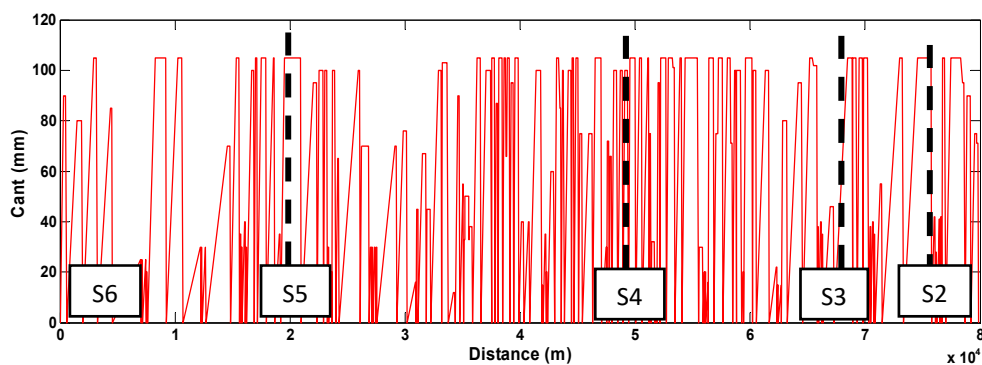
(b)

Figure 5.8 Track transition curve

5.2.1.8 Ruling Gradient

It is defined as the steepest climb between two points on the railway track (Figure 5.9). A train can haul only half or even less weight on 1 % gradient (1 in 100) when compared to that on plane section. Thus providing decent ruling gradient generally helps in limiting the load that train can pull, which includes the weight of the train vehicle also. The gradient on sharp curves is effectively steeper when comparing to the same gradient on straight tracks. In order to compensate this issue, the ruling gradient provided must be reduced marginally on the sharp curves to maintain the ruling grade constant all over. Gradients (slope) can be expressed as per mille, ‰ (in each thousand). Figure 5.9 shows the recorded ruing gradient of the measured railway track using TRV, which has drastic variation from constant section to curved section beyond station 3.
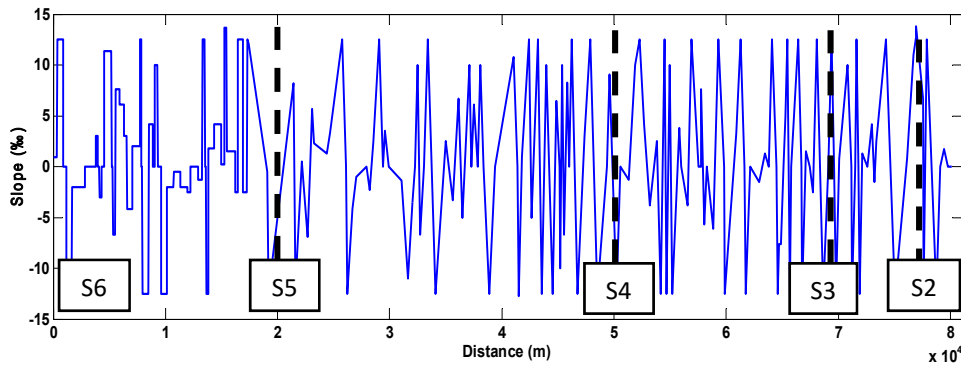
Figure 5.9 Ruling gradient of track

The measured vertical and lateral responses on the car body and axle-box mounted accelerometers are plotted along with the RMS plots in the Appendix: B for all stations.

5.2.2 Track profile estimation from commercial train vehicle

Railway infrastructure maintenance of train vehicles and tracks, are important for guaranteeing the safety of the system. Track irregularity is the key factor of external excitation for a train system. An advantage of using in-service railway vehicle for track maintenance is a simple and robust method. Lately, numerous track geometry estimation methods using inertial sensors by acceleration data are proposed. [116] developed low-cost Train Intelligent Monitoring System (TIMS) for monitoring railway track irregularities in local railways and also train position identification method using GPS sensor and train velocity where there is no

connection with tachometer signal. The RMS of vertical and lateral acceleration values are being considered as threshold for vertical and lateral track geometry respectively.

A number of research works have been carried out using vibration response of ordinary vehicles [57, 58, 62, 117]. When only dynamic acceleration response is observed, the location of an accelerometer in the vehicle is critical. Similarly, when only angular velocity is measured, there are certain undetectable frequency ranges which exist due to the difference in vehicle wheel base length. Therefore, observing either acceleration or angular velocity is not enough to capture the exact dynamic response [118-121]. Also in order to process both acceleration and angular velocity, transfer function method is not sufficient to describe the model since it is designed for single-input and single-output model. Instead, the state-space representation needs to be utilized in order to achieve multi-input model.

The acceleration data measured at car-body floor level is extremely reliant on the primary and secondary suspensions, and thus the consequence of the track irregularities are challenging to extract from such data. The significant aim of this present research is to recommend an approach for track monitoring by simple acceleration and angular velocity measurements by utilizing a small number of prevalent sensors attached to car body and bogie mass of in-service vehicles. In this section, an experimental study is carried out in local Japanese in-service railway network to identify track profile from acceleration and angular velocity measurements on train car body. Prevalent sensing devices such as smartphones are potentially utilized in train body motion measurement. However, the applicability of such measurement for track profile estimation is not clarified yet. To evaluate track profile from measurements obtained from car-body responses, a data assimilation inverse analysis based augmented state Kalman filter (ASKF) is utilized to solve the problem using 4 DOF simplified train model. The efficiency of the proposed approach is also validated.

5.2.2.1 Onboard sensing system

The sensor considered for the measurement purpose is of smartphone based iPod touch which utilize the Dynamic Response Intelligent Monitoring System (iDRIMS) quantitatively obtained from dynamic response of a driving vehicle [119, 121]. Yet, the earlier mechanism of iDRIMS has limitations. Generally, iDRIMS have two significant points: (a) a modest and low cost arrangement which can be easily attached on to any locations of the body of a commercial vehicle devoid of the requirement of vehicle adjustment and (b) an application which can estimate road condition from measured data on the vehicle body with the capability to compensate for the difference in the vehicle's dynamic features and drive speeds. Apple's iPhone and iPod touch [122] are employed as measurement devices with an iOS application named iDRIMS measurement application. The application is established with the

requirements of precise sampling timing and simple handling operation assuming commercial vehicle drivers as the operator. iDRIMS can measure acceleration, angular velocity, and GPS signals simultaneously. The application can also capture photo and movie data. The vehicle responses are obtained at a sampling frequency of 100Hz and GPS signal is obtained with a sampling frequency of 1Hz. In order to precisely obtain the measurement data from vehicle and also to avoid coordinate transformation, the smartphone was mounted on a plane surface, such as train car body floor. The dynamic response data for in-service commercial train vehicle (as shown in Figure 5.10) are collected from two types of sensors: namely, (a) RTRI sensor: developed by Railway Technical Research Institute (RTRI), Tokyo, Japan and (b) smartphone based iPod touch with iDRIMS application (Figure 5.11 (b)). The sensors are placed on the floor of the driver room, which is approximately directly above the front bogie. The two different iPod touch of 5th generation was used for the measurement purpose (black and blue colored) which is firmly attached on the top and side surface of the RTRI sensor box (Figure 5.11 (a)). The black and blue iPod touches are referred as iPod touch-1 and iPod touch-2 respectively, in the following sections. The sensor directions are illustrated in Figure 5.12.

Figure 5.10 Local railway line and train car
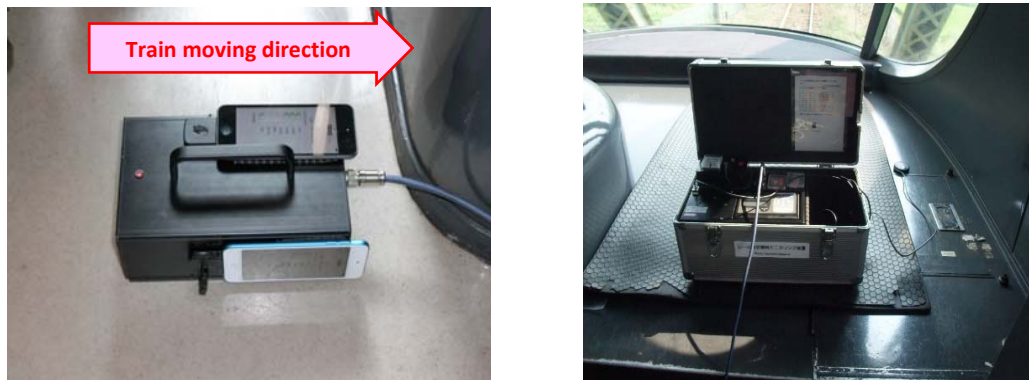
(a) Sensor setup and Onboard data management system in driver cabin

(b) Smartphone Application: iDRIMS

Figure 5.11 Sensor placements on in-service vehicle car body
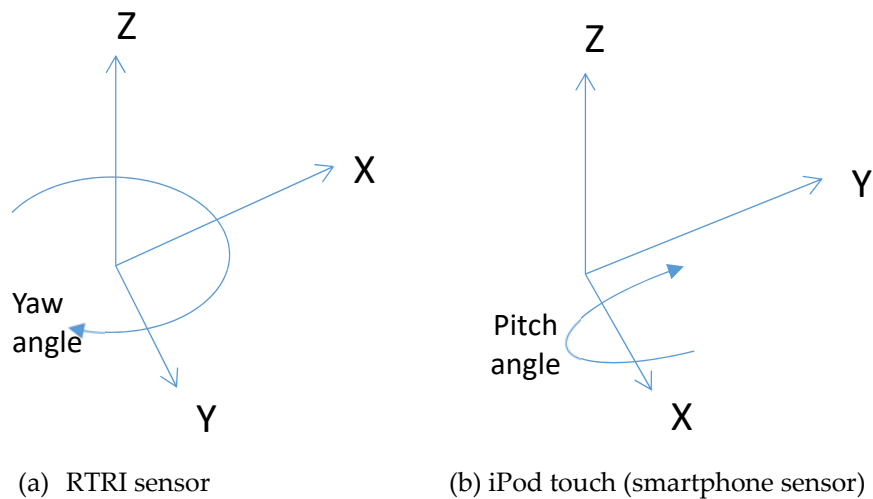
(a) RTRI sensor   (b) iPod touch (smartphone sensor)

Figure 5.12 Sensor direction

The RTRI sensor can only measure acceleration and yaw angle while smartphone based sensor can measure acceleration and pitch rate. Table 5.2 illustrates the RTRI sensor configuration properties. The RTRI sensor is used to cross check the measured dynamic response from iPod touch. The signal acquired from RTRI sensor is with 5000 Hz sampling frequency. The vertical car body acceleration collected from all sensors are plotted as shown in the Figure 5.13 (a-b) for the up train (station 1 to 6) and down train (station 6 to 1) respectively. The plots show that, the vertical acceleration data collected from both iPod touches are in good agreement with the RTRI sensor attached on car body floor. Figures 5.13 (c-d), show the comparison results for yaw angular velocity for the up train both is time and frequency domain and it shows clearly

from Power spectral density (PSD) plots that blue iPod touch is closely having good correlation with RTRI sensor.

Table 5.2 RTRI Sensor configuration properties

Channel	Signal	Range for data recorder	Sensitivity	Range of sensor
1	Acceleration x	5V	0.5G/V	-2G ~ 2G
2	Acceleration y	5V	0.5G/V	-2G ~ 2G
3	Acceleration z	5V	0.5G/V	-2G ~ 2G
4	Sound	5V	97dB/V	57 ~ 111 db
5	Yaw angular velocity	5V	4deg/sec/V	-6deg/sec ~ 6deg/sec
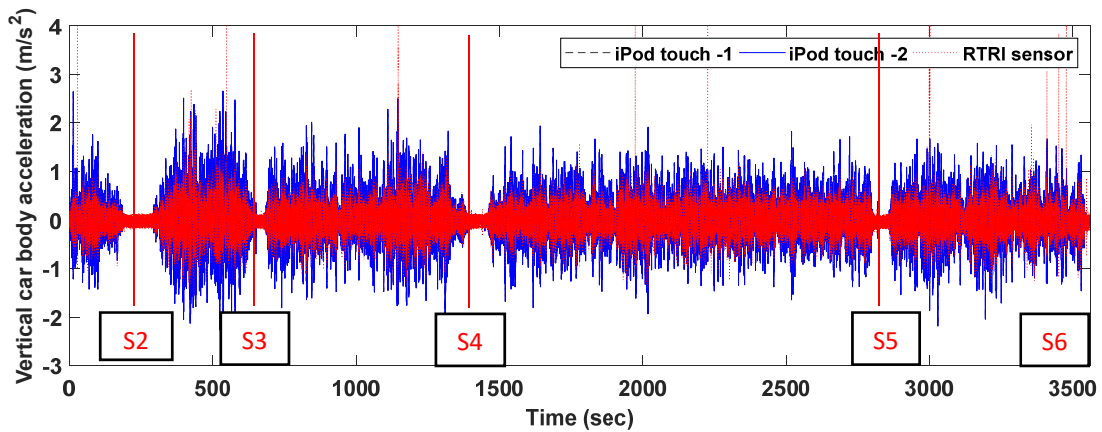
(a) Comparison of Vertical car body acceleration: Up train data
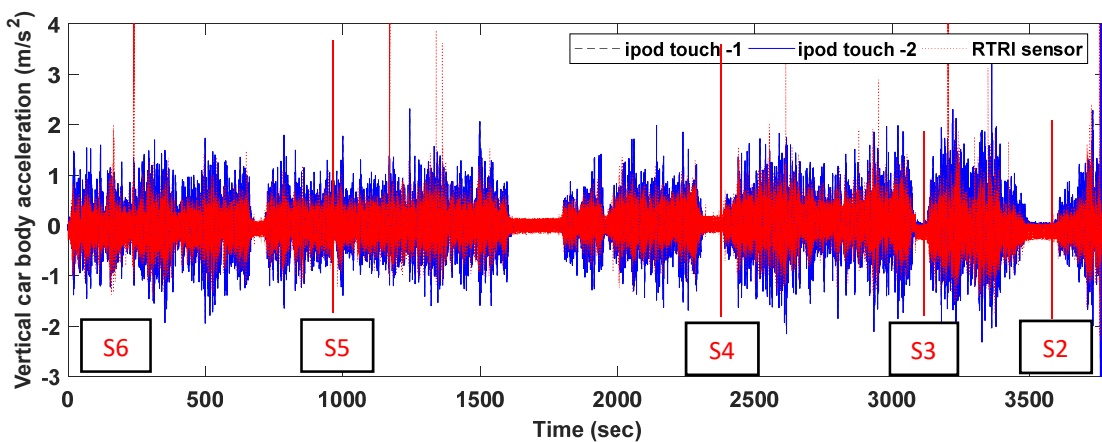
(b) Comparison of Vertical car body acceleration: Down train data
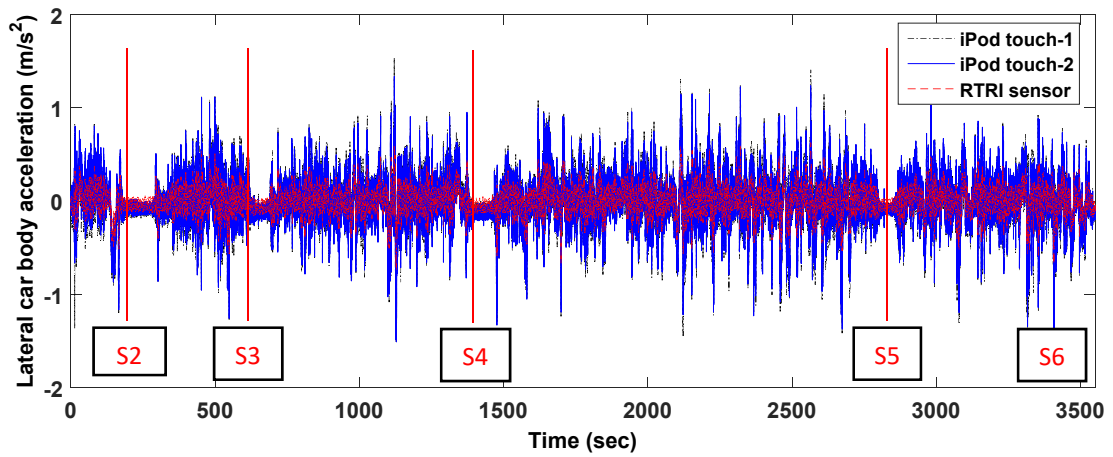
(c) Comparison of Lateral car body acceleration: Up train data
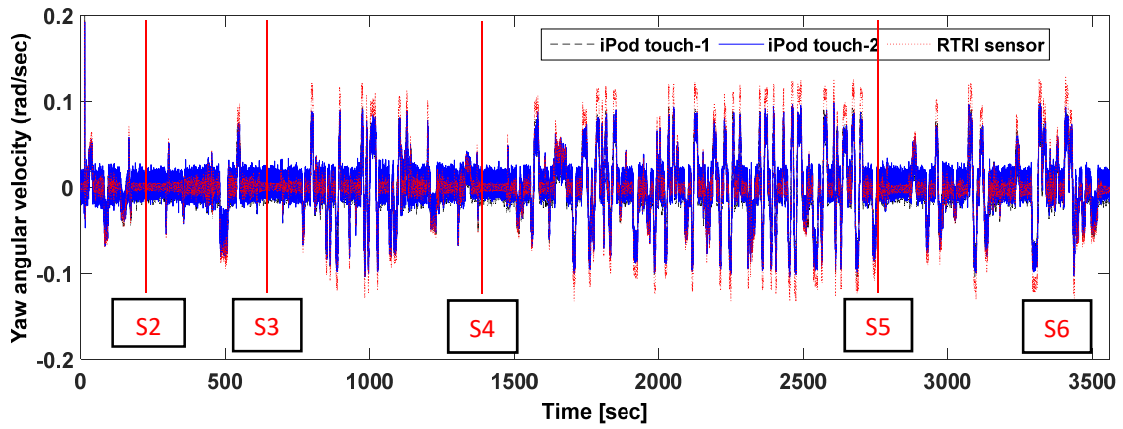
(d) Yaw angular velocity comparison
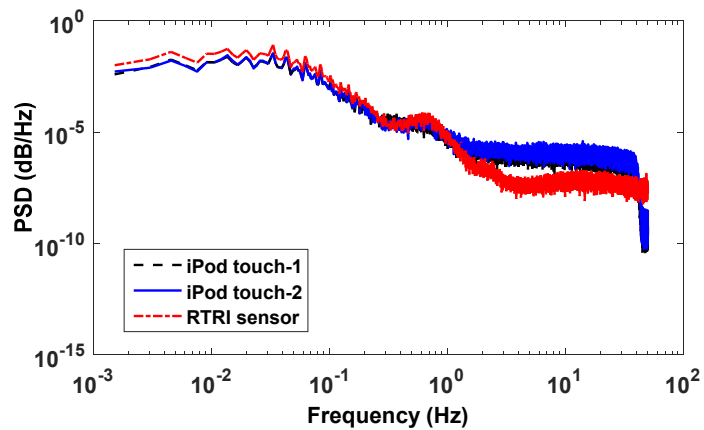
(e) PSD plots

Figure 5.13 Comparison of sensors for validation

119

The velocity profile obtained from two iPod touches are compared with each other for up train side of the running train as shown in the Figure 5.14. The vertical and lateral car body acceleration measurements obtained from both iPod touches are compared and plotted in the Figures 5.15 and 5.16 for the up train side of the traversing vehicle respectively. In order to consider the comfort level of the car body, a low pass filter of 8 Hz is applied with the transition band of stopping frequency at 10 Hz to the measured acceleration data (Figure 5.15 (d-f)). Both the responses are compared in the frequency domain by utilizing PSD approach and also compared in time domain using RMS method.
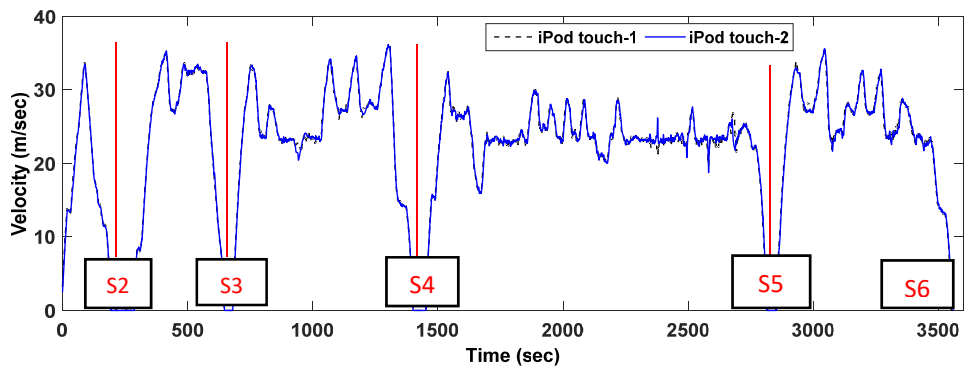
Figure 5.14 Velocity profile comparison between two iPod touches: Up train side
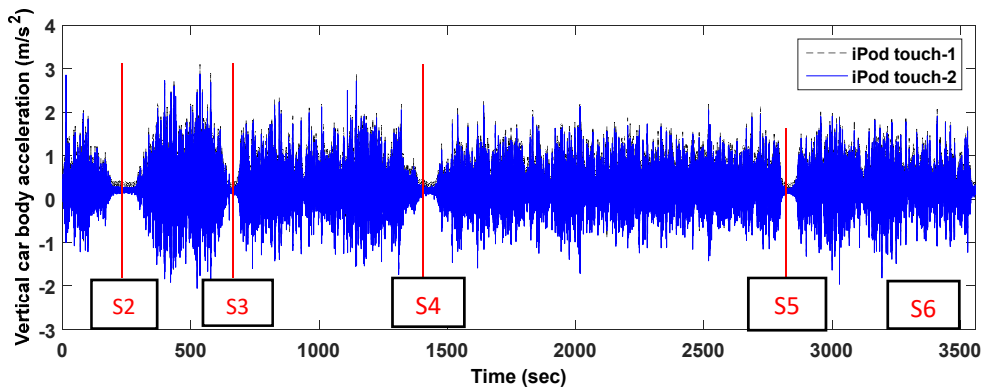
(a) Up train side

(b) RMS plot

120
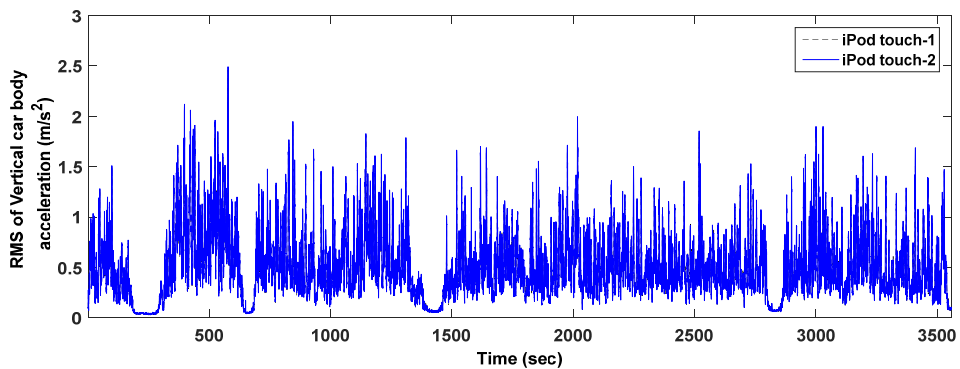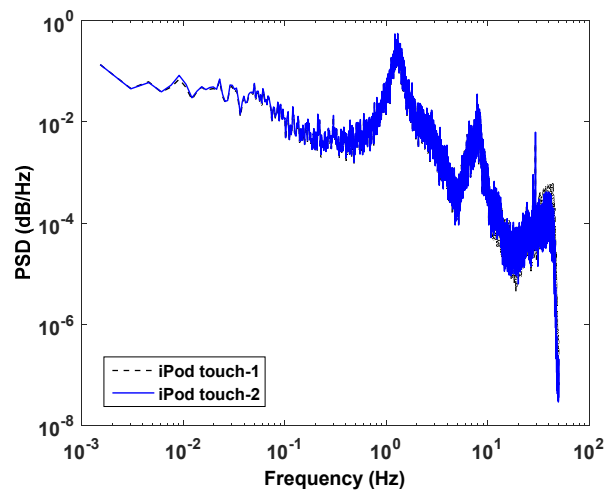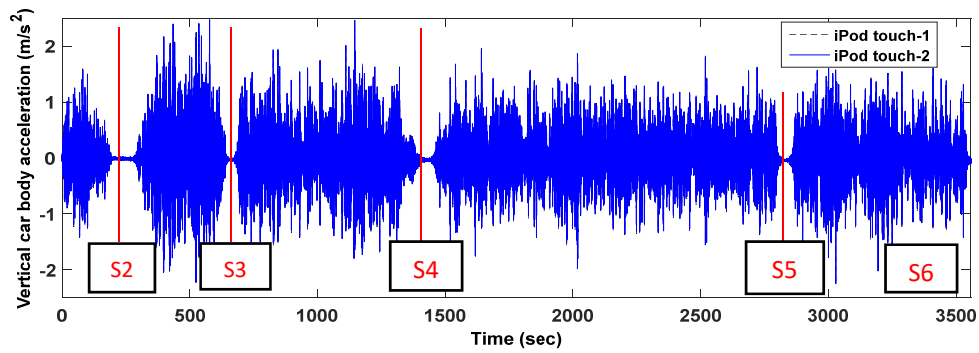
(c) PSD plot

(d) A low pass filter of 8 Hz is applied with the transition band of stopping frequency at
10 Hz
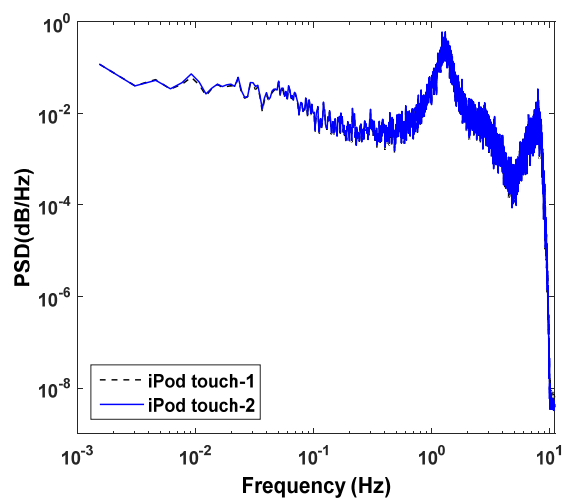
(e) PSD plot (filtered waveform with the gain dropped at 8 Hz to 10 Hz)
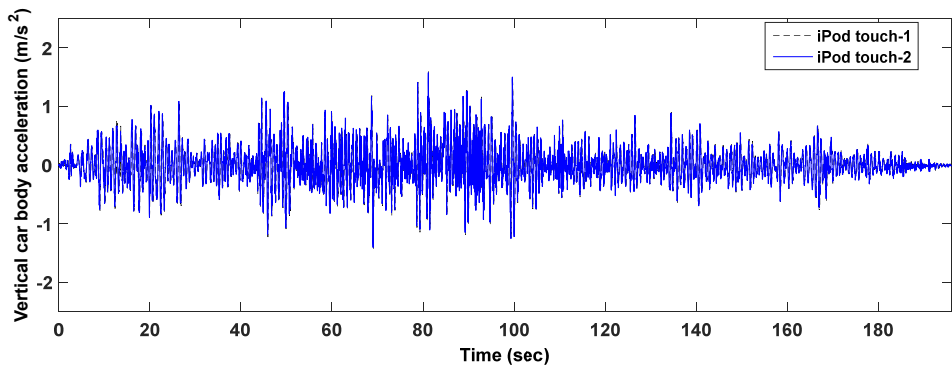
(f)   For station 1-2 (filtered waveform with the gain dropped at 8 Hz to 10 Hz)

Figure 5.15 Car body vertical acceleration measurement: Up train side
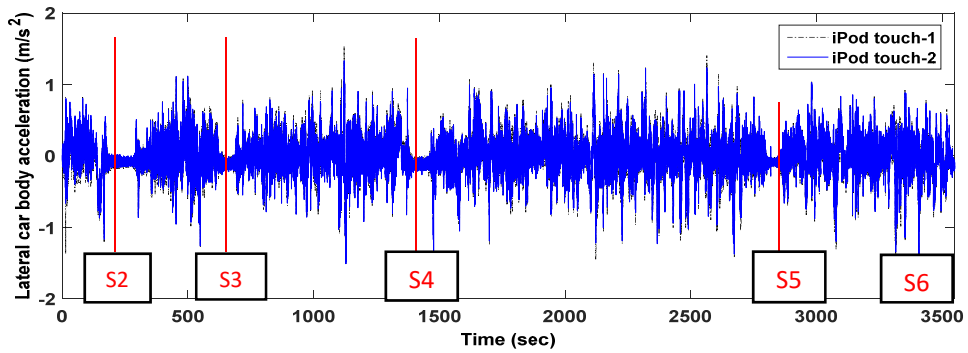
(a)   Lateral car body acceleration
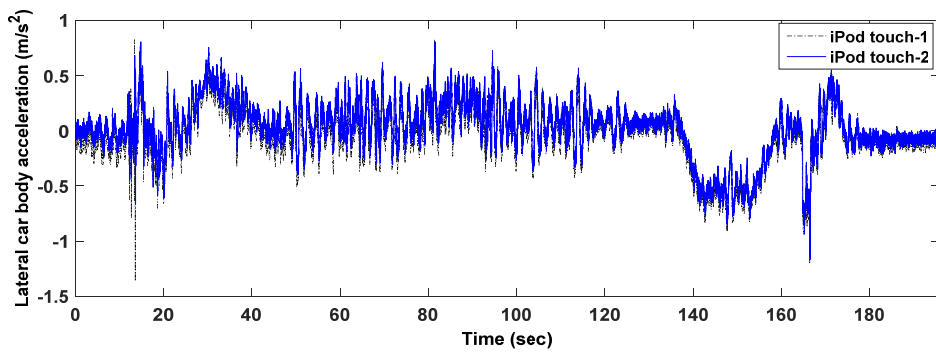
(b) For station 1-2 (zoomed response)

(c) RMS plot

122
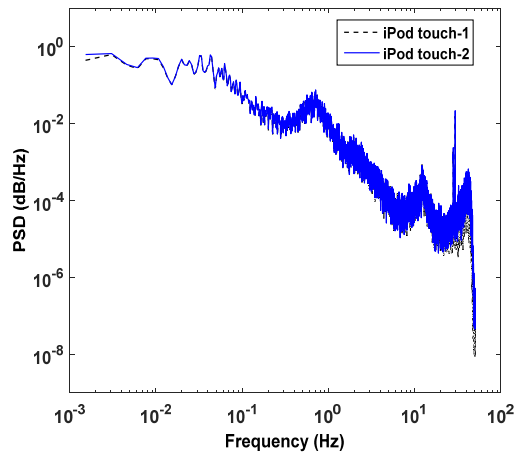
(d) PSD plot

Figure 5.16 Car body lateral acceleration measurement: Up train side

The car body pitch rate measurement and yaw rate measurement obtained from both iPod touches are compared and plotted in the Figures 5.17 and 5.18 for the up train side of the traversing vehicle respectively. Both the responses are compared in the time domain (RMS plot) and frequency domain (PSD) and it is found to have slight deviation with each other. The measurement responses obtained from smartphones mounted on car body floor for down train traversing vehicle are illustrated in Appendix: C.
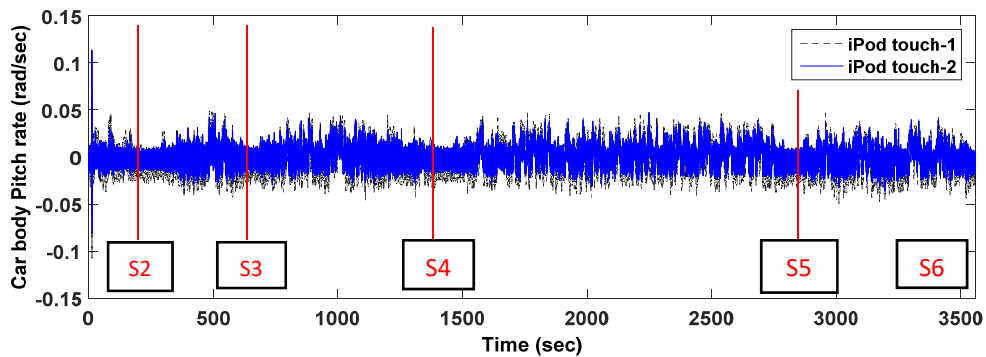
(a) Car body pitching angular velocity: Up train side

(b) RMS plot

123
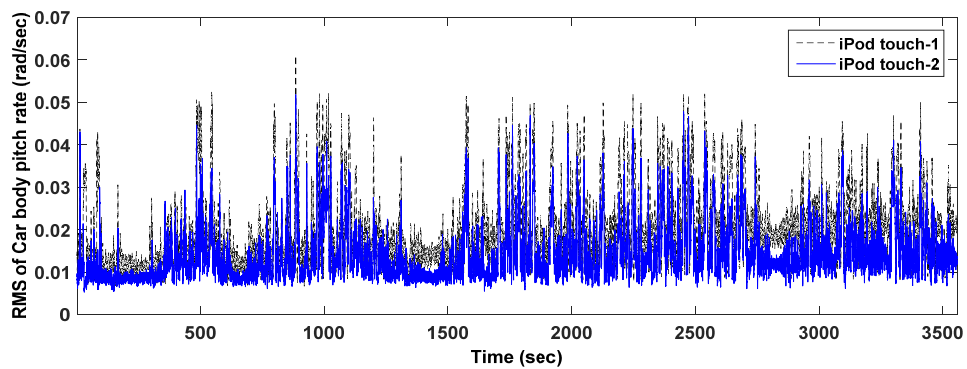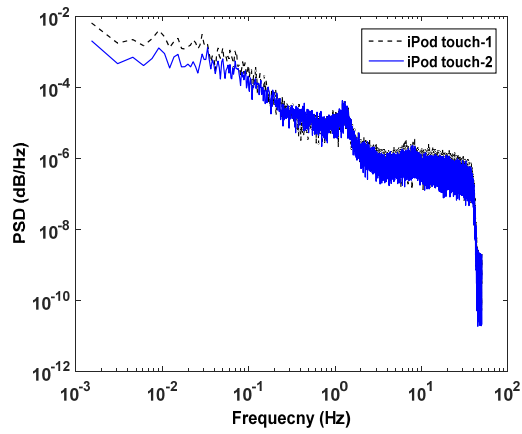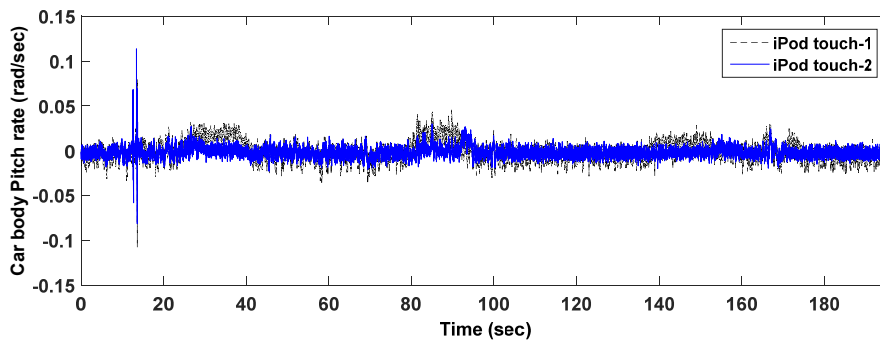
(c) PSD plot

(d) For station 1-2 (zoomed response)

Figure 5.17 Car body pitch rate response and its RMS and PSD plots: Up train
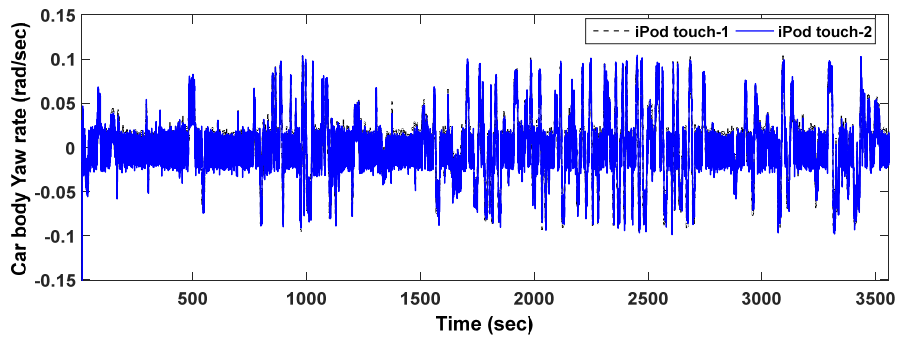
(a) Car body yawing angular velocity: Up train side
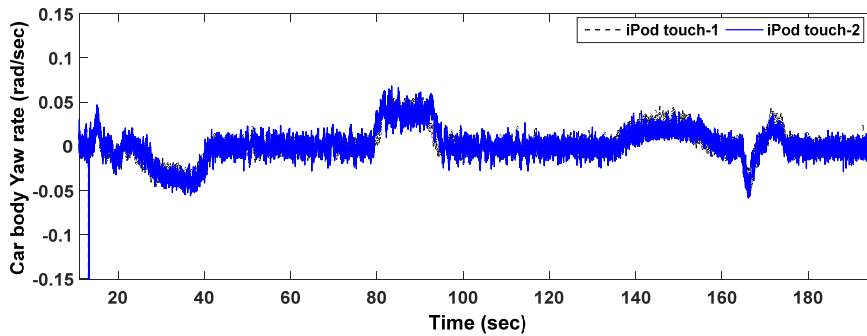
(b) Zoomed responses for Station 1-2

124
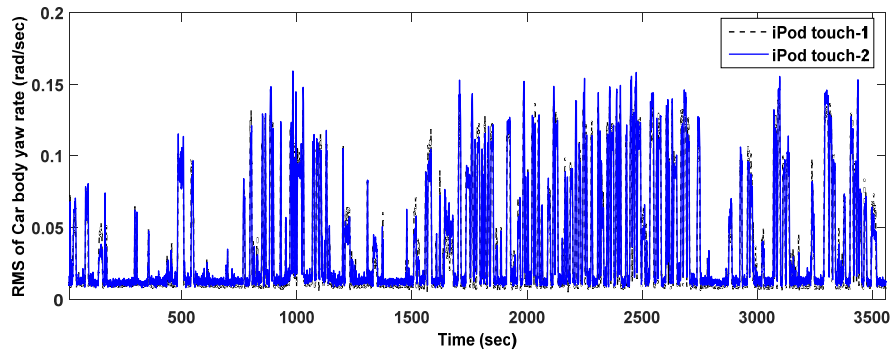
(c) RMS plot
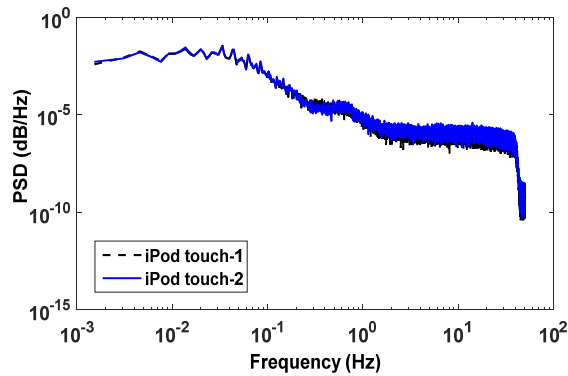
(d) PSD plot

Figure 5.18 Car body yawing angular velocity measurement: Up train side

5.2.2.2 Distance sampling method for on-board measured data

In order to make the track condition monitoring simple and easy, a technique is required to convert the on-board measured data to the distance sampling data. The track irregularity measured data obtained from TRV and the in-service vehicle measurement responses do not correlate well. Henceforth, it is required to correlate well with the on-board measured data. In [123], explains a methodology to extract the true distance sampling data by comparing the yaw angular velocity measured on car body of the in-service train and the transition curve data of the respective track section. By manually correlating these two responses, it is feasible to extract the more precise distance sampling data which can be further utilized in the inverse analysis problem in order to compare with the estimated results from Kalman filtering techniques. Figure 5.19 illustrates the comparison of the yaw rate angle measured by iPod touch-2 (blue) mounted on car body floor of in-service train and the easement curve (desired curve radius) of the track section measured using TRV. The low pass filter is applied to the iPod data in order to the cross correlation function is utilized for the comparison and lag difference is maintained to be zero in all cases. It shows high correlation among the plots and the distance sampling data is extracted and utilized later for the comparison purpose.

125
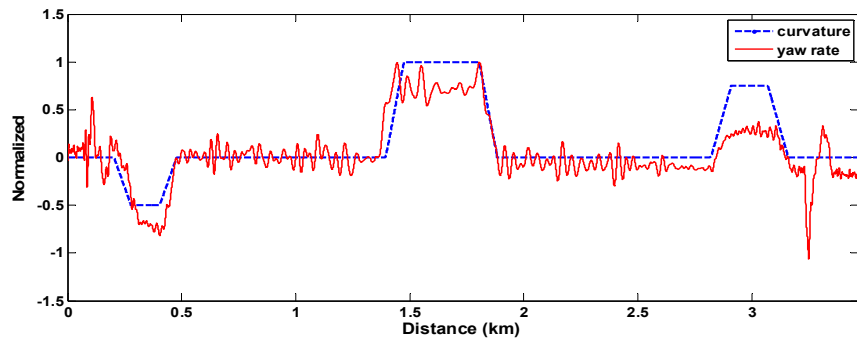
(a) Station 1-2
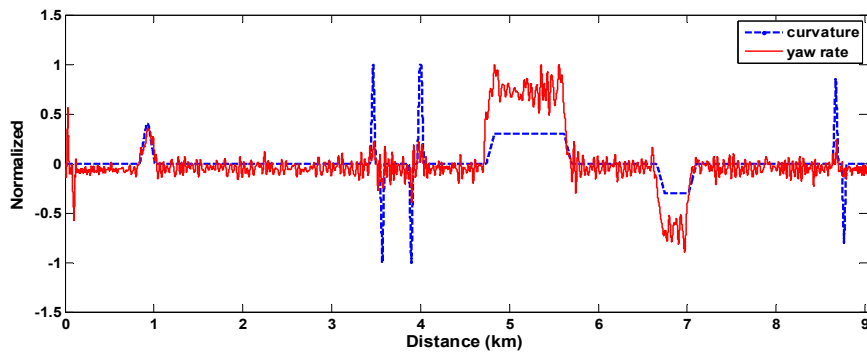
(b) Station 2-3
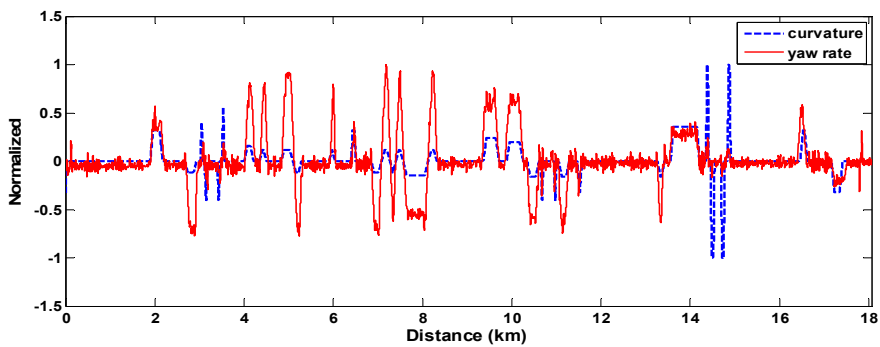
(c) Station 3-4

(d) Station 4-5

126
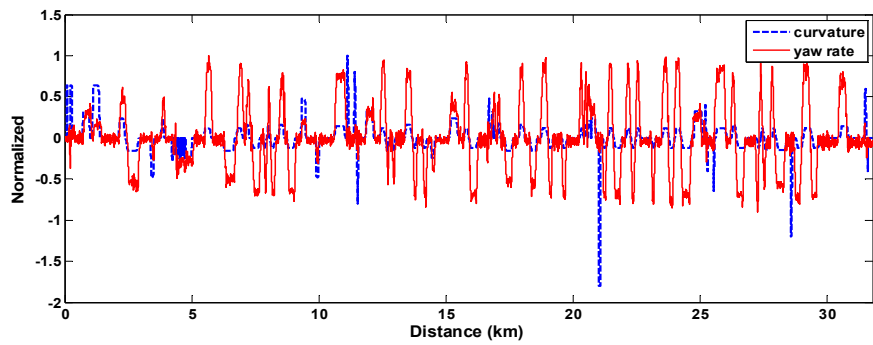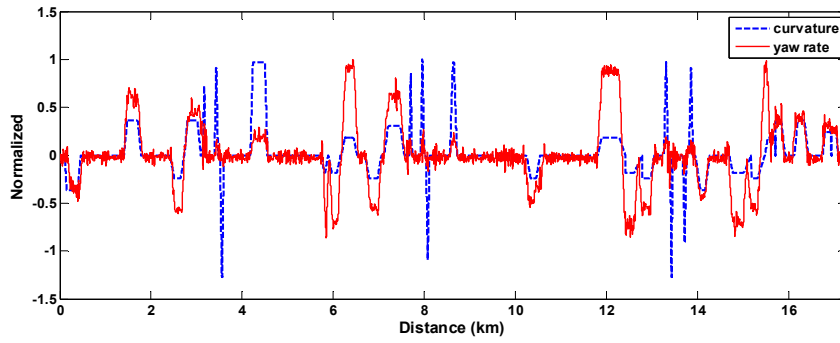
(e) Station 5-6

Figure 5.19 Comparison of yaw angular velocity and transition curve data for all stations

5.3 Converting true profile to 10 m chord versine waveform

As per [115], a relationship between a true track irregularity and its measured one by 10 m - chord versine method can be mathematically expressed as,

$$p(x) = q(x) - \frac{q(x+5)+q(x-5)}{2} \qquad (5.1)$$

where $p(x)$ represents the 10 m – chord versine and $q(x)$ represents the true track geometry. In the above equation (5.1), an independent variable 'x' is the distance measured along the actual track and not an originally defined one. In order to validate this indirect theory for converting the original track profile to 10 m chord versine waveform, a restored true track profile is utilized and the above equation (5.1) is used to convert it. Figure 5.20 shows the comparison plot for the true and estimated 10 m chord versine for the track profile. In the Figure 5.20 (b), it shows clear deviation with the true measured versine waveform. Thus, in frequency domain, PSD plots show the variation because the measured 10 m chord versine is for the bandwidth of the 6 - 60 m wavelength. Hence, by incorporating the band pass filter with cut off spatial frequency of 0.0166 – 0.166 cycle/m is considered and the results are illustrated in Figure 5.21. Thus, the estimated and true 10 m chord versine waveforms are in good agreement.
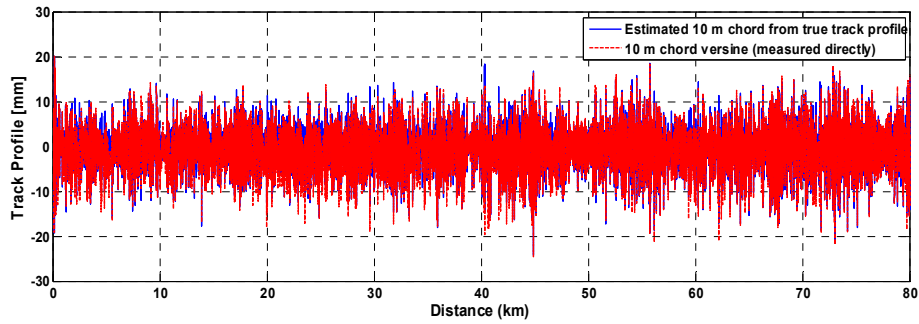
(a)
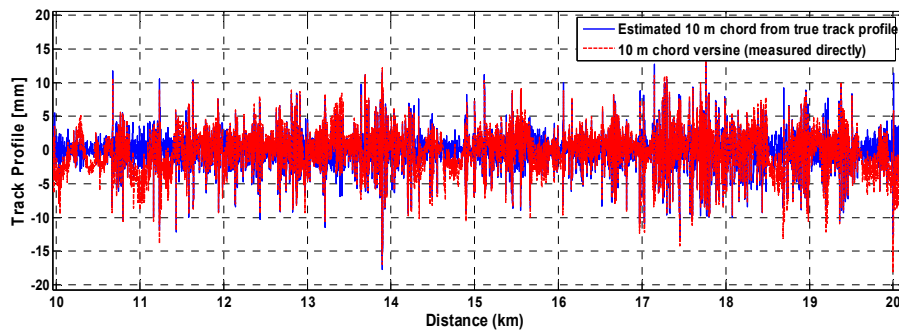
(b) Zoomed response (10 -20 km)
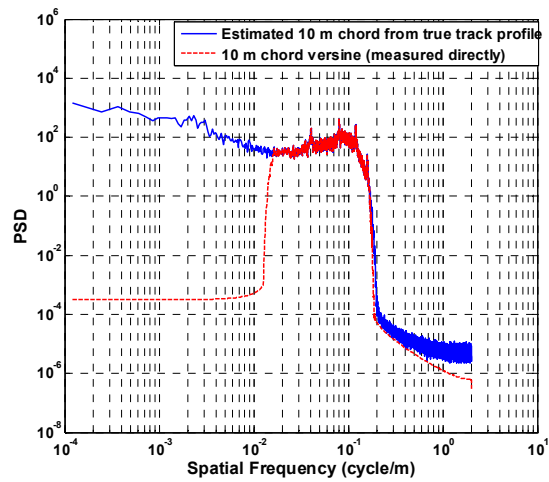
(c) PSD plot

Figure 5.20 Comparison result for true and estimated 10 m chord versine for left rail
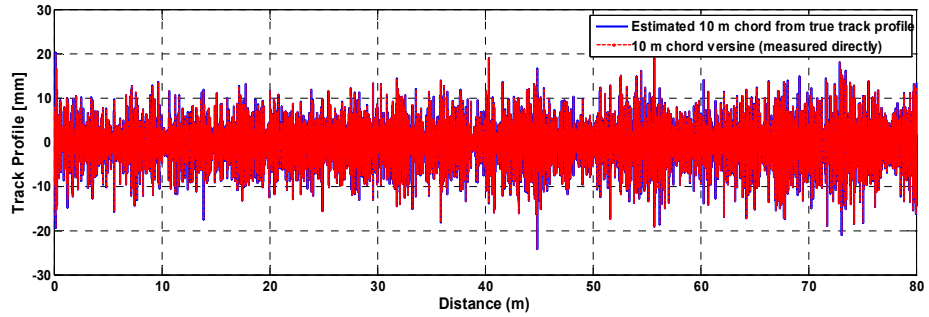
(a) After band pass filter (spatial frequency: 0.0166 – 0.166 cycle/m)
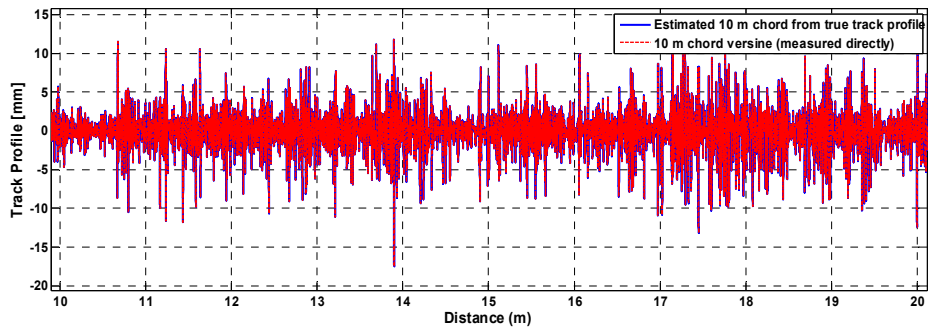
(b) Zoomed response (10 – 20 km)
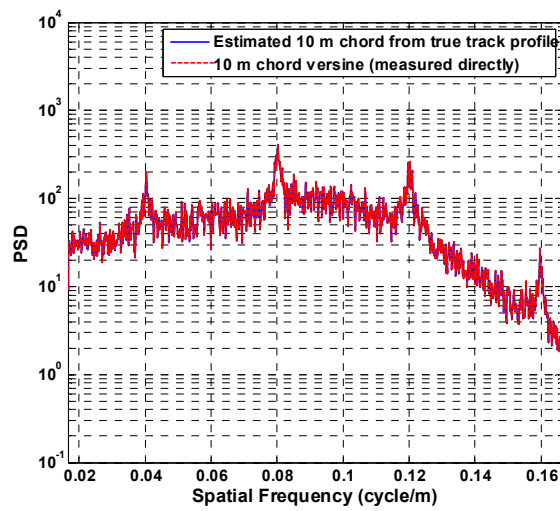
(c) PSD plot

Figure 5.21 Comparison results for 10 m chord versine for left rail: after filter

5.4 Vehicle modelling and inverse analysis for estimating vertical track irregularity

In order to analysis the measured responses, the appropriate vehicle model need to be considered for implementing an inverse analysis using augmented state Kalman filtering (ASKF) technique. Since the measurement is carried out only on the car body of the train, the simplified train model with averaged track geometry is considered for inverse analysis, as shown in the Figure 5.22. It represents the sensor placement on the car body floor just above the front bogie mass. The measured responses are car body vertical acceleration and pitching angular velocity. Inverse analysis is incorporated with various measurement noise levels generated as a random walk driven by Gaussian white noise and also initial condition error in the Kalman filter iteration in order to approximately obtain the exact profile. For true track profile, restored waveform from 10 m chord measuring system for left rail - vertical track irregularity, is considered for comparison with the estimated track profile (Figure 5.7). A typical case of track profile after using band pass filter with cut off spatial frequency of 0.0166 – 0.166 cycle/m, by incorporating noise level of 5 % (standard deviation of measured response and random error). The vehicle parameter model given in Table 3.3 is considered for the inverse analysis [94, 95]. The parameters of the model are approximated based on the real vehicle. The filter considered in this simulation helps to evaluate wavelengths ranging between 6 m – 60 m, which covers ranges comprising from short to long wavelength irregularities as mentioned in [96].
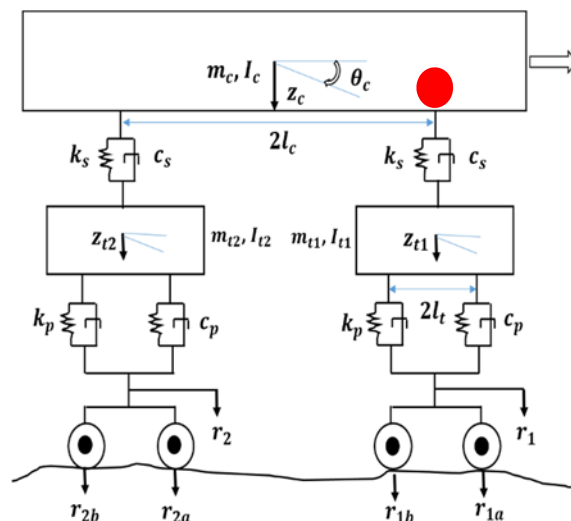
Figure 5.22 Simplified train model with averaged geometry: for vertical displacement

The inverse analysis is carried out using the proposed approaches for the measurement responses obtained while the train is traversing from station 1 to 6 (up train) which is about 80 km distance. In order to show the better performance among the smartphone sensors, the measured responses are compared with RTRI sensor with higher sampling frequency and found that iPod touch-2 (blue) is comparatively performing better compared to iPod touch-1 (black). This is due to the car body pitch rate response measured by iPod touch-1 (black) is found deviating slightly compared to that of the iPod touch-2. This may cause the variation in the track profile estimation.

5.4.1 Restored track irregularity waveform for vertical irregularity

The left track profile irregularity (Figure 5.7 (A)) is considered as the true track profile for the comparison purpose with the estimated results obtained from Kalman filter inverse analysis technique. Figures 5.23 (a-b) represent the results on reconstructing track geometry profile for station 1-2, using a Kalman filter and inverse modelling for iPod touch-2 (blue) sensor. The plot shows the comparison of the track profile obtained from extended ASKF methods with true profile obtained from TRV after carrying out the distance sampling method (as discussed in Figure 5.19). In order to compare the frequency content of estimated and true profile, PSD results, calculated using Welch's method are obtained and shown in Figure 5.23 (c). In Appendix: D, Figures D.1 - D.4, show the estimated responses and also zoomed-responses of track geometry profile for station 2-6, using a Kalman filter and inverse modelling for iPod touch-2 (blue) sensor. Also PSD plots are shown for the comparison in frequency domain. The Federal Railroad Administration (FRA) Class 4 (very poor) track profile is compared with the inverse analyses results in PSD plots to convey the current status of the existing the track profile section. Figure 5.23 (d) gives the comparison of estimation error for Approach (a) and (b) which has value less than ± 5 mm. The statistical metrics like Root Mean Square Deviation (RMSD) is utilized to quantify the error among the estimated profile with true one. The extended ASKF techniques are performed for all stations from 1 to 6 and the statistical metric, RMSD is calculated to obtain the quantitative difference between both approaches as illustrated in Table 5.3. Also, Approach (a) performs better than Approach (b). The results are influenced much by the spiral easement curve, cant, ruling gradient and also by integration error accumulations. These parameters influence the train dynamics and thus, measured acceleration and pitch rate at car body floor is highly affected. These influences need to be further investigated in future research. In future, the upgraded model which considers bogie pitching motion can be utilized to improve the estimated results.
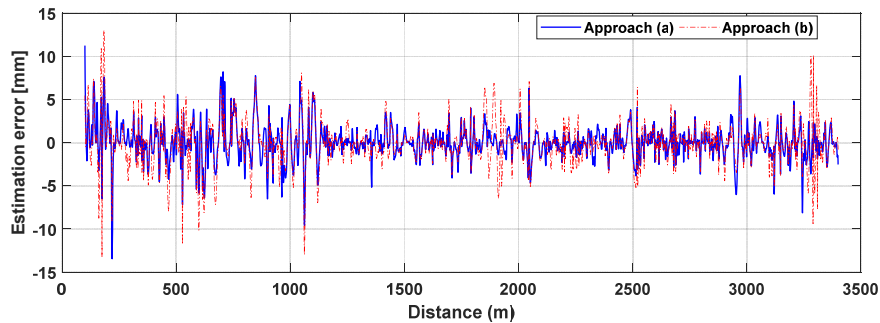
(a) For station 1-2

(b) Zoomed responses (0.5 – 1.5 km)
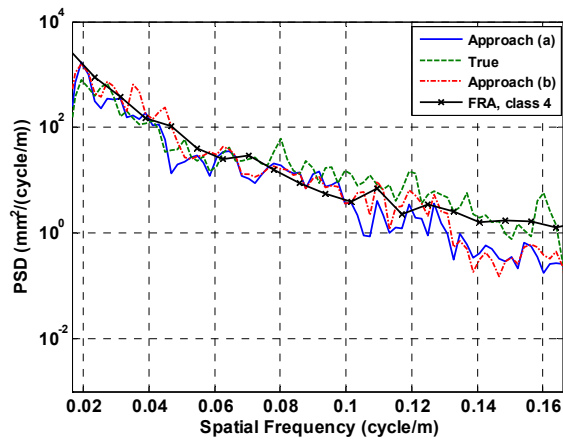
(c) PSD plot

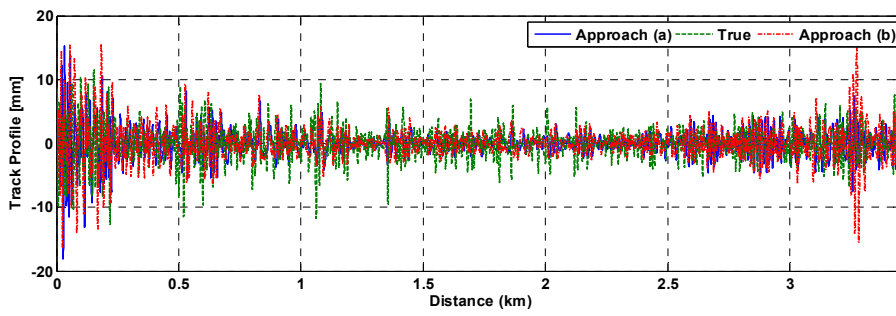(d) Estimation error after misfit criteria (100 m to 3400 m)

Figure 5.23 Estimation results for restored left vertical track profile for station 1-2

Table 5.3 Comparison of statistical metrics for estimation results on 4 DOF simplified train vehicle model: restored waveform for vertical irregularity
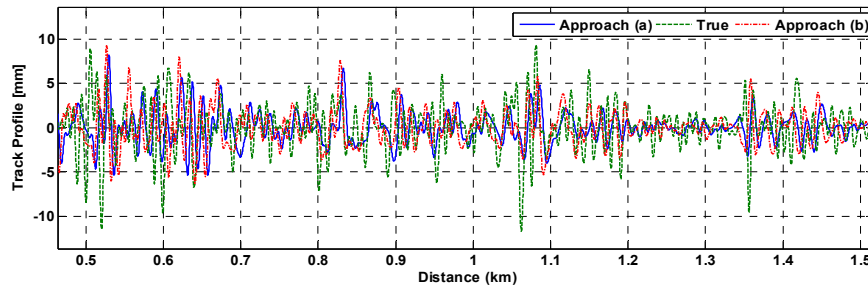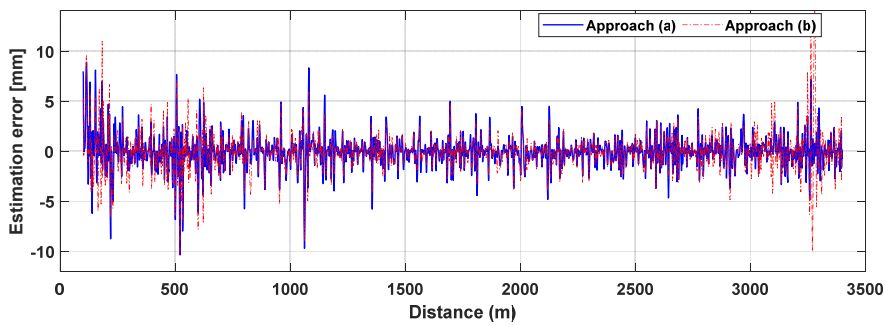
Station	Distance (km)	Approach (a)			Approach (b)		
		RMSD (%)	CC	RMSE (mm)	RMSD (%)	CC	RMSE (mm)
1-2	3.5	61.4	0.84	1.97	77.1	0.81	2.46
2-3	9	80.2	0.86	3.08	94.7	0.83	3.65
3-4	18.1	108.3	0.82	3.67	115.9	0.79	3.94
4-5	31.8	118.7	0.80	4.21	120.5	0.78	4.28
5-6	17.4	120.3	0.74	3.91	123.2	0.74	4.01

5.4.2 10 m chord versine waveform for vertical irregularity

Figure 5.24 represents the results on reconstructing 10 m chord versine waveform for station 1-2, using a Kalman filter and inverse modelling for iPod touch-2 (blue) sensor. The plot shows the comparison of track profile obtained from extended ASKF methods with true versine obtained from TRV. In order to compare the frequency content of estimated and true profile, PSD results, calculated using Welch's method are obtained and shown in Figure 5.24 (c). In Appendix: D, Figures D.5 - D.8, show the estimated responses and also zoomed-responses of 10 m chord versine waveform of track geometry for station 2-6, using a Kalman filter and inverse modelling for iPod touch-2 (blue) sensor. Also PSD plots are shown for the comparison in frequency domain. Figure 5.24 (d) gives the comparison of estimation error for Approach (a) and (b) which has value less than ± 5 mm. The statistical metrics like RMSD is utilized to quantify the error among the estimated profile with true one as illustrated in Table 5.4. Also, Approach (a) performs better than Approach (b). As discussed early, the results might be influenced by the spiral easement curve, cant, ruling gradient and also by integration error accumulations. These influences need to be further investigated in future research. In future, the upgraded model which considers bogie pitching motion can be utilized to improve the estimated results.

(a) For station 1-2

(b) Zoomed responses (0.5 – 1.5 km)
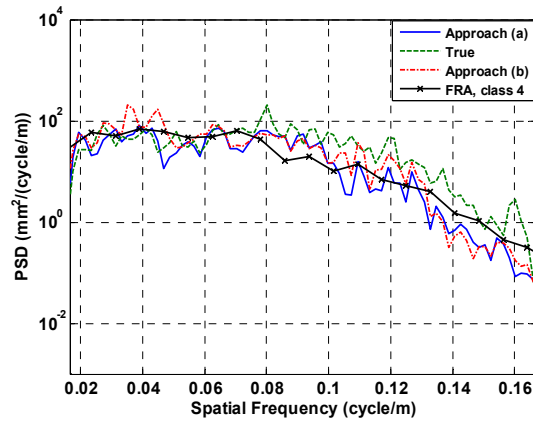
(c) PSD plot

(d) Estimation error after misfit criteria (100 m to 3400 m)

Figure 5.24 Estimation results for 10 m chord versine: left vertical track profile for station 1-2

Table 5.4 Comparison of statistical metrics for estimation results on 4 DOF simplified train vehicle model: 10 m chord versine waveform for vertical irregularity

Station	Distance (km)	Approach (a)			Approach (b)		
		RMSD (%)	CC	RMSE (mm)	RMSD (%)	CC	RMSE (mm)
1-2	3.5	67.8	0.74	1.37	77.9	0.72	1,81
2-3	9	77.2	0.79	2.25	78.4	0.76	2.28
3-4	18.1	95.47	0.73	2.30	101.8	0.70	2.45
4-5	31.8	104.4	0.71	2.47	108.8	0.70	2.57
5-6	17.4	93.5	0.74	2.94	121.3	0.72	3.81

From Table 5.3 and 5.4, the inferences can be drawn as below,

- The relative error is comparatively lesser for Approach (a) than Approach (b).
- For Approach (a) in both the cases, it is found that relative error is slightly higher for true track profile waveform comparing than 10 m chord versine. Because the restored waveform does not include an extra component due to curvature effect. In order to overcome this effect, the 10 m chord versine is more general and flexible method.
- PSD plot obtained using the proposed algorithm aids to approximately evaluate under which category of irregularity the measured rail track profile section falls. This is achieved by comparing the PSD results with the track irregularity power spectrum obtained from FRA- Classes.
- By employing the obtained track irregularity PSD, the track maintenance team can ensure the safety and comfort of railway transportation system.
- The RMSD error can be attributed to following reasons. The real train vehicle primary suspension and secondary suspension systems usually has nonlinearity especially at high drive speed or large track input due to irregularities on the rail. However, this nonlinearity cannot be reproduced in by a linear 4 DOF simplified train vehicle model implemented in this study. Though large modelling error can be compensated by increasing the system noise covariance, the track profile estimation accuracy may be sacrificed.
- The RMSE value gives the dimensional metric error for overall rail track. According to track irregularity tolerance limit, maintenance of track can be done.
- Secondly, the simplified half car model cannot represent the bogie pitching motion of a real train vehicle which often occurs to be significant under different conditions.

## 5.5 Vehicle modelling and inverse analysis for estimating lateral track irregularity

The lateral / alignment irregularity is the significant factor affecting the wheel-rail contact geometry relationship. Poor maintenance of horizontal track geometry can effect in unwanted vehicle dynamic responses leading to poor ride quality, distorted flange contact and deterioration during climb [124, 125]. At rail joints, there is an influence of the disturbances of shocks/ vibrations and also at crossings or turnouts transient vehicle vibration occurs. These forces effect in causing different level of track degradation due to variation in the frequencies corresponding to the vehicle Eigen frequencies. Henceforth, beyond certain level of track irregularity, the traversing of train vehicles will be risky and it might cause lateral track shift or derailment. In order to arrive at the conclusion that the obtained 10 m chord versine alignment is following the track geometry it can be compared to the measured cross levels of the measured track sections. Curvature effect is also incorporated in the alignment signal as this is a chord offset signal [126]. Figure 5.25 illustrates the comparison plot between the 10 m chord versine left alignment waveform with the cross level waveform of the measured track sections and it shows good correlation with each other.
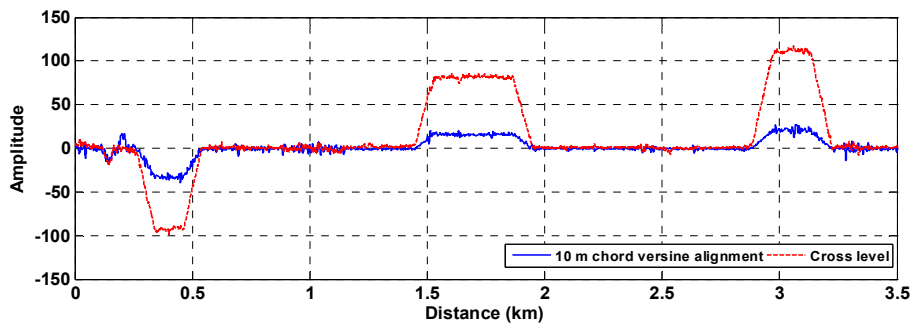
(a) Station 1-2
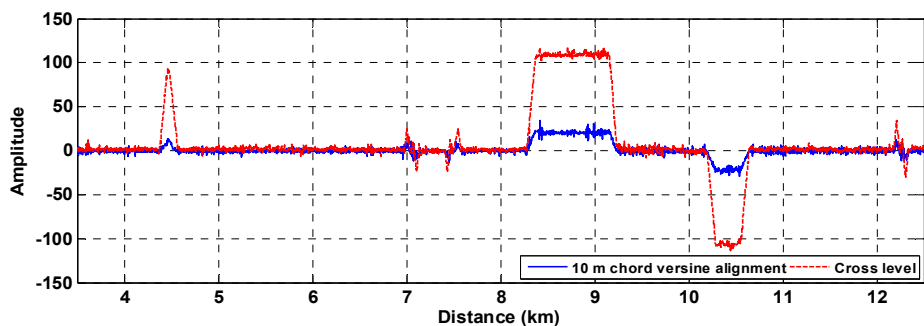
(b) Station 2-3
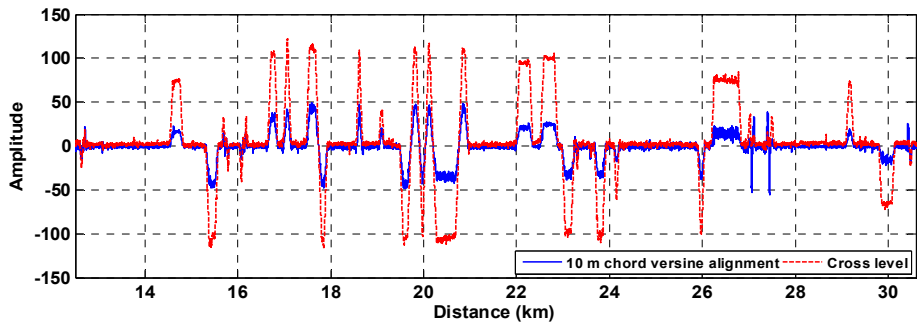
(c) Station 3-4
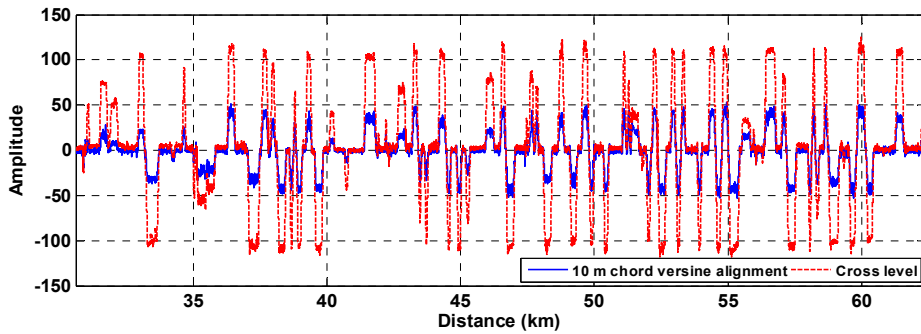
Station 4-5
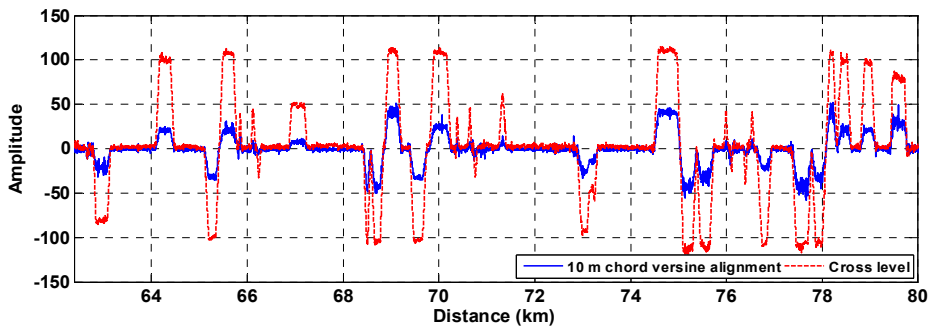
Station 5-6

Figure 5.25 Correlation plot between 10 m chord versine left alignment waveform and the track section cross levels for all stations

In order to analysis the measured responses, the appropriate vehicle model need to be considered for implementing an inverse analysis using ASKF technique. Since the measurement is carried out only on the car body of the train, the simplified train model with averaged geometry is considered for inverse analysis, as shown in the Figure 5.26. It represents the sensor placement on the car body floor just above the front bogie mass. The measured responses are car body lateral acceleration and yawing angular velocity. Inverse analysis is incorporated with various measurement noise levels generated as a random walk

137

driven by Gaussian white noise and also initial condition error in the Kalman filter iteration in order to approximately obtain the exact profile. For true track profile, alignment waveform obtained from 10 m chord measuring system for left rail track irregularity, is considered for comparison with the estimated track profile (Figure 5.7 (a)). A typical case of track profile after using band pass filter with cut off spatial frequency of 0.0166 – 0.166 cycle/m, by incorporating noise level of 5 % (standard deviation of measured response and random error). The vehicle parameter model given in Table 3.3 is considered for the inverse analysis [94, 95]. The parameters of the model are approximated based on the real vehicle. The filter considered in this simulation helps to evaluate wavelengths ranging between 6 m – 60 m, which covers ranges comprising from short to long wavelength irregularities as mentioned in [96].
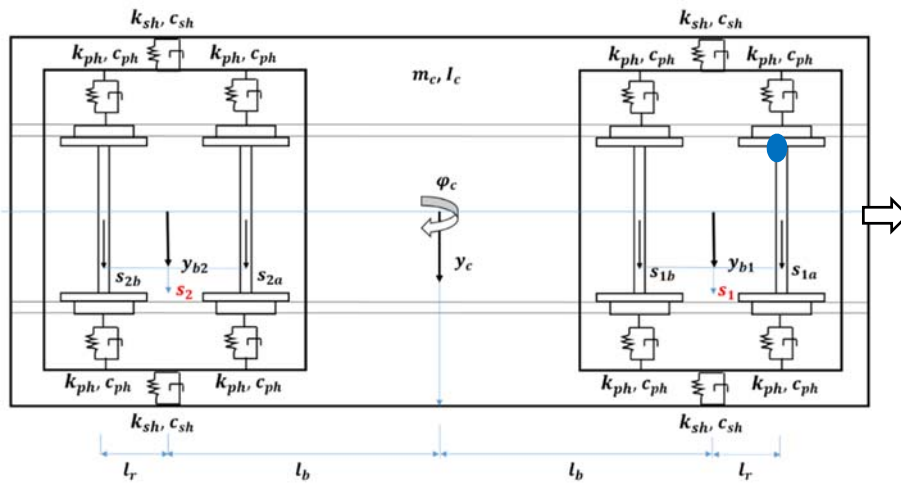
Figure 5.26 Simplified train model with averaged geometry: for lateral displacement

5.5.1 Restored track irregularity waveform for lateral irregularity

The left track profile irregularity (Figure 5.7 (B)) is considered as the true track profile for the comparison purpose with the estimated results obtained from Kalman filter inverse analysis technique. Figures 5.27 (a-b) represent the results on reconstructing track geometry profile for station 1-2, using a Kalman filter and inverse modelling for iPod touch-2 (blue) sensor. The plot shows the comparison of the track profile obtained from extended ASKF methods with true profile. In Appendix: D, Figures D.9 - D.12, show the estimated responses and also zoomed-responses of track geometry profile for station 2-6, using a Kalman filter and inverse modelling for iPod touch-2 (blue) sensor. Also PSD plots are shown for the comparison in frequency domain. The Federal Railroad Administration (FRA) Class 4 (very poor) track profile is compared with the inverse analyses results in PSD plots to convey the current status of the existing the track profile section.

(a) For station 1-2
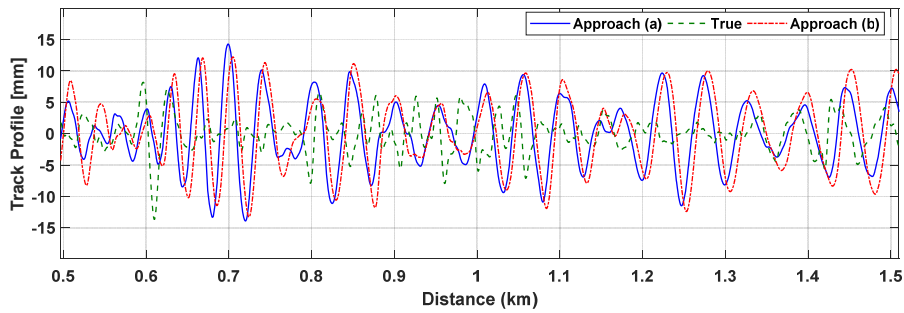
(b) Zoomed responses (0.5 – 1.5 km)
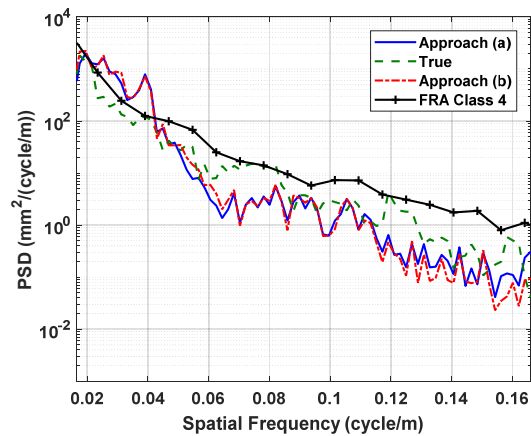
(c) PSD plot
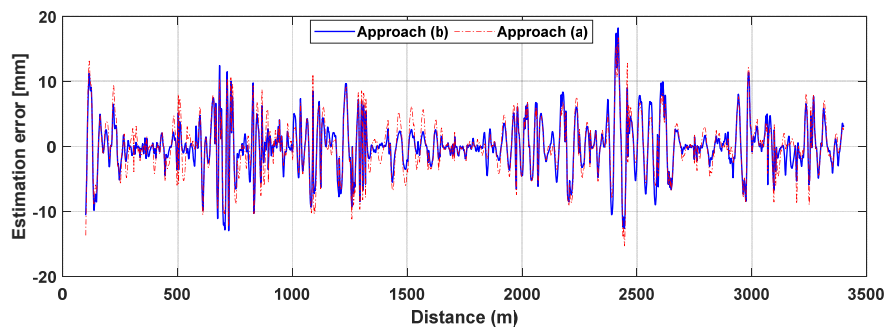
(d) Estimation error after misfit criteria (100 m to 3400 m)

Figure 5.27 Estimation for restored left alignment profile for station 1-2

Figure 5.27 (d) gives the comparison of estimation error for Approach (a) and (b) which has value less than ± 7 mm. The statistical metrics like Root Mean Square Deviation (RMSD) is utilized to quantify the error among the estimated profile with true one. The extended ASKF techniques are performed for all stations from 1 to 6 and the statistical metric, RMSD is calculated to obtain the quantitative difference between both approaches as illustrated in Table 5.5. Also, Approach (a) performs better than Approach (b). The results are influenced much by the wheel – rail flange contact, gauge, cross level, spiral easement curve, transition gradient and also by integration error accumulations. These parameters influence the train dynamics and thus, measured acceleration and pitch rate at car body floor is highly affected. These influences need to be further investigated in future research.

Table 5.5 Comparison for restored waveform for lateral irregularity

Station	Distance (km)	Approach (a)			Approach (b)		
		RMSD (%)	CC	RMSE (mm)	RMSD (%)	CC	RMSE (mm)
1-2	3.5	106.3	0.66	3.82	112.3	0.65	4.03
2-3	9	91.1	0.81	2.36	134.5	0.81	3.49
3-4	18.1	89.1	0.62	4.79	91.5	0.61	4.92
4-5	31.8	106.4	0.80	3.99	128.8	0.75	4.84
5-6	17.4	0.80	0.66	2.31	103.6	0.66	2.32

5.5.2 10 m chord versine alignment waveform for accounting lateral irregularity

Figure 5.28 represents the results on reconstructing 10 m chord versine left alignment waveform for station 1-2, using a Kalman filter and inverse modelling for iPod touch-2 (blue) sensor. The plot shows the comparison of track profile obtained from extended ASKF methods with true versine obtained from TRV. Also PSD plots are shown for the comparison in frequency domain. Figure 5.28 (d) gives the comparison of estimation error for Approach (a) and (b) which has value less than ± 3 mm. The statistical metrics like RMSD is utilized to quantify the error among the estimated profile with true one as illustrated in Table 5.10. Also, Approach (a) performs better than Approach (b). The results might be influenced by various factors as discussed in Section 5.5.1. In Appendix: D, Figures D.9 – D.12, show the estimated responses and also zoomed-responses of 10 m chord versine alignment waveform of track geometry for station 2-6, using a Kalman filter and inverse modelling for iPod touch-2 sensor (blue).
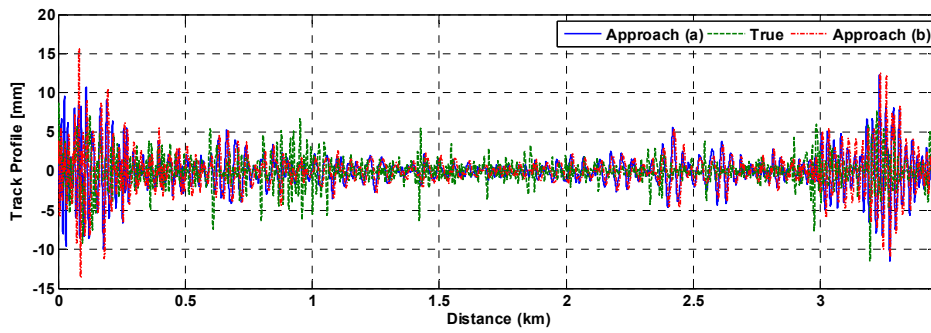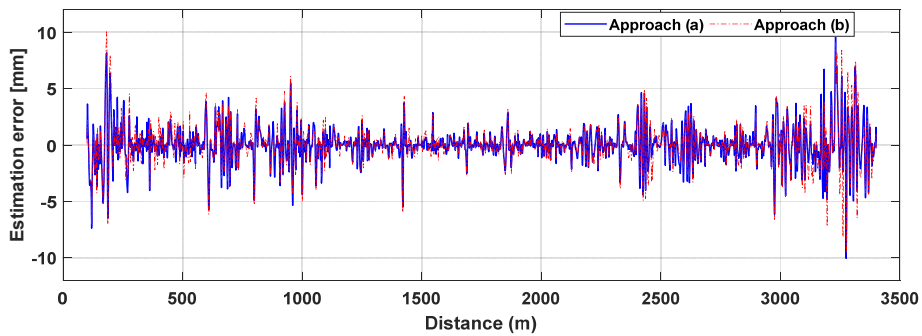
(a) For station 1-2
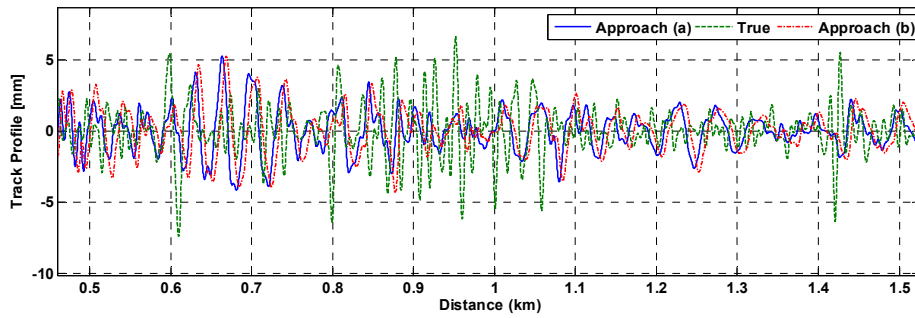
(b) Zoomed responses (0.5 – 1.5 km)
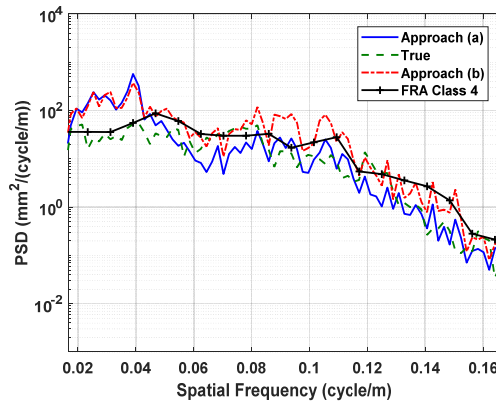
(c) PSD plot

(d) Estimation error after misfit criteria (100 m to 3400 m)

Figure 5.28 Estimation for 10 m chord versine left alignment profile for station 1-2

Table 5.6 Comparison for 10 m chord versine waveform for lateral irregularity

Station	Distance (km)	Approach (a)			Approach (b)		
		RMSD (%)	CC	RMSE (mm)	RMSD (%)	CC	RMSE (mm)
1-2	3.5	96.3	0.69	1.59	103.2	0.67	1.76
2-3	9	101.5	0.74	1.56	106.8	0.70	1.64
3-4	18.1	95.7	0.68	1.77	107.1	0.63	1.98
4-5	31.8	117.5	0.73	2.01	117.8	0.71	2.02
5-6	17.4	104.2	0.70	1.84	114.7	0.66	2.01

From Tables 5.5 and 5.6, the inferences can be drawn as below,

- The relative error is comparatively lesser for Approach (a) than Approach (b).
- PSD plot obtained using the proposed algorithm aids to approximately evaluate under which category of irregularity the measured rail track profile section falls. This is achieved by comparing the PSD results with the track irregularity power spectrum obtained from FRA- Classes.
- By employing the obtained track irregularity PSD, the track maintenance team can ensure the safety and comfort of railway transportation system.
- The RMSD error can be attributed to two reasons. First, the real train vehicle primary suspension and secondary suspension systems usually has nonlinearity especially at high drive speed or large track input due to irregularities on the rail. However, this nonlinearity cannot be reproduced in by a linear 4 DOF simplified train vehicle model implemented in this study. Though large modelling error can be compensated by increasing the system noise covariance, the track profile estimation accuracy may be sacrificed.
- According to RMSE value and track irregularity tolerance limit, maintenance of track can be done.
- Secondly, the simplified half car model cannot represent the bogie yawing motion of a real train vehicle which often occurs to be significant under different conditions.
- From the PSD plots, it is found that lateral profile is affected by hunting motion phenomenon at the wavelength of around 35 – 45 m (0.0285 – 0.0222 cycle/m). (refer section 5.5.3)
- Also the lateral track profile is affected from the angle of attack – the tangential angle on the contact point between wheels and rails. This is one of the prevailing limitations that define the curving performance of train and it predominantly affects lateral force. The vehicle can make different lateral deflections depending on angles of attacks.

- These influences need to be further investigated in future research. In future, the upgraded model which considers bogie yawing motion can be utilized to improve the estimated results.

5.5.3 Hunting oscillation

The hunting phenomenon often occurs when train vehicle runs at high speed, and presents a coupled oscillation of the wheelset in its lateral displacement and yaw angle. This kind of motion is caused by wheel conicity and the flange clearance between the wheel and the rail. When the train runs on the straight line, once the centerline of the wheelset has an offset, the difference of the travel distance between the two wheels will cause the turning of the moving direction of the wheelset [90]. Thus the two wheels will rotate around one instantaneous center, shown as Figure 5.29 (a). The path of the hunting motion is shown in Figure 5.29 (b) and it is approximated by a sine wave of wavelength. The sine path due to the hunting motion can be calculated by equation (5.8) [127],

$$z(x) = A_h \sin\left(\frac{2\pi vt}{L_h} + \varphi_{hijl}\right) \tag{5.8}$$

Where v is the speed of the train, L_h is the wavelength of the hunting motion with bogie, and φ_{hijl} is the random initial angle of the wheel. The wavelength is calculated by equation (4.9),

$$L_h = 2\pi \sqrt{\frac{br}{\lambda}\left[1 + \left(\frac{S_0}{2b}\right)^2\right]} \tag{5.9}$$

where r is the rolling radius at the center of the wheel tread, $2b$ is the distance between the two contact points of the wheel treads with rails, S_0 is the distance between the two axels of the bogie, λ is the contact angle between the wheel tread and the rail surface as shown in Figure 5.29 (b). Substituting the data of local in-service train, S_0 = 2.25 m; $2b$ = 1.067 m; $2r$ = 0.81 m; λ = 1/40 into equation (5.9), one can obtain the wavelength of the hunting motion L_h is 43 meters.
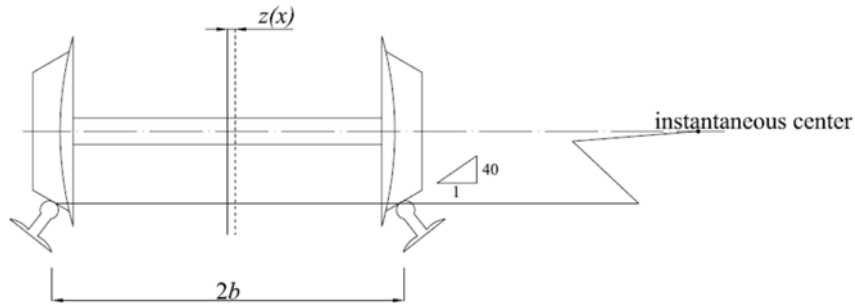
(a) Instantaneous center of hunting motion
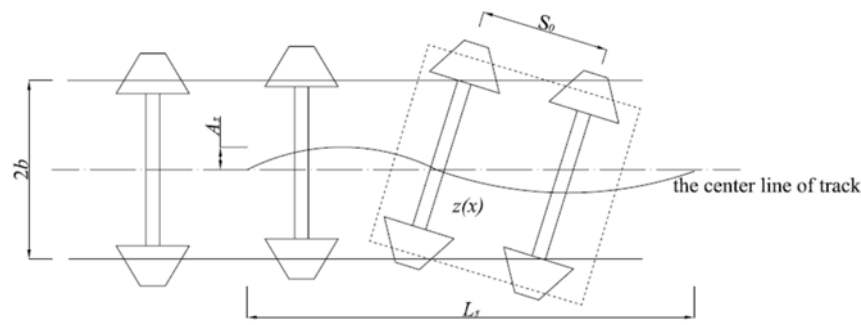
(b) Wheel path during self-oscillation

Figure 5.29 Phenomenon of Hunting Oscillation

5.6   Discussions and Summary

The rail track profile estimation from the in-service vehicle response measurement by employing inverse analysis based on extended ASKF method is being studied. The smartphones are mounted on the train car body to collect the vehicle dynamic responses. Inverse analysis is carried out to estimate both the vertical and lateral track irregularity by reconstructing the track profile geometry for restored true track profile as well as converted 10 m chord versine waveform. The further studies are being conducted for the effective track profile estimation using practical sensors and its installation locations on in-service train vehicle. Thus, depending upon the sensors availability and feasible sensor placement locations in the real field measurement, rail track geometry can be reconstructed using inverse analysis modelling and extended ASKF estimation algorithm with proposed approaches. Also, the estimated vertical track profile irregularity using simplified train model (4 DOF) is performing poor because bogie pitching motion is not considered. Thus, in future research, by utilizing 6 DOF train model accounting for vertical displacement which considers bogie pitching motion, rail track profile can be estimated accurately using proposed ASKF method. Similarly, the estimated lateral track profile irregularity using 4 DOF simplified train model can be improved by considering the yawing angular velocity in the bogie mass by utilizing 6 DOF train model for accounting lateral displacement, by using proposed ASKF method.

144

Chapter 6 CONCLUSIONS

6.1 Conclusions

The research detailed in this dissertation has developed a robust inverse analysis scheme for the track geometry estimation from local in-service train responses. The proposed algorithm is tested by measurement and verified by the numerical simulation to be effective, resulting in the realization of the dynamic characteristics of vehicles and track irregularity estimation.

Chapter 1, provides the importance of railway infrastructure in Japan and the wide background of this present research study. The railways track maintenance problem has a long history, ever since 1920. A good deal of literature about the past and existing track maintenance technologies and current methodologies can be found in detail. In most of those studies or technologies, the track geometry car has been used, which is cost effective and time consuming. A state-of-the-art-review of the research work on the track geometry estimation especially on the indirect mechanism- response based, including numerical analyses and measurement investigations, have been discussed in that chapter. Recently researchers have focused on reconstructing track geometry from the in-service vehicle responses.

To obtain the theoretical and mathematical proof of state space representation model for implementing the Kalman filter based inverse analysis technique, Observability Rank Condition method is carried out in Chapter 2. The observability analyses have been presented, which helps to theoretically obtain the appropriate sensor types and their placements for estimating vertical and lateral track profiles. Accelerations and angular velocities are assumed to be observed variables. The second derivative of the track profile is set as the variable to be identified, so that non-static components of the profile is obtained as its double integral. This chapter provides the basic knowledge on the vehicle dynamics. The vehicle is modelled by assuming to have a rigid body motion. Different types of vehicle models are considered with appropriate sensor types and their locations, for the numerical analyses and the results have been presented. The two approaches to obtain the second derivative of profile as an observable state variable are examined. Approach (a) includes the second derivative of the profile in the state vector. Although the system is unobservable the augmented state variable is observable.

Approach (b) alters state space model by taking the first derivative of the system equation. The second derivative component is observable. These analyses indicate that the track profile can be estimated by placing practical sensors on car body floor and bogie masses.

To investigate the proposed approach, a numerical study on extension of Augmented State Kalman Filter is carried out for track profile estimation from the in-service vehicle response measurements and are well described in Chapter 3. Measurements like acceleration and angular velocities are assumed to be observed variables. The two approaches to obtain the second derivative of profile as an observable state variable are examined as explained in the Chapter 2. The performances are compared numerically for simplified train models (4 DOF) and 6 DOF train model, accounting for both vertical and lateral displacements and found to be in good agreement. In order to obtain the quantitative comparison of two waveforms, phase-shift correction is carried out using the misfit criteria through Hilbert transform. The statistical metrics like RMSE, RMSD, CC are utilized for obtaining the single-valued misfit between two waveforms.

In Chapter 4, the Multi-Body Simulations (MBS) using SIMPACK: Rail, are carried out to replicate the real field test. MBS are performed to investigate the influence from different factors under various scenarios, namely straight track and splined track sections. The sensors are placed just above the rail tracks on both the sides and used to measure the acceleration and angular velocity responses from the car body and both bogie masses of running train model on simulated track excitations. These vehicle measurement responses are utilized to estimate the vertical and lateral track profile using the 6 DOF train model and it is validated for the proposed estimation algorithm. The suggested sensor placement strategy is verified with all possible sensor location results. For straight track section (ideal case), it shows a good agreement for vertical track profile while it can estimate only above 8 m wavelength irregularity for lateral track profile. The statistical metrics are utilized for comparison between various cases and the proposed approach is verified. Also, MBS are carried out for understanding the influence of rolling motion of train vehicle. So, similar track excitations are given for both left and right rail and MBS is carried out.

For curved track section, the results show good agreement for vertical track profile estimation, while it shows large variation for lateral profile estimation. This is due to hunting oscillation phenomenon. Exactly the splined section of the track cannot be evaluated, because of wheel-rail interaction problem. In the track curvature part, the wheel – rail contact point moves inward and outward accordingly for left and right rail. The lateral track excitation is not influencing the vehicle dynamics of the train model. So, this phenomenon could not replicate in the collected vehicle responses. This need to be further investigated.

In Chapter 5, the railway track geometry estimation from in-service local train vehicle responses are demonstrated in detailed manner. The rail track profile is reconstructed from

vehicle response measurements by employing inverse analysis based on extended ASKF analyses as described in Chapter 3. Inverse analysis is carried out to estimate both the vertical and lateral track irregularity by reconstructing the track profile geometry for restored true track profile as well as converted 10 m chord versine waveform. The results are found with slight deviations due to simplified 4 DOF model and other phenomenon like hunting oscillation motion. This is due to practical limitations of sensor placement only on the car body. In future experimental measurements, the optimal sensor placement is recommended to mount sensors on car body and bogie masses. Thus, by utilizing 6 DOF train model accounting for bogie pitching/yawing motion, rail track profile can be estimated more precisely. It is also verified using the proposed estimation algorithm by performing numerical simulations in previous chapters.

In summary, this dissertation proposes and realizes an inverse analysis scheme for the railway track profile estimation from in-service vehicle response measurements. The results obtained from numerical analyses and real field experiments exposed that the recommended data assimilation method, ASKF: Approach (a) is efficient for condition assessment of local railway track lines with satisfactory correctness. Successful completion of this research indicates this approach is expected to provide not only an accurate inverse analysis technique, but also useful information for the safety and maintenance of railway infrastructure.

6.2   Future research

Application of proposed inverse analysis technique adopted in this present research study for efficient track geometry estimation from the in-service vehicle response measurements have proved the merit of the proposed methodology. Using the estimation algorithm scheme, this study shows that it is possible to capture the track irregularities successfully even for the local commercial railway networks. The advantages and effectiveness of numerical schemes addressed in this study might lead to a promising future application of numerical simulations for train vehicle dynamic analysis. In this study, however, several assumptions have been employed such as simple linear vehicle train model for the inverse analysis method under state space representation. These certainly simplify the inverse problem but the drawbacks yet remain to be solved in future. It will be interesting to investigate how the regularized estimation algorithm based on Augmented State Kalman Filter (ASKF) technique will perform for higher degree of freedom (DOF) train vehicle models. Not only had more detailed model with additional DOF to describe, but also robust model to investigate both vertical and lateral irregularities for condition monitoring of railway tracks need to be studied in future. Therefore, advanced suspension train vehicle models are need to be utilized for incorporating the non-linearity effects. Future research can be the introduction of nonlinear vehicle rigid body

motion models. Improving robustness in railway track geometry estimation even under the circumstance of non-linearity using proper data assimilation technique is another possible direction.

In the multi-body simulation, more works should be devoted for refining numerical analysis and modelling of the train-track system to capture more detailed behavior of wheel-rail interaction such that the measured responses from car body and bogie mass can be utilized for reconstructing the track geometry estimation using the proposed inverse analysis technique. These would be very helpful to understand the vehicle structure dynamics further. In the framework of railway infrastructure safety management, dynamic characteristic behavior of in-service train vehicle can be viewed as an initial step. Hence, development of a robust online monitoring system using the above methodology schemes would be the next logical direction of this research study.

The Kalman filter address the optimum linear filtering problem in a straightforward manner to obtain the optimal a priori and a posteriori states estimates. Optimal smoothing is a method to improve the estimating accuracy using not only the previous measurement data but also the later information as well. A fixed-interval smoothing algorithm, Rauch-Tung-Striebel (RTS) smoothing technique is considered as a high computationally efficient method, which can be introduced to improve the state estimation. Still, the technique need to be improved and with further investigations can be successfully implemented.

APPENDIX: A ESTIMATED TRACK PROFILE FROM MULTI-BODY SIMULATION APPROACH

A.1 Track profile estimation from Multi-Body Simulation approach

In this section, the estimation results from Multi-Body Simulation (MBS) approach, for vehicle parameter SET-I (as illustrated in Table 4.1) are shown in the Figure A.1 and A.2 for vertical and lateral right track profile under different excitations (Figure 4.3) for the average train speed (90 km/h) respectively. Similar conclusions are obtained as left track profile estimation as discussed in the section 4.5.1.1. The measurement set M3 ($\ddot{z}_c$ $\dot{\theta}_c$ $\ddot{z}_{t1}$ $\dot{\theta}_{t1}$) is performing close to M2 ($\ddot{z}_c$ $\dot{\theta}_c$ $\ddot{z}_{t1}$ $\dot{\theta}_{t1}$ $\ddot{z}_{t2}$ $\dot{\theta}_{t2}$). Correspondingly, the measurement set A3 ($\ddot{y}_c$ $\dot{\varphi}_c$ $\ddot{y}_{b1}$ $\dot{\varphi}_{b1}$) is performing close to A2 ($\ddot{y}_c$ $\dot{\varphi}_c$ $\ddot{y}_{b1}$ $\ddot{y}_{b2}$ $\dot{\varphi}_{b1}$ $\dot{\varphi}_{b2}$). The statistical metrics are evaluated after applying misfit criteria and results are given in Table A.1. It has error value less than ± 0.5 mm for vertical and lateral track profile geometry. Hence, the optimal sensor placement can be at car body and front bogie mass (measurement set: M3 and A3).
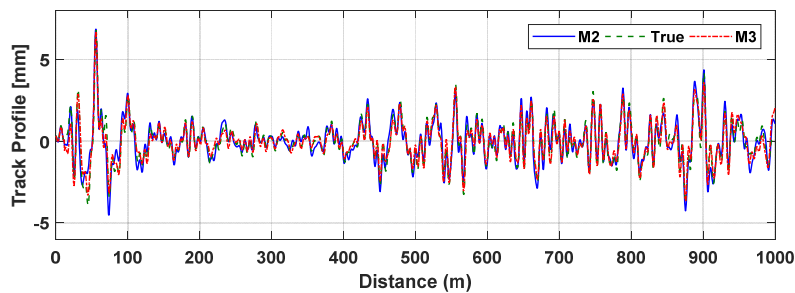
(a) Comparison plot
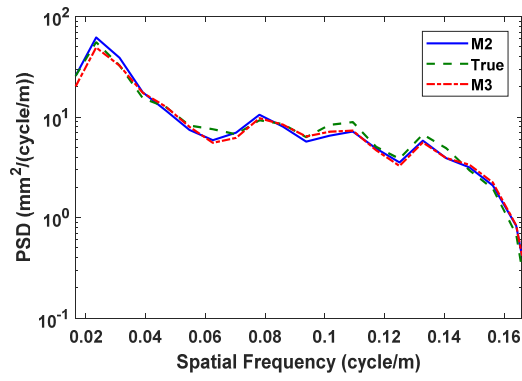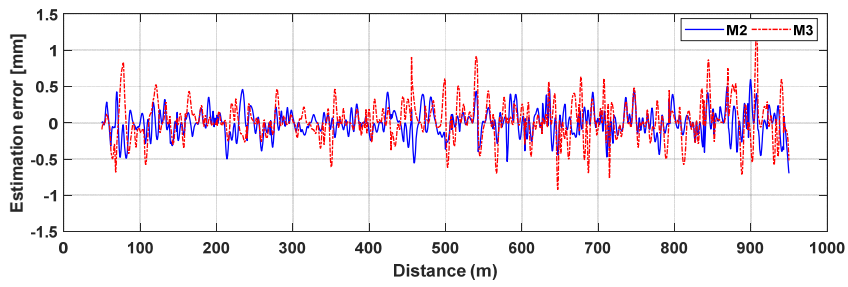
(b) PSD plot

(c) Estimation error after misfit criteria (for track length 50m to 950m)

Figure A.1 Estimation of vertical right track irregularity (for SET-I)
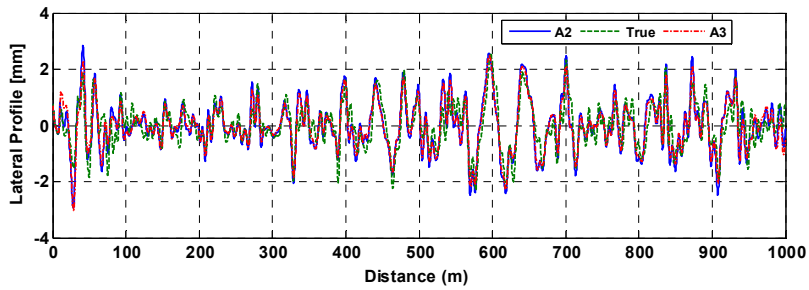
(a) Comparison plot
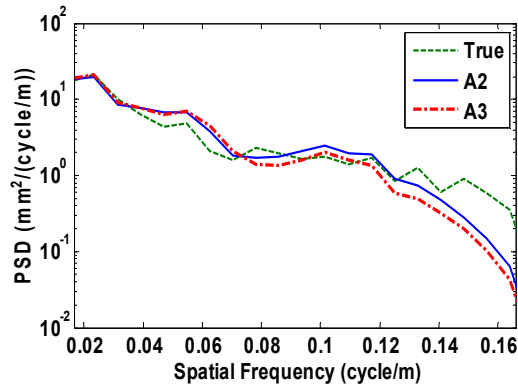
(b) PSD plot
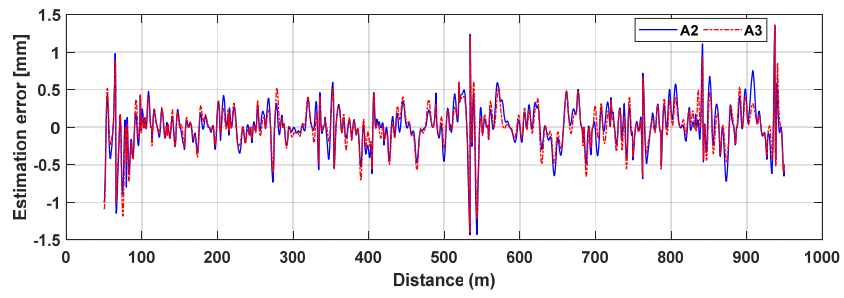
(c) Estimation error after misfit criteria (for track length 50m to 950m)

Figure A.2 Estimation of lateral right track irregularity (for SET-I)

Table A.1 Comparison of right track profile using statistical metrics under different excitation (for vehicle parameter SET-I)

Track profile	Measurement: Approach (a)	Statistical Metrics		
		RMSD (%)	CC	RMSE (mm)
Vertical	M2	15.1	0.99	0.18
	M3	21.4	0.98	0.25
Lateral	A2	32.9	0.96	0.27
	A3	32.7	0.96	0.25

APPENDIX: B   TRACK RECORDING VEHICLE: MEASURED RESPONSES

B.1 Car-body accelerometers

In order to estimate the riding comfort for existing track displacements, the car body vibration response can be utilized for maintaining the track geometry. The accelerometers and gyroscopes attached to the Track Recording Vehicle (TRV) car body just above the rear bogie are examined and the collected vibration data responses are shown for the existing track conditions. The car body vibration measurements vary with track irregularities due to various reasons such as vehicle parameter properties, train speed and varying load conditions. Still, the track condition can be approximately assessed using the root mean square (RMS) metrics from the acceleration data measured on the car body. The measurements are obtained when train running from Station 6 to Station 1. The vertical acceleration response of car body and its calculated RMS value plot are shown in the Figure B.1. The lateral acceleration response of car body and its calculated RMS value plot are shown in the Figure B.2.
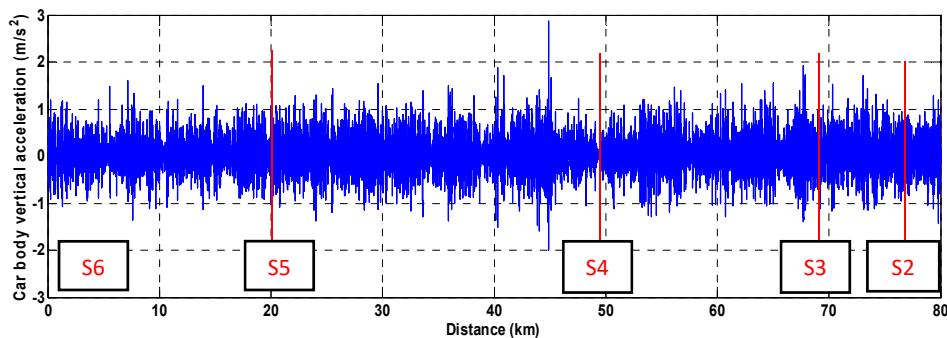
(a) Vertical acceleration of car body

152
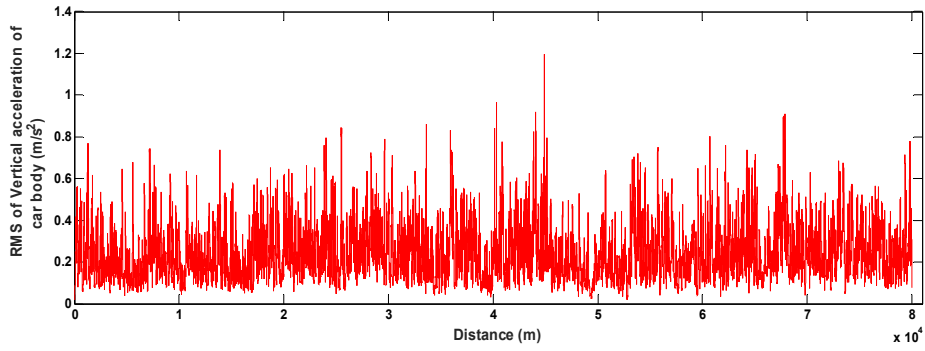
(b) RMS of vertical acceleration of car body

Figure B.1 Car body vertical acceleration response and its RMS plot
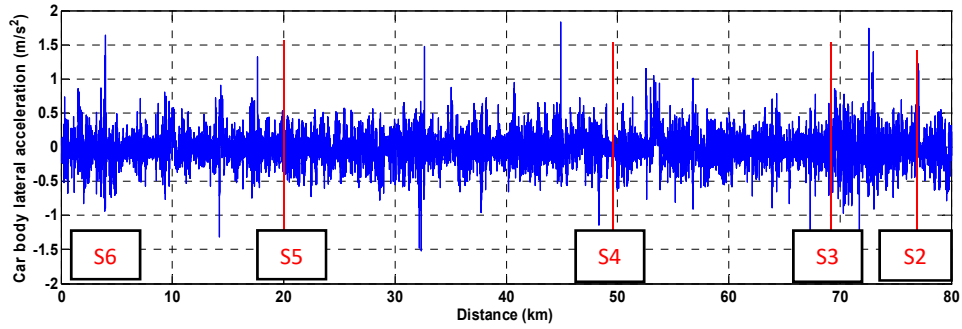
(a) Lateral acceleration of car body
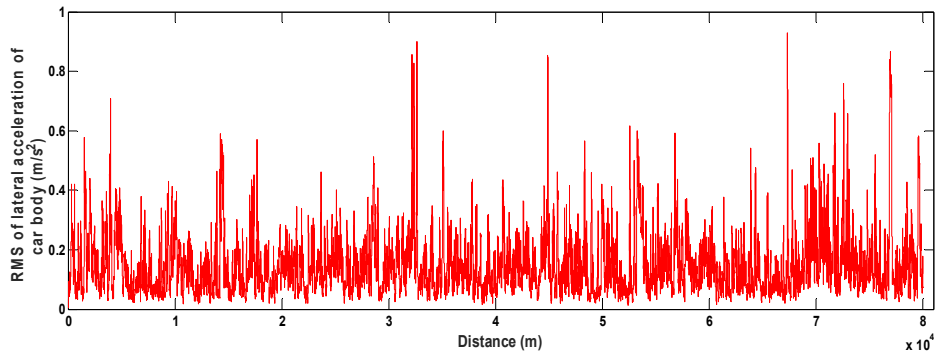
(b) RMS of lateral acceleration of car body

Figure B.2 Car body lateral acceleration response and its RMS plot

B.2 Axle-Box-Mounted accelerometers

One reasonable alternate to evaluate the track geometry, is to mount the inertial sensor type like accelerometers on to the axle-box or the bogie mass of an in-service train vehicle. Tentatively, the displacement information (track profile) can be basically obtained through double integration approach which typically results in impractical data due to an offset drift. The important reasons for such drifts are low-frequency error or direct current (DC) offsets caused by electrical or mechanical hysteresis in the sensor/cables and non-zero initial condition of the data. For the current study, the vibration data collected from axle-box mounted sensor is from the front axle in the rear bogie. The distance between the two wheels of the same bogie is 2.25 m. The vertical acceleration response from axle-box-mounted accelerometers and its calculated RMS value plot are shown in the Figures B.3 and B.4 respectively for left and right rails. The lateral axle-box-mounted acceleration response and its calculated RMS value plot are shown in the Figure B.5.
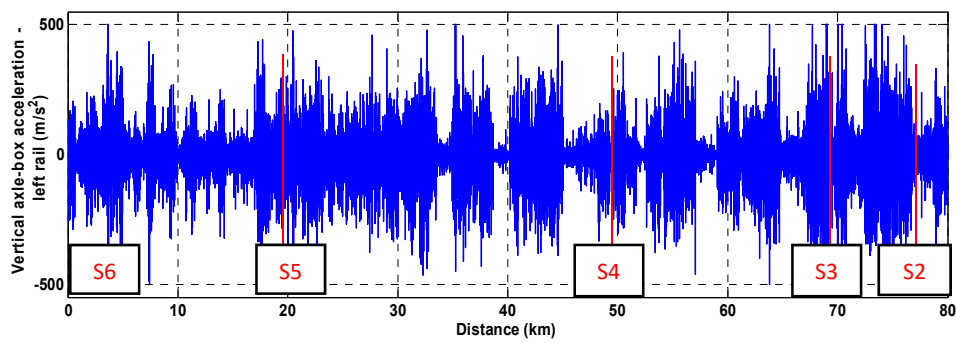
(a) For left rail
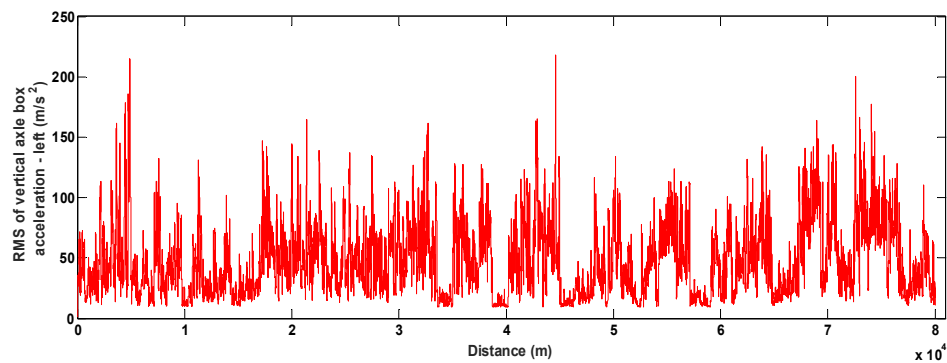
(b) RMS plot

Figure B.3 Vertical axle-box mounted accelerometer response for left rail

154
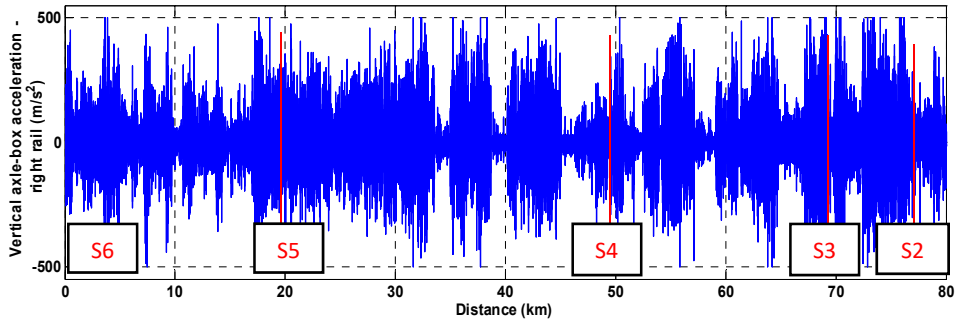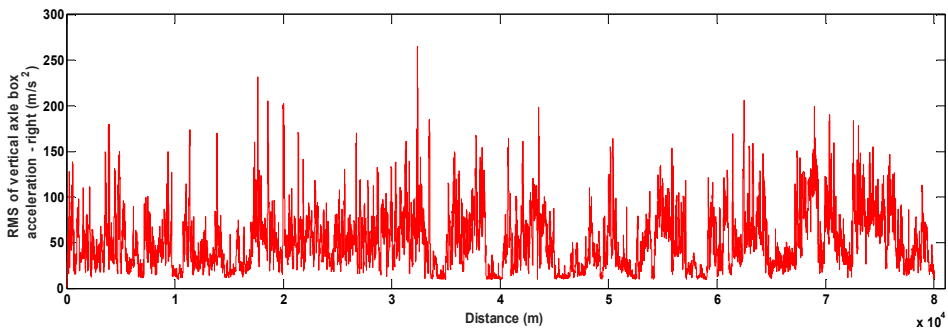
(a) For right rail

(b) RMS plot

Figure B.4 Vertical axle-box mounted accelerometer response for right rail
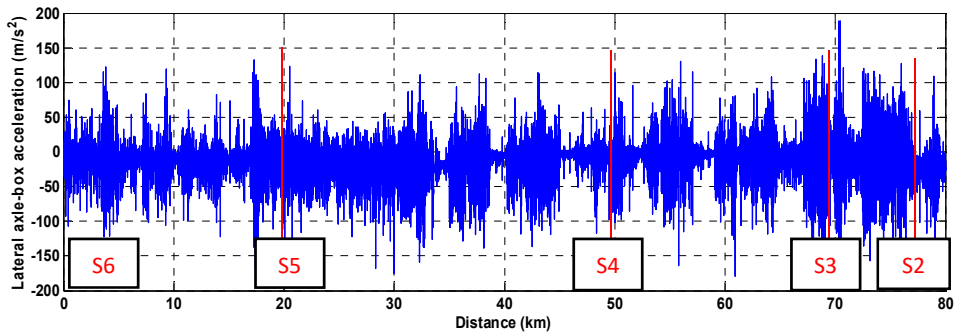
(a) Lateral acceleration of axle-box
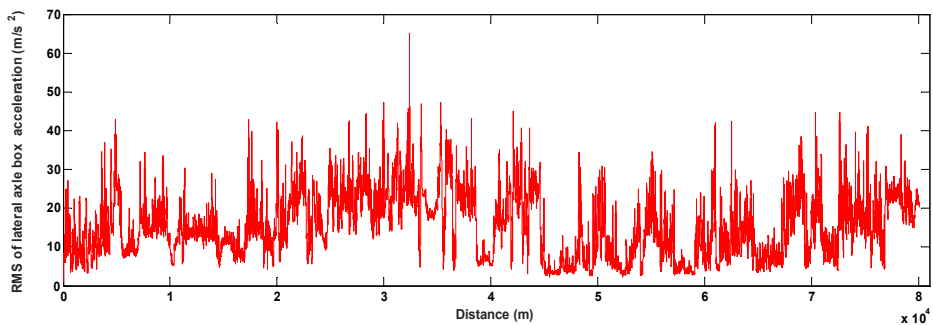
(b) RMS of lateral acceleration of axle-box

Figure B.5 Axle-box lateral acceleration response and its RMS plot

155

APPENDIX: C IN- SERVICE TRAIN VEHICLE RESPONSES

C.1 Smartphone Responses from Car-body: Down-Train side

The velocity profile obtained from two iPod touches (black: iPod touch-1 and blue: iPod touch-2) are compared with each other for down train side of running train as shown in the Figure C.1. The vertical car body acceleration measurement and pitch rate car body measurement obtained from both iPod touches are compared and plotted in the Figures C.2 and C.3 respectively.
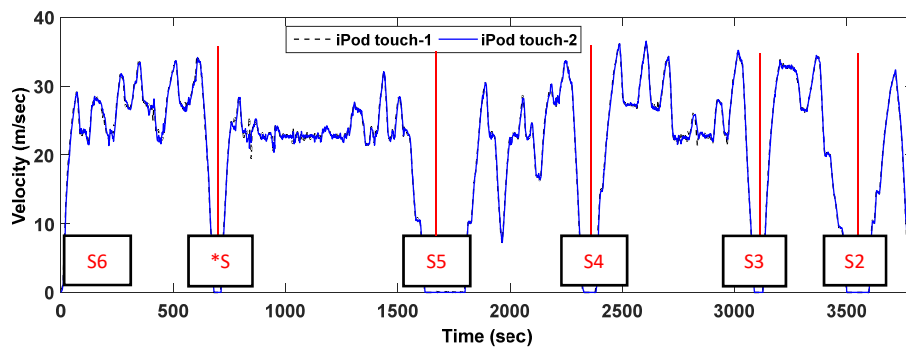
(a) Down train side (*S – extra station for halt)

Figure C.1 Velocity profile comparison between two iPod touches
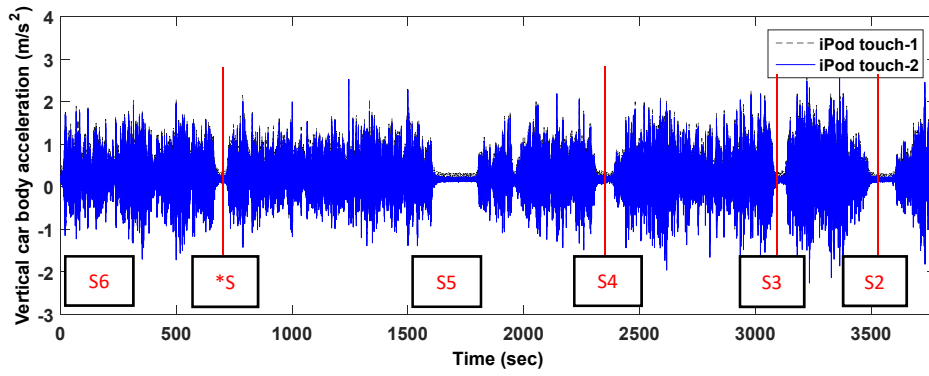
(a) Down train side
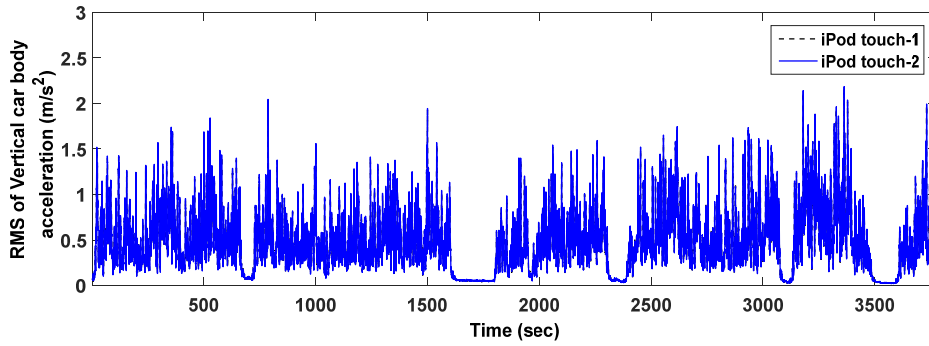
(b) RMS plot
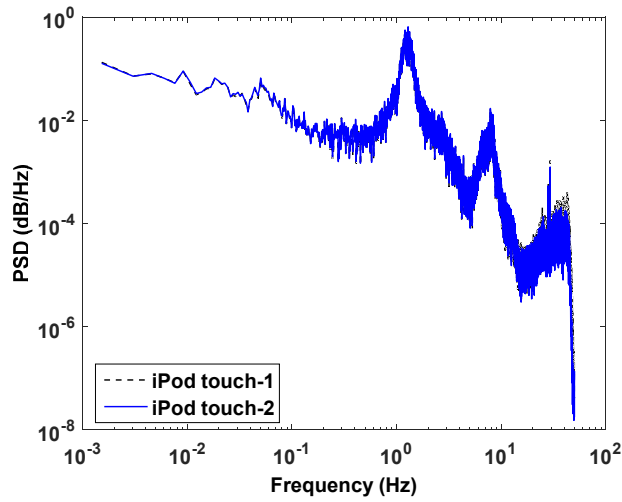
(c) PSD plot

Figure C.2 Car body vertical acceleration measurement: Down train side
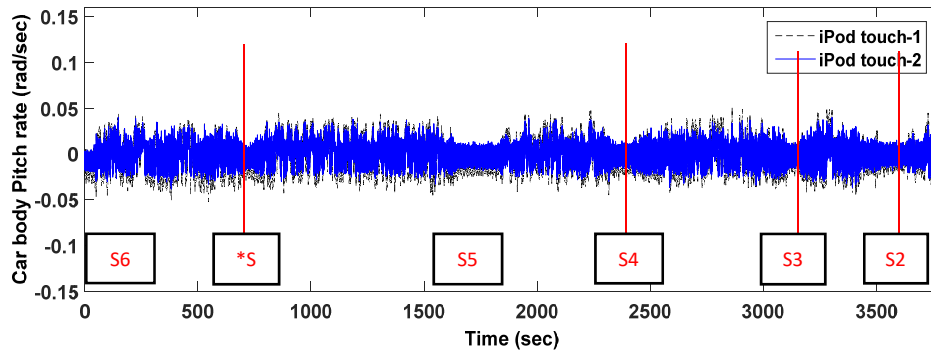
(a) Down train side
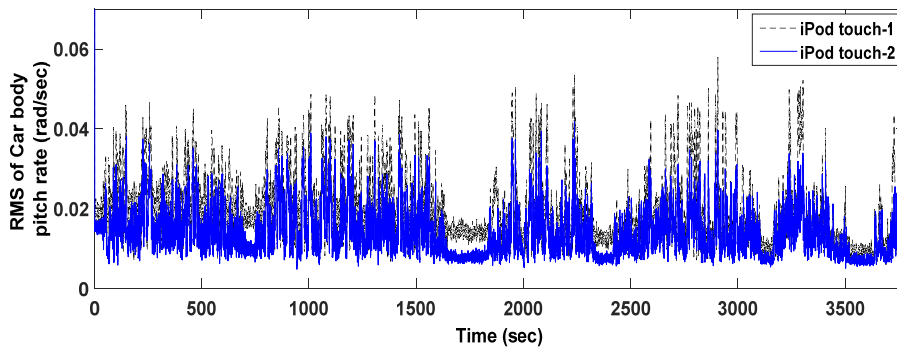
(b) RMS plot
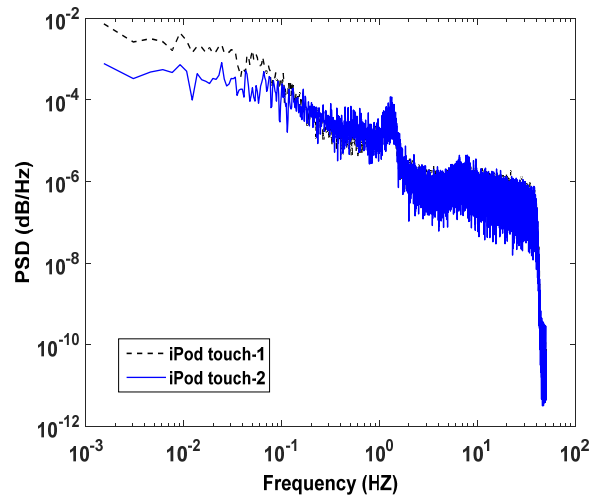
(c) PSD plot

Figure C.3 Car body pitch rate response and its RMS and PSD plots: Down train side

158

APPENDIX: D   ESTIMATED TRACK PROFILE FROM SMARTPHONE RESPONSES

D.1 Track irregularity waveform for vertical and lateral profile

In this section, the left track irregularity waveform for vertical as well as lateral profile is shown in the following below figures. Figures D.1 – D.4, show the estimated responses and also zoomed-responses of restored waveform of vertical track geometry for station 2-6, using a Kalman filter and inverse modelling for iPod touch-2 (blue) sensor. Similarly, Figures D.5 – D.8, show the estimated responses and also zoomed-responses of 10 m chord versine waveform of vertical track geometry for station 2-6. In Figures D.9 – D. 12, show the estimated responses and also zoomed-responses of 10 m chord versine waveform of lateral track geometry for station 2-6 respectively. From Figure D.10 for Station 3-4, it can be seen that the restored true profile from the TRV has some spike around 14 - 15 km along the track section. This might be due to rail crossing which is verified from the location.
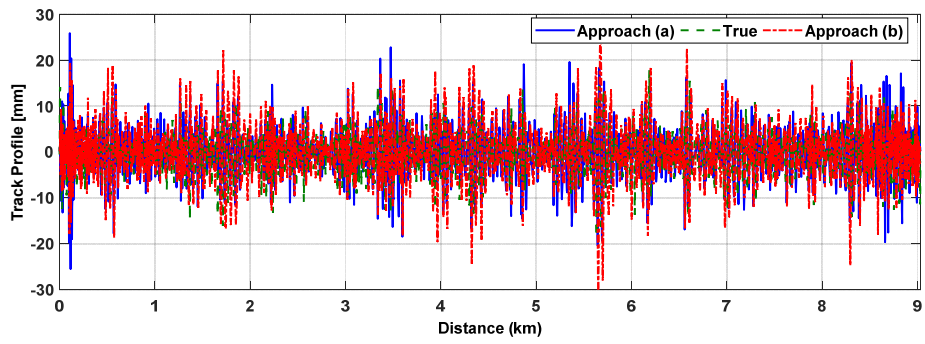
(a) For station 2-3
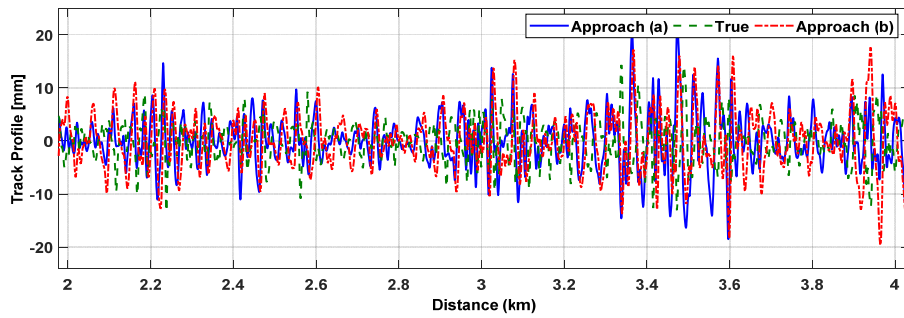
(b) Zoomed responses (2 – 4 km)
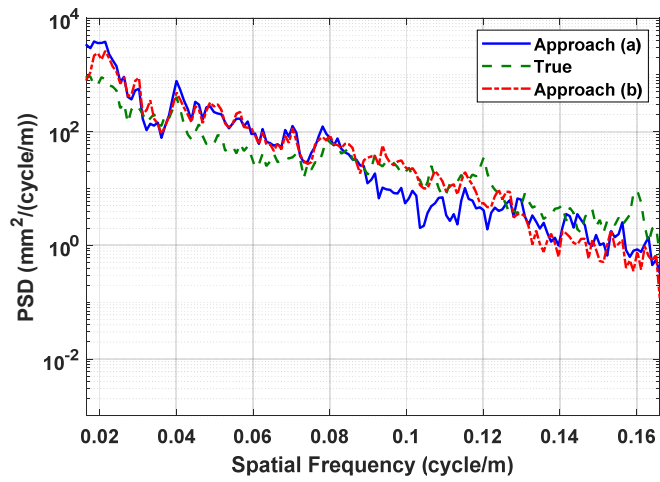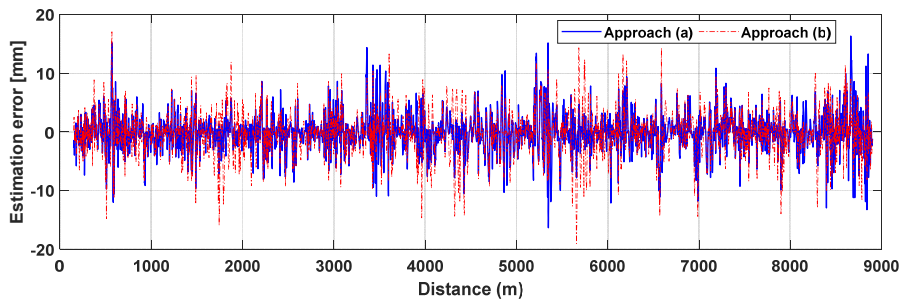
(c) PSD plot

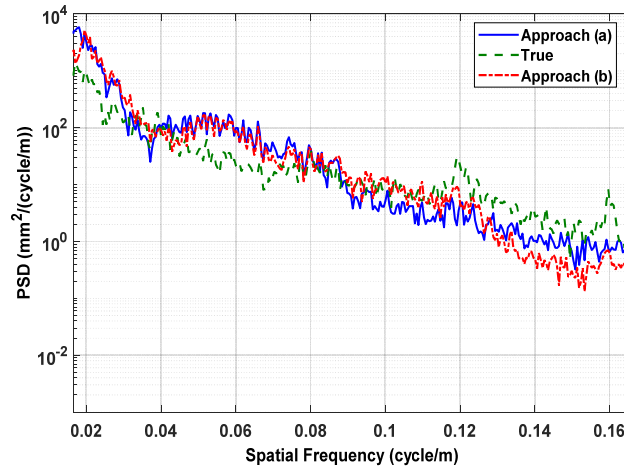(d) Estimation error after misfit criteria (150 m to 8900 m)

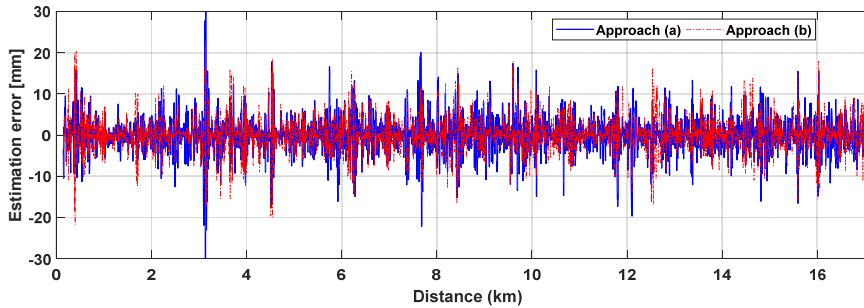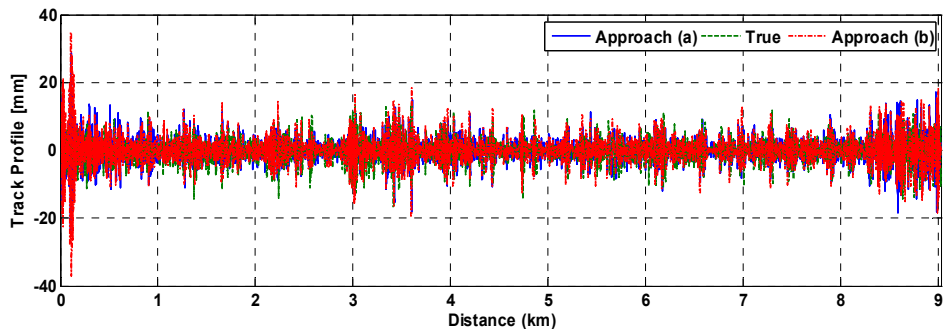Figure D.1 Estimation results for restored left vertical track profile for station 2-3
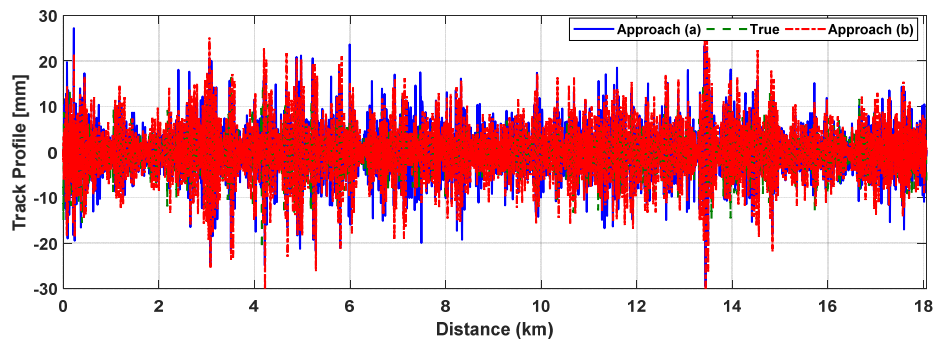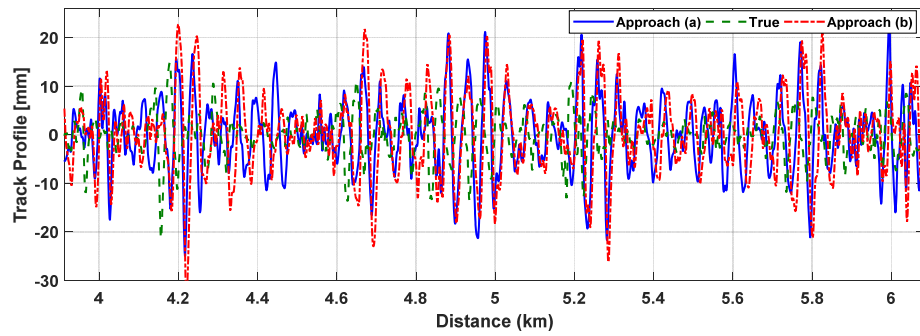
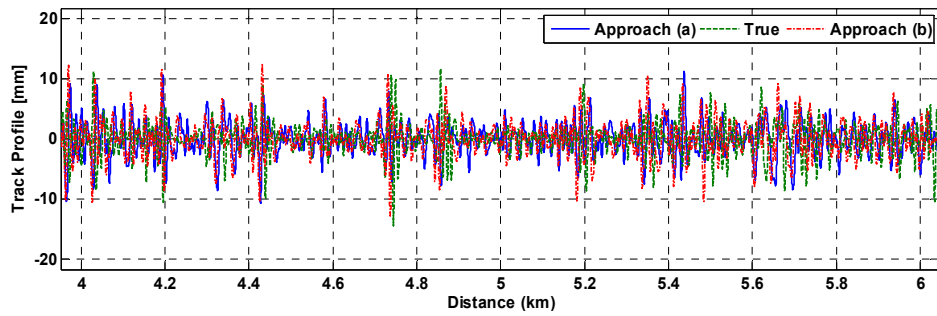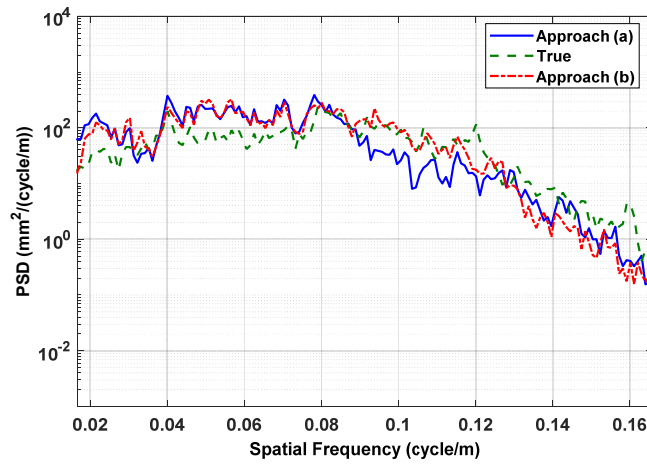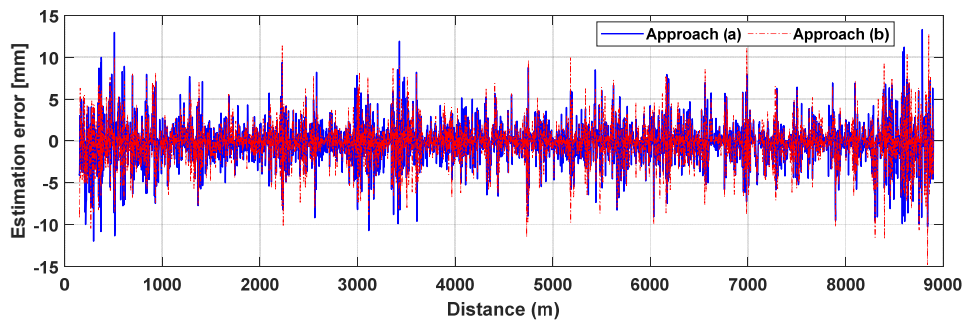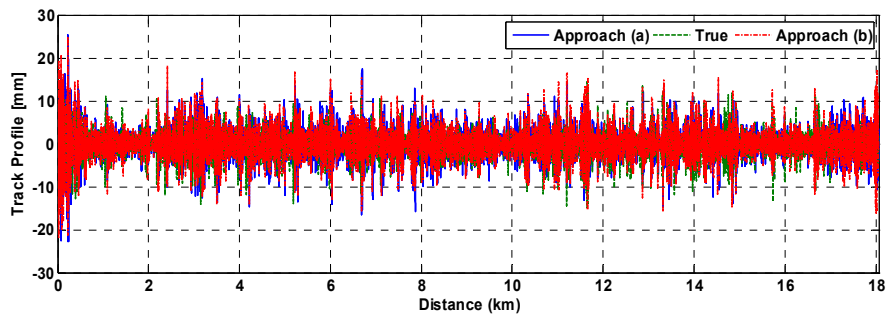(a) For station 3-4

(b) Zoomed response (4-6 km)
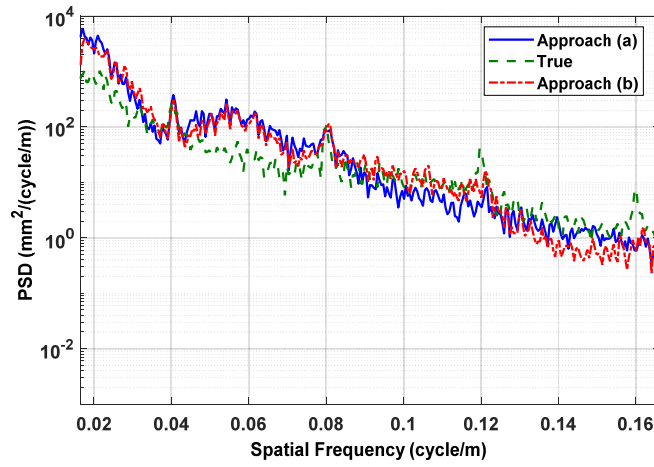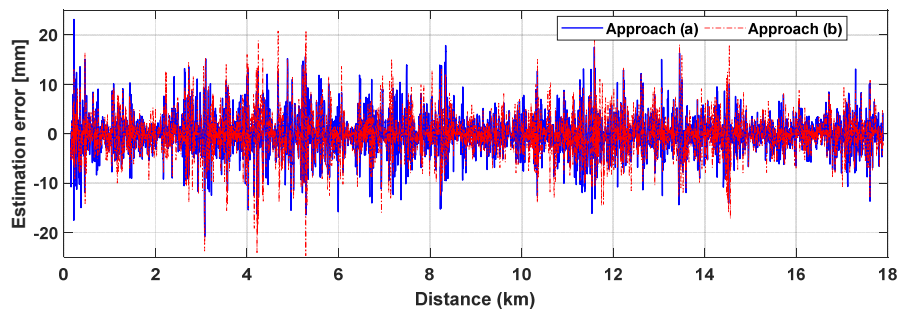
(c) PSD plot

(d) Estimation error after misfit criteria (150 m to 17.9 km)

Figure D.2 Estimation results for restored left vertical track profile for station 3-4
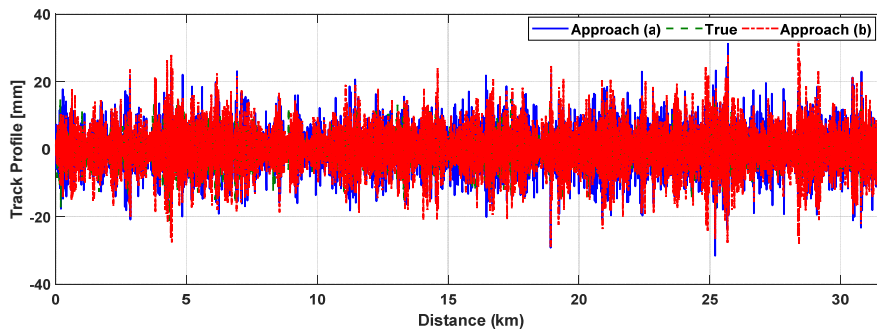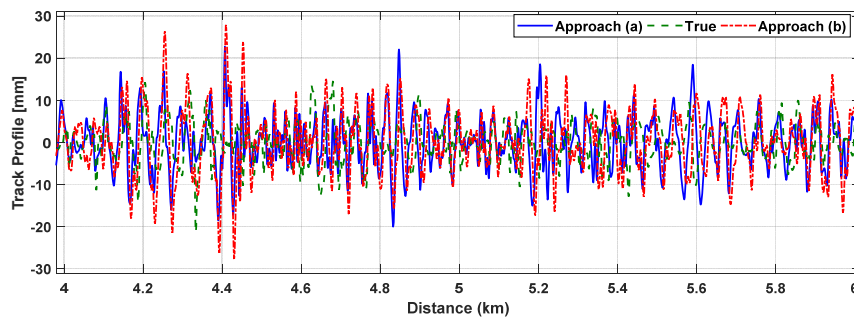
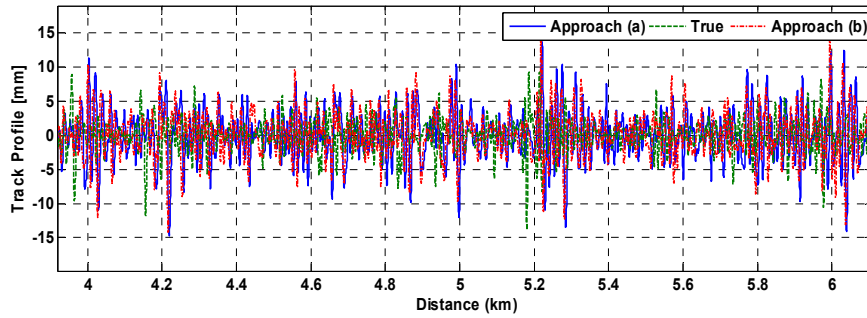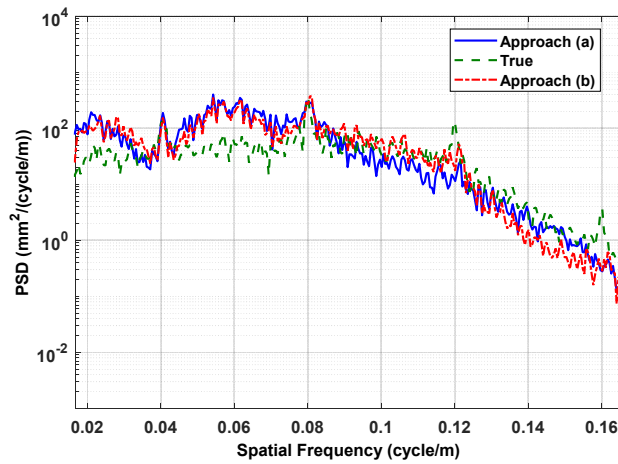(a) For station 4-5

(b) Zoomed responses (4-6 km)
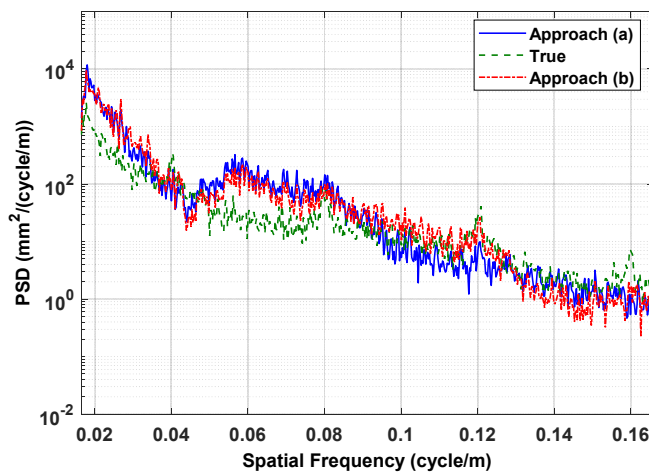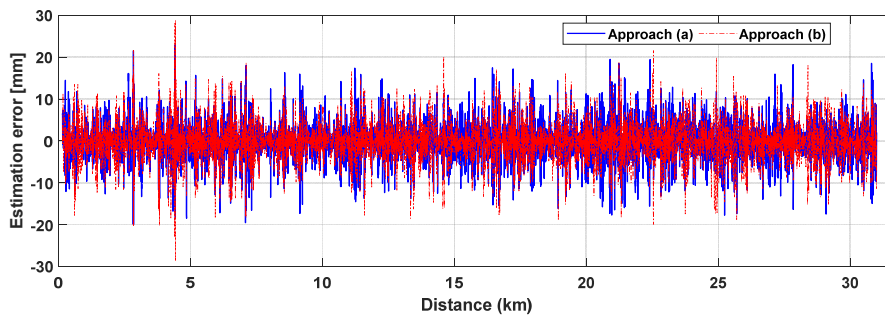
(c) PSD plot

(d) Estimation error after misfit criteria (150 m to 31 km)

Figure D.3 Estimation results for restored left vertical track profile for station 4-5
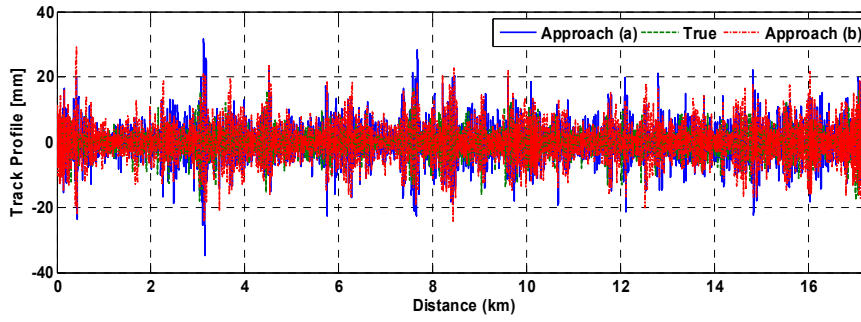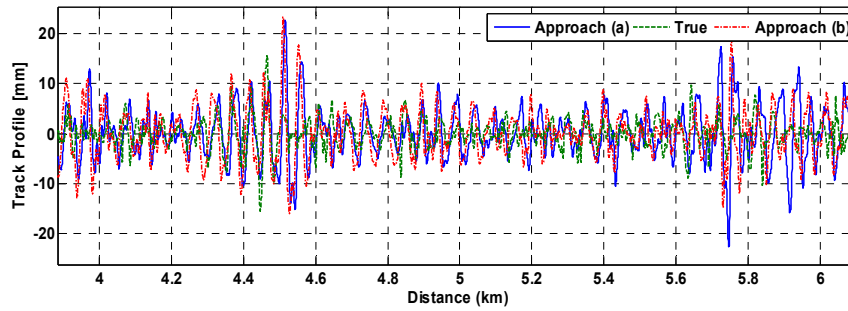
(a) For station (5-6)

(b) Zoomed response (4-6 km)

(c) PSD plot

(d) Estimation error after misfit criteria (150 m to 17.1 km)

Figure D.4 Estimation results for restored left vertical track profile for station 5-6

(a) For station 2-3

(b) Zoomed responses (4 – 6 km)

(c) PSD plot

(d) Estimation error after misfit criteria (150 m to 8900 m)

Figure D.5 Estimation results for 10 m chord versine: left vertical track profile for station 2-3
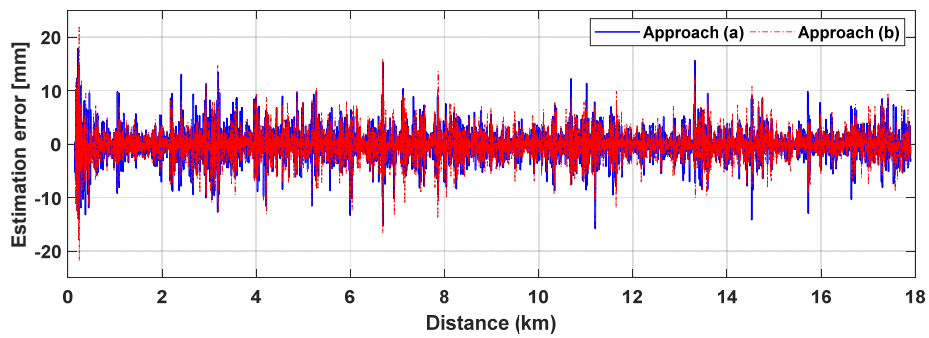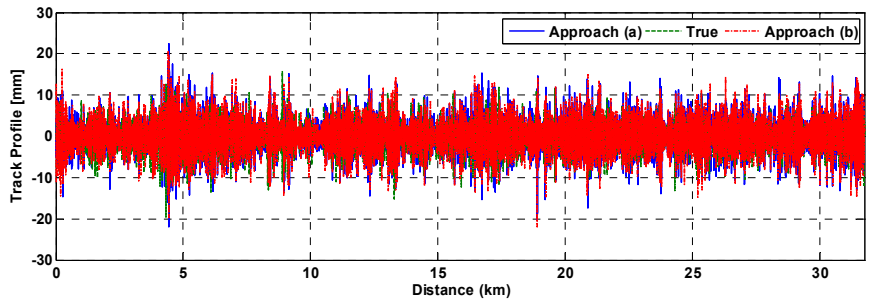
(a) For station 3-4

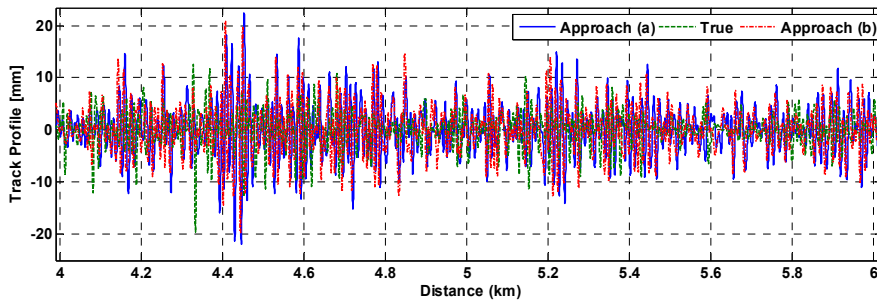(b) Zoomed response (4 -6 km)

(c) PSD plot

(d) Estimation error after misfit criteria (150 m to 17.9 km)
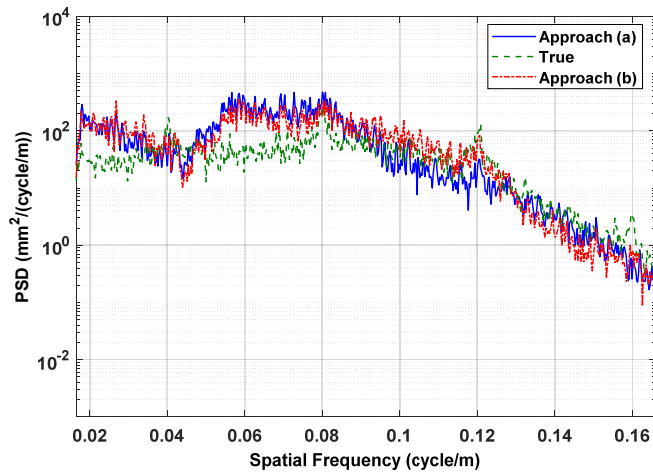
Figure D.6 Estimation results for 10 m chord versine: left vertical track profile for station 3-4
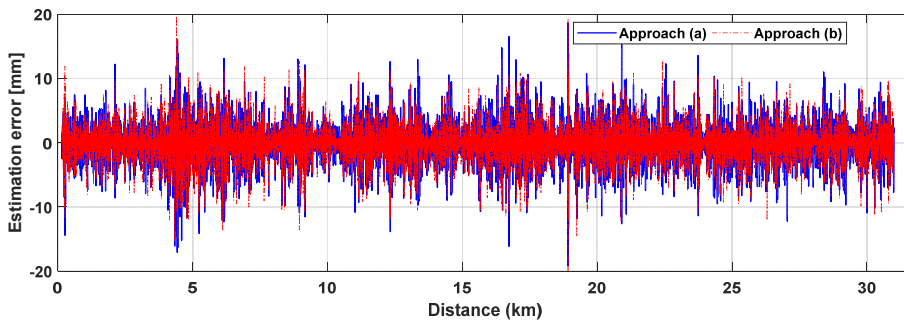
(a) For station 4-5

(b) Zoomed response (4 -6 km)

(c) PSD plot

(d) Estimation error after misfit criteria (150 m to 31 km)

Figure D.7 Estimation results for 10 m chord versine: left vertical track profile for station 4-5

(a) For station 5-6

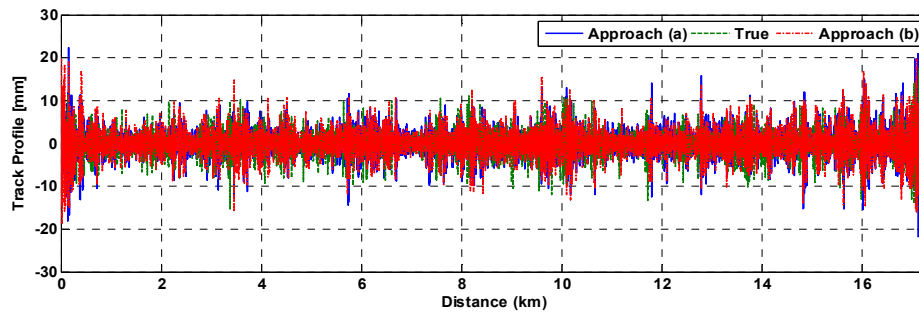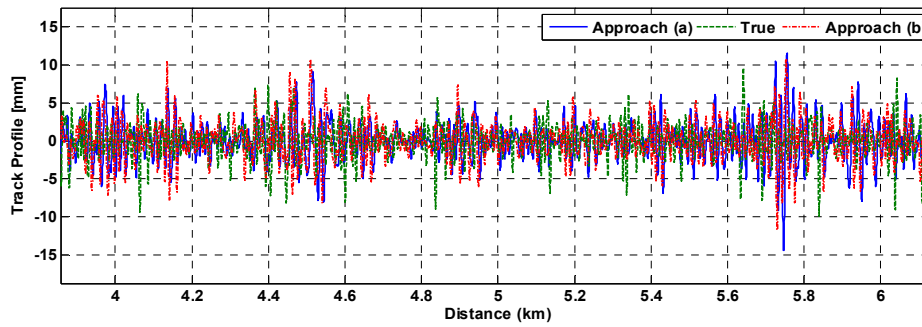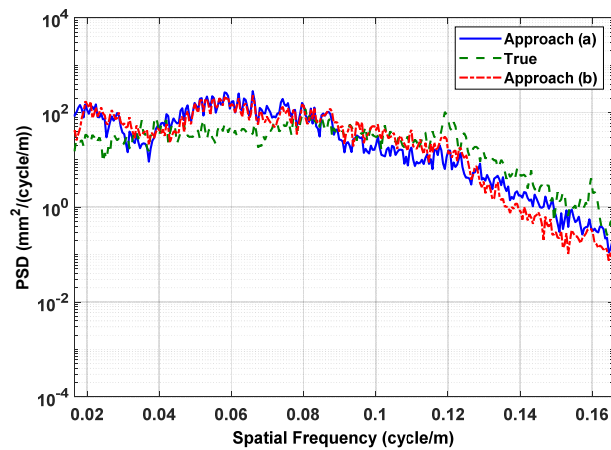

(b) Zoomed response (4 -6 km)

(c) PSD plot

(d) Estimation error after misfit criteria (150 m to 17.1 km)

Figure D.8 Estimation results for 10 m chord versine: left vertical track profile for station 5-6

(a) For station 2-3

(b) Zoomed responses (1-3 km)

(c) PSD plot

(d) Estimation error after misfit criteria (150 m to 8900 m)

Figure D.9 Estimation results for restored waveform: left alignment profile for station 2-3
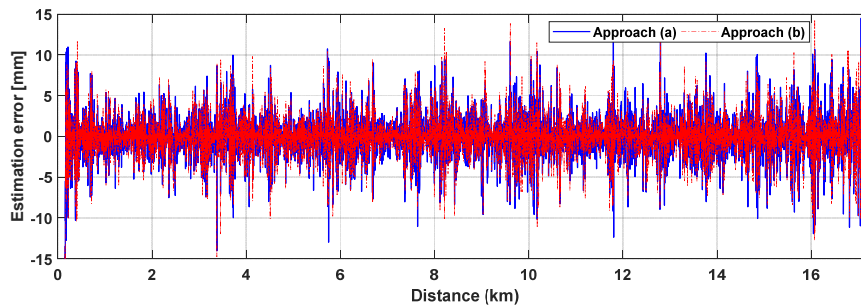
(a) For station 3-4

(b) Zoomed response (4 -6 km)
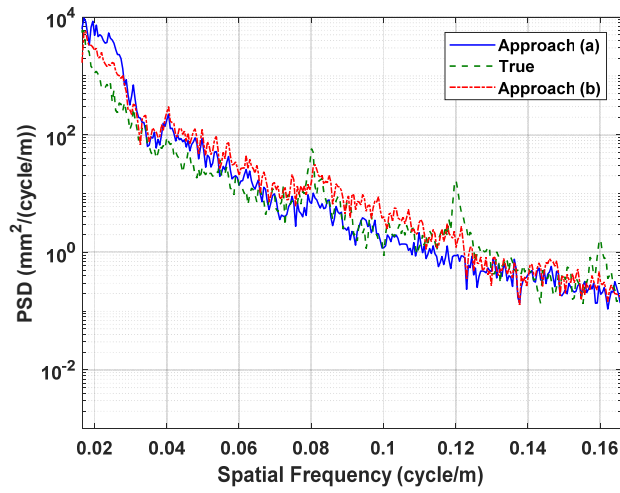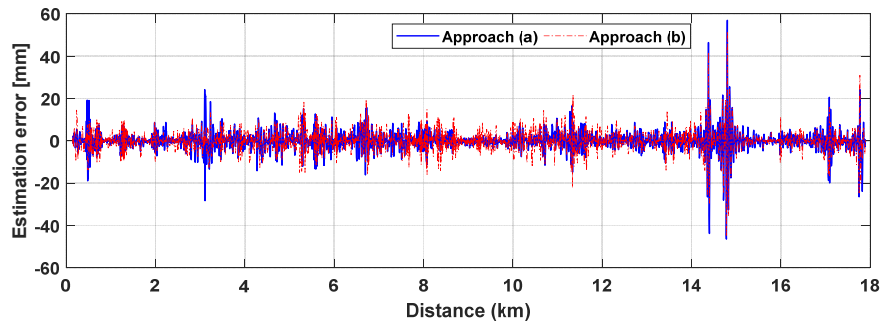
(c) PSD plot

(d) Estimation error after misfit criteria (150 m to 17.9 km)

Figure D.10 Estimation results for restored waveform: left alignment profile for station 3-4
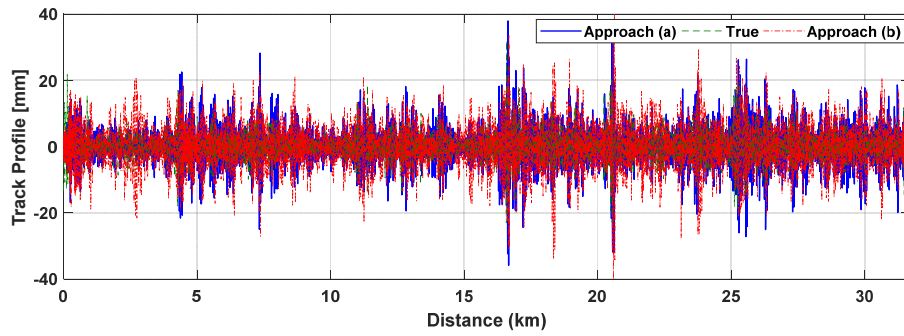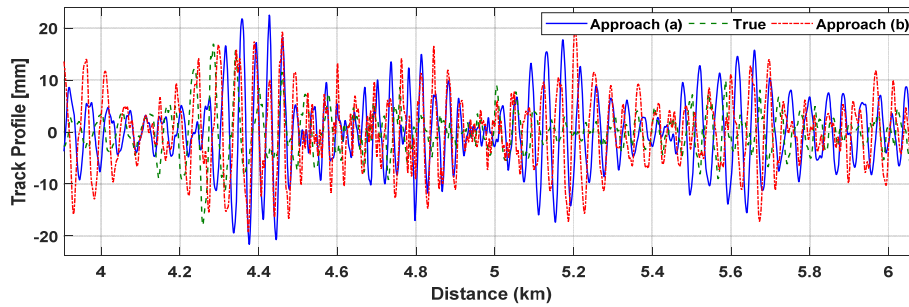
(a) For station 4-5

(b) Zoomed responses (2-4 km)
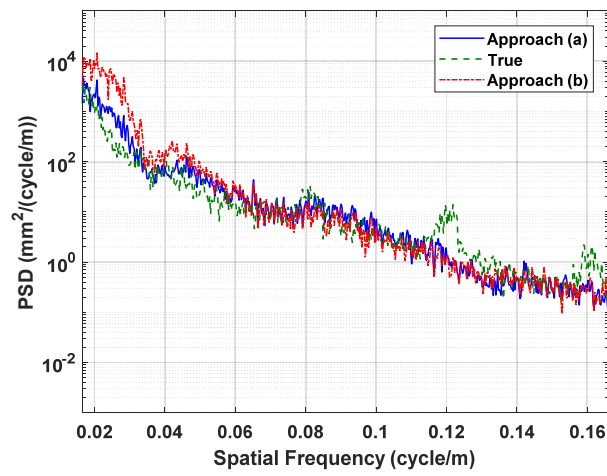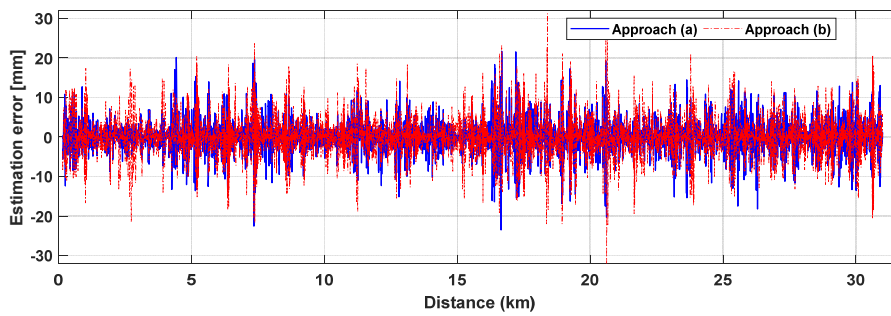
(c) PSD plot

(d) Estimation error after misfit criteria (150 m to 31 km)

Figure D.11 Estimation results for restored waveform: left alignment profile for station 4-5
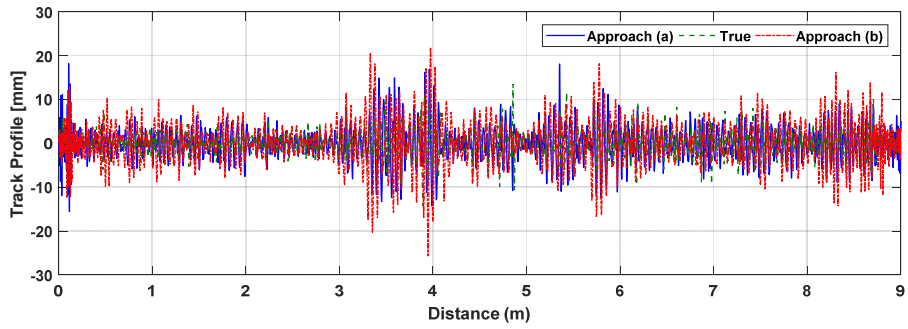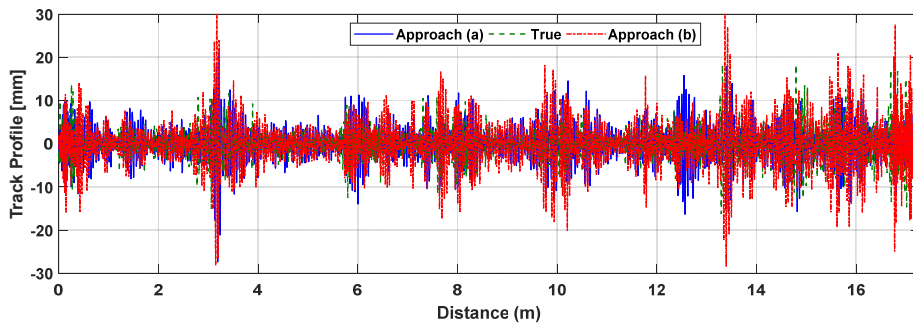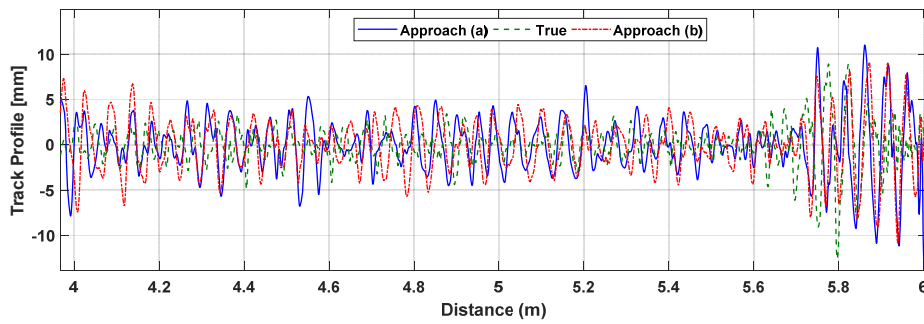
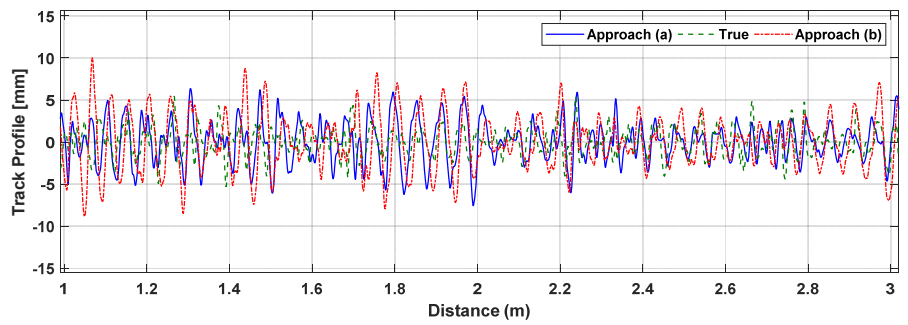(a) For station 5-6

(b) Zoomed response (4-6 km)
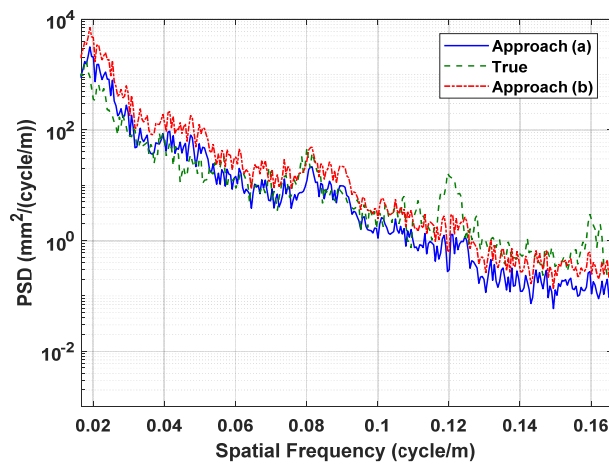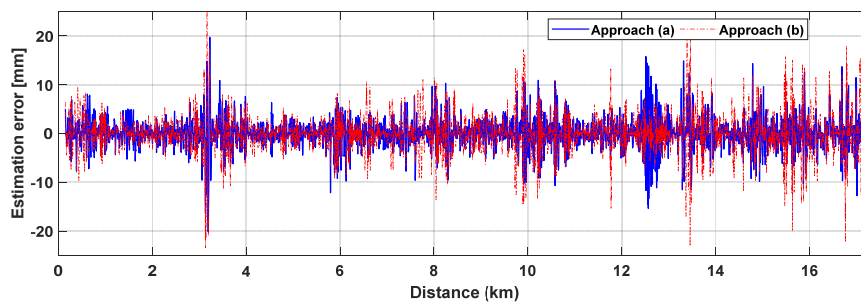
(c) PSD plot

(d) Estimation error after misfit criteria (150 m to 17.1 km)

Figure D.12 Estimation results for restored waveform: left alignment profile for station 5-6

(a) For station 2-3

(b) Zoomed responses (1-3 km)
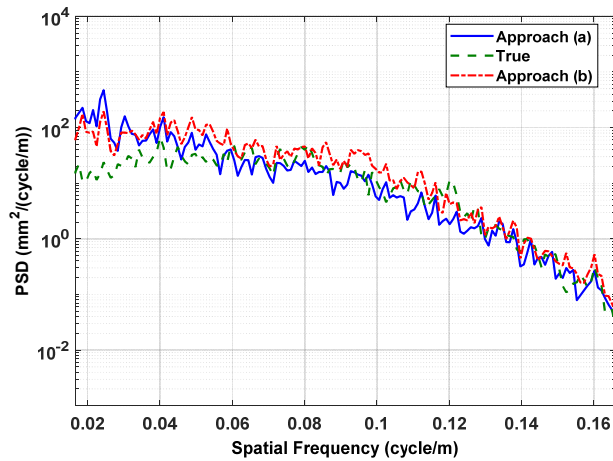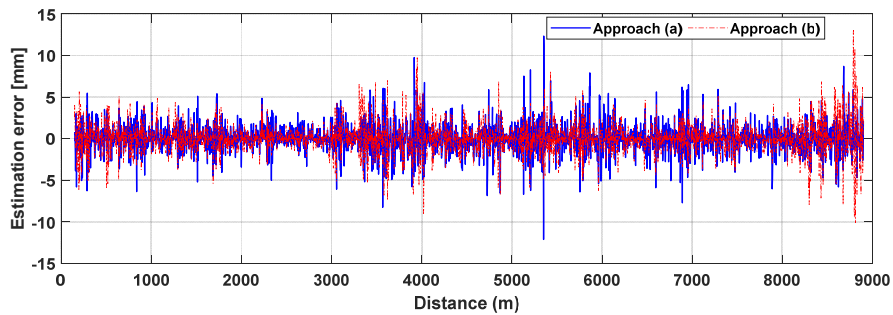
(c) PSD plot

(d) Estimation error after misfit criteria (150 m to 8900 m)

Figure D.13 Estimation for 10 m chord versine left alignment profile for station 2-3
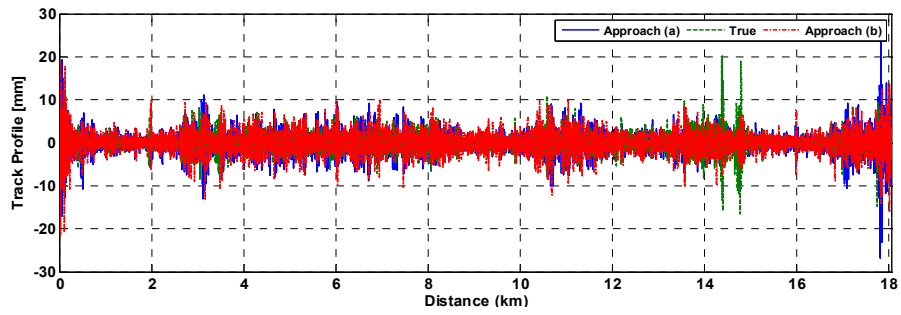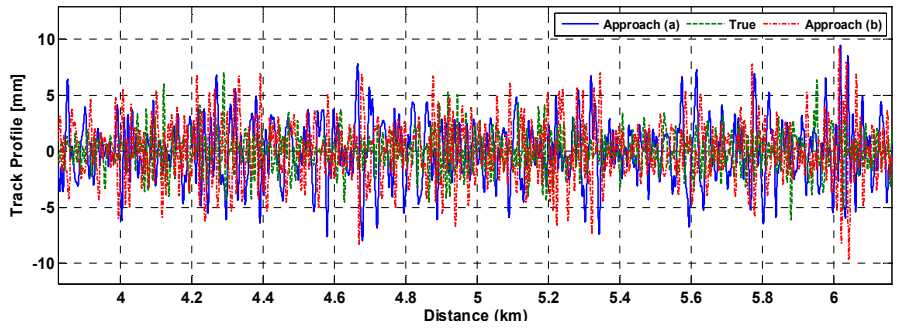
(a) For station 3-4

(b) Zoomed response (4 -6 km)
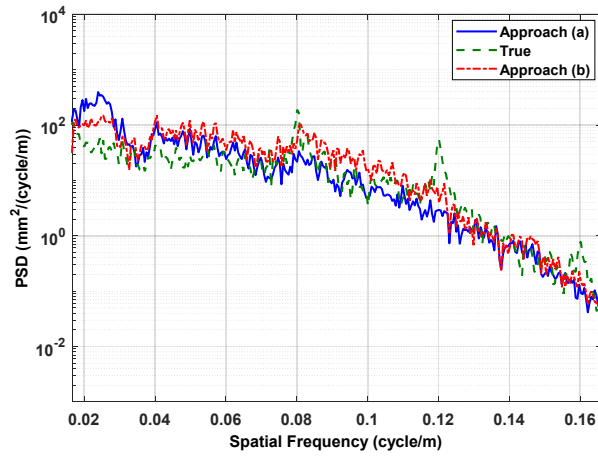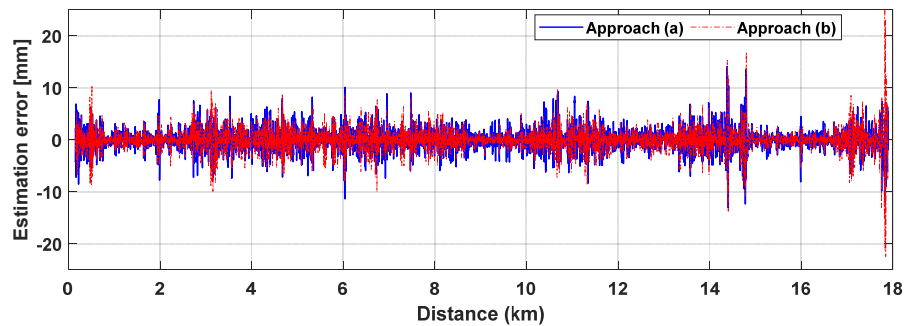
(c) PSD plot

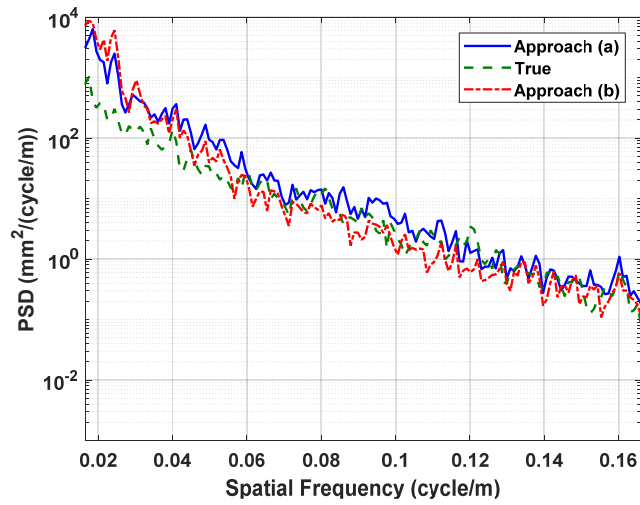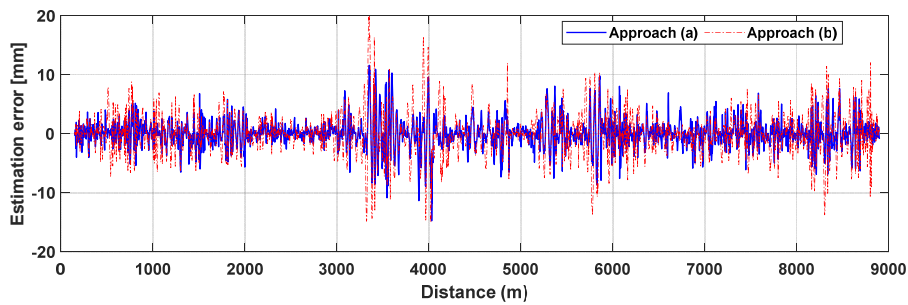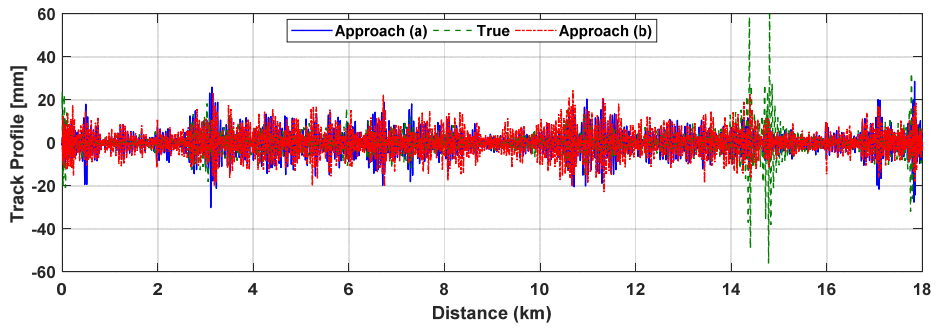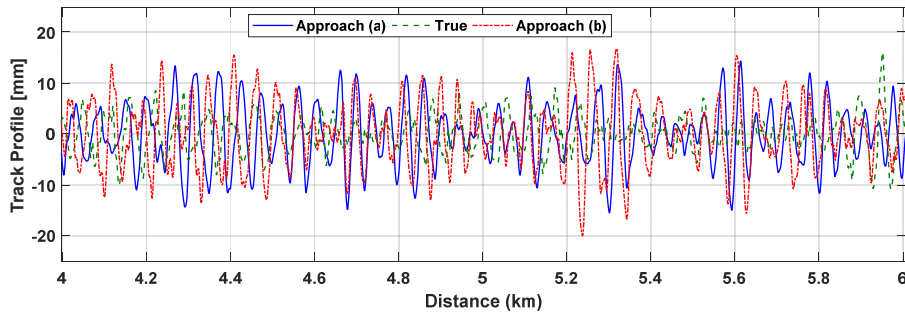(d) Estimation error after misfit criteria (150 m to 17.9 km)

Figure D.14 Estimation for 10 m chord versine left alignment profile for station 3-4
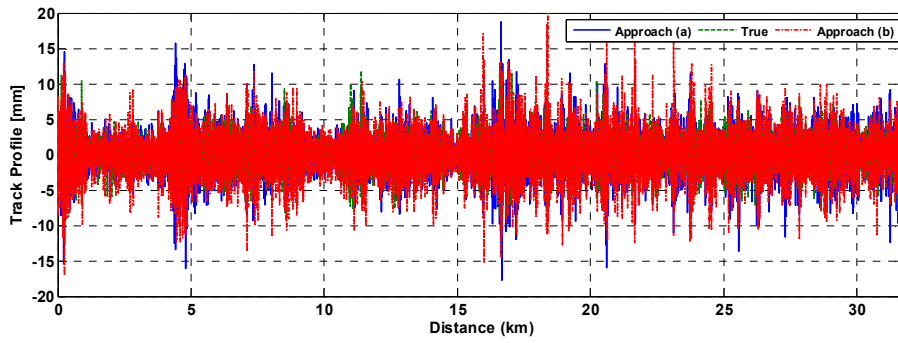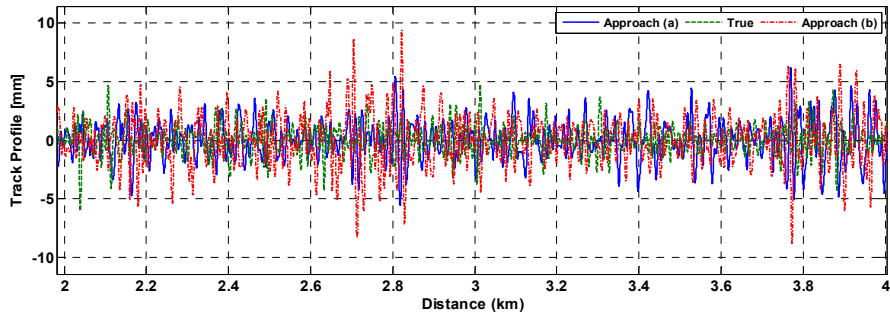
(a) For station 4-5

(b) Zoomed responses (2-4 km)
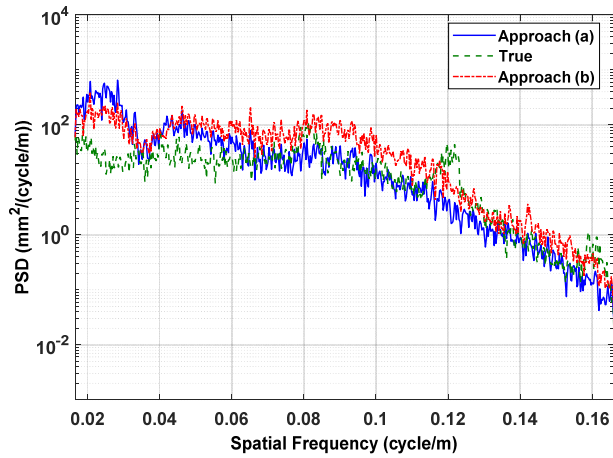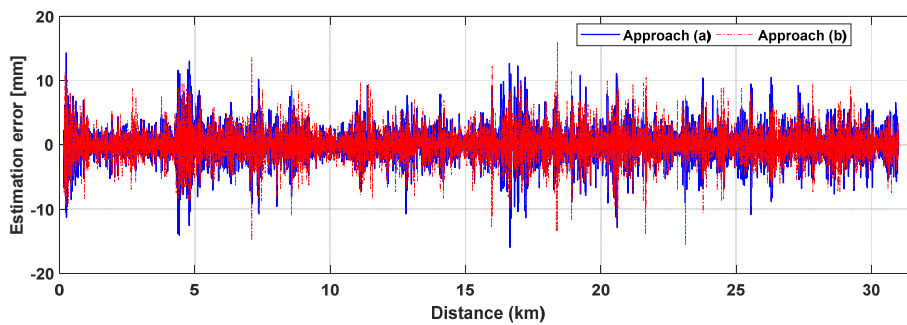
(c) PSD plot

(d) Estimation error after misfit criteria (m to m)

Figure D.15 Estimation for 10 m chord versine left alignment profile for station 4-5
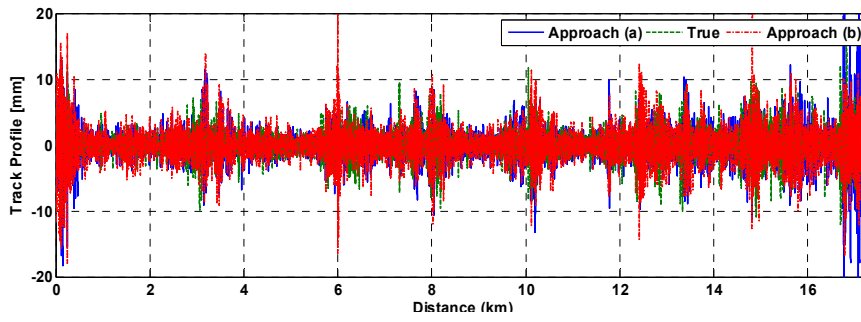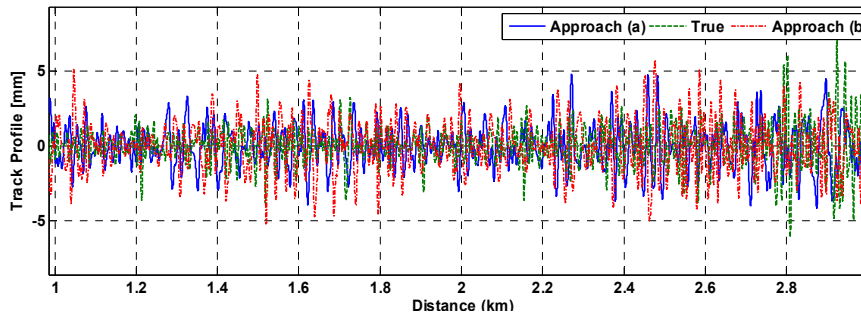
(a) For station 5-6

(b) Zoomed response (1-3 km)
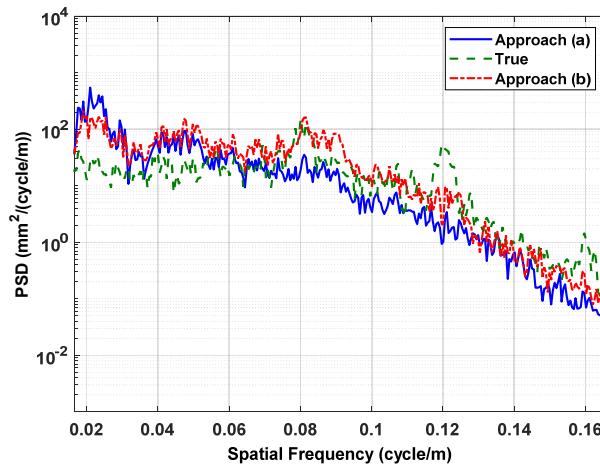
(c) PSD plot
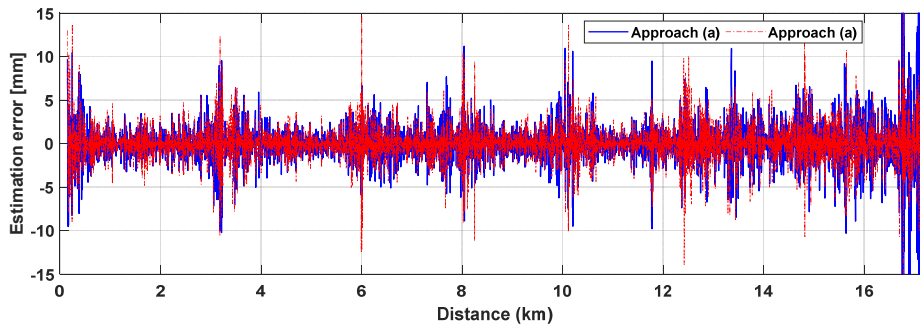
(d) Estimation error after misfit criteria (150 m to 17.1 km)

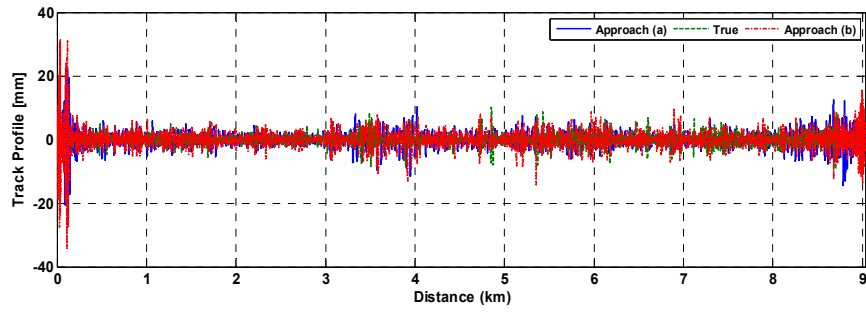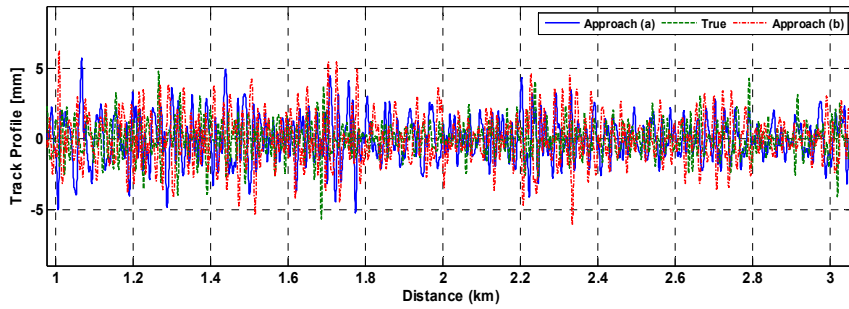Figure D.16 Estimation for 10 m chord versine left alignment profile for station 5-6

REFERENCES

[1] Takatsu, T., *The history and future of high-speed railways in Japan.* Japan Railway & Transport Review, 2007. **48**: p. 6-21.

[2] Garg, V., *Dynamics of railway vehicle systems*. 2012: Elsevier.

[3] Li, Q., et al. *Rail inspection meets big data: methods and trends*. in *Network-Based Information Systems (NBiS), 2015 18th International Conference on*. 2015. IEEE.

[4] Haigermoser, A., et al., *Road and track irregularities: measurement, assessment and simulation.* Vehicle System Dynamics, 2015. **53**(7): p. 878-957.

[5] Berggren, E.G., M.X. Li, and J. Spännar, *A new approach to the analysis and presentation of vertical track geometry quality and rail roughness.* Wear, 2008. **265**(9): p. 1488-1496.

[6] Guler, H., *Prediction of railway track geometry deterioration using artificial neural networks: a case study for Turkish state railways.* Structure and Infrastructure Engineering, 2014. **10**(5): p. 614-626.

[7] Sadeghi, J. and H. Askarinejad, *Development of track condition assessment model based on visual inspection.* Structure and Infrastructure Engineering, 2011. **7**(12): p. 895-905.

[8] Weston, P., et al., *Perspectives on railway track geometry condition monitoring from in-service railway vehicles.* Vehicle System Dynamics, 2015. **53**(7): p. 1063-1091.

[9] Ackroyd, P., et al. *Remote ride quality monitoring of Acela train set performance*. in *ASME/IEEE 2002 Joint Rail Conference*. 2002. American Society of Mechanical Engineers.

[10] McAnaw, H.E., *The system that measures the system.* NDT & E International, 2003. **36**(3): p. 169-179.

[11] Wang, C., et al. *On-line monitoring of railway deformation using acceleration measurement*. in *Intelligent Control and Automation, 2006. WCICA 2006. The Sixth World Congress on*. 2006. IEEE.

[12] Bocciolone, M., et al., *A measurement system for quick rail inspection and effective track maintenance strategy.* Mechanical Systems and Signal Processing, 2007. **21**(3): p. 1242-1254.

[13] Alfi, S. and S. Bruni, *Estimation of long wavelength track irregularities from on board measurement.* 2008.

[14] Scott, G., E. Chillingworth, and M. Dick. *Development of an unattended track geometry measurement system*. in *Proceeding of the 2010 Joint Rail Conference*. 2010.

[15] Erhard, F., K. Wolter, and M. Zacher. *Improvement of track maintenance by continuous monitoring with regularly scheduled high speed trains*. in *Railway Engineering–10th International Conference & Exhibition*. 2009.

[16] Westeon, P., et al., *Monitoring vertical track irregularity from in-service railway vehicles.* Proceedings of the institution of mechanical engineers, Part F: Journal of Rail and Rapid Transit, 2007. **221**(1): p. 75-88.

[17] Weston, P., et al., *Monitoring lateral track irregularity from in-service railway vehicles.* Proceedings of the Institution of Mechanical Engineers, Part F: Journal of Rail and Rapid Transit, 2007. **221**(1): p. 89-100.

[18] Ward, C.P., et al., *Condition monitoring opportunities using vehicle-based sensors.* Proceedings of the Institution of Mechanical Engineers, Part F: Journal of Rail and Rapid Transit, 2011. **225**(2): p. 202-218.

[19] Stewart, E., et al., *Using bogie-mounted sensors to understand the dynamics of third rail current collection systems.* Proceedings of the Institution of Mechanical Engineers, Part F: Journal of Rail and Rapid Transit, 2011. **225**(2): p. 219-227.

[20] Lee, J., et al., *Track condition monitoring by in-service trains: a comparison between axle-box and bogie accelerometers.* 2011.

[21] Lee, J.S., et al., *A mixed filtering approach for track condition monitoring using accelerometers on the axle box and bogie.* IEEE Transactions on Instrumentation and Measurement, 2012. **61**(3): p. 749-758.

[22] Heirich, O., et al. *Measurement and analysis of train motion and railway track characteristics with inertial sensors*. in *Intelligent Transportation Systems (ITSC), 2011 14th International IEEE Conference on*. 2011. IEEE.

[23] Molodova, M., et al. *Axle box acceleration for health monitoring of insulated joints: A case study in the Netherlands*. in *Intelligent Transportation Systems (ITSC), 2014 IEEE 17th International Conference on*. 2014. IEEE.

[24] YAZAWA, E. and K. TAKESHITA, *Development of measurement device of track irregularity using inertial mid-chord offset method.* Quarterly Report of RTRI, 2002. **43**(3): p. 125-130.

[25] Kaito, K., et al., *The Study of Train Intelligent Monitoring System Using Acceleration of Ordinary Train.* 2006.

[26] Hayashi, Y., et al., *Real time fault detection of railway vehicles and tracks.* 2006.

[27] Naganuma, Y., et al., *Condition monitoring of Shinkansen tracks using commercial trains.* 2008.

[28] Czop, P., K. Mendrok, and T. Uhl, *Application of inverse linear parametric models in the identification of rail track irregularities.* Archive of Applied Mechanics, 2011. **81**(11): p. 1541-1554.

[29] Tsunashima, H., et al., *Condition monitoring of railway track using in-service vehicle*, in *Reliability and safety in railway*. 2012, InTech.

[30] Tsunashima, H., Y. Naganuma, and T. Kobayashi, *Track geometry estimation from car-body vibration.* Vehicle System Dynamics, 2014. **52**(sup1): p. 207-219.

[31] Hung, C. and W. Hsu, *Influence of long-wavelength track irregularities on the motion of a high-speed train.* Vehicle System Dynamics, 2017: p. 1-18.

[32] Minbashi, N., et al., *Geometrical Degradation Analysis of Railway Turnouts Using Power Spectral Density.* Journal of Transportation Engineering, Part A: Systems, 2017. **143**(8): p. 04017035.

[33] Furukawa, A., *A method to predict vertical vehicle motion caused by track irregularities.* Proceedings of the Institution of Mechanical Engineers, Part F: Journal of Rail and Rapid Transit, 2017. **231**(4): p. 431-443.

[34] Mukhopadhyay, S., H. Luş, and R. Betti, *Modal parameter based structural identification using input–output data: minimal instrumentation and global identifiability issues.* Mechanical Systems and Signal Processing, 2014. **45**(2): p. 283-301.

[35] Nagayama, T., et al., *Structural identification of a nonproportionally damped system and its application to a full-scale suspension bridge.* Journal of structural engineering, 2005. **131**(10): p. 1536-1545.

[36] Siringoringo, D.M. and Y. Fujino, *System identification of suspension bridge from ambient vibration response.* Engineering Structures, 2008. **30**(2): p. 462-477.

[37] Papadimitriou, C., *Optimal sensor placement methodology for parametric identification of structural systems.* Journal of sound and vibration, 2004. **278**(4): p. 923-947.

[38] Papadimitriou, C. and G. Lombaert, *The effect of prediction error correlation on optimal sensor placement in structural dynamics.* Mechanical Systems and Signal Processing, 2012. **28**: p. 105-127.

[39] Castro-Triguero, R., et al., *Robustness of optimal sensor placement under parametric uncertainty.* Mechanical Systems and Signal Processing, 2013. **41**(1): p. 268-287.

[40] Sun, H. and O. Büyüköztürk, *Optimal sensor placement in structural health monitoring using discrete optimization.* Smart Materials and Structures, 2015. **24**(12): p. 125034.

[41] Wang, J., S. Law, and Q. Yang, *Sensor placement methods for an improved force identification in state space.* Mechanical Systems and Signal Processing, 2013. **41**(1): p. 254-267.

[42] Wang, S.-H., E. Wang, and P. Dorato, *Observing the states of systems with unmeasurable disturbances.* IEEE transactions on Automatic Control, 1975. **20**(5): p. 716-717.

[43] Darouach, M., M. Zasadzinski, and S.J. Xu, *Full-order observers for linear systems with unknown inputs.* IEEE transactions on automatic control, 1994. **39**(3): p. 606-609.

[44] Kalman, R.E., *Mathematical description of linear dynamical systems.* Journal of the Society for Industrial and Applied Mathematics, Series A: Control, 1963. **1**(2): p. 152-192.

[45] Hermann, R. and A. Krener, *Nonlinear controllability and observability.* IEEE Transactions on automatic control, 1977. **22**(5): p. 728-740.

[46] Pan, J. and R. Wang. *Nonlinear observability in the structural dynamic identification.* in *Smart Structures and Materials.* 2005. International Society for Optics and Photonics.

[47] Anguelova, M., *Nonlinear observability and identifiability: General theory and a case study of a kinetic model for S. cerevisiae.* 2004.

[48] Sedoglavic, A. *A probabilistic algorithm to test local algebraic observability in polynomial time.* in *Proceedings of the 2001 international symposium on Symbolic and algebraic computation.* 2001. ACM.

[49] Franco, G., R. Betti, and R.W. Longman, *On the uniqueness of solutions for the identification of linear structural systems.* Journal of applied Mechanics, 2006. **73**(1): p. 153-162.

[50] Goshen-Meskin, D. and I. Bar-Itzhack, *Observability analysis of piece-wise constant systems. I. Theory.* IEEE Transactions on aerospace and electronic systems, 1992. **28**(4): p. 1056-1067.

[51] Dawkins, J.J. *Model based off-road terrain profile estimation.* in *American Control Conference (ACC), 2014.* 2014. IEEE.

[52] Doumiati, M., et al. *Estimation of road profile for vehicle dynamics motion: experimental validation.* in *American Control Conference (ACC), 2011.* 2011. IEEE.

[53] Türkay, S. and H. Akçay, *A study of random vibration characteristics of the quarter-car model.* Journal of sound and vibration, 2005. **282**(1): p. 111-124.

[54] Zhao, B., S. Takada, and T. Nagayama. *Development of response-based road profile estimation using multiple observables.* in *JSCE Annual Meeting at Okayama.* 2015.

[55] Chatzis, M.N., E.N. Chatzi, and A.W. Smyth, *On the observability and identifiability of nonlinear structural and mechanical systems.* Structural Control and Health Monitoring, 2015. **22**(3): p. 574-593.

[56] Li, Z., et al., *Improvements in axle box acceleration measurements for the detection of light squats in railway infrastructure.* IEEE Transactions on Industrial Electronics, 2015. **62**(7): p. 4385-4397.

[57] Asakawa, H., et al. *Development and application of road monitoring system using dynamic response of vehilces*. in *11th East Asia-Pacific Conference on Structural Engineering and Construction, EASEC-11*. 2008.

[58] Asakawa, H., et al., *Development of A Simple Pavement Diagnostic System Using Dynamic Responses of An Ordinary Vehicle*. Journal of Japan Society of Civil Engineers, Ser. E1 (Pavement Engineering), 2012. **68**: p. 20-31.

[59] Imine, H., Y. Delanne, and N. M'sirdi, *Road profile inputs for evaluation of the loads on the wheels*. Vehicle System Dynamics, 2005. **43**(sup1): p. 359-369.

[60] Imine, H., Y. Delanne, and N. M'sirdi, *Road profile input estimation in vehicle dynamics simulation*. Vehicle System Dynamics, 2006. **44**(4): p. 285-303.

[61] Johnsson, R. and J. Odelius. *Methods for road texture estimation using vehicle measurements*. in *International Conference on Noise and Vibration Engineering: 17/09/2012-19/09/2012*. 2012. Katholieke Universitat.

[62] Nagayama, T., et al., *Road condition evaluation using the vibration response of ordinary vehicles and synchronously recorded movies*. Proceedings of the SPIE Smart Structures and Materials+ Nondestructive Evaluation and Health Monitoring, 2013: p. 86923A.

[63] Kalman, R.E., *A new approach to linear filtering and prediction problems*. Journal of basic Engineering, 1960. **82**(1): p. 35-45.

[64] Kalman, R.E. and R.S. Bucy, *New results in linear filtering and prediction theory*. Journal of basic engineering, 1961. **83**(1): p. 95-108.

[65] Ma, C.-K., et al., *A study of an inverse method for the estimation of impulsive loads*. International journal of systems science, 1998. **29**(6): p. 663-672.

[66] Parloo, E., et al., *Force identification by means of in-operation modal models*. Journal of Sound and Vibration, 2003. **262**(1): p. 161-173.

[67] Vanlanduit, S., et al., *On-line identification of operational loads using exogenous inputs*. Journal of Sound and Vibration, 2005. **285**(1): p. 267-279.

[68] Lu, Z. and S. Law, *Identification of system parameters and input force from output only*. Mechanical Systems and Signal Processing, 2007. **21**(5): p. 2099-2111.

[69] Liu, J.-J., et al., *Input force estimation of a cantilever plate by using a system identification technique*. Computer Methods in Applied Mechanics and Engineering, 2000. **190**(11): p. 1309-1322.

[70] Ma, C.-K., J.-M. Chang, and D.-C. Lin, *Input forces estimation of beam structures by an inverse method*. Journal of Sound and Vibration, 2003. **259**(2): p. 387-407.

[71] Ma, C.-K. and C.-C. Ho, *An inverse method for the estimation of input forces acting on non-linear structural systems*. Journal of Sound and Vibration, 2004. **275**(3): p. 953-971.

[72] Smyth, A. and M. Wu, *Multi-rate Kalman filtering for the data fusion of displacement and acceleration response measurements in dynamic system monitoring.* Mechanical Systems and Signal Processing, 2007. **21**(2): p. 706-723.

[73] Kim, J., K. Kim, and H. Sohn, *Autonomous dynamic displacement estimation from data fusion of acceleration and intermittent displacement measurements.* Mechanical Systems and Signal Processing, 2014. **42**(1): p. 194-205.

[74] Hwang, J.-s., A. Kareem, and W.-j. Kim, *Estimation of modal loads using structural response.* Journal of Sound and Vibration, 2009. **326**(3): p. 522-539.

[75] Chatzi, E.N. and A.W. Smyth, *The unscented Kalman filter and particle filter methods for nonlinear structural system identification with non-collocated heterogeneous sensing.* Structural control and health monitoring, 2009. **16**(1): p. 99-123.

[76] Chatzis, M., E. Chatzi, and A. Smyth, *An experimental validation of time domain system identification methods with fusion of heterogeneous data.* Earthquake Engineering & Structural Dynamics, 2015. **44**(4): p. 523-547.

[77] Lourens, E., et al., *An augmented Kalman filter for force identification in structural dynamics.* Mechanical Systems and Signal Processing, 2012. **27**: p. 446-460.

[78] Naets, F., J. Cuadrado, and W. Desmet, *Stable force identification in structural dynamics using Kalman filtering and dummy-measurements.* Mechanical Systems and Signal Processing, 2015. **50**: p. 235-248.

[79] Chatzi, E.N. and C. Fuggini, *Online correction of drift in structural identification using artificial white noise observations and an unscented Kalman filter.* Smart Structures and Systems, 2015. **16**(2): p. 295-328.

[80] Azam, S.E., E. Chatzi, and C. Papadimitriou, *A dual Kalman filter approach for state estimation via output-only acceleration measurements.* Mechanical Systems and Signal Processing, 2015. **60**: p. 866-886.

[81] Azam, S.E., et al., *Experimental validation of the Kalman-type filters for online and real-time state and input estimation.* Journal of Vibration and Control, 2017. **23**(15): p. 2494-2519.

[82] Kim, K., et al., *Dynamic displacement estimation by fusing biased high-sampling rate acceleration and low-sampling rate displacement measurements using two-stage Kalman estimator.* Smart Structures and Systems, 2016. **17**(4): p. 647-667.

[83] Liu, L., et al., *Improved Kalman filter with unknown inputs based on data fusion of partial acceleration and displacement measurements.* Smart Structures and Systems, 2016. **17**(6): p. 903-915.

[84] Fauriat, W., et al., *Estimation of road profile variability from measured vehicle responses.* Vehicle System Dynamics, 2016. **54**(5): p. 585-605.

[85] Giurgiutiu, V. and C.A. Rogers. *Recent advancements in the electro-mechanical (E/M) impedance method for structural health monitoring and NDE*. in *Proc. SPIE*. 1998.

[86] Park, G. and D.J. Inman, *Structural health monitoring using piezoelectric impedance measurements.* Philosophical Transactions of the Royal Society of London A: Mathematical, Physical and Engineering Sciences, 2007. **365**(1851): p. 373-392.

[87] Fries, R. and B. Coffey, *A state-space approach to the synthesis of random vertical and crosslevel rail irregularities.* J. Dyn. Sys., Meas., Control, 1990. **112**(1): p. 83-87.

[88] Berawi, A., *Improving railway track maintenance using power spectral density*. 2013, Universidade Do Porto.

[89] Su, D., et al., *Vibration of reinforced concrete viaducts under high-speed train passage: measurement and prediction including train–viaduct interaction.* Structure and Infrastructure Engineering, 2010. **6**(5): p. 621-633.

[90] Su, D., *Prediction of bridge vibration incorporating dynamic interaction with high-speed trains and its comparison with measurement*, in *Department of Civil Engineering*. 2009, The University of Tokyo: Japan.

[91] Kristeková, M., et al., *Misfit criteria for quantitative comparison of seismograms.* Bulletin of the seismological Society of America. 2006. 96(5): p. 1836-1850.

[92] Kristeková, M., et al., *Time-frequency misfit and goodness-of-fit criteria for quantitative comparison of time signals*. Geophysical Journal International. 2009. 178(2): p. 813-825.

[93] Claus, H. and W. Schiehlen, *Modeling and simulation of railway bogie structural vibrations.* Vehicle System Dynamics, 1998. **29**(S1): p. 538-552.

[94] JRCEA, *Investigation committee of railway technical specification in civil engineering. (In Japanese)*, ed. J.R.C.E. Association. 2002, Japan: Ministry of Land, Infrastructure, Transport and Tourism: Railway technical specification (civil engineering).

[95] JSME, *Dynamics of Rolling Stock (In Japanese)*, ed. J.S.o.M. Engineers. 1996: Denkisya-Kenkyukai.

[96] Standard, B., *Railway applications/Track-Track geometry quality.* BS EN, 2003: p. 13848-1.

[97] Bruni, S., et al., *Control and monitoring for railway vehicle dynamics.* Vehicle System Dynamics, 2007. **45**(7-8): p. 743-779.

[98] Goodall, R. and C. Roberts. *Concepts and techniques for railway condition monitoring*. in *Railway Condition Monitoring, 2006. The Institution of Engineering and Technology International Conference on*. 2006. IET.

[99] Sunaga, Y., I. Sano, and T. IDE, *A method to control the short wave track irregularities utilizing axlebox acceleration.* Railway Technical Research Institute, Quarterly Reports, 1997. **38**(4).

[100] Naganuma, Y. and Y. Sato, *Track state control with use of real time digital data processing.* International Journal of Heavy Vehicle Systems, 2000. **7**(1): p. 82-95.

[101] Kojima, T., H. Tsunashima, and A. Matsumoto, *Fault detection of railway track by multi-resolution analysis.* 2006.

[102] Real, J., et al., *Determination of rail vertical profile through inertial methods.* Proceedings of the Institution of Mechanical Engineers, Part F: Journal of Rail and Rapid Transit, 2011. **225**(1): p. 14-23.

[103] Ngigi, R., et al. *Modern techniques for condition monitoring of railway vehicle dynamics.* in *Journal of Physics: Conference Series.* 2012. IOP Publishing.

[104] Perrin, G., et al., *Track irregularities stochastic modeling.* Probabilistic Engineering Mechanics, 2013. **34**: p. 123-130.

[105] Cantero, D. and B. Basu, *Railway infrastructure damage detection using wavelet transformed acceleration response of traversing vehicle.* Structural Control and Health Monitoring, 2015. **22**(1): p. 62-70.

[106] Chiacchiari, L. and G. Loprencipe, *Measurement methods and analysis tools for rail irregularities: a case study for urban tram track.* Journal of Modern Transportation, 2015. **23**(2): p. 137-147.

[107] OBrien, E.J., et al., *Determination of longitudinal profile of railway track using vehicle-based inertial readings.* Proceedings of the Institution of Mechanical Engineers, Part F: Journal of Rail and Rapid Transit, 2017. **231**(5): p. 518-534.

[108] Mori, H., et al., *Development of compact size onboard device for condition monitoring of railway tracks.* Journal of mechanical systems for transportation and logistics, 2013. **6**(2): p. 142-149.

[109] Ogino, M., et al., *Development of Track Condition Monitoring System Based on Compact Onboard Sensing Devices (Japanese Title: 小型レール診断装置を用いた軌道状態診断システムの開発).* IEEJ Transactions on Industry Applications, 2015. **135**: p. 395-402.

[110] Kobayashi, T., Y. Naganuma, and H. Tsunashima, *Condition monitoring of shinkansen tracks based on inverse analysis.* International Journal of Performability Engineering, 2014. **10**(5): p. 443-452.

[111] ODASHIMA, M., et al., *Track geometry estimation of a conventional railway from car-body acceleration measurement.* Mechanical Engineering Journal, 2017. **4**(1): p. 16-00498-16-00498.

[112] Grassie, S.L., *Measurement of railhead longitudinal profiles: a comparison of different techniques.* Wear, 1996. **191**(1-2): p. 245-251.

[113] Insa, R., et al., *On the filtering effects of the chord offset method for monitoring track geometry.* Proceedings of the Institution of Mechanical Engineers, Part F: Journal of Rail and Rapid Transit, 2012. **226**(6): p. 650-654.

[114] Nielsen, J., et al., *Overview of methods for measurement of track irregularities important for ground-borne vibration.* Railway Induced Vibration Abatement Solutions (RIVAS), 2013.

[115] Yoshimura, A., *Theory and practice for restoring an original waveform of a railway track irregularity.* Railway Technical Research Institute, Quarterly Reports, 1995. **36**(2).

[116] Ishii, Y., et al. *The Study of Train Intelligent Monitoring System using acceleration of ordinary trains*. in *Proceedings of Asia-Pacific Workshop on Structural Health Monitoring, Yokohama Japan (CD)*. 2006.

[117] Fujino, Y., et al. *Development of vehicle intelligent monitoring system (VIMS)*. in *Proc. of SPIE Vol*. 2005.

[118] Makihata, N., et al., *Large-scale road surface evaluation using dynamic responses of commercial vehicles.* ICE Virtual Library essential engineering knowledge, 2016.

[119] Zhao, B. and T. Nagayama, *IRI Estimation by the Frequency Domain Analysis of Vehicle Dynamic Responses.* Procedia Engineering, 2017. **188**: p. 9-16.

[120] Zhao, B., et al. *IRI Estimation by the Frequency Domain Analysis of Vehicle Dynamic Responses and Its Large-scale Application*. in *Adjunct Proceedings of the 13th International Conference on Mobile and Ubiquitous Systems: Computing Networking and Services*. 2016. ACM.

[121] Zhao, B., et al., *Vehicle Model Calibration in the Frequency Domain and its Application to Large-Scale IRI Estimation.* Journal of Disaster Research, 2017. **12**(3): p. 446-455.

[122] Apple. *www.apple.com*. 2017.

[123] Tanaka, H., Saruki, Y. and Haga, A. *Distance Sampling Method of On-board Measured Data for Portable Track Condition Monitoring Device*. in *17th Railway Technology Union Symposium (J-RAIL2010)*. 2010. Japan.

[124] Alfi, S., A. De Rosa, and S. Bruni, *Estimation of lateral track irregularities from on-board measurement: effect of wheel-rail contact model.* 2016.

[125] Wang, L., et al., *The effect of track alignment irregularity on wheel-rail contact geometry relationship in a turnout zone.* Journal of Modern Transportation, 2012. **20**(3): p. 148-152.

[126] Furukawa, A. and A. Yoshimura, *Identification of rolling stock lateral dynamic characteristics and their track irregularity maintenance applications.* Quarterly Report of RTRI, 2005. **46**(1): p. 7-12.

[127] TANIFUJI, K. and T. SAKUYAMA, *The Characteristics of Wheel Wear in Shinkansen Electric Cars and Its Effect on the Running Vibration: In Case of Conical-Shaped Wheels with a*

Conicity of 1/40. JSME international journal. Ser. 3, Vibration, control engineering, engineering for industry, 1988. **31**(2): p. 457-464.

[128] Arnold, M., et al., *Numerical methods in vehicle system dynamics: state of the art and current developments.* Vehicle System Dynamics, 2011. **49**(7): p. 1159-1207.

[129] Iwnicki, S., *Future trends in railway engineering.* Proceedings of the Institution of Mechanical Engineers, Part C: Journal of Mechanical Engineering Science, 2009. **223**(12): p. 2743-2750.

[130] Spiryagin, M., et al., *Design and simulation of rail vehicles*. 2014: CRC Press.

[131] Wickens, A., *Fundamentals of rail vehicle dynamics: guidance and stability, 2003.* Swets & Zeitlinger Publishers, Lisse.

[132] Baeza, L. and H. Ouyang, *A railway track dynamics model based on modal substructuring and a cyclic boundary condition.* Journal of Sound and Vibration, 2011. **330**(1): p. 75-86.

[133] Dietz, S., G. Hippmann, and G. Schupp, *Interaction of vehicles and flexible tracks by co-simulation of multibody vehicle systems and finite element track models.* Vehicle system dynamics, 2002. **37**(sup1): p. 372-384.

[134] Lei, X. and L. Mao, *Dynamic response analyses of vehicle and track coupled system on track transition of conventional high speed railway.* Journal of Sound and Vibration, 2004. **271**(3): p. 1133-1146.

[135] Netter, H., et al., *New aspects of contact modelling and validation within multibody system simulation of railway vehicles.* Vehicle System Dynamics, 1998. **29**(S1): p. 246-269.

[136] Schupp, G., C. Weidemann, and L. Mauer, *Modelling the contact between wheel and rail within multibody system simulation.* Vehicle System Dynamics, 2004. **41**(5): p. 349-364.

[137] Sun, Y.Q. and M. Dhanasekar, *A dynamic model for the vertical interaction of the rail track and wagon system.* International Journal of Solids and Structures, 2002. **39**(5): p. 1337-1359.

[138] Sun, Y.Q., M. Dhanasekar, and D. Roach, *A three-dimensional model for the lateral and vertical dynamics of wagon-track systems.* Proceedings of the Institution of Mechanical Engineers, Part F: Journal of Rail and Rapid Transit, 2003. **217**(1): p. 31-45.

[139] Evans, J. and M. Berg, *Challenges in simulation of rail vehicle dynamics.* Vehicle System Dynamics, 2009. **47**(8): p. 1023-1048.

[140] Ling, L., et al., *A 3D model for coupling dynamics analysis of high-speed train/track system.* Journal of Zhejiang University SCIENCE A, 2014. **15**(12): p. 964-983.

[141] Zhai, W., K. Wang, and C. Cai, *Fundamentals of vehicle–track coupled dynamics.* Vehicle System Dynamics, 2009. **47**(11): p. 1349-1376.

[142] Polach, O. and J. Evans, *Simulations of running dynamics for vehicle acceptance: application and validation.* Int J Railway Technol, 2013. **2**(4): p. 59-84.

[143] Rulka, W. and A. Eichberger, *Simpack an analysis and design tool for mechanical systems.* Vehicle system dynamics, 1993. **22**(S1): p. 122-126.

[144] Bosso, N. and N. Zampieri, *Long train simulation using a multibody code.* Vehicle System Dynamics, 2017. **55**(4): p. 552-570.

[145] Wang, Y., Y. Qin, and X. Wei. *Track irregularities estimation based on acceleration measurements*. in *Measurement, Information and Control (MIC), 2012 International Conference on*. 2012. IEEE.

[146] Weidemann, C., *State-of-the-art railway vehicle design with multi-body simulation.* Journal of mechanical systems for transportation and logistics, 2010. **3**(1): p. 12-26.

[147] Kalker, J., *A fast algorithm for the simplified theory of rolling contact.* Vehicle system dynamics, 1982. **11**(1): p. 1-13.

[148] Nefzger, A., *Geometrie der Berührung zwischen Radsatz und Gleis.* Eisenbahntechnische Rundschau ETR, 1974(3): p. 113.